Développement de transducteurs électromagnétiques acoustiques pour l'estimation d'épaisseur minimale sur des tuyaux corrodés en acier

par

Aurélien THON

THÈSE PAR ARTICLES PRÉSENTÉE À L'ÉCOLE DE TECHNOLOGIE SUPÉRIEURE COMME EXIGENCE PARTIELLE À L'OBTENTION DU DOCTORAT EN GÉNIE Ph.D.

MONTRÉAL, LE 31 JUILLET 2023

ÉCOLE DE TECHNOLOGIE SUPÉRIEURE UNIVERSITÉ DU QUÉBEC

PRÉSENTATION DU JURY

CETTE THÈSE A ÉTÉ ÉVALUÉE

PAR UN JURY COMPOSÉ DE:

M. Pierre Bélanger, directeur de thèse
Département de génie mécanique à l'École de technologie supérieure

M. Ricardo Izquierdo, président du jury
Département de génie électrique à l'École de technologie supérieure

M. Ricardo Zednik, membre du jury
Département de génie mécanique à l'École de technologie supérieure

M. Nicolas Quaegebeur, examinateur externe
Département de génie mécanique à l'Université de Sherbrooke

ELLE A FAIT L'OBJET D'UNE SOUTENANCE DEVANT JURY ET PUBLIC

LE 13 JUILLET 2023

À L'ÉCOLE DE TECHNOLOGIE SUPÉRIEURE

REMERCIEMENTS

Je tiens tout d'abord à remercier les membres du jury d'avoir accepté d'évaluer ce travail. Merci pour le temps que vous m'avez attribué, vos conseils et vos remarques.

Ensuite, je remercie tout particulièrement mon directeur de recherche le professeur Pierre Bélanger, pour son accompagnement et ses conseils lors de ce doctorat, plus anciennement de ma maîtrise, mais également lors de nombreux projets annexes.

Ce projet n'aurait pas été possible sans le partenaire de cette thèse : Evident Industrial (anciennement Olympus). Un grand merci à tous les employés qui ont contribué de près ou de loin à mes travaux, je pense en particulier à Alain et Guillaume.

Je tiens à remercier tous les membres du PulÉTS, anciens et nouveaux, avec qui j'ai passé d'excellents moments que ce soit au laboratoire ou lors d'activités extérieures : Guillaume, Victor, Baptiste, Frédéric, Timothé, Geoffrey, Sévan, Arthur, Anthony, Cherif, Mathieu, Nicolas (12), Aubin, Damien, Thibault, Jorge, Bupesh, Rafeal, Tony, Adrien, les deux Hugo.

Bien sûr, je remercie ma famille, mes parents, mes frères, ma sœur, mes grands-parents pour leurs soutiens inconditionnels dans tout ce que j'ai entrepris.

Développement de transducteurs électromagnétiques acoustiques pour l'estimation d'épaisseur minimale sur des tuyaux corrodés en acier

Aurélien THON

RÉSUMÉ

Le contrôle non destructif (CND) par ondes guidées regroupe diverses techniques visant à scanner des structures comme des plaques ou des tuyaux sur de moyennes à longues distances. Les résultats peuvent aller de la caractérisation d'un défaut, nature et taille, à l'estimation des propriétés du matériau inspecté. Un phénomène largement surveillé est la corrosion. Cette réaction chimique dégrade des matériaux comme de l'acier et peut engendrer une altération de propriétés mécaniques, la création de concentrateur de contrainte ou bien une perte locale d'épaisseur. Ce dernier cas est particulièrement important dans les industries pétrochimiques puisqu'une surface corrodée non surveillée peut aboutir à la rupture d'un tuyau et donc à une fuite de produit potentiellement nocif pour les humains et l'environnement. Le filtrage structurel est une méthode permettant ce suivi. Cette technique utilise les relations de dispersion des modes d'onde guidée d'ordre élevé, ou relations des vitesses de phases et de groupes avec la fréquence et l'épaisseur du guide d'onde. Les ondes guidées de cisaillement horizontal, ondes SH, sont favorisées pour les inspections par filtrage structurel par rapport aux ondes de Lamb du fait de la simplicité d'interprétation de leurs courbes de dispersion, de leur faible sensibilité aux chargements fluides non visqueux en surface et du fait qu'elles ne se convertissent pas en modes de Lamb lorsqu'elles interagissent avec un défaut parallèle à la direction de polarisation. Cependant les ondes SH sont connues pour être difficiles à exciter et à détecter à l'aide de transducteurs piézoélectriques conventionnels. Les transducteurs électromagnétiques acoustiques ou EMAT rendent la transduction de mode SH relativement simple. Les concepts existants sont majoritairement des sondes mono-éléments, comme des EMAT à aimants permanents et périodiques ou PPM EMAT, limitant les capacités d'excitation et les techniques de traitement de données utilisables par rapport à des sondes multi-éléments.

Les travaux présentés dans ce document reposent sur des résultats obtenus par simulation éléments finis et par des mesures expérimentales. Ils ont permis de démontrer que : (1) une sonde PPM EMAT lorsqu'elle optimisée pour une inspection sur un tuyau en acier permet une reconstruction rapide du profil d'épaisseur d'une région corrodée ; (2) un EMAT multi-éléments conçu pour la transduction d'onde SH peut permettre l'utilisation de technique avancée d'excitation et d'algorithmes de traitements de données comme des transformées de Fourier à deux dimensions avec des performances similaires à celles de sondes piézoélectrique ; (3) cette dernière sonde lorsqu'elle est utilisée sur un tuyau en acier a permis l'estimation de l'épaisseur minimale selon diverses positions avec une erreur maximale de 0.4 mm et un positionnement à 10 mm près pour une distance de propagation totale de 600 mm.

Mots-clés: Ultrasons, Ondes guidées, Corrosion, Onde de cisaillement horizontal, EMAT, Sonde multi-élément

Development of electromagnetic acoustic transducers for minimum thickness estimation on corroded steel pipes

Aurélien THON

ABSTRACT

Guided waves nondestructive testing, NDT, includes various techniques to scan structures such as plates or pipes over medium to long distances. The results can range from the characterization of a defect, nature and size, to the estimation of the properties of the inspected material. A widely monitored phenomenon is corrosion. This chemical reaction degrades materials such as steel and can lead to an alteration of mechanical properties, the creation of stress concentrators or a local loss of thickness. This last case is particularly important in the petrochemical industry since an unmonitored corroded surface can lead to a pipe rupture and therefore to a leak of product potentially harmful to humans and the environment. Structural filtering is a method allowing this monitoring. It uses the high order guided wave mode dispersion relationships, or phase and group velocity relationships with the frequency and the waveguide thickness. Shear horizontal guided waves, SH waves, are favored for structural filtering inspections over Lamb waves because of the simplicity of interpretation of their dispersion curves, their low sensitivity to non-viscous surface loads, and the fact that they do not convert into Lamb modes when interacting with a defect parallel to the direction of polatization. However, SH waves are known to be difficult to excite and detect using conventional piezoelectric transducers. Electromagnetic acoustic transducers or EMAT make SH mode transduction relatively simple but existing concepts are mostly single-element probes, such as periodic and permanent magnets EMATs or PPM EMATs, limiting the excitation capabilities and data processing techniques that can be used with multi-element probes.

The work presented in this thesis is based on results obtained by finite element simulations and experimental measurements and has demonstrated that : (1) a PPM EMAT when optimized for steel pipe inspection allows rapid reconstruction of the thickness profile of a corroded region ; (2) a multi-element EMAT probe designed for SH wave transduction can allow the use of advanced excitation techniques and data processing algorithms such as two-dimensional Fourier transforms with similar performance to piezoelectric probes ; (3) this probe when used on a steel pipe allowed the estimation of the minimum thickness at various positions with a maximum error of 0.4 mm and a positioning with an error of 10 mm for a total propagation distance of 600 mm.

Keywords: Ultrasound, Guided wave, Corrosion, Shear horizontal waves, EMAT, Multi-element probe

TABLE DES MATIÈRES

Page

LISTE DES TABLEAUX

LISTE DES ABRÉVIATIONS, SIGLES ET ACRONYMES

CND   Contrôle Non Destructif

CPU   Unité centrale de traitement (Central Processing Unit)

EMAT   Transducteurs électromagnétiques-acoustiques

GPU   Unité de traitement graphique (Graphics Processing Unit)

PPM EMAT   Transducteurs électromagnétiques-acoustiques à aimants périodiques et permanents

FE   Éléments finis

FFT   Transformée de Fourier rapide (Fast Fourier Transform)

2D-FFT   Transformée de Fourier rapide à deux dimensions (Fast Fourier Transform)

P   Onde de longitudinale, ou de pression

ROI   Région d'intérêt

SH   Onde de cisaillement polarisé dans la direction horizontale

SV   Onde de cisaillement polarisé dans la direction verticale

LISTE DES SYMBOLES ET UNITÉS DE MESURE

$\frac{\partial}{\partial}$	Dérivée partielle
α	Coefficient d'atténuation
λ	Premier coefficient de Lamé
λ_x	Longueur d'onde selon l'axe $\vec{x}$
μ	Second coefficient de Lamé
ν	Coefficient de Poisson
ρ	Masse volumique
ϕ	Potentiel scalaire
Φ	Potentiel vectoriel
ω	Fréquence angulaire ou pulsation
B	Densité du flux magnétique
b	Épaisseur
cos	Fonction cosinus
E	Module de Young
F	Force
F_M	Force magnétostrictive
F_L	Force de Lorentz
f	Fréquence
f_D	Décalage Doppler
g	Gramme
H	Champ magnétique
Hz	Hertz
I	Intensité de l'onde

J	Courant induit
I_0	Amplitude initiale de l'onde
k_x	Nombre d'onde selon l'axe $\vec{x}$
m	Mètre
N	Nombre d'élément de la sonde
Pa	Pascal
s	Seconde
sin	Fonction sinus
t	Temps
tan	Fonction tangente
V_G	Vitesse de groupe
V_P	Vitesse de phase

INTRODUCTION

La corrosion désigne une dégradation par réaction chimique d'oxydation d'un matériau. Ces attaques peuvent prendre différentes formes. Une corrosion uniforme peut être observée sur une surface par une perte d'épaisseur ainsi qu'une modification locale des propriétés mécaniques de la structure. Les piqûres de corrosion sont une forme beaucoup plus locale. Ici le principal effet sur un matériau est la création de concentrateur de contrainte qui peuvent être la source de fissures de fatigue provoquant une rupture de la pièce. Si deux métaux différents sont en contact et en présence d'eau alors l'un des matériaux agira comme une anode et l'autre comme une cathode. L'anode sera progressivement dégradée et un dépôt pourra être visible sur la cathode, il s'agit d'une corrosion galvanique. Ces attaques peuvent par exemple se produire au niveau des joints de grains de matériau métallique, produisant ainsi une attaque par corrosion invisible à la surface du matériau. Un cas de corrosion peut également être observés dans des assemblages, une infiltration d'eau aboutit à une corrosion caverneuse. Des solutions existent pour prévenir ces dégradations comme l'utilisation de matériaux peu réactifs (aciers inoxydables, aluminium) ou bien l'utilisation de traitements de surface comme la galvanisation qui permettent de retarder ou ralentir la propagation de la corrosion. Ces solutions ne sont pas entièrement fiables et des attaques peuvent quand même se produire suivant l'environnement auquel sera exposé la pièce et des efforts auquel elle sera soumise.

Le contrôle non destructif ou CND regroupe un ensemble de techniques visant à évaluer les capacités d'une pièce à remplir sa fonction sans la détériorer. Une multitude de principes physiques sont utilisés dans ce but allant de la simple inspection visuelle, comme le ressuage et la magnétoscopie, à des procédés plus complexes comme de la radiographie, des inspections par courants de Foucault ou bien un contrôle par ondes ultrasonores (Krautkrämer & Krautkrämer, 1990; García-Martín, Gómez-Gil & Vázquez-Sánchez, 2011; Lopez *et al.*, 2018). Le choix de la technique optimale dépend de nombreux paramètres. La considération du matériau inspecté est primordiale : un matériau non conducteur (ex : une céramique) ne pourra être inspecté par

courants de Foucault, un matériau trop dense (ex : du tungstène) atténuera très fortement des rayons X et les composites sont réputés pour être des matériaux fortement atténuants pour les ondes ultrasonores. La position et la nature des défauts influent également ce choix. Des défauts non débouchants ne seront pas détectés par ressuage et certaines inclusions métalliques, suivant leur nature, sont complexes à observer par courants de Foucault ou magnétoscopie. Finalement même si une technique est utilisable l'accessibilité des régions à inspecter est souvent un critère déterminant. Si un désassemblage, ou un arrêt de fonctionnement est nécessaire alors cela peut entraîner une perte importante de temps et donc d'argent.

La corrosion est un phénomène très surveillé dans le CND. Dans un cas simple de mesure d'épaisseur d'une surface corrodée sans obstacle alors une sonde ultrasonore mono-élément et une mesure de temps de vol en pulse-écho permet d'obtenir rapidement une valeur précise de l'épaisseur. Mais lorsque l'on considère des pièces comme des tuyaux ou des pipelines alors des régions sont inaccessibles du fait des supports, des couches d'isolant ou bien d'un enterrement partiel. Dans ce cas l'utilisation d'ondes guidées est particulièrement intéressante du fait de leur capacité à se propager sur de longues distances. A basse fréquence les modes fondamentaux peuvent être utilisés pour scanner rapidement de longues sections de rails ou de tuyau et pour localiser des défauts (Alleyne, Lowe & Cawley, 1998; Alleyne, Pavlakovic, Lowe & Cawley, 2001; Cawley, Lowe, Alleyne, Pavlakovic & Wilcox, 2003). En augmentant la fréquence une multitude de modes peuvent se propager. Ces modes d'ordre élevé peuvent par exemple être utilisés pour estimer précisément l'épaisseur de guide d'onde avec des techniques comme la tomographie ultrasonore ou bien le filtrage structurel. La tomographie ultrasonore (Bélanger, Cawley & Simonetti, 2010; Huthwaite & Simonetti, 2013; Zimmermann, Huthwaite & Pavlakovic, 2021) permet de cartographier la vitesse d'une onde dans la région d'inspection. Ensuite les relations de dispersion reliant les vitesses de phases des modes à la fréquence et à l'épaisseur du guide d'onde sont utilisées pour obtenir une reconstruction de l'épaisseur. Deux inconvénients majeurs sont à noter pour cette option. Tout d'abord la technique

nécessite d'utiliser un grand nombre de sondes positionnées très précisément les unes par rapport aux autres. Ensuite les algorithmes utilisés pour traiter les données sont lourds tant en terme de temps d'exécution que de ressources nécessaires. La seconde méthode, le filtrage structurel (Bélanger, 2014; Thon & Bélanger, 2019; Thon, Painchaud-April, Le Duff & Bélanger, 2022; Suresh & Balasubramaniam, 2020), utilisent l'existence de fréquences de coupure pour les modes d'ondes guidées d'ordre élevé. En effet toutes les ondes guidées peuvent être séparées en deux catégories : (1) les modes fondamentaux capables de se propager quelque soit la fréquence et l'épaisseur du guide d'onde et (2) les modes d'ordre élevé contraints à ne se propager que lorsque le produit de la fréquence et de l'épaisseur est au-dessus d'une valeur seuil appelée valeur de coupure. Si l'on considère une pièce comportant une zone corrodée, assimilable à une perte d'épaisseur, alors le produit fréquence-épaisseur subira un décalage et si la sévérité de la corrosion est suffisante alors ce mode sera coupé et ne pourra plus se propager. Les modes affectés sont alors soit convertis vers des modes capables de se propager soit réfléchis (Nurmalia, Nakamura, Ogi, Hirao & Nakahata, 2012; Nakamura, Ogi & Hirao, 2013).

Les ondes guidées les plus utilisées : les ondes de Lamb et les ondes de cisaillement horizontale, ou ondes SH. Ces dernières sont en général préférées du fait de la simplicité lors de l'interprétation des courbes de dispersion mais aussi de leur faible sensibilité au chargement de surface dû à l'absence de déplacement hors plan. Ce dernier point est particulièrement important lorsque l'on souhaite réaliser une inspection sur un tuyau sans arrêter son fonctionnement ou sans avoir à le démonter de ses supports. La principale difficulté réside alors dans le mécanisme de transduction de l'onde SH. Les sondes piézoélectriques nécessitent l'utilisation de couplant visqueux pour être capables de transmettre une contrainte de cisaillement du cristal à la pièce à inspecter. Cette couche de couplant a tendance à se dégrader au moindre mouvement de la sonde. Les sondes électromagnétiques acoustiques ou EMAT , sont des transducteurs utilisant principalement des forces de Lorentz ou des forces magnétostrictives. Ces efforts sont générés directement dans la pièce inspectée ce qui donne aux EMAT leur caractère sans contact. Dans la plupart des

cas d'inspection par ondes guidées SH des EMAT à aimants périodiques et permanents, ou PPM EMAT, sont utilisés, permettant la génération et la détection d'une onde guidée SH avec une sonde mono-élément. Mais les travaux présents dans la littérature approximent souvent les tuyaux par des plaques en aluminium ignorant ainsi la courbure et le caractère ferromagnétique du tuyau souvent en acier. De plus cette structure de sonde est limitante car elle exclut en émission des techniques d'excitation comme les excitations en vitesse de phase et en réception des algorithmes de traitement de données comme les transformées de Fourier à deux dimensions.

Les travaux menés au cours de cette thèse ont visé à répondre à ces problèmes. Le premier chapitre présentera les connaissances en ondes guidées et en mécanismes de transduction nécessaires à la compréhension de ce projet. Le second chapitre est un article publié dans le journal NDT & E Internationnal présentant une étude sur l'optimisation d'un PPM EMAT pour reconstruire le profil d'épaisseur d'un défaut usiné sur un tuyau en acier. Le troisième chapitre est un article publié dans le journal NDT & E Internationnal détaillant une nouvelle structure d'EMAT multi-élément permettant la génération et la réception d'onde SH sur des tuyaux en acier avec des performances similaires à celle d'un transducteur piézoélectrique en cisaillement. Le dernier article propose une application de cette sonde pour une inspection par filtrage structurel en utilisant l'onde réfléchie permettant ainsi une mesure de l'épaisseur et un positionnement du défaut. Cette thèse se clôture par une conclusion et des recommandations.

CHAPITRE 1

REVUE DE LITTÉRATURE

1.1   Les ondes ultrasonores

Les ondes ultrasonores sont des perturbations mécaniques se propageant dans un matériau à des fréquences supérieures à 20 kHz, soit au-delà du spectre audible par l'humain. Leur utilisation dans le domaine du contrôle non destructif a commencé vers la fin du 20e siècle et leur comportement est largement détaillé dans des ouvrages de références comme (Cheeke, 2012; Gazanhes & Jessel, 1976; Shull, 2016).

1.1.1   Les ondes de volumes

Les ondes de volumes peuvent être observés dans le cas de la propagation d'une perturbation mécanique dans un milieu en théorie infini ou semi-infini. En pratique on considère un milieu comme infini quand ses dimensions sont grandes comparées à la longueur d'onde. Dans un milieu à trois dimensions, trois sous-catégories d'ondes de volume peuvent se propager. Premièrement les ondes longitudinales, souvent appelées ondes de pression, (P) ont un déplacement de particules et une direction de propagation colinéaires. Les ondes de cisaillements ont un déplacement de particules perpendiculaire à la direction de propagation, deux composantes peuvent être dissociées : la composante verticale (SV) et la composante horizontale (SH). Les déformées dues à la propagation de ces ondes sont présentés sur la figure 1.1. Pour l'intégralité de cette thèse l'hypothèse d'un milieu homogène et isotrope est faite.

1.1.1.1   Les équations de propagation

Dans un cas unidimensionnel les équations de propagation ont été formulé au 18e siècle par d'Alembert :

$$\frac{\partial^2 u}{\partial t^2} = V^2 \frac{\partial^2 u}{\partial x^2} \qquad (1.1)$$
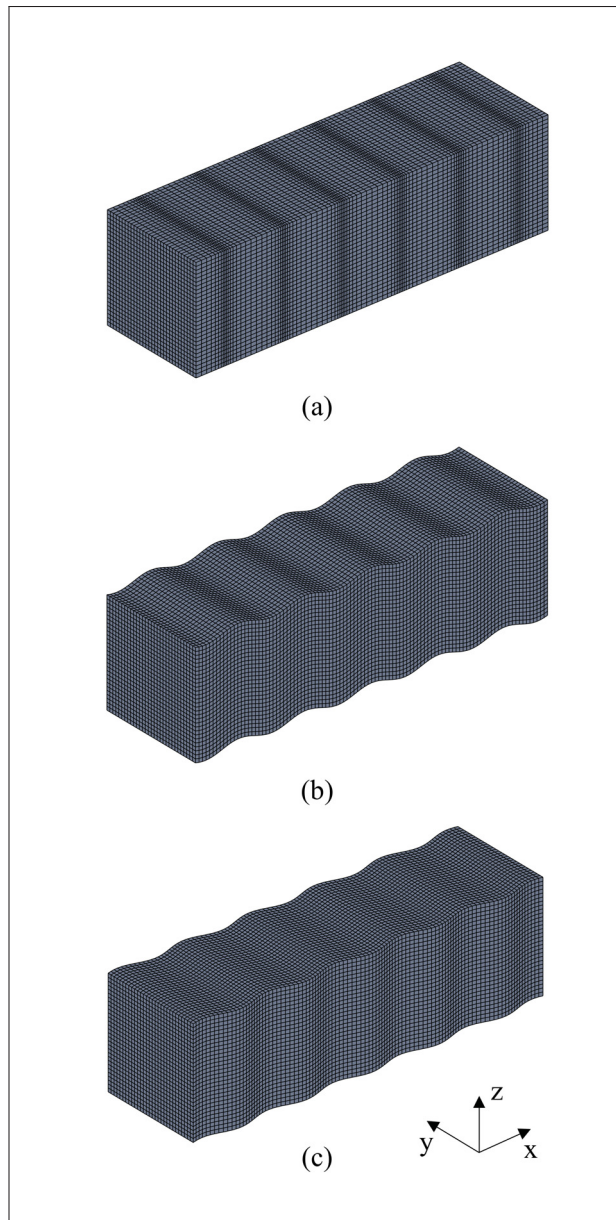
Figure 1.1   Déformées de milieu homogène et isotrope dues à la propagation d'onde : (a)
longitudinale (L), (b) de cisaillement verticale (SV) et de cisaillement horizontale (SH)

Où u est de déplacement, V est la vitesse de l'onde, x est la position selon l'axe x et t est le
temps. Il est possible de décomposer la solution $u(x, t)$ en deux termes, f lié à la propagation
selon $\vec{x}$ et g selon $-\vec{x}$ (Voir figure 1.1 pour le système d'axes) soit :

$$u(x,t) = f(x - Vt) + g(x + Vt) \tag{1.2}$$

Si on fait l'hypothèse d'une onde sinusoïdale alors on peut écrire :

$$u(x,t) = A\cos(\omega t - kx) \tag{1.3}$$

Avec A l'amplitude, $\omega = \frac{2\pi}{T}$ la pulsation de l'onde et T sa période, et $k = \frac{\omega}{T} = \frac{2\pi}{\lambda_x}$ le nombre d'onde et λ_x la longueur d'onde.

Dans le cas plus complexe d'une propagation dans une milieu tri-dimensionnel alors l'équation du mouvement dans un milieu isotrope et homogène peut être obtenue grâce à l'équation de Navier sans force de volume :

$$\rho\frac{\partial^2\overrightarrow{u}}{\partial t^2} = (\lambda + \mu)\vec{\nabla}(\vec{\nabla} \cdot \overrightarrow{u}) + \mu\nabla^2\overrightarrow{u} \tag{1.4}$$

Avec ρ la densité du milieu, λ et μ les coefficients de Lamé décrivant le milieu de propagation. En effectuant une décomposition de Helmholtz on peut séparer $\vec{u}$ comme la somme gradient du champ scalaire ϕ et du rotationnel d'un champ vectoriel Φ :

$$\overrightarrow{u} = \vec{\nabla}\phi + \vec{\nabla} \times \Phi = \overrightarrow{u_L} + \overrightarrow{u_S} \tag{1.5}$$

Avec $\overrightarrow{u_L}$ et $\overrightarrow{u_S}$ respectivement un champ de déplacement avec un rotationnel nul et un champ de déplacement avec une divergence nulle. En combinant l'équation 1.4 et l'équation 1.5 on peut démontrer qu'une onde de volume peut être décomposée en une composante longitudinale et une composante de cisaillement :

$$\frac{\partial^2 \phi}{\partial t^2} = V_L^2 \nabla^2 \phi \tag{1.6}$$

$$\frac{\partial^2 \Phi}{\partial t^2} = V_S^2 \nabla^2 \Phi \tag{1.7}$$

Où V_L est la vitesse longitudinale et V_S la vitesse en cisaillement.

$$V_L = \sqrt{\frac{\lambda + 2\mu}{\rho}} \tag{1.8}$$

$$V_S = \sqrt{\frac{\mu}{\rho}} \tag{1.9}$$

Deux ondes peuvent donc se propager dans un matériau isotrope et homogène : une onde de cisaillement et une onde longitudinale.

1.1.1.2 L'atténuation

L'atténuation d'une onde désigne la perte d'amplitude qu'elle subit au cours de sa propagation. Ce phénomène est souvent modélisé par une décroissance exponentielle (Cheeke, 2012) :

$$I(x) = I_0 e^{-2\alpha x} \tag{1.10}$$

Où $I(x)$ est l'intensité de l'onde à une position x, I_0 est son intensité initiale et α est le coefficient d'atténuation. Ce coefficient dépend de plusieurs facteurs comme la diffusion, la diffraction ou bien l'absorption contribuant tous à la perte d'intensité de l'onde. Divers paramètres comme les propriétés et la géométrie du matériau inspecté ou la fréquence de l'onde ont donc une influence

sur l'atténuation. Une règle générale est que ce coefficient augmente avec la fréquence. La prise en compte de l'atténuation est donc un point crucial lors de l'inspection par onde ultrasonore vu que celle-ci peut fortement réduire la distance maximale d'inspection.

1.1.2   Les ondes guidées

Dans la partie précédente deux hypothèses ont été effectuées : celle d'un matériau homogène et isotrope et celle d'un milieu infini ou semi-infini. Lorsque la structure inspectée est d'épaisseur finie comme une plaque ou un tuyau par exemple alors des ondes guidées peuvent se former. Celles-ci sont dues aux réflexions successives des ondes de volume longitudinales et de cisaillement sur les parois du guide d'onde. Deux catégories d'ondes peuvent être distinguées : les ondes de cisaillement horizontales et les ondes de Lamb.

1.1.2.1   Les ondes de cisaillement horizontales

Considérons une plaque d'épaisseur b dans laquelle se propage une onde SH selon la direction $\vec{x}$ et avec un déplacement des particules selon $\vec{z}$, tel que décrit sur la figure 1.2. Une méthode simple et efficace pour obtenir les équations de propagation pour les ondes SH a été développé par (Cheeke, 2012).
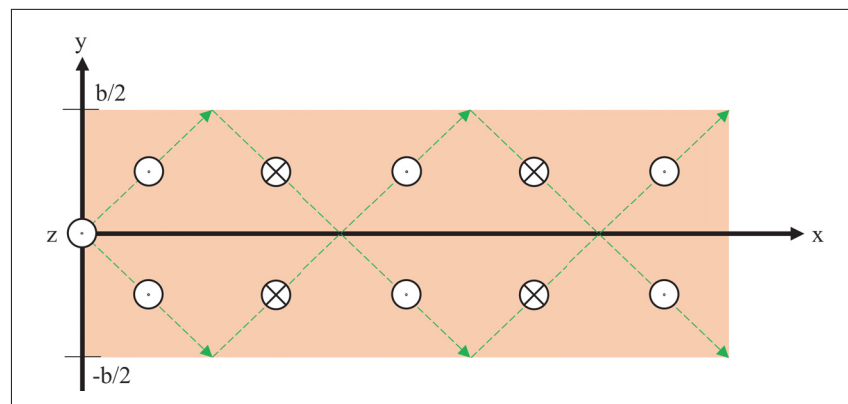
Figure 1.2   Propagation d'une onde guidée SH dans une plaque d'épaisseur b selon la direction $\vec{x}$ grâce aux réflexions successives des ondes de volume SH sur les parois de la plaque

Si on décompose le nombre d'onde de l'onde SH (figure 1.3), alors on peut écrire :

$$k_s^2 = k_x^2 + k_y^2 + k_z^2 = \frac{\omega^2}{V_S^2} \tag{1.11}$$

Où ω est la pulsation. Selon la direction $\vec{y}$, en utilisant les conditions aux frontières du guide d'onde on peut montrer que k_y doit être un multiple de $\frac{\pi}{b}$. Montrant ainsi qu'une infinité de modes d'ondes guidées SH peuvent se propager.

$$k_y = \frac{n\pi}{b}, n \in \mathbb{N} \tag{1.12}$$

Sachant que l'onde SH se propage dans le plan $(\vec{x},\vec{y})$ alors on peut en déduire que k_z est nul, $k_z = 0$.

En injectant les équations 1.12 et 1.13 dans 1.11 on obtient alors :

$$k_{SH,n}^2 = k_x^2 = \left(\frac{\omega}{V_S}\right)^2 - \left(\frac{n\pi}{b}\right)^2, n \in \mathbb{N} \tag{1.13}$$

De plus la définition du nombre d'onde nous donne :

$$k_{SH,n} = \frac{\omega}{V_p}, n \in \mathbb{N} \tag{1.14}$$

Avec V_p la vitesse de phase. En combinant les deux dernières équations il est alors possible de calculer la vitesse de phase de tous les modes SH :

$$V_p = V_S \left(\frac{2fb}{\sqrt{4(fb)^2 - n^2 V_S^2}} \right), n \in \mathbb{N} \tag{1.15}$$

Où b est l'épaisseur du guide d'onde. La seconde vitesse caractéristique d'une onde guidée, la vitesse de groupe V_g, est définie par :

$$V_g = \frac{\partial \omega}{\partial k} \tag{1.16}$$

$$V_g = V_S \sqrt{1 - \frac{(n/2)^2}{(fb/V_S)^2}}, n \in \mathbb{N} \tag{1.17}$$

Les équations 1.16 et 1.18, permettent de tracer les courbes de dispersion pour les modes SH. Ces courbes représentent l'évolution des vitesses de phases et de groupe des modes SH en fonction de la fréquence f et de l'épaisseur b. Ces deux variables sont parfois représentées sur un même axe sous la forme d'un produit fréquence-épaisseur fb. La figure 1.3 montre les courbes de dispersions pour une onde guidée SH sur une plaque d'acier ($\rho = 8000$ kg/m^3, E = 210 GPa, $\nu = 0.30$).

La première observation que l'on peut faire sur ces courbes est la présence d'un mode fondamental SH$_0$ capable de se propager quelque soit la valeur du produit fréquence-épaisseur. Pour ce mode fondamental les vitesses de groupe et de phase sont égales à la vitesse d'une onde de volume en cisaillement V_S. Ce mode est dit non dispersif, ce qui est confirmé par les équations 1.15 et 1.17 si on les applique pour $n = 0$. Pour les modes d'ordre élevé, $n \geqslant 1$, on observe la présence d'asymptotes verticales pour chacun des modes où la vitesse de phase tend vers l'infini et où la vitesse de groupe tend vers 0. Selon les équations 1.15 et 1.17, lorsque l'on a $n \geqslant 1$, alors ces asymptotes sont positionnées à des produits fréquence-épaisseur fb égaux à :

$$fb = \frac{nV_s}{2}, n \in \mathbb{N} \tag{1.18}$$

Lorsque cette position est atteinte le mode n'est alors plus capable de se propager et il est alors réfléchi ou converti dans un mode capable de se propager (Nurmalia *et al.*, 2012; Nakamura
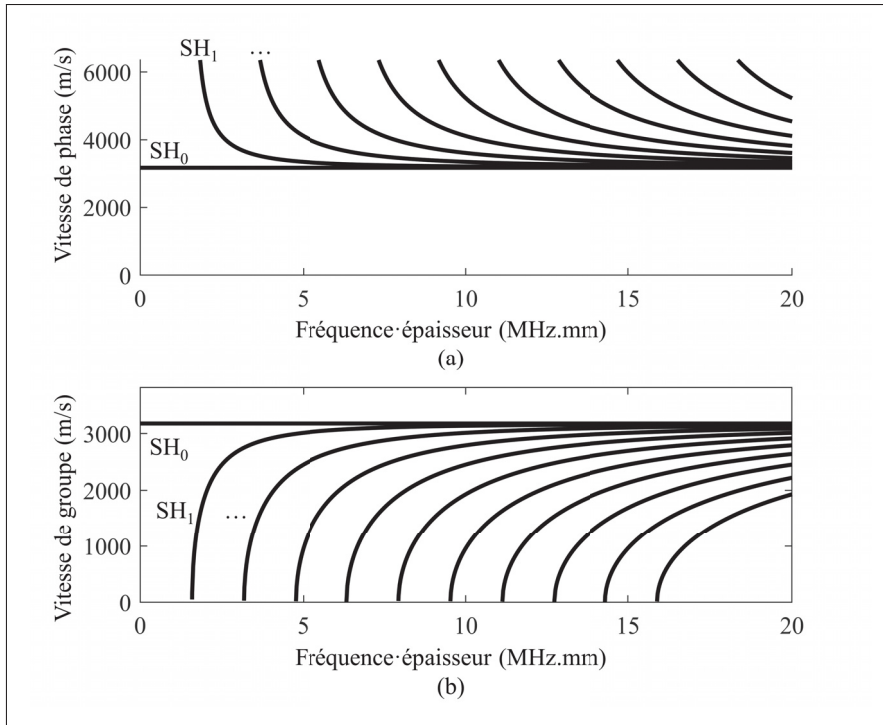
Figure 1.3   Courbe de dispersions en vitesses de phase et de groupe pour les modes d'onde
guidée SH sur une plaque d'acier ($\rho = 8000 \, \text{kg/m}^3$, E = 210 GPa, $\nu = 0.30$)

et al., 2013). La détection de cette coupure permet donc une estimation de l'épaisseur minimale
du guide d'onde. Cette technique est souvent appelée filtrage structurel.

1.1.2.2   Les ondes de Lamb

Lorsque des ondes de volume P et S, polarisé dans la direction verticale ou SV, sont contraintes
de se propager dans un guide d'onde alors leurs réflexions successives produisent des ondes
de Lamb. Ces deux modes de propagation sont couplés dans le sens où les réflexions sur les
parois entraînent des conversions entres ces modes du fait de la loi de Snell. Dans notre cas on
considérera que le guide d'onde est une plaque d'épaisseur b et que aucune transmission ne
s'effectue dans l'air. On a donc pour l'onde réfléchie à l'intérieur de la plaque :

$$\frac{\sin \theta_i}{V_i} = \frac{\sin \theta_{rL}}{V_L} = \frac{\sin \theta_{rS}}{V_S} \tag{1.19}$$

Avec θ_i et V_i respectivement l'angle et la vitesse de l'onde de volume incidente (P ou SV), θ_{rL} et V_L l'angle et la vitesse de l'onde de volume P réfléchie et θ_{rS} et V_S l'angle et la vitesse de l'onde de volume SV réfléchie. La figure 1.4 illustre ce phénomène de conversion de mode dans le cas où l'onde incidente est une onde P.
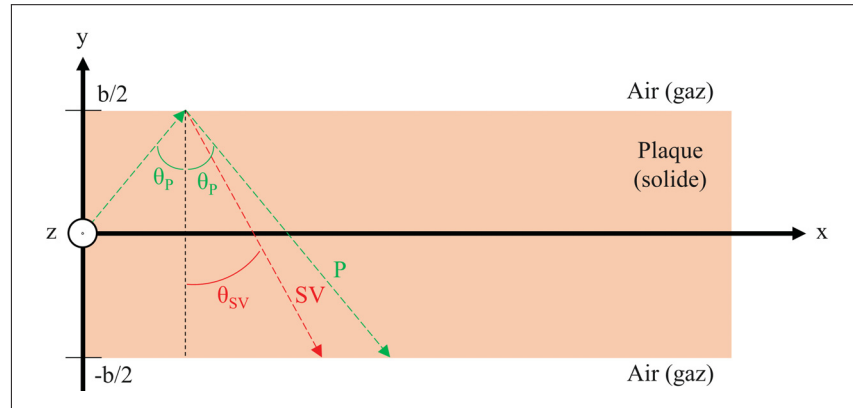
Figure 1.4   Propagation d'une onde de Lamb dans une plaque d'épaisseur b selon la direction $\vec{x}$ grâce aux réflexions successives des ondes de volume P (vert) et SV (rouge)

Le couplage de ces deux ondes lors de la propagation implique qu'il faut considérer la composante de cisaillement mais aussi la composante longitudinale lors de la décomposition en nombre d'onde. On obtient alors :

$$k_s^2 = k_{sx}^2 + k_{sy}^2 + k_{sz}^2 = \frac{\omega^2}{V_S^2} \tag{1.20}$$

Et

$$k_l^2 = k_{lx}^2 + k_{ly}^2 + k_{lz}^2 = \frac{\omega^2}{V_l^2} \tag{1.21}$$

Comme pour les ondes SH aucune propagation ne s'effectue selon la direction $\vec{z}$, $k_{sz} = k_{lz} = 0$. De plus d'après la figure 1.4 illustrant les premières réflexions des ondes SV et P aboutissant à

une onde de Lamb on en déduit que les nombres d'ondes partiels selon la direction de propagation sont égaux, soit $k_{sx} = k_{lx} = k_x$.

$$k_{sy}^2 = \frac{\omega^2}{V_S^2} - k_x^2 \tag{1.22}$$

$$k_{ly}^2 = \frac{\omega^2}{V_l^2} - k_x^2 \tag{1.23}$$

Les équations de Rayleigh-Lamb (Lamb, 1917) permettent d'obtenir des relations permettant de décrire les modes de Lamb symétrique :

$$\frac{\tan\left(k_{sy}\frac{b}{2}\right)}{\tan\left(k_{ly}\frac{b}{2}\right)} = -\frac{4k_x^2 k_{ly} k_{sy}}{\left(k_{sy}^2 - k_x^2\right)^2} \tag{1.24}$$

Et antisymétrique :

$$\frac{\tan\left(k_{sy}\frac{b}{2}\right)}{\tan\left(k_{ly}\frac{b}{2}\right)} = -\frac{\left(k_{sy}^2 - k_x^2\right)^2}{4k_x^2 k_{ly} k_{sy}} \tag{1.25}$$

Les relations de dispersions peuvent alors être obtenues en injectant les équations 1.22 et 1.23 dans l'équation 1.24 pour les modes symétriques, ou modes S, et dans l'équation 1.25 pour les modes anti-symétriques, ou modes A. Le problème est que ces équations sont transcendantales et doivent être résolues de manière numérique avec des logiciels comme DISPERSE (Pavlakovic, Lowe, Alleyne & Cawley, 1997) ou CIVA, un logiciel de simulation. La figure 1.5 montre les courbes de dispersions pour les ondes de Lamb dans une plaque d'acier ($\rho = 8000$ kg/m^3, E = 210 GPa, $\nu = 0.30$) en fonction du produit fréquence-épaisseur.
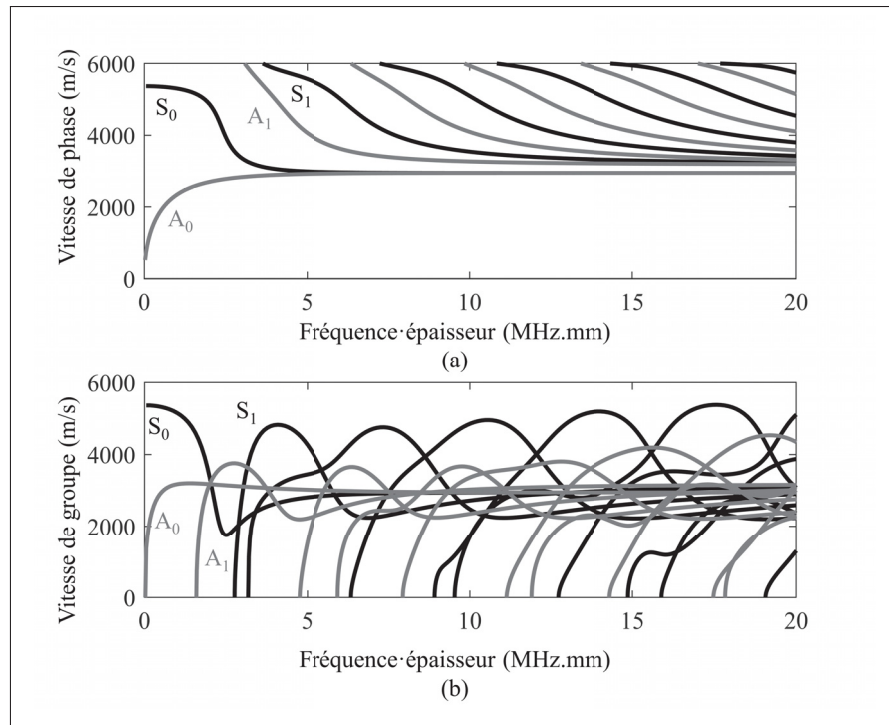
Figure 1.5   Courbes de dispersion en vitesses de phase et de groupe pour les modes
d'ondes guidées de Lamb symétriques S (noir) et anti-symétriques (gris) sur une plaque
d'acier ($\rho = 8000$ kg/m^3, E = 210 GPa, $\nu = 0.30$)

1.1.2.3   Pourquoi utiliser les ondes SH ?

Dans le domaine du contrôle non destructif par ondes guidées ultrasonores les ondes SH sont très souvent préférées aux ondes de Lamb (Bélanger, 2014; Koodalil, Rajagopal & Balasubramaniam, 2021a; Sun *et al.*, 2021b; Thon & Bélanger, 2019; Zimmermann *et al.*, 2021). Ce choix est fait pour plusieurs raisons :

1. La répartition régulière des modes SH d'ordre élevé dans le domaine fréquentiel permet une estimation de l'épaisseur minimale du guide d'onde sur une base plus régulière qu'avec des ondes de Lamb.

2. L'absence d'intersection dans les courbes de dispersions des modes SH permet une identification plus facile des modes se propageant.

3. Contrairement aux ondes de Lamb, les modes SH sont caractérisés par une absence de déplacement hors plan, rendant ces ondes très peu sensibles aux chargements de surfaces fluides non visqueux. En théorie cette caractéristique permet une inspection d'un pipeline pendant son fonctionnement.

4. Lorsqu'une onde SH interagit avec un défaut parallèle à la direction du déplacement des particules alors aucune conversion vers un autre type d'onde guidée ne se produira (Graff, 1991; Krautkrämer & Krautkrämer, 1990; Petcher, Burrows & Dixon, 2014).

1.1.2.4 L'approximation d'un tuyau par une plaque

Figure 1.6   Photo du tuyau utilisé lors de cette thèse avec une épaisseur de 10.2 mm et un diamètre extérieur de 323.8 mm

La principale hypothèse dans la partie précédente est que le guide d'onde est une plaque. Dans le cas où la structure inspectée est un tuyau, comme c'est le cas dans ce projet, d'autres modes peuvent se propager comme des modes de flexions (axisymétriques et non-axisymétriques) et de torsion (axisymétriques et non-axisymétriques). Des études, (Luo, Zhao & Rose, 2005; Velichko & Wilcox, 2009), ont démontré que l'assimilation d'un tuyau par une plaque de même épaisseur est une hypothèse valable lorsque le ratio entre l'épaisseur du tuyau et son diamètre extérieur est inférieur à 5-10%. Si l'on considère le tuyau inspecté lors de ce doctorat (figure 1.6) avec une épaisseur de 10.2 mm et un diamètre extérieur de 323.8 mm alors ce ratio est de 3.1%. Une seconde vérification de la validité de cette hypothèse peut être faite à l'aide du logiciel DISPERSE. La figure 1.7 présente les courbes de dispersions pour les modes SH dans le tuyau inspecté et une plaque d'acier de même épaisseur, soit 10.2 mm. Comme on peut le voir la différence entre ces deux courbes est minime et celles-ci se superposent bien. Pour la suite lorsque les équations analytiques seront nécessaires, les équations décrites dans la section 1.1.2.1 seront considérées comme valables dans le cas du tuyau inspecté.
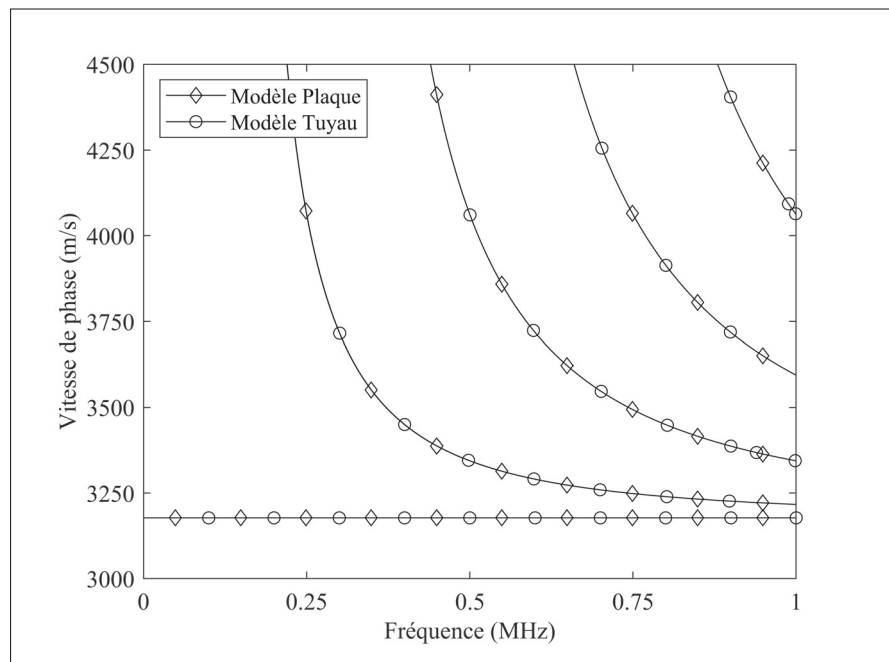
Figure 1.7   Comparaison entre les courbes de dispersions des modes SH dans une plaque d'acier de 10.2 mm d'épaisseur et dans un tuyau ayant une épaisseur nominale de 10.2 mm et un diamètre extérieur de 323.8 mm

1.2 Les mécanismes de transduction

1.2.1 Les transducteurs

1.2.1.1 Les transducteurs piézoélectriques

L'effet piézoélectrique désigne la capacité de certains matériaux à générer sous l'effet d'une différence de potentiel électrique une déformation mécanique et inversement. Cet effet est la base de la technologie des sondes les plus utilisées dans le domaine du contrôle non destructif ultrasonore : les sondes piézoélectriques (figure 1.8). Les sondes piézoélectriques sont en général composées de divers éléments. :

1. Le cristal piézoélectrique permet la conversion entre l'énergie électrique et l'énergie mécanique. Le matériau le plus utilisé dans l'industrie est le titano-zirconate de plomb ou PZT. La polarisation du cristal se fait en le soumettant à un champ électrique puissant. La direction de ce champ induira le type d'onde généré.

2. La couche absorbante, à l'intérieur du boîtier de la sonde permet d'atténuer l'onde qui se propage à l'intérieur de la sonde afin que le signal reçu soit majoritairement dû à l'onde se propageant dans la pièce inspectée.

3. La couche d'adaptation a une impédance acoustique $Z = \rho * V$ comprise entre celle du cristal piézoélectrique et celle du matériau inspecté. Son rôle est de faciliter le transfert d'énergie mécanique entre le cristal et la pièce.

4. Les électrodes sont fixées sur le cristal piézoélectrique pour permettre le câblage de la sonde.

5. La couche de couplant n'est pas incluse physiquement dans la sonde mais elle est nécessaire pour garantir un couplage efficace et constant entre la surface inférieure de la sonde et la pièce inspectée. Pour des ondes longitudinales ce couplant peut-être un gel ou bien simplement de l'eau. Dans le cas des ondes de cisaillement l'eau ou les gels couramment utilisées ne permettent pas un transfert de l'énergie et des couplants plus visqueux doivent être utilisés.
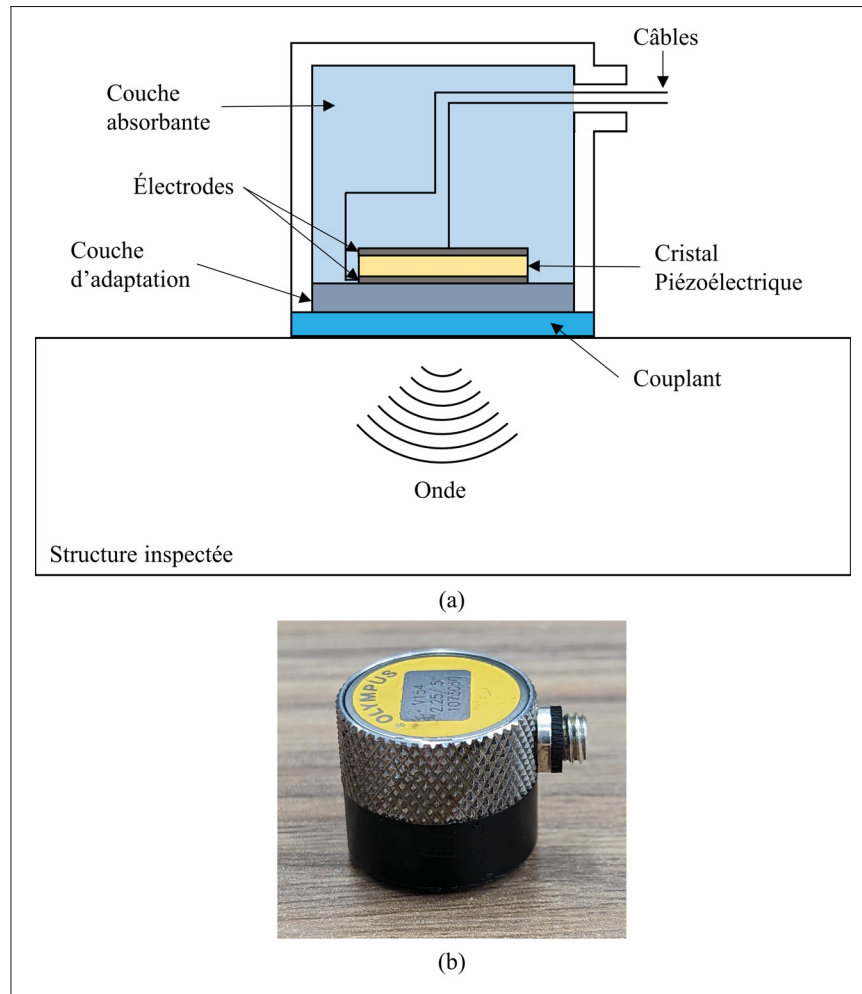
Figure 1.8   (a) Schéma de principe d'une sonde piézoélectrique et (b) Photo de la sonde mono-élément Olympus V154-RM

Les principales limitations de cette technologie sont : (1) les faibles performances lorsqu'elle est utilisée au-dessus d'un revêtement et (2) la température de Curie des éléments piézoélectriques. La température de Curie désigne le seuil à partir duquel le cristal perdra sa propriété piézoélectrique. Cette dégradation est progressive à partir d'une température plus faible souvent appelée température maximale de fonctionnement.

1.2.1.2 Les transducteurs électromagnétiques acoustiques

Les transducteurs électromagnétiques acoustiques, ou EMAT, sont des sondes utilisant majoritairement deux forces : les forces de Lorentz, dues à l'interaction entre un courant induit dans un matériau conducteur et un champ magnétique, et les forces magnétostrictives, dues à la capacité des matériaux ferromagnétiques à se déformer selon la direction d'un champ magnétique. On peut donc calculer les forces générées par un EMAT, F, de la manière suivante :

$$F = F_L + F_M \tag{1.26}$$

Avec F_L les forces de Lorentz, F_M les forces magnétostrictives. Un EMAT est composé, dans son état le plus basique, de deux éléments : une bobine et un aimant permanent. La bobine peut soit être faite à la main, permettant une grande liberté dans la forme de la bobine, mais également imprimée sur un PCB rigide ou flexible, permettant une grande répétabilité de fabrication et des bobines plus fines et denses. Les aimants les plus utilisés dans l'industrie sont composé de néodyme. Ces aimants sont, tous comme les éléments piézoélectriques, limités par leur température de Curie à partir de laquelle ils perdent leur aimantation permanente. Le principal avantage par rapport aux transducteurs piézoélectriques est que ces sondes sont considérées comme étant sans contact, du fait que la génération des forces se produit directement dans le matériau inspecté. Ce point est particulièrement intéressant dans le cas d'inspection au-dessus d'un revêtement ou dans le cas de la transduction d'une onde de cisaillement, l'utilisation d'un couplant visqueux n'étant plus nécessaire.

Des EMAT mono-éléments composés d'un aimant et d'une ou plusieurs bobines peuvent être utilisés dans des techniques d'inspection par onde de volume pour détecter des défauts comme des fissures (Parra-Raad, Khalili & Cegla, 2020). La version la plus utilisée lorsque l'on considère une inspection par onde guidée sont les EMAT à aimants permanents et périodiques ou PPM EMAT. Ces EMATs sont composés d'une bobine plane et allongée et d'un jeu d'aimants dont la direction de polarisation varie périodiquement avec une période égale à la longueur

d'onde excitée (Vasile & Thompson, 1979; Ribichini, 2011). Ce type d'EMAT et ses variants ont été utilisés à de nombreuses reprises pour l'inspection de plaque et/ou de tuyau corrodé (Bélanger, 2014; Suresh & Balasubramaniam, 2020; Thon & Bélanger, 2019). Des structures plus complexes d'EMAT multi-éléments ont été développées pour permettre de l'imagerie par onde ultrasonore (Isla & Cegla, 2017; Pucci, Raillon, Taupin & Baqué, 2019).

Toutes les configurations citées précédemment lorsqu'elles sont utilisées sur un matériau ferromagnétique et conducteur comme de l'acier sont susceptibles de générer des forces de Lorentz et des forces magnétostrictives. Il a été montré que le principal effet de la superposition de ces deux forces est une réduction de l'amplitude de l'onde SH générée de environ 30% par rapport à un modèle ne considérant que les forces de Lorentz, mais aucun effet ne se produit sur les fréquences et nombres d'onde excités (Sun, Sinclair & Filleter, 2021a). Les forces générées par un EMAT seront donc approximées par les forces de Lorentz soit :

$$F \approx F_L = J_e \times B \tag{1.27}$$

Avec J_e les courants induits par la sonde dans le matériau, et B le champ magnétique généré par le ou les aimants. Cette hypothèse est souvent faite dans la littérature (Isla & Cegla, 2016, 2017; Ribichini, Cegla, Nagy & Cawley, 2012a; Ribichini, Nagy & Ogi, 2012b).

1.2.1.3   Les lasers

Pour la génération d'une onde ultrasonore par laser deux méthodes existent : la méthode par ablation et celle par effet thermoélastique. Dans le premier cas un faisceau laser de forte puissance est concentré sur une zone. Ceci entraîne une attaque par vaporisation du matériau inspecté et la force de réaction permet de générer une onde ultrasonore. La méthode thermoélastique utilise un laser de plus faible puissance pour chauffer localement la surface d'une pièce. Le gradient de température crée alors un champ de contrainte permettant la transduction d'une
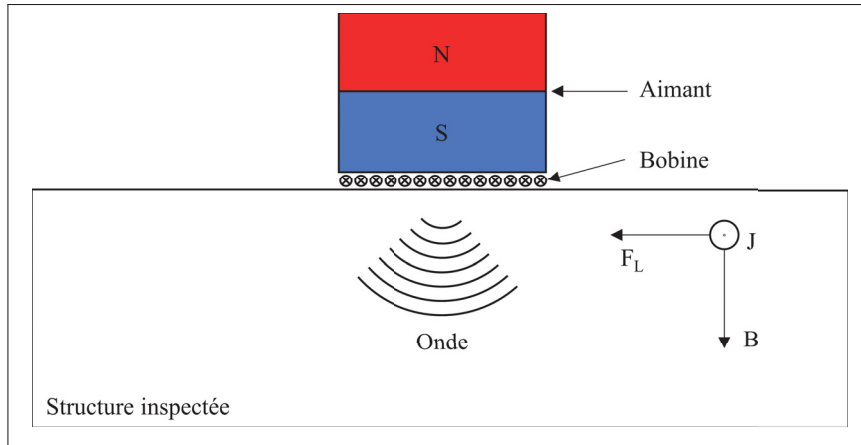
Figure 1.9   Schéma de principe d'un EMAT basé sur les forces de Lorentz

onde. Ces deux méthodes n'ont pas été retenues pour la suite du fait du prix des équipements et de leur encombrement important rendant complexe voire impossible une mesure sur un site d'exploitation.

En réception la mesure à l'aide de vibromètres lasers repose sur deux principes physiques : l'effet Doppler et l'interférométrie. L'effet Doppler est expérimenté dans la vie de tous les jours avec comme cas le plus connu le changement de tonalité d'un véhicule en fonction de son mouvement. Une onde lorsque sa source se déplace subit un décalage dans le domaine fréquentiel qui est appelé décalage Doppler, f_D :

$$f_D = \frac{2V}{\lambda} \tag{1.28}$$

Avec V la vitesse de l'onde et λ se longueur d'onde. Le second phénomène utilisé est l'interférométrie ou l'étude des interférences dues à la superposition dans une onde de deux faisceaux cohérents. Si l'on appelle I_1 et I_2 l'intensité de ces deux faisceaux alors l'intensité totale de l'onde I est :

$$I = I_1 + I_2 + 2\sqrt{I_1 I_2} \cos\left(\frac{2\pi (d_1 - d_2)}{\lambda}\right) \tag{1.29}$$

Avec d_1 la distance parcourue par le faisceau 1 et d_2 celle parcourue par le faisceau 2. Il est donc possible à l'aide de ces deux phénomènes d'obtenir à distance le déplacement et la vitesse d'une onde. Même si l'encombrement est important cette technologie reste intéressante en laboratoire pour permettre des mesures indépendantes de l'impédance, contrairement à des acquisitions faites avec des sondes tels que des EMAT ou des transducteurs piézoélectriques.

1.2.2   Les techniques d'excitation

La technique la plus basique d'excitation est d'utiliser un transducteur mono-élément. Dans ce cas le seul contrôle que l'on a est le signal utilisé et l'amplitude des modes excités ne dépendra que du spectre fréquentiel du signal et de l'excitabilité des différents modes. Cette sonde peut également être associée avec un sabot permettant de concentrer l'énergie des modes excités autour d'une vitesse de phase dépendant de l'angle du sabot. Le problème est que cette vitesse de phase ne peut être modifiée sans changer le sabot utilisé.

1.2.2.1   Les excitations en peigne
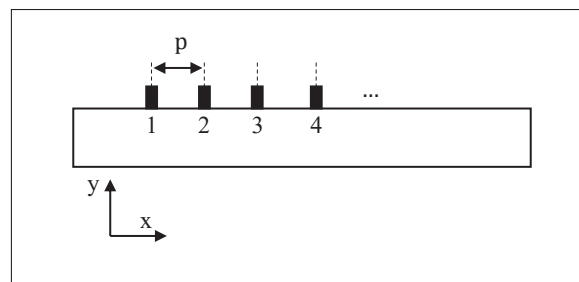
Figure 1.10   Schéma d'une sonde multi-élément. Les numéros représentent la position de l'élément dans le transducteur, et p le pas de la sonde

Une excitation en peigne est obtenue lorsque tous les éléments d'un transducteur multi-éléments sont activés en même temps par le même signal. Ceci permet de concentrer les modes excités autour d'une longueur d'onde égale au pas de la sonde, ou distance entre deux éléments. Joseph L. Rose (Rose, 2014) a montré que l'amplitude $A_n(\omega, x)$ d'un mode d'ordre n peut être exprimée de la manière suivante :

$$A_n(\omega, x) = U \cdot F(\omega) \cdot C_n(x) \cdot H(\omega, x) \tag{1.30}$$

où U est le déplacement des particules, $F(\omega)$ la réponse fréquentielle des éléments, $C_n(x)$ un terme de couplage entre les efforts en surface du guide d'onde et les modes d'onde guidée excités et :

$$H(\omega, x) = \sum_{i=1}^{N} e^{j[\omega t \pm k_x \cdot (x - x_i))]} = \frac{\sin(N\frac{k_x p}{2})}{\sin(\frac{k_x p}{2})} e^{j[\omega t \pm k_x \cdot (x - x_c))]} \tag{1.31}$$

avec $\pm$ négatif dans le cas où la propagation se fait selon $+\vec{x}$ et positif selon $-\vec{x}$ (Voir figure 1.10 pour les axes), p est le pas de la sonde, N le nombre d'éléments de la sonde, ω la pulsation, $k_x = \frac{\omega}{V_p}$ le nombre d'onde selon la direction $\vec{x}$ et x_c le centre de la sonde. $|H(\omega, x)|$ est maximale lorsque p est un multiple de la longueur d'onde $\lambda = \frac{2\pi}{k_x}$, montrant ainsi que les modes sont excités autour d'une longueur d'onde égale au pas de la sonde ou à un de ses multiples. Il est possible de prédire les modes excités lors d'une excitation en peigne en multipliant $|H(\omega, x)|$ par le spectre fréquentiel du signal utilisé. La figure 1.11 (a) montre les régions des courbes de dispersions excitées lors d'une excitation en peigne autour d'une longueur d'onde de 6.4 mm. La figure 1.11 (b) et la figure 1.11 (c) montrent la combinaison de cette excitation avec des signaux sinusoïdaux de 10 cycles centrés respectivement autour de 520 et 705 kHz et fenêtrés par une fonction de Hann.

1.2.2.2 Les excitations en vitesse de phase

Une évolution de cette méthode d'excitation a été proposée par divers chercheurs (Li & Rose, 2001; Zhu & Rose, 1999; Veit & Bélanger, 2020), en ajoutant une loi de retard lors de l'excitation
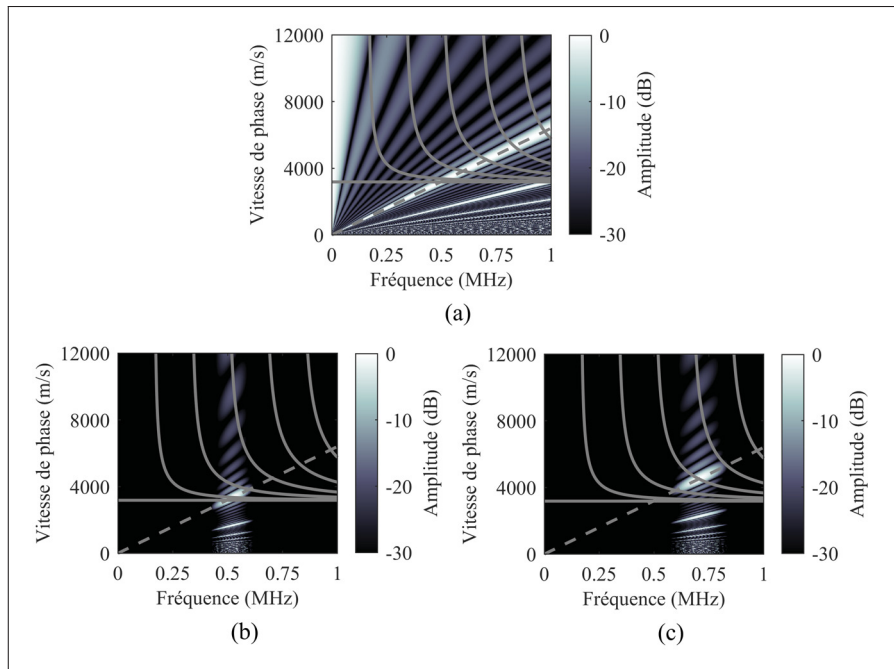
Figure 1.11   (a) Cartographie de l'énergie due à une excitation en peigne avec un transducteur de 20 éléments autour d'une longueur d'onde de 6.4 mm, Modes excités lorsque cette excitation est associée à un signal de 10 cycles centré sur une fréquence de 520 kHz (b) et 705 kHz (b) et fenêtré par une fonction de Hann. Dans ce cas le guide d'onde considéré est une plaque d'acier (ρ = 8000 kg/m^3, E = 210 GPa, ν = 0.30) de 9.53 mm d'épaisseur. Les courbes pleines en grises sont les courbes de dispersions des modes SH. La droite grise en pointillé correspond à la longueur d'onde de l'excitation

des différents éléments. Si l'on considère un incrément de temps t_0 pour la loi de retard alors l'équation 1.31 devient :

$$H(\omega, x) = \sum_{i=1}^{N} e^{j[w(t-t_i))\pm k(x-x_i))]} = \frac{\sin(N\pi(\frac{p}{\lambda} \pm \frac{t_0}{T}))}{\sin(\pi(\frac{p}{\lambda} \pm \frac{t_0}{T}))} e^{j\left[w(t-\frac{N-1}{2}t_0)\pm k(x-x_c)\right]} \quad (1.32)$$

où T est la période. De la même manière on remarque que $|H(\omega, x)|$ est maximal $\frac{p}{\lambda} \pm \frac{t_0}{T} = m$ avec $m \in \mathbb{N}$. Ici l'excitation dépend toujours du pas de la sonde mais également le l'incrément de temps utilisé, permettant ainsi de modifier les régions excitées sans changer de caractéristique physique du transducteur. Lorsque l'on considère la direction de propagation selon $+\vec{x}$ un cas

particulier se produit lorsque $m = 0$. L'équation 1.32 n'est pas définie pour $m = 0$ mais $|H(\omega, x)|$ étant continu au voisinage de $m = 0$ on peut alors en déduire que :

$$V_p = \frac{\lambda}{T} = \frac{p}{t_0} \tag{1.33}$$

Cette technique d'excitation permet donc une excitation des modes autour d'une vitesse de phase contrôlable. En associant le bon signal avec cette méthode d'excitation il est donc en théorie possible d'exciter n'importe quelle partie des courbes de dispersions. La figure 1.12 (a) montre les régions des courbes de dispersions excitées lors d'une excitation autour d'une vitesse de phase de 3600 m/s. La figure 1.12 (b) et la figure 1.12 (c) montrent la combinaison de cette excitation avec des signaux sinusoïdaux de 10 cycles centrés respectivement autour de 330 et 630 kHz et fenêtrés par une fonction de Hann.

1.3 L'estimation de l'épaisseur d'un guide d'onde

1.3.1 Le filtrage structurel

Le filtrage structurel est une technique utilisant le phénomène de coupure des modes d'ordre élevé en fonction du produit fréquence épaisseur (Bélanger, 2014; Thon & Bélanger, 2019; Suresh & Balasubramaniam, 2020). Comme démontré sur la figure 1.3 et la figure 1.5 les modes d'ordre élevé sont contraints de se propager au dessus d'un seuil fréquence épaisseur de coupure. Une réduction d'épaisseur décalera la valeur du produit fréquence épaisseur et les modes seront alors soit en partie ou soit totalement coupés. Les modes coupés pourront être réfléchis ou convertis vers d'autres modes capables de se propager (Nurmalia *et al.*, 2012; Nakamura *et al.*, 2013).

Deux options sont possibles lorsqu'on envisage une estimation d'épaisseur par filtrage structurel : 1) une mesure en transmission, ou 2) une mesure en réflexion. Dans le premier cas, deux sondes
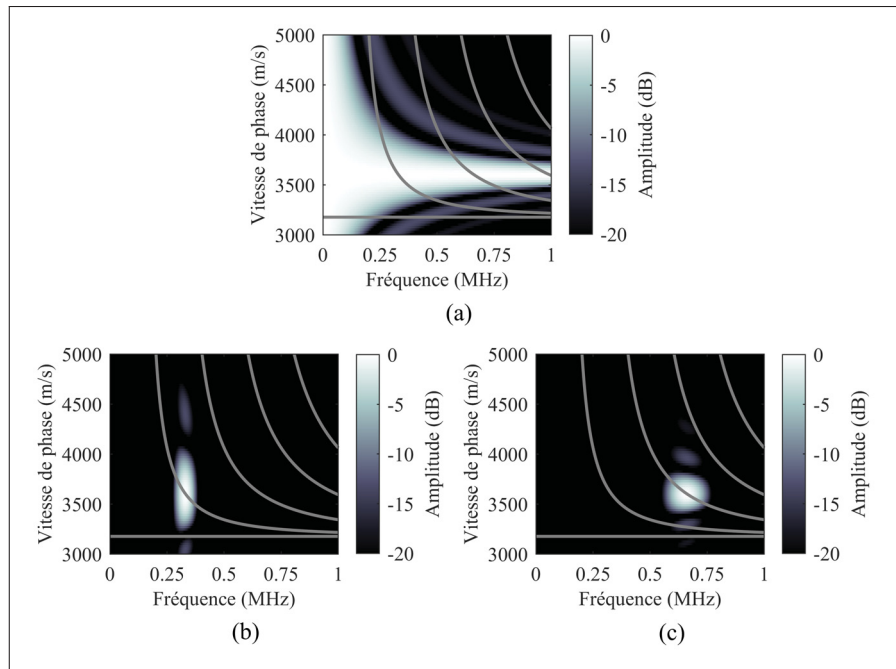
Figure 1.12 (a) Cartographie de l'énergie due à une excitation en vitesse avec un transducteur de 20 éléments autour d'une vitesse de phase de 3600 m/s, Modes excités lorsque cette excitation est associé à un signal de 10 cycles centré sur une fréquence de 330 kHz (b) et 630 kHz (b) et fenêtré par une fonction de Hann. Dans ce cas le guide d'onde considéré est une plaque d'acier (ρ = 8000 kg/m^3, E = 210 GPa, ν = 0.30) de 9.53 mm d'épaisseur. Les courbes pleines en grises sont les courbes de dispersions des modes SH

sont nécessaires, l'une en amont et l'autre en aval de la région d'intérêt (ROI). La mesure des fréquences de coupure des différents modes qui ont pu se propager permet grâce à l'équation 1.18 d'en déduire l'épaisseur minimale du guide d'onde entre les deux transducteurs. En termes de position, la seule information disponible est que le défaut se situe entre la sonde émettrice et la sonde réceptrice. De plus, lorsque le défaut est trop profond, l'amplitude de l'onde après le défaut risque d'être trop faible pour être détectée. La deuxième option, une mesure en réflexion, permet d'effectuer des mesures avec au minimum une sonde. La mesure d'épaisseur se fait de la même manière mais à partir de la partie réfléchie de l'onde guidée. Le principal intérêt est de permettre grâce à une mesure de temps de vol de positionner le défaut. Contrairement à la mesure en transmission, des mesures complexes peuvent se produire pour des défauts superficiels lorsque l'énergie réfléchie est trop faible.
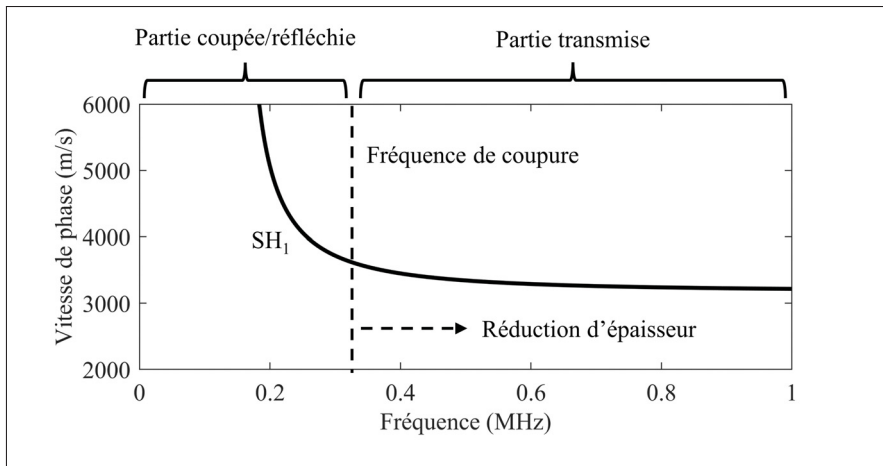
Figure 1.13   Schéma de principe pour une méthode de filtrage structurel utilisant SH$_1$ sur une plaque d'acier (ρ = 8000 kg/m^3, E = 210 GPa, ν = 0.30) d'une épaisseur de 10.2 mm

1.3.2   La tomographie par onde guidée

L'objectif de la tomographie par onde guidée est de reconstruire une carte d'épaisseur de la ROI. L'acquisition est réalisée avec une multitude de sondes placées tout autour de la ROI. Une première émission est réalisée sur une sonde et la réception sur l'intégralité des transducteurs. L'élément émetteur est changé jusqu'à ce que toutes les combinaisons de sondes émettrices et réceptrices aient été effectuées.

Au niveau du traitement des données la difficulté réside dans la reconstruction de la carte de vitesse de l'onde sur la ROI. La solution la plus simple est de considérer l'onde comme un rayon ayant une propagation linéaire (Hinders & McKeon, 1999; Leonard & Hinders, 2005; Volker, Mast & Bloom, 2010; Belanger & Cawley, 2009; Willey, Simonetti, Nagy & Instanes, 2014). Le calcul du temps d'arrivée pour chaque combinaison permet d'obtenir la carte désirée. Cette technique implique que l'hypothèse d'assimiler l'onde par un rayon est valide. Ceci est vérifié dans le cas où les défauts sont grands par rapport à la longueur d'onde et à la largeur du champ ultrasonore. Lorsque la dimension du défaut est plus faible la diffraction de l'onde commence à être trop importante pour être négligée. Dans ce cas des algorithmes de

tomographie par diffraction peuvent être utilisés (Bélanger *et al.*, 2010; Huthwaite & Simonetti, 2011; Zimmermann *et al.*, 2021).

Une fois cette carte de vitesse obtenue, il est possible avec les relations de dispersion des modes d'ondes guidées (Voir équation 1.15 pour les ondes guidées SH) de convertir cette carte en une carte d'épaisseur. La tomographie permet donc, par cette carte d'épaisseur, de positionner et dimensionner un défaut. Cependant des inconvénients importants sont à noter. Tout d'abord un nombre important de sondes doivent être utilisées et positionnées précisément les unes par rapport aux autres. Le schéma d'acquisition implique un nombre conséquent de courbes à stocker. Les algorithmes d'acquisition sont également lourds que ce soit en termes de temps de calcul que de ressources nécessaires.

Ces désavantages rendent la tomographie par onde guidée peu compatible avec des mesures sur chantiers du fait du temps et des équipements nécessaires. La méthode retenue pour cette thèse est donc le filtrage structurel.

1.4   L'extraction de l'amplitude des modes

Comme on peut le voir à l'aide de l'équation 1.18 deux étapes primordiales sont nécessaires à l'estimation de l'épaisseur minimale d'un guide d'onde par filtrage structurel : 1) la mesure de la fréquence de coupure et 2) l'identification de l'ordre du mode. Pour cette étape des transformées de Fourier à une ou deux dimensions peuvent être utilisées.

1.4.1   Transformée de Fourier à une dimension

Fourier a démontré que n'importe quelle fonction continue et périodique est décomposable en une somme de fonctions sinusoïdales, appelée série de Fourier. Si on considère g comme une fonction périodique de période T et intégrable sur $\left[\frac{-T}{2}, \frac{T}{2}\right]$ alors :

$$g(t) = \sum_{n=-\infty}^{+\infty} c_n(g) e^{j2\pi\frac{n}{T}t} \tag{1.34}$$

$$c_n(g) = \frac{1}{T} \int_{\frac{-T}{2}}^{\frac{T}{2}} g(t)e^{-j2\pi\frac{n}{T}t}dt \tag{1.35}$$

Les $c_n(g)$ sont appelés coefficients de Fourier de la fonction g. La transformée de Fourier $\hat{g}$ est une extension des séries de Fourier dans le cas de fonction continue, non périodique mais intégrable sur l'ensemble des réels $\mathbb{R}$:

$$\hat{g}(\omega) = \frac{1}{\sqrt{2\pi}} \int_{-\infty}^{+\infty} g(t)\mathrm{e}^{-\mathrm{i}\omega t} \, \mathrm{d}t \tag{1.36}$$

où ω est la pulsation. Dans le cas de signaux issus de mesures expérimentales ou de simulations les fonctions sont échantillonnées et donc non continues, on utilise alors la version discrète de la transformée de Fourier X :

$$X(f) = \sum_{n=0}^{N-1} x(nTe)\mathrm{e}^{-2\mathrm{i}\pi fnTe} \tag{1.37}$$

avec x un signal de N incréments échantillonnés avec une période Te. Le calcul du spectre d'une fonction n'est pas réalisé à partir de l'équation 1.37 mais à partir de l'algorithme de transformée de Fourier rapide développé par J. W. Cooley et J. W. Tukey (Cooley & Tukey, 1965). L'utilisation de l'algorithme de transformée Fourier rapide (fft) permet donc d'obtenir l'amplitude d'un signal en fonction de la fréquence. Dans le cas d'une onde guidée, si l'on fait l'hypothèse d'aucune superposition des modes dans le domaine fréquentiel, cette opération permettra d'identifier un mode se propageant et de détecter une éventuelle coupure. Cependant suivant les paramètres d'excitation et les possibles conversions de modes ce critère peut ne pas être vérifié. En effet Nurmalia et Nakamura (Nurmalia *et al.*, 2012; Nakamura *et al.*, 2013) ont démontré que lorsqu'une onde guidée interagit avec un défaut présentant une variation rapide d'épaisseur alors des conversions de modes peuvent se produire.

1.4.2   Transformée de Fourier à deux dimensions

D. Alleyne et P. Cawley (Alleyne & Cawley, 1991) ont proposé une extension à deux dimensions des transformées de Fourier. En échantillonnant une onde guidée selon plusieurs points répartis à des intervalles réguliers selon la direction de propagation une matrice de l'amplitude de l'onde en fonction du temps et de la distance parcourue est obtenue. En appliquant une fft successivement sur chacune des dimensions de cette matrice il est alors possible d'extraire l'amplitude des modes se propageant selon leurs fréquences et nombres d'ondes. La superposition de cette figure et des courbes de dispersions permet d'identifier les modes pouvant se propager. A l'aide de l'équation 1.14 la figure obtenue peut être convertie en une cartographie de l'énergie en fonction de la fréquence et de la vitesse de phase. Cette technique est plus complète dans le sens où elle permet d'extraire l'amplitude de chacun des modes mêmes s'ils se situent à la même position dans le domaine fréquentiel. La difficulté est que cela nécessite plusieurs prises de mesures à des positions différentes, ce qui peut être réalisé en déplaçant une sonde, un vibromètre laser ou en utilisant une sonde multi-éléments. Cette technique est illustrée par la figure 1.14.

1.5   Retour au projet et présentation des articles

1.5.1   Conclusion de la revue de la littérature

Les ondes guidées ultrasonores, et plus particulièrement les ondes guidées SH, permettent grâce à leur relation de dispersion une estimation de l'épaisseur d'un guide d'onde. Cette caractéristique est intéressante dans le cas d'une inspection de structure corrodée comme un tuyau. En effet pour une onde guidée une attaque par corrosion sur une surface peut être assimilée à une perte d'épaisseur. Si cette perte d'épaisseur est suffisamment importante alors certains modes d'ordre élevés seront affectés et ils seront complètement ou partiellement coupés. Les parties affectées de ces modes seront alors soit réfléchies soit converties vers un mode capable de se propager. Ces premières informations permettent d'établir un protocole de mesure. Tout d'abord un transducteur générera une onde SH dans le matériau. Cette onde se propagera ensuite dans le guide d'onde et dans le cas de la présence d'un défaut alors une partie sera transmise à
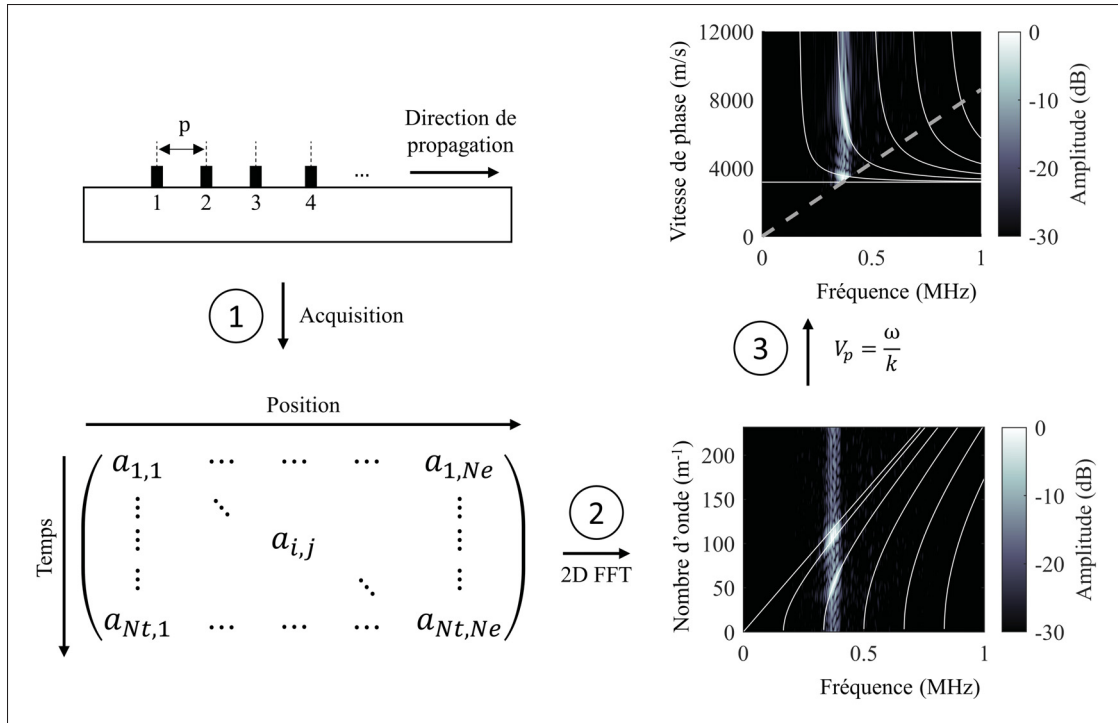
Figure 1.14   Schéma de principe d'une FFT à deux dimensions appliquée sur une onde
guidée se propageant dans un guide d'onde. L'acquisition est réalisée à N_e positions, chaque
trace temporelle comporte N_t échantillons et le terme $a_{i,j}$ désigne l'amplitude mesuré à la
position j pour l'incrément temporel i

travers la région corrodée et une partie sera réfléchie. La mesure d'une de ces deux composantes
permet l'estimation de l'épaisseur et un positionnement dans le cas de l'onde réfléchie.

Le choix de la sonde a été fait dans l'optique de permettre une acquisition fiable et répétable.
Comme dit précédemment la transduction d'une onde SH par une sonde piézoélectrique nécessite
l'utilisation d'un couplant visqueux qui se dégrade lorsque la sonde est déplacée. Le choix
d'utiliser un EMAT a donc été fait à l'origine de ce projet, la couche de couplant étant inutile. Les
sondes les plus utilisées dans la littérature pour l'inspection par filtrage structurel sont les PPM
EMAT permettant une excitation et une détection contrôlée d'onde guidée SH. Le problème dans
le cas de cette structure est que les travaux ont été souvent réalisés sur des plaques en aluminium,
ignorant donc la géométrie et le caractère ferromagnétique des tuyaux majoritairement en acier.

De plus ces EMAT sont des sondes mono-élément rendant impossible, sans déplacer la sonde, l'utilisation de transformées de Fourier à deux dimensions pour l'identification des modes.

1.5.2   Objectifs et méthodologie

L'objectif principal de cette thèse est de fournir des EMATs compatibles avec des méthodes d'estimation d'épaisseur de plaques ou de tuyaux par filtrage structurel. Cet objectif inclus : 1) la prise en compte de la géométrie et du caractère ferromagnétique des structures inspectées et 2) le développement de sondes compatibles avec des méthodes d'excitations, comme les excitations en vitesse de phase, et avec des algorithmes de traitement de données polyvalents comme les transformées de Fourier à deux dimensions.

Ces objectifs ont été atteints en trois étapes lors de cette thèse :

1. La structure d'un PPM EMAT a été optimisée pour permettre une transduction plus efficace de modes SH dans un tuyau en acier. Cette étude a démontré l'importance des distances de décollage de la bobine et des aimants par rapport au tuyau dans le cas d'un matériau ferromagnétique. La configuration optimale utilisant des aimants incurvés et une bobine flexible a permis la reconstruction du profil d'épaisseur d'une région corrodée sur un tuyau.

2. Un nouveau modèle d'EMAT multi-éléments a été proposé. Cette configuration permet la transduction d'onde guidée SH avec des performances similaires à celle d'une sonde piézo-électrique multi-éléments de cisaillement. Le principal intérêt de ce nouveau transducteur et de permettre des techniques d'excitation plus performantes comme les excitations en vitesse de phase et aussi l'utilisation de techniques de traitement de données comme les transformées de Fourier à deux dimensions.

3. La dernière étape a été de tester cette sonde sur un tuyau en acier. Le même tuyau que pour le PPM EMAT a été utilisé. Une technique de filtrage structurel en utilisant en émission une série d'excitations en vitesse de phase et en réception l'onde réfléchie par le défaut a permis d'estimer l'épaisseur du tuyau selon trois positions différentes avec une erreur maximale de

0.4 mm. L'utilisation de l'onde réfléchie a également permis un positionnement de la région corrodée avec une erreur de 10 mm pour une distance de propagation totale de 600 mm.

Les travaux réalisés lors de ces trois étapes ont permis la rédaction et la publication de trois articles, présentés dans les chapitres suivants, et de trois brevets (voir annexes).

Pour chacune de ces étapes la méthodologie suivante a été utilisé :

1. Réalisation de modèles éléments finis pour simuler le comportement des différentes configurations retenues.
2. Mesures expérimentales dans les mêmes configurations que pour les simulations éléments finis.
3. Évaluation des sondes considérées selon divers critères comme : l'amplitude de l'onde générée, la précision de l'estimation d'épaisseur ou une comparaison de leurs capacités par rapport à des technologies existantes.

Trois logiciels ont été utilisés lors de cette thèse. Comsol Multiphysics, un logiciel de simulation par éléments finis qui permet de créer des modèles multi-physiques. Il sera particulièrement utile pour modéliser le champ magnétique généré par les aimants et les courants de Foucault induits par la bobine. Pogo FEA (Huthwaite, 2014), un logiciel qui permet de simuler la propagation d'ondes ultrasonores. Sa particularité est qu'il utilise des processeurs de cartes graphiques (GPU) pour permettre une résolution plus rapide des modèles par rapport à des logiciels utilisant des unités centrales de traitement (CPU). Enfin les algoritmes de traitement de données seront exécutés sur MATLAB.

CHAPITRE 2

OPTIMIZATION OF A LORENTZ FORCES EMAT FOR THE RECONSTRUCTION OF THE CIRCUMFERENTIAL THICKNESS PROFILE OF A STEEL PIPE USING HIGH ORDER SHEAR HORIZONTAL MODE

Aurélien THON[1,2] , Guillaume Painchaud-April[3] , Alain Le Duff[3] , Pierre Bélanger[1,2]

[1] Piezoelectricity and Ultrasonics Technologies and Materials Laboratory at ÉTS (PULÉTS), 1100 Notre-Dame Ouest, Montréal, Québec, Canada H3C 1K3

[2] Département de Génie mécanique, École de Technologie Supérieure, 1100 Notre-Dame Ouest, Montréal, Québec, Canada H3C 1K3

[3] Evident Industrial, 3415 Rue Pierre-Ardouin, Québec, Québec, Canada G1P 0B3

2.1   Abstract

Corrosion is a chemical reaction affecting a wide range of materials. Safety-critical structures in the oil, gas, petrochemical, and many other industries need a fast, reliable screening technique that can be performed without operational disruption. Partially accessible structures such as pipes at supports or under a layer of insulation are particularly challenging. In this respect, high-order shear horizontal (SH) guided wave modes can be used in medium- to long-range thickness gauging thanks to their cutoff frequency-thickness product. As the wave propagates, a reduction in the thickness behaves like a low-pass filter for high-order modes. It has been demonstrated that periodic and permanent magnet electromagnetic acoustic transducers (PPM EMAT) can be used for transmission and reception. This paper presents a comparative study between different PPM EMAT configurations on a 323.8 mm diameter, 10.2 mm thick steel pipe. Finite element (FE) simulations and experimental measurements are used to compare the effectiveness of the different configurations to measure the thickness in four intervals : less than 5.4 mm, between 5.4 and 7 mm, between 7 and 8 mm, and between 8 mm and 10.2 mm, thus allowing to detect thickness losses of up to 50% of the nominal thickness of the waveguide.

2.2   Introduction

The inspection of corroded structures is crucial across many industries, including oil, gas and civil infrastructure (Garverick, 1994). Affected areas are often difficult to reach due to other structures, such as pipe support (Britton, 2002) and insulation (Vogelaere, 2009), impeding access. This makes it impossible to use standard thickness gauging methods such as point-by-point ultrasonic thickness gauging (Krautkrämer & Krautkrämer, 1990). These techniques are simply not compatible with the need of the industry for a reliable and rapid thickness gauging process.

Given the ability of ultrasonic guided waves to propagate over long distances, they are commonly used to screen long sections of pipes for different types of defects (Cawley, 2002; Rose, Cho & Avioli, 2009). Methods based on these waves generally use low frequency guided waves in order to excite only non-dispersive fundamental guided wave modes (Alleyne *et al.*, 2001, 1998; Mudeg, 2001). Performing a pulse-echo measurement allows to locate a corroded area or other types of defects. However, accurately measuring the remaining thickness of the waveguide is not possible.

Imaging methods such as ultrasonic guided wave tomography can be used to overcome this problem. A detailed thickness map of the inspection area is obtained, but this requires using a dense array of transducers, high-level control over the position of each transducer, and heavy data processing (Bélanger *et al.*, 2010; Ho, Billson & Hutchins, 2007; Huthwaite & Simonetti, 2013; Zimmermann *et al.*, 2021).

Defect quantification is an important part of non-destructive testing. The use of high frequency guided waves allows in theory to detect small defects. The disadvantage is that the dispersion of high order modes and the increasing attenuation with frequency makes these measurements more complex. These measurements are even more complex when considering the use of electromagnetic acoustic transducers (EMAT). Recent work has shown that deep neural networks can allow accurate quantification of small defects such as microcracks (Sun *et al.*, 2021b).

Another solution is to use high-order shear horizontal modes (SH). Each of these modes has a characteristic frequency-thickness product below which they can no longer propagate. Depending on the shape of the thickness transition, two behaviors are possible for high order modes. When the variation is smooth and progressive then the majority of the energy of the mode is reflected. On the contrary if the defect is abrupt then the mode will be converted into a lower order mode capable of propagating under the defect and when the thickness allows it may be converted into its original state (Nurmalia *et al.*, 2012; Nakamura *et al.*, 2013). By identifying the modes propagating through a corroded area, it is possible to estimate the minimum thickness of the waveguide. One advantage of using SH waves is that they can be easily generated using Periodic and Permanent Magnet Electromagnetic Acoustic Transducers (PPM EMAT). No surface preparation is then necessary. Several recent papers (Bélanger, 2014; Thon & Bélanger, 2019; Suresh & Balasubramaniam, 2020) have demonstrated the value of using such a technique. Some limitations of these studies are the use of plate approximation, they only consider single defect, and propagation is through the center of large defects.

The contribution of this study is to compare different configurations of PPM EMAT in the case of an inspection by high-order shear horizontal modes on a steel pipe and choose the one that will allow the most accurate reconstruction of the pipe thickness profile. The ferromagnetic nature of the pipe and the alteration induced on the shape of the magnetic field lines are considered. The effect of the liftoff between the coil and the conductive pipe are also analyzed. The paper first presents the materials and methods including a description of the inspected pipe as well as the dimensions and shapes of the defects. Then, the required theoretical background on SH waves and EMAT is addressed. At the end of the first section, a description of the simulation models using Comsol Multiphysics® and Pogo® (Huthwaite, 2014), as well as that of the experimental setup, are presented. Section 3 presents, analyzes, and compares the results obtained using the finite element model and experimental measurements. This article ends with a discussion in section 4 and conclusions in section 5.

2.3   Materials and methods

2.3.1   Inspected Pipe
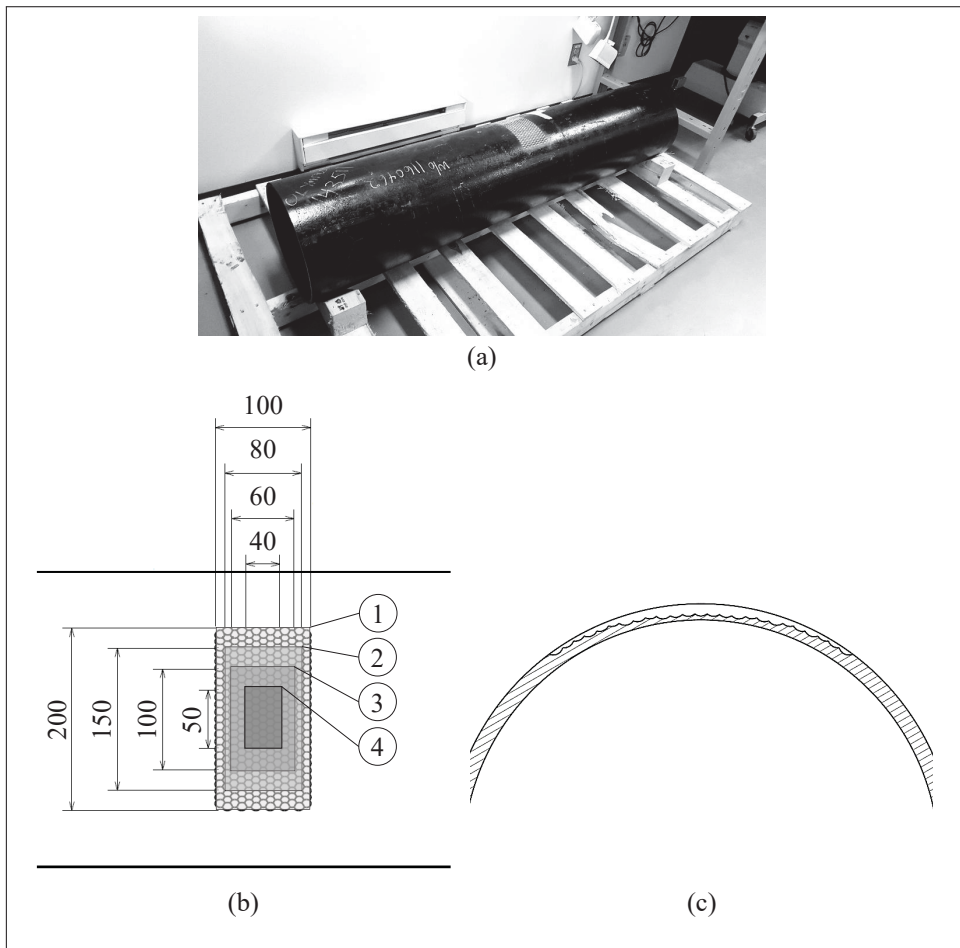
Figure 2.1   (a) Steel pipe used for both simulations and experiments, (b) Dimensions of the different steps, (c) Cross-section of the pipe at the center of the defect showing the minimum thickness profile of the pipe. All dimensions are in mm

To test the probes and the various inspection parameters, a steel pipe was used Fig. 2.1 (a). Its outer diameter was 323.8 mm, and its nominal thickness was 10.2 mm. To simulate a progressive corroded zone, the thickness profile was machined using spherical pockets, as shown in Fig. 2.1 (b). The dimensions and minimum remaining thickness of each region are summarized in Table 2.1. The machined thickness profile mimics a large corrosion patch, with an increasing

depth towards the center. Using milled spherical pockets also adds a degree variability to the thickness profile for waves propagating through the profile.

Tableau 2.1   Dimensions of each region

Zone	Axial Dimensions (mm)	Circumferential Dimensions (mm)	Minimum Thickness (mm)
1	100	200	7.2
2	80	150	6
3	60	100	4
4	40	50	2.5

2.3.2   Plate approximation

The use of ultrasonic guided waves in nondestructive testing enables rapid inspections over long distances. In a pipe, several modes, such as flexural (axisymmetric and non-axisymmetric) and torsional modes (axisymmetric and non-axisymmetric), can propagate. PPM EMAT can easily generate torsional modes. Numerous studies have shown that using a plate approximation for a pipe will hold, provided the ratio between the thickness and outer diameter of the pipe is below 5 to 10% and when the frequency used is below the first cutoff frequency (Luo *et al.*, 2005; Velichko & Wilcox, 2009). In the context of this study, the ratio is 3.1% and the frequencies used will be greater than the first cutoff frequency

Fig. 2.2 shows the phase velocity dispersion curves of shear horizontal modes, obtained using the Civa® simulation package, in a 10.2 mm plate and a pipe with a diameter of 323.8 mm and a thickness of 10.2 mm, both made of steel (ρ = 8000 kg/m^3, E = 210 GPa, v = 0.30). It can be seen that the error between the two curves is negligible. The maximum error on the frequency range used remains less than 1%. As the circumferential propagation of guided waves are not used in this paper, the dispersion curves of a flat plate are used instead, and the EMAT configurations are developed for a curved 10.2 mm plate.
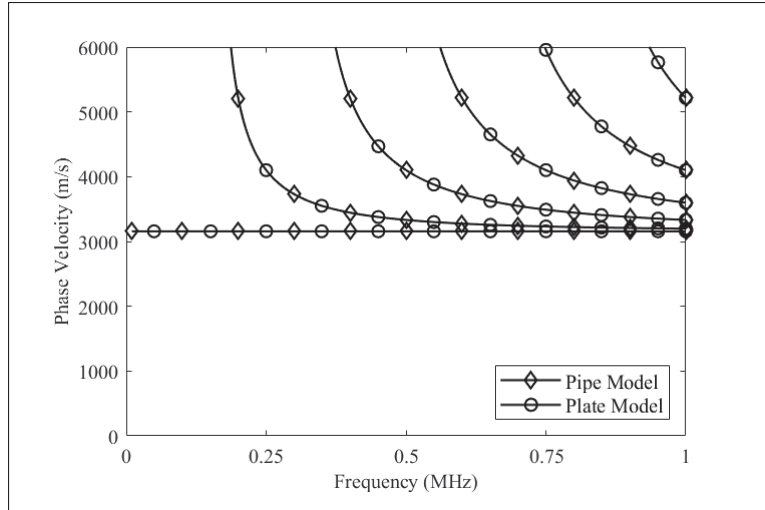
Figure 2.2   Comparison between phase velocity dispersion curves in a 323.8 mm diameter
and 10.2 mm thick steel pipe and in a 10.2 mm thick steel plate

2.3.3   Guided wave propagation

Guided waves are mechanical perturbations that propagate between two boundaries forming a waveguide, such as a plate or a pipe. These can be separated into Lamb waves (symmetric and anti-symmetric), and shear horizontal (SH) guided waves. When impinging a defect or a feature parallel to the direction of polarization, SH waves will not convert to Lamb modes (Graff, 1991; Krautkrämer & Krautkrämer, 1990; Petcher *et al.*, 2014). Unlike Lamb waves, SH waves are less sensitive from the loading of non-viscous fluid. Finally, as the dispersion curves show, the cutoff frequency-thickness product of the high-order SH modes are evenly distributed along the frequency-thickness product axis. This allows the estimation of the thickness at regular intervals.

Eq. 2.1 and Eq. 2.2 allow to compute the phase and group velocity of shear horizontal modes :

$$V_{p,n} = V_S \left(\frac{2fb}{\sqrt{4(fb)^2 - n^2 V_S^2}} \right) \tag{2.1}$$

$$V_{g,n} = V_S \sqrt{1 - \frac{(n/2)^2}{(fb/V_S)^2}} \qquad (2.2)$$

where $V_{p,n}$ and $V_{g,n}$ are respectively the phase and group velocity of the n-order mode, V_S is the bulk shear wave velocity, f is the frequency, and b is the thickness of the waveguide. The fundamental mode SH_0 can propagate at all frequency-thickness products. High-order modes are constrained to propagate only above a given cutoff frequency-thickness product. When this value is reached, the mode's phase velocity tends towards infinity, and the group velocity towards zero, this mode can no longer propagate, and is then reflected or converted to a lower-order mode (Cheeke, 2012).
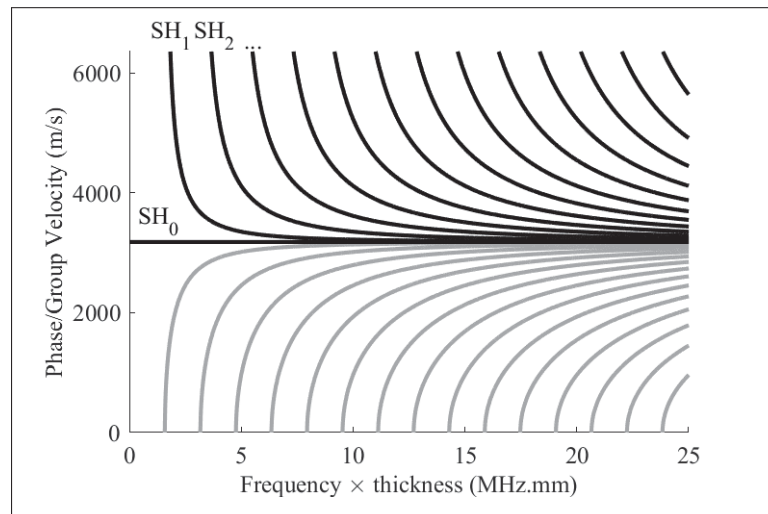
Figure 2.3   SH waves phase (black) and group (gray) velocity dispersion curves in a steel plate (ρ = 8000 kg/m^3, E = 210 GPa, v = 0.30)

In metallic materials, corrosion takes the form of a chemical weathering by an oxidizer. This involves wear of the affected surfaces, which can be likened to a local loss of thickness. For a high-order shear horizontal mode, this shifts the frequency-thickness product. If the severity of the defect is sufficient, then the mode can reach its cutoff threshold. The energy of this mode is then no longer able to propagate. By identifying the last mode capable of propagating and the first mode filtered out, the waveguide thickness can be estimated. Considering a plate of a given thickness b, the cutoff frequency-thickness product of SH_n can be obtained using Eq. 2.3 :

$$fb = \frac{nV_S}{2} \qquad (2.3)$$

where V_S is the bulk shear wave velocity. Using multiple modes allows to increase the number of detection thresholds. However, the excitation and detection of high-order modes become more complex as the frequency increases. Cheeke (Cheeke, 2012) modeled the attenuation using Eq. 2.4 :

$$I = I_0 e^{-2\alpha x} \qquad (2.4)$$

where I is the intensity of the wave at a distance x from its source, I_0 is the initial intensity, and α is the attenuation coefficient depending on the material properties and increasing with the frequency. In addition to attenuation, the ultrasonic wave is also subject to scattering when it encounters a defect. Moreover, high-order modes can be described as dispersive. The difference between their phase and group velocities involves an alteration in the waveform in the time domain along with its propagation. The experimental use of high order mode over a large propagation distance are therefore more complex than is the case for the first SH modes. In this project, the inspection distance (42 cm) was set by the maximum separation distance of the scanner (Olympus HSMT Compact) used to position the two probes.

2.3.4   Electromagnetic acoustic transducer

Electromagnetic acoustic transducers or EMAT is a transducer technology that relies mainly on two forces : Lorentz forces for conductive materials and magnetostrictive forces for ferromagnetic materials. In the case of an inspection on steel, the two forces mentioned above come into play and the force F generated by an EMAT can be calculated as follows :

$$F = F_L + F_M \tag{2.5}$$

where F_L are the Lorentz forces and F_M are the magnetostrictive forces. PPM EMATs (Fig. 2.4) are a category of probes whose arrangement of magnets and coil allows the generation and the detection of SH guided waves. A set of permanent magnets generates an alternating magnetic field with a period λ. An elongated coil is supplied with a current corresponding to the emission signal. The proximity of the coil to the conductive waveguide induces the eddy currents necessary for transduction.

PPM EMAT generates both Lorentz and magnetostrictive forces. Under the magnets, the currents induced by the coil are perpendicular to the static magnetic field generated by the magnets, so Lorentz forces can be induced in the material. When moving away from the center of a magnet the magnetic field rotates and ends up being parallel to the current induced by the coil, magnetostrictive forces are then generated. These two mechanisms occur at the same frequency and wavelength and as shown in (Sun *et al.*, 2021a) the main effect of the coexistence of these two forces is to reduce the amplitude of the generated SH waves by approximately 30% compared to a model relying purely on Lorentz forces. The combination of these two forces imply only a loss of amplitude, and no change in the frequency and wavelength excited, only the Lorentz forces will be considered for analytical models and finite element simulations and the forces F will be considered equal to :

$$F \approx F_L = J_e \times B \tag{2.6}$$

where J_e is the eddy current induced by the coil and B is the magnetic field generated by the magnet array.
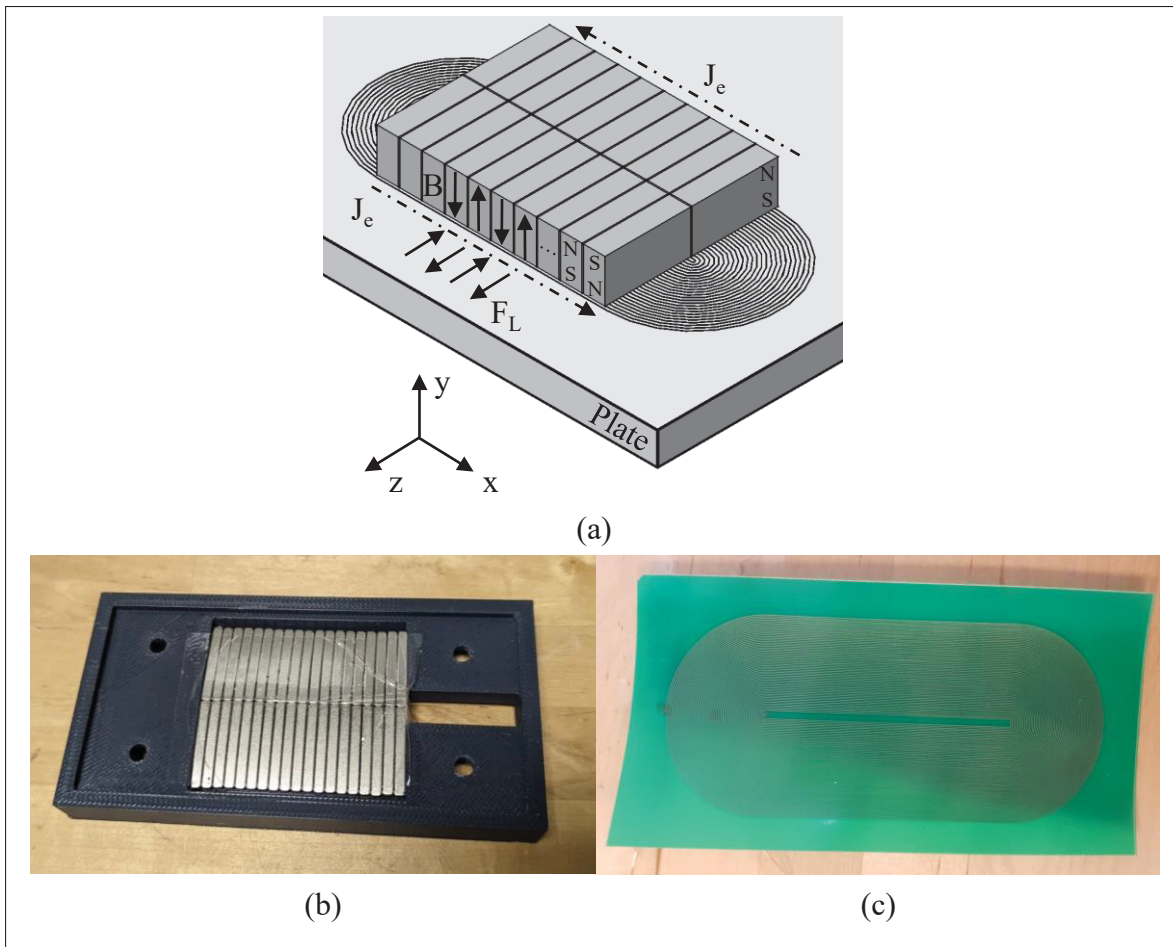
Figure 2.4 (a) Schematic diagram of a PPM EMAT on a plate, (b) Magnet array of a PPM EMAT composed of 2x20 curved magnets in neodynium grade N55 and (c) 60 turns flexible racetrack coil used for each of the EMATs presented in this article

Tableau 2.2 Dimensions of the 60 turns flexible coil

Number of turns	Track Width	Distance between tracks	Linear region dimension	Total Dimension
60	0.2 mm (8 mils)	0.2 mm (8 mils)	65 mm x 52 mm	115.5 mm x 52 mm

To optimize the generation of Lorentz forces, four configurations, with different magnets setups, are studied in this paper. For each configuration the coil is realized on a flexible PCB and its dimensions are given in the table Table 2.2. The pitch is set to 3.2 mm, the elevation to 50.8 mm, and the aperture to 64 mm (20 magnets in the direction of propagation). Fig. 2.5 and Table 2.3

show the magnet arrangements, along with their dimensions and direction of magnetization. The first configuration (1) corresponds to a PPM EMAT comprising a set of rectangular magnets Fig. 2.5 (a) and a flat coil. This is the standard configuration for transduction in a plate. When considering an inspection on a pipe, the liftoff between this configuration and the pipe is not constant, and increases as one moves away from the center of the probe. Since the pipe is ferromagnetic, it has a lower reluctance than air, and will tend to attract magnetic flux lines. The amplitude of the eddy currents generated by the coil decreases as a function of its distance to the conductor. This has the effect of locally altering the direction of the magnetic flux lines, the amplitude of the eddy currents, and thus, the shape of the Lorentz forces generated by this configuration. The second configuration (2) uses the same type of magnet, but in this case, the coil is flexible and follows the curvature of the pipe. This allows the quantification of the influence of the distance from the coil on the generated force field. The third case (3) ensures constant and minimal spacing of the magnets and coil from the pipe by using curved magnets and a flexible coil Fig. 2.5 (c) whose inner diameter is equal to the outer diameter of the pipe plus a lift-off distance due to the probe casing (1 mm). Finally, the last case (4) is considered using small rectangular magnets Fig. 2.5 (b) and a flexible coil. This solution has the advantage of reducing the magnet liftoff relative to the pipe using only readily available magnets.

Tableau 2.3   Geometry and magnetization direction of the magnets

Pitch (mm)	Length (mm)		Height (mm)	Magnetization direction	Model
3.2	25.4		6.4	Height	Fig. 5 (a)
3.2	12.7		6.4	Height	Fig. 5 (b)
	Inner Radius (mm)	Arc (degree)			
3.2	162.9	9	6.4	Radial	Fig. 5 (c)

2.3.5   Constant wavenumber excitation

A constant wave number excitation or a comb excitation allows the control of the excited modes according to the distance between each element of a probe or pitch. All elements are activated at the same time with the same signal. J. L. Rose (Rose, 2014) has shown that in this configuration
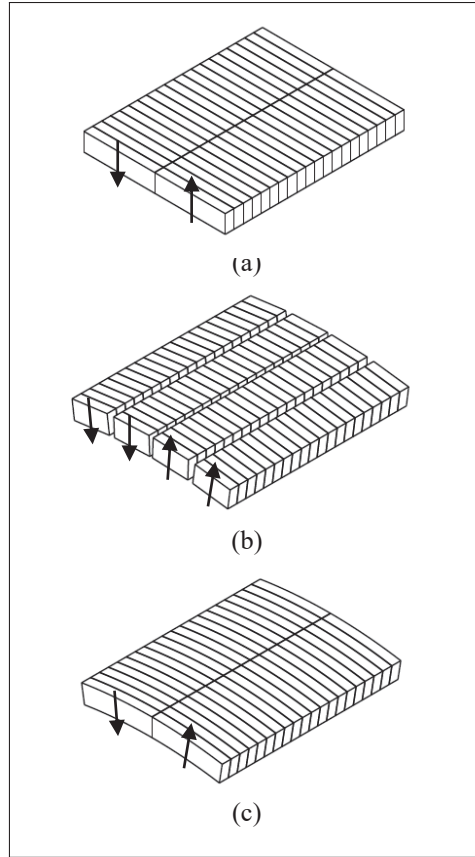
Figure 2.5   Diagram of the three magnet setups used; the arrows represent the direction of magnetization of the magnets

the modes will be excited around a wavelength equal to the pitch or one of its multiple. The amplitude $A_n(\omega, x)$ of the n-th mode will then be :

$$A_n(\omega, x) = U \cdot F(\omega) \cdot C_n(x) \cdot H(\omega, x) \tag{2.7}$$

where U is the particle displacement, $F(\omega)$ is the frequency response of the elements, $C_n(x)$ is the coupling coefficient between the waveguide surface traction and the guided wave mode and

$$H(\omega, x) = \sum_{i=1}^{N} e^{j[\omega t \pm k_x \cdot (x - x_i)]} = \frac{sin(N\frac{k_x p}{2})}{sin(\frac{k_x p}{2})} e^{j[\omega t \pm k_x \cdot (x - x_c)]} \tag{2.8}$$

where $\pm$ is negative for the direction of propagation +x and positive for the direction of propagation -x (see Fig. 2.4 (a) for axis system), p is the pitch, N is the number of elements, ω is the angular frequency, $k_x = \frac{\omega}{V_p}$ is the wavenumber component along the direction of propagation x and x_c is the center of the transducer array. $|H(\omega, x)|$ reaches a maximum when p is equal to a multiple of $\lambda = \frac{2\pi}{k_x}$. The modes will then be excited at a wavelength equal to an integer times p. By using a PPM EMAT it is possible to perform this type of excitation without having to use a multielement probe. To apply it to a PPM EMAT p will be equal to the distance between two magnets having the same direction of magnetization and N will be equal to the number of magnets divided by two.

By multiplying $|H(\omega, x)|$ by the frequency content of the signal used it is then possible to obtain Fig. 2.6 (a) showing the amplitude of a comb excitation on a phase velocity frequency map for an excitation with a PPM EMAT composed of 20 magnets of 3.2 mm in the direction of propagation and a 20-cycle Hann-windowed toneburst centered around a frequency of 500 kHz. By using long signals it is then possible to concentrate the energy around a specific point of the dispersion curves allowing a pure excitation of a high order mode. In this case, in reception, the amplitude of the modes can easily be extracted from the A-scans using a Fourier transform.

Tableau 2.4 Excitation frequencies and cutoff thicknesses of SH_0 to SH_4 in a 10.2 mm thick steel pipe (ρ = 8000 kg/m^3, E = 210 GPa, ν = 0.30) for an excitation centred around a wavelength of 6.4 mm

	SH_0	SH_1	SH_2	SH_3	SH_4
Excitation frequency (kHz)	500	524	588	682	795
Cutoff thickness (mm)	/	3	5.4	7	8

Table 2.4 and Fig. 2.6 (b) shows the excitation frequencies of the first shear horizontal guided wave modes. Due to the wavelength of the emission (6.4 mm) and the thickness of the steel plate (10.2 mm), the excitation frequencies of SH_0 and SH_1 are very close. In fact, only 24 kHz separates these two values. Detecting the cutoff of SH_1 may then be complicated since SH_0 will still be able to propagate unless the waveguide breaks completely.
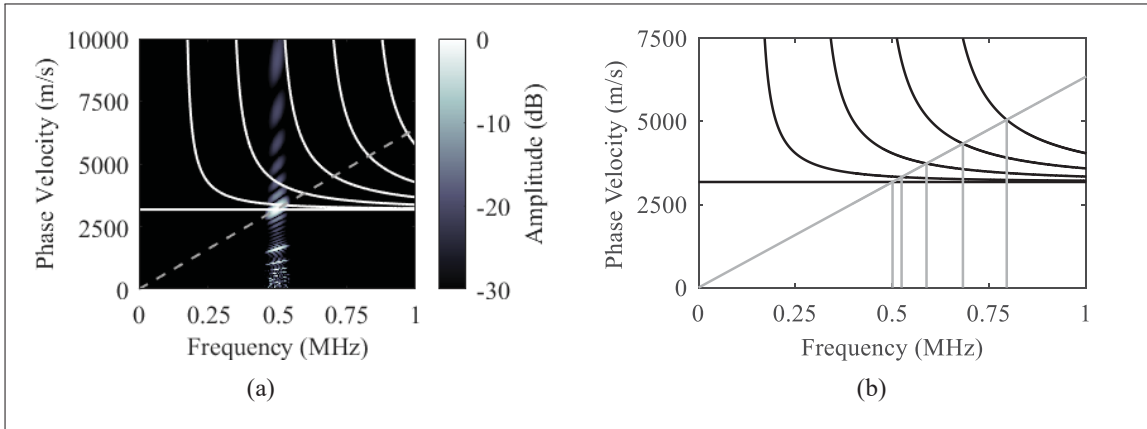
Figure 2.6 (a) Excitation energy obtained with comb excitation generated with a PPM EMAT composed of 20 magnets of 3.2 mm in the direction of propagation and a 20 cycles Hann-windowed toneburst centered around a frequency of 500 kHz. (b) Phase velocity dispersion curves in a 10.2 mm thick steel plate ($\rho = 8000$ kg/m³, E = 210 GPa, $v = 0.30$), the diagonal gray line correspond to the wavenumber associated with the pitch of the magnet, 3.2 mm, and the vertical line to the excitation frequency from SH_0 to SH_4

2.3.6 Ultrasonic beam

It is essential to know the near-field size and the angle of divergence of the ultrasonic beam. If the defect is too close to the EMAT or too small as compared to the ultrasonic beam's width, its effect on the propagation of the ultrasonic wave may not be strong enough to be detected. The near-field length N and the divergence angle from the inspection line to the -6 dB line θ can be calculated as follows (Olympus, 2004) :

$$N = \frac{D^2}{4\lambda} \tag{2.9}$$

$$\sin(\theta) = 0.44\frac{\lambda}{D} \qquad (2.10)$$

where D is the dimension of the transducer in the direction perpendicular to the propagation direction, λ is the wavelength.

2.3.7   Finite element model

The generation of an ultrasonic wave by an EMAT involves various physical phenomena such as magnetism, induction, and continuous media mechanics. Some software such as Comsol Multiphysics can simulate all these phenomena. However, because of the size of the models, results cannot be obtained within a suitable timeframe, which is why only the Lorentz forces were simulated in Comsol in the present study. The size of the model can then be reduced to an area close to the EMAT. These forces were then imported into Pogo (Huthwaite, 2014), a graphics processing unit (GPU) accelerated solver. This type of solver allows ultrasonic propagation simulations on large models, while maintaining a reasonable computation time as compared to standard central processing unit (CPU) FE codes. The hypothesis of a weak coupling is then made meaning that the propagation of the ultrasonic waves simulated by Pogo will not have any influence on the electromagnetic simulation in Comsol.

Lorentz forces were modeled using Comsol Multiphysics models of Fig. 2.7 (a) composed of four elements : (1) a steel pipe corresponding to that described in Fig. 2.1, (2) the corresponding set of neodymium magnets, (3) an elongated 60-turn coil below the magnets, and (4) air above the pipe encompassing the coil and magnets, to ensure mesh continuity. The different regions are described by their magnetic permeability and electrical conductivity.

The geometry of the Pogo model Fig. 2.7 (b) was developed from the technical drawings used to machine the pipe Fig. 2.1 (a) to ensure high precision, including in areas of defects. Mechanically, the pipe material is described using three parameters : density, Young's modulus and Poisson ratio (ρ = 8000 kg/m^3, E = 210 GPa, ν = 0.30). The signals used are 20-cycle Hann windowed toneburst centered around the excitation frequencies of SH$_0$ to SH$_4$ (See Table 2.3). A distance

50

of 420 mm was imposed between the emission (Tx) and reception (Rx) probe with the defect in the center of the zone. Absorbing boundaries designed with the Absorbing Layer with Increasing Damping (ALID) method were added at both ends of the pipe to reduce the echoes' amplitude and simulate an infinite pipe. (Cook, Malkus, Plesha & Witt, 2007; Ribichini, 2011).
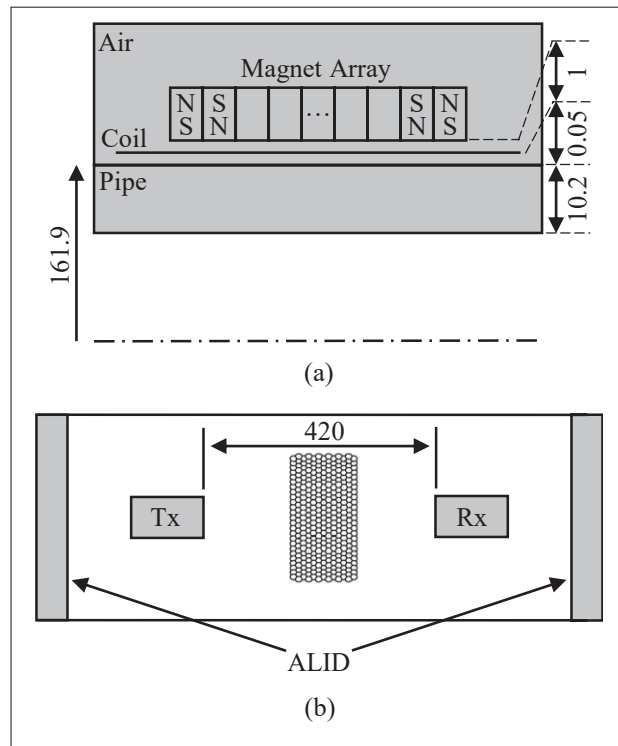
Figure 2.7   (a) Schematic of the model used to compute Lorentz Forces using Comsol Multiphysics 5.5. (b) Schematic of the model used in Pogo to simulate the wave propagation. Dimensions are in mm

2.3.8   Experimental setup

Measurements, like simulations, were performed in a pitch-catch configuration. Thus, two identical EMATs were used in all measurements. To ensure the position and orientation of the magnets and the coil, casings were 3D-printed. These casings were designed to be compatible with the Olympus HSMT Compact scanner. This will ensure high repeatability in the position and orientation of the probes. The version of the scanner used allowed a maximum separation distance of the EMATs of 420 mm, equivalent to the distance used during the simulations. The

signal was generated using MATLAB and sent as a command to a Keysight 33500B function generator. A Ritec RPR-4000 High Power Pulser Receiver amplified the signal from the generator and then fed it to the transmitting EMAT. For the acquisition setup, an adjustable differential amplifier set to an amplification of 80 dB (x10,000) made the signal detectable by a Keysight infiniiVision DSOX3014T oscilloscope. An increase in the signal-to-noise ratio of the waveforms was achieved by averaging and filtering the received signals. Broadband filters (50 kHz - 1.5 MHz) were used not to remove any feature in the frequency domain considered.

2.4 Results

2.4.1 Ultrasonic field simulation

The first point of comparison between the four EMAT configurations (see section 2.4) is the shape of the ultrasonic field generated. This can be approximated analytically using Eq. 2.9 and Eq. 2.10. These equations were obtained empirically for rectangular piezoelectric probes. In the case of an EMAT, it is then necessary to know the shape of the Lorentz force field. However, the shape of this region is influenced by eddy currents and the magnetic field, both depending on the distance from the pipe and the orientation of the magnets and the coil. As explained in section 2.7, Lorentz forces were simulated using Comsol Multiphysics according to the four configurations selected. The elevation was measured considering the width of the force field when the amplitude is greater than half of the maximum amplitude (-6 dB). In an optimal case, the distribution of forces is uniform and covers the entire surface of the pipe under the EMAT, and the elevation is then 50.8 mm.

Fig. 2.8 (a) shows the map of the forces induced in the pipe by an EMAT with rectangular magnets and a flat coil. The effective elevation of the probe is then 24.3 mm. This large deviation from the reference value is due to the increasing liftoff of the coil and magnets at the edge of the EMAT. In the case of Fig. 2.8 (b) the position and shape of the magnets remain unchanged, but the coil follows the curvature of the pipe. The height of the coil is therefore uniform. The elevation increases to 41.7 mm. By using curved magnets (Fig. 2.8 (c)) or smaller magnets
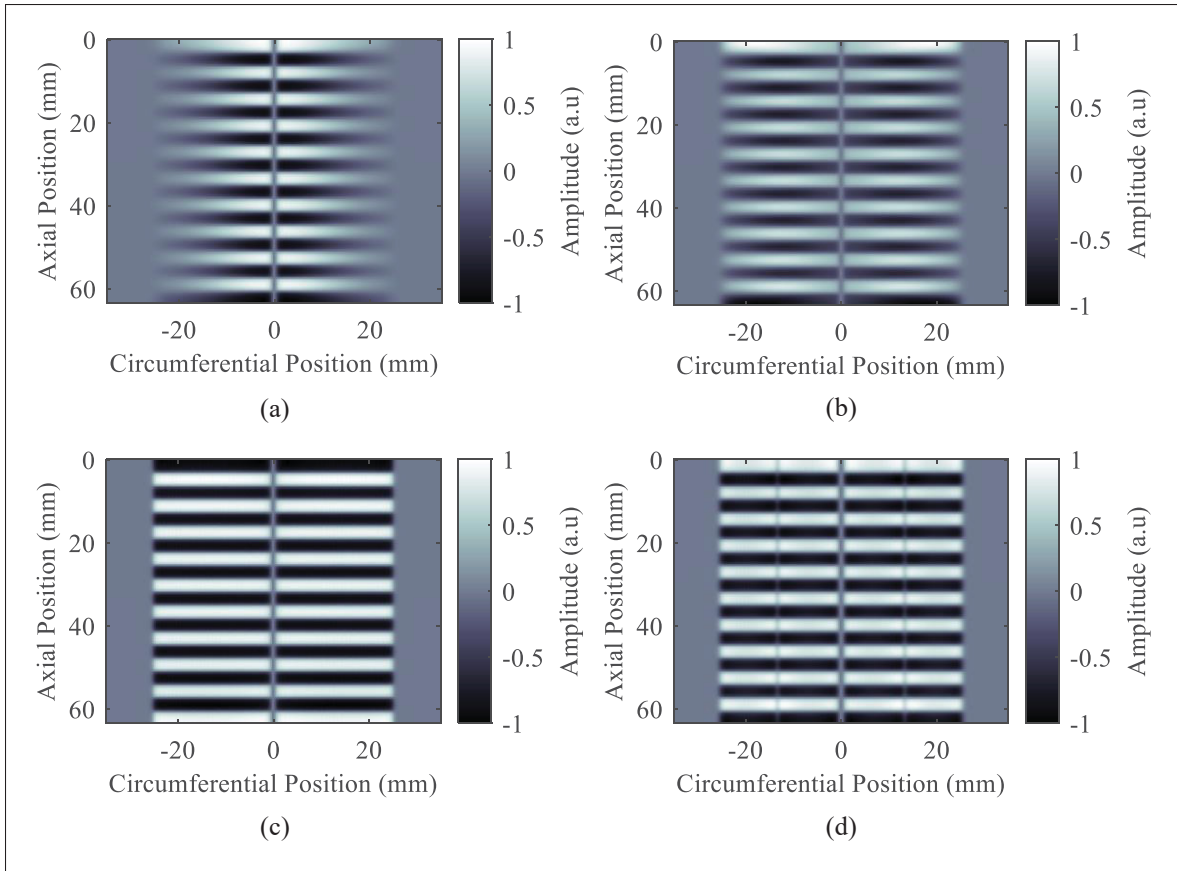
Figure 2.8   Maximum amplitude of Lorentz Forces generated along the shear horizontal direction on a steel pipe with a diameter of 323.8 mm and a thickness of 10.2 mm by different PPM EMAT configurations : (a) Rectangular magnets and flat coil, (b) Rectangular magnets and curved coil, (c) Curved magnets and coils, and (d) Small magnets and curved coil

following the pipe surface better (Fig. 2.8 (d)) elevations of 50.7 and 50.6 mm, closer to the reference value, are obtained.

This variation in the effective elevation of the probe, according to Eq. 2.9 and Eq. 2.10, induces an alteration in the shape of the ultrasonic field generated. A reduction of the elevation reduces the size of the near-field of the probe and increases the angle of divergence of the ultrasound beam. If the beam is too wide with respect to the dimensions of the defect, then the defect may not be detected correctly. To quantify this effect, the Lorentz forces were imported into a pipe of uniform thickness in Pogo, and the displacement field of the wave propagation was monitored

on the outer surface nodes. The diffraction pattern of the probe was then obtained (Fig. 2.9). The near-field of the transducer is measured as the distance from the EMAT to the distinct appearance of a conical shape in the displacement field and the angle of divergence equal to half the angle of the mentioned cone. The values obtained can then be compared with the analytical values resulting from Eq. 2.9 and Eq. 2.10.
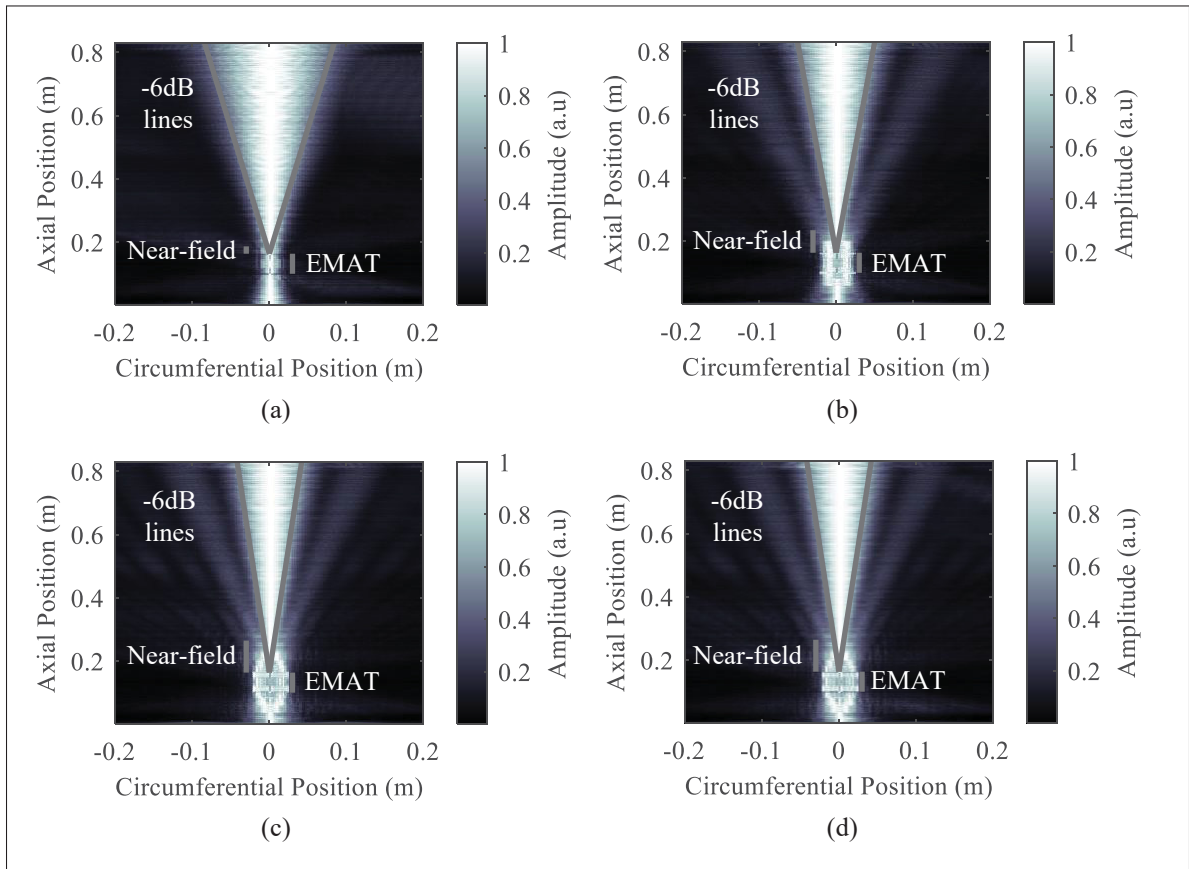
Figure 2.9   Ultrasonic field generated on a steel pipe with a diameter of 323.8 mm and a thickness of 10.2 mm by different PPM EMAT configurations : (a) Rectangular magnets and flat coil, (b) Rectangular magnets and curved coil, (c) Curved magnets and coils, and (d) Small magnets and curved coil

Fig. 2.9 and Table 2.5 show the diffraction patterns of the different EMAT configurations selected. The analytical values N_{a_n}, θ_{a_n} are therefore in good agreement with the N_{f_e}, θ_{f_e} simulations. Fig. 2.9 (a) corresponds to the diffraction pattern for an EMAT with a flat coil and rectangular magnets. This case represents the most divergent configuration since the angle obtained is 106%

Tableau 2.5   Near-field N and divergence angle θ values of the ultrasonic beam for different EMAT configurations

Case	N_{a_n}	N_{f_e}	θ_{a_n}	θ_{f_e}
a	23.2 mm	25.3 mm	6.6°	7.2°
b	68.5 mm	71.2 mm	3.8°	4.3°
c	101.2 mm	108.4 mm	3.2°	3.6°
d	100.8 mm	107.8 mm	3.2°	3.6°
ref	100.8 mm	/	3.2°	/

greater than the reference value obtained for an elevation of 50.8 mm. By using a flexible coil that best follows the curvature of the pipe (Fig. 2.9 (b)) this effect is reduced since an increase of 19% is noted. Finally, the cases of Fig. 2.9 (c) and Fig. 2.9 (d) present results similar to the reference case.

2.4.2   Thickness profile reconstruction

In view of the results of the last section, the least divergent cases are c and d. To confirm the performance of these configurations, simulations and experiments were carried out with each EMAT to reconstruct the thickness profile of the pipe. In the strategy, 20-cycle Hann windowed tonebursts centered around the excitation frequency of SH_1 to SH_4 Table 2.3 were used, thus allowing to excite the modes one by one. The 20-cycle Hann windowed toneburst represents a tradeoff between the temporal duration and the bandwidth required to excite the modes individually. When the amplitude of a mode dropped 20 dB below its amplitude without a defect or if the corresponding lobe in the signal's frequency spectrum was no longer visible, it was considered as unable to propagate.

Fig. 2.10 shows three scans performed at three different positions along the circumference of the pipe, with EMATs manufactured with small magnets Fig. 2.5 (b). The first (Fig. 2.10 (a) and (Fig. 2.10 (e)) corresponds to a reference measurement without any defect on the inspection line. Specifically, the measurements were taken 130 mm from the center of the defect on the circumferential axis. At this position, the thickness on the inspection line corresponds to the nominal thickness of the pipe. By analyzing the frequency content of the various A-Scans, one

realizes that all the modes from SH_1 to SH_4 can propagate. It should be noted that the amplitude of SH_4 is much lower than that of the other modes. It is therefore deduced that the thickness of the waveguide must lie between the nominal thickness of the pipe, 10.2 mm, and the cutoff thickness of SH_4, 8 mm. In the second case (Fig. 2.10 b) and (Fig. 2.10 (e)), the inspection line passes through the defect, and the minimum thickness is 6 mm. Here, a significant reduction in the amplitude of the reception signals can be seen, which is characteristic of the presence of a defect. The presence of SH_1 and SH_2 can nevertheless be noted in the frequency content of the signals. SH_3 and SH_4 were not detected. The thickness must therefore be between the cutoff thickness of SH_3, 7 mm, and that of SH_2, 5.4 mm. For the last position at 30 mm from the center of the defect the minimum thickness along the inspection line is 2.5 mm. It can be noticed that the SH_1 and SH_2 modes are visible and that the SH_3 and SH_4 modes were cut. The method therefore predicts that the thickness should be between 7 and 5.4 mm. This error is most likely due to the fact that this inspection line is located near a zone where the thickness varies rapidly. As shown in (Nurmalia *et al.*, 2012; Nakamura *et al.*, 2013) a mode cutoff can manifest itself in two different ways. In the case of an abrupt thickness variation, a high order mode can be converted into a lower order mode when it passes under a defect and when the thickness allows it, it may convert back to its initial state. On the contrary if the variation is progressive then the mode will be entirely reflected and no energy will propagate through the defect. A second possibility is that due to the diffraction of the generated wave a part of the ultrasonic field was not affected by the same zone of the defect (Fig. 2.1 b).

The method was applied for other inspection lines through the machined area. The scanner was moved in increments of 10 mm from the center of the defect until it reached a position where the defect no longer had an effect on the propagation of the wave, i.e., around 130 mm.

Fig. 2.11 shows the results obtained by simulation using the developed model. The oscillating curve represents the actual thickness profile of the pipe, and the gray boxes correspond to the estimated thickness range obtained with the method described above. First, it can be observed that the cutoff of SH_1 is not detected in any of the cases. This is most likely due to the proximity of its excitation frequency from SH_0 when considering an excitation around a wavelength of
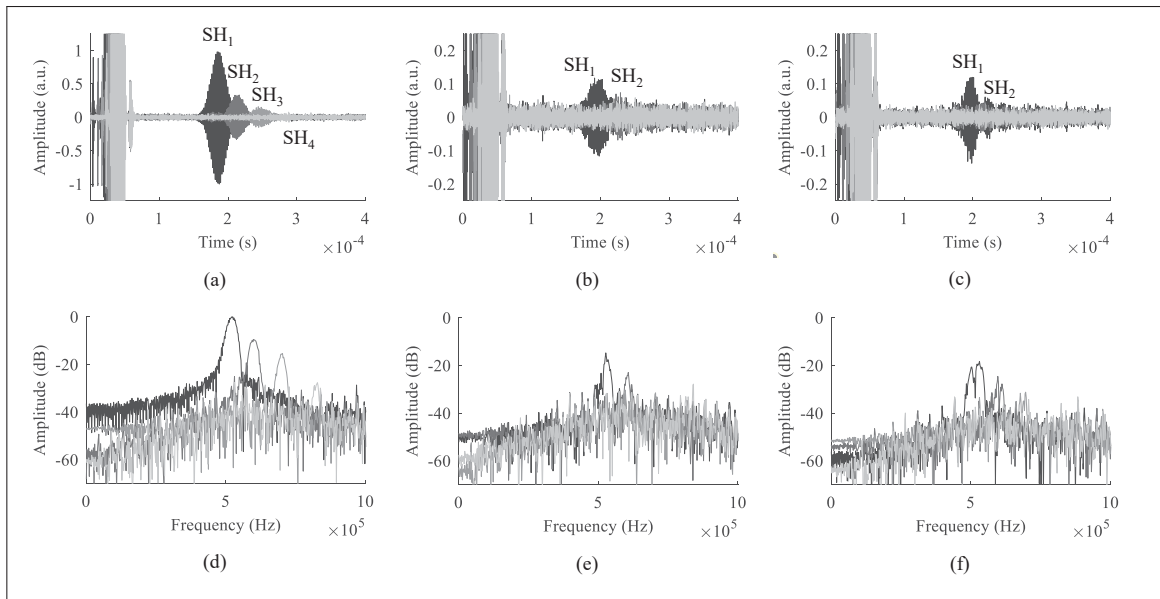
Figure 2.10 Experimental A-scans obtained with an excitation from SH_1 to SH_4 with 20-cycle Hann windowed signals centered respectively at 524, 588, 682 and 795 kHz in a configuration using small magnets and a curved coil with an inspection line positioned at 130 mm (a), 60 mm (b) and 30 mm (c) from the center of the defect as well as their respective frequency contents (d), (e) and (f)

6.4 mm in a 10.2 mm thick steel pipe. Individually energizing these two modes or extracting the amplitude of a particular mode are complex endeavors. in each of the figures, some errors (circled) are visible. They are located in areas where the thickness varies rapidly. Once the thickness has stabilized, the estimates are reliable. Fig. 2.11 (c) and Fig. 2.11 (d) are identical, which is consistent with the similarities between the ultrasonic fields generated by these EMATs (See Fig. 2.8 and Fig. 2.9)

The results of the experimental scans are shown in Fig. 2.12. Fig. 2.12 (a) shows the most important drawback of the configuration with flat magnets and the coil. The liftoff of the magnets and the coil from the pipe induces a significant loss of energy in the Lorentz force generation. This implies a low signal-to-noise ratio in the measured signals. SH_4 was not detected at any position, even in a defect-free case. In addition, the general loss of amplitude due to the presence of the defect implies a premature detection of high-order mode cutoffs. At the positions where the defect is the most severe, only noise is received, and no waveform is detected. The problem
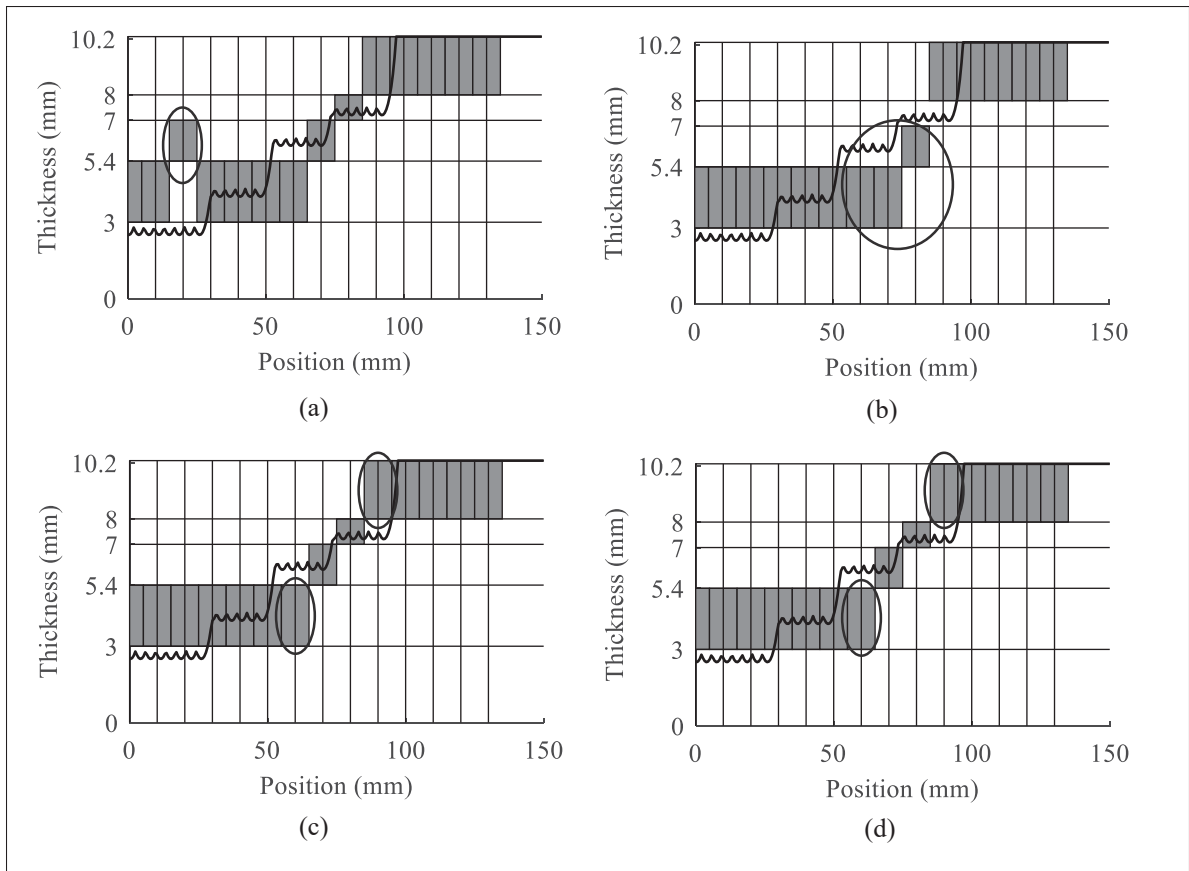
Figure 2.11   Reconstruction by simulation of the thickness profile of the steel pipe machined for this project using the different EMAT configurations selected : (a) Rectangular magnets and flat coil, (b) Rectangular magnets and curved coil, (c) Curved magnets and coils, and (d) Small magnets and curved coil. The oscillating lines represent the actual profile of the pipe. The gray boxes represent the thickness range predicted. The horizontal lines represent the cutoff thicknesses of SH_1 to SH_4. The vertical lines represent the position of the inspection lines

is solved with the other EMAT configurations. In Fig. 2.12 (b) and Fig. 2.12 (d) , some errors are still present when the variation in thickness is too steep, but the shape of the damaged area is discernible. The last case with curved magnets Fig. 2.12 (c) is the only configuration that allowed an error-free reconstruction of the pipe thickness profile.
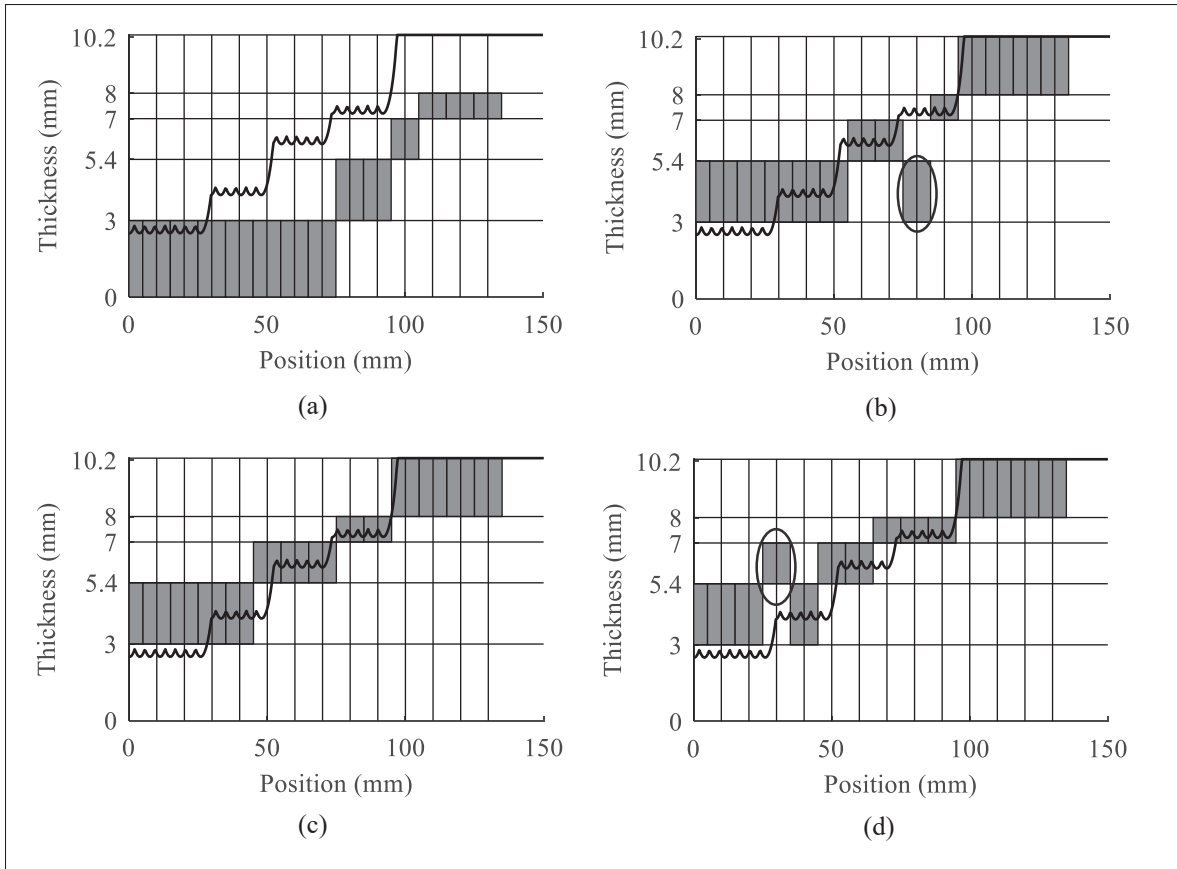
Figure 2.12   Experimental reconstruction of the thickness profile of the steel pipe machined using the different EMAT configurations selected : (a) Rectangular magnets and flat coil, (b) Rectangular magnets and curved coil, (c) Curved magnets and coils, and (d) Small magnets and curved coil. The oscillating lines represents the actual profile of the pipe. The gray boxes represent the thickness range predicted. The horizontal lines represent the cutoff thicknesses of SH_1 to SH_4. The vertical lines represent the position of the inspection lines

2.5   Discussion

In an industrial context, the main objective of pipe inspection is to detect potential leakage and dangerous situations corresponding to cases of high thickness losses. Table 2.4 as well as Fig. 2.11 and Fig. 2.12 show that the first high-order modes detect the most significant losses, as SH_0 can propagate regardless of the thickness of the waveguide ; the principal detection limit of this method is the cut-off thickness of SH_1. With the excitation method used, SH_1 detects a loss of more than 70% of the nominal thickness and SH_2 50%. Increasing the frequency would excite

more modes and thus multiply the number of detection thresholds, but this would only concern superficial regions of the waveguide. The technique described in this document efficiently used high order modes from SH_2, thus allowing experimental detection of thickness losses exceeding 50% of the nominal thickness.

Among the four configurations discussed, the solution using curved magnets is the one that allows obtaining the best reconstruction of the pipe thickness profile. The constant and minimal gap between the different components of the EMAT and the pipe allows to minimize the losses of magnetic field strength, eddy currents, and therefore, Lorentz forces. This is only valid, however, when considering an axial measurement on a pipe of a given diameter. The configuration using small rectangular magnets (Fig. 2.5 (c)) and a flexible PCB coil showed similar results either during simulations or during experimental measurements. The main advantage of this EMAT is that it allows a reconstruction of the pipe profile using only readily available components, and therefore, without using magnets designed for a single pipe diameter.

By comparing both the simulation results and the experimental measurements, a number of errors are visible. Their causes can be multiple, such as inconsistencies in the estimation of the properties of the steel during simulation, or a positioning error during the experimental scan. The relative position of the two EMATs with respect to each other is controlled precisely using the scanner, but that of the scanner with respect to the defect is only managed manually. These errors can also be classified into two categories : an overestimation and an underestimation of the thickness. Overestimating the thickness of a waveguide during an inspection is risky since the severity of a defect is minimized. A dangerous situation close to a structural failure may not be detected. Conversely, an underestimation will allow a faster detection of a defect, and even though this can lead to premature maintenance operations, the probability of failure is reduced.

The use of the first high-order SH mode, SH_1, has been limited, due to its proximity to the fundamental SH_0 mode on dispersion curves. Its cutoff thickness, therefore, could not be used. One solution to facilitate their separation would be to increase the central wavelength of the excitation. This will have the effect of reducing the excitation frequencies of the modes and

increasing the difference between SH_0 and SH_1. On the other hand, according to Eq. 2.3, this will also increase the cutoff thickness of the other modes. For example, if an excitation around a wavelength of 16 mm is considered, the excitation frequency of SH_0 and SH_1 are then respectively 200 kHz and 250 kHz, i.e., representing a spacing twice as large as in the case discussed in this article. However, the cutoff thickness of SH_1 is then 6.4 mm. The first cutoff threshold will therefore be higher than that in the context of this project, which was 5.4 mm, i.e., the cutoff thickness of SH_2 (Fig. 2.13). In addition, high-order modes will be excited in a more dispersive region.
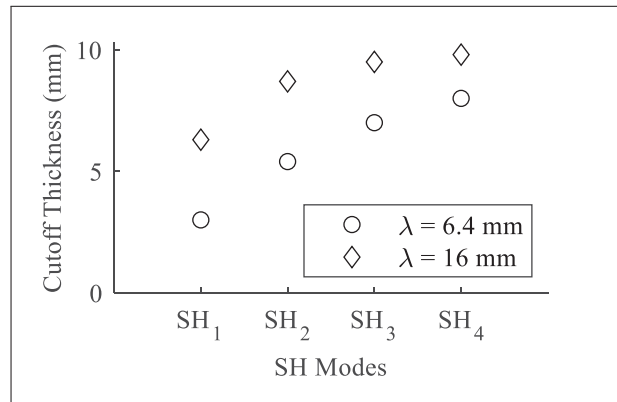
Figure 2.13   Cutoff thickness from SH_1 to SH_4 on a steel plate (ρ = 8000 kg/m^3, E = 210 GPa, v = 0.30) of 10.2 mm nominal thickness for an excitation centered around a wavelength of 6.4 mm and 16 mm

2.6   Conclusion

A comparative study of four PPM EMAT configurations and their ability to reconstruct the thickness profile of a steel pipe by structural filtering was carried out. FE simulations were used to predict the effect of magnets and coil geometry on the generated shear horizontal ultrasonic guided waves. The results obtained were verified experimentally. The simulation of the ultrasonic fields of the different EMAT configurations showed that the liftoff distance between magnets and the coil from the pipe could have a significant impact on the generation of the ultrasonic wave. Experimentally, this manifested itself in the form of a significant loss of signal-to-noise ratio, which can complicate the excitation or detection of high-order SH modes. The optimal

configuration, including a flexible PCB coil and curved magnets, allowed the pipe thickness profile to be reconstructed using the cutoffs from SH_2 to SH_4, respectively 5.4, 7, and 8 mm. This technique, therefore, makes it possible to detect a loss of 50% of the thickness of the waveguide, at the very most.

CHAPITRE 3

DEVELOPMENT OF A LINEAR ARRAY ELECTROMAGNETIC ACOUSTIC TRANSDUCER FOR SHEAR HORIZONTAL GUIDED WAVE INSPECTION

Aurélien THON[1,2] , Guillaume Painchaud-April[3] , Alain Le Duff[3] , Pierre Bélanger[1,2]

[1] Piezoelectricity and Ultrasonics Technologies and Materials Laboratory at ÉTS (PULÉTS), 1100 Notre-Dame Ouest, Montréal, Québec, Canada H3C 1K3

[2] Département de Génie mécanique, École de Technologie Supérieure, 1100 Notre-Dame Ouest, Montréal, Québec, Canada H3C 1K3

[3] Evident Industrial, 3415 Rue Pierre-Ardouin, Québec, Québec, Canada G1P 0B3

3.1 Abstract

Ultrasonic guided wave screenings have proven to be fast and reliable in detecting various types of defects in plate-like structures. Today, low frequency ultrasonic guided waves are routinely used to screen long sections of pipelines. For many years, ultrasonic guided waves at frequencies beyond the cutoff of the first high-order mode attracted interest in the research community due to the plurality of modes that can propagate. During operation at a frequency beyond the cutoff of the first high-order mode, the transduction mechanism becomes crucial for selectively exciting and detecting a single high-order mode or a group of high-order modes. Ultrasonic comb transducers allow to selectively excite and detect high-order ultrasonic guided waves at a desired wavelength. Linear array transducers are even more flexible, and allow virtually full control in the frequency wavenumber space. High-order shear horizontal (SH) modes have multiple potential applications including, for example, remote thickness gauging and crack monitoring. However, these modes are notoriously difficult to excite and detect using conventional piezoelectric transducers. Electromagnetic acoustic transducers (EMAT) make the excitation and detection of SH modes relatively simple. Periodic permanent magnet (PPM) EMAT can be used to selectively excite and detect high-order SH modes based on a desired wavelength. However, in some applications, it may be necessary to excite and detect high-order

SH modes with more control in the frequency wavenumber space. In this paper, a novel EMAT linear array is proposed using a configuration similar to a PPM EMAT but with individual coils wrapped around the magnets. The performance of the EMAT linear array in transmission and reception is demonstrated in simulations and experimentally on a 9.53 mm steel plate. The results show a successful transmission and detection of SH_0 to SH_4 for a 300 to 800 kHz frequency range.

3.2 Materials and methods

3.2.1 Guided wave propagation

Ultrasonic guided waves are mechanical perturbations forced to propagate between two boundaries. These two boundaries form a waveguide characterized by its thickness and its mechanical properties : density, Young's modulus and Poisson's ratio, in the case of a homogeneous and isotropic material. Depending on the polarization of the displacement, ultrasonic guided waves can be grouped into two categories : (1) Lamb waves, including both symmetric and antisymmetric modes, and (2) SH waves. Depending on the thickness of the waveguide and the frequency, it is possible to differentiate two types of modes that can propagate. On the one hand, the fundamental modes, S_0, A_0, and SH_0 can propagate regardless of the frequency-thickness product. On the other hand, the high-order modes are constrained to propagating only above a certain frequency-thickness product threshold, known as the cutoff frequency-thickness product. Dispersion curves represent the phase and group velocities of the different modes that can propagate in a structure as a function of the frequency-thickness product. In the case of SH waves, these can be calculated analytically with Eq. 3.1 and Eq. 3.2, and are plotted as a function of the frequency-thickness product shown in Fig. 3.1 (a) :

$$V_{p,n} = V_S \left(\frac{2fb}{\sqrt{4(fb)^2 - n^2 V_S^2}} \right) \tag{3.1}$$

$$V_{g,n} = V_S \sqrt{1 - \frac{(n/2)^2}{(fb/V_S)^2}} \qquad (3.2)$$

where $V_{p,n}$ and $V_{g,n}$ are respectively the phase and group velocity of the n_{th}-order mode, V_S is the bulk shear wave velocity, f is the frequency, and b is the thickness of the waveguide. For Lamb waves (Fig. 3.1 (b)), the transcendental equations must be solved numerically, and tools including DISPERSE® or CIVA® can be used (Rose, 2014).

The waveguide considered in this project is a 9.53 mm steel plate. This material will be considered as homogeneous and isotropic, with a density of $\rho = 8000$ kg/m^3, a Young's modulus of $E = 210$ GPa and a Poisson's ratio of $\nu = 0.3$.

When considering an ultrasonic guided wave packet, the received signals can include a plurality of modes, thus making the received waveform complex. One of the most reliable methods to separate and extract the amplitude of the different modes consists in performing a two-dimensional Fourier transform or 2D-FFT (Alleyne & Cawley, 1991). This technique requires that several measurements be taken at regular intervals in the direction of propagation. In simulation, a reception on a large quantity of points is not problematic. Experimentally, several options are possible, such as using a laser vibrometer, scanning a single-element probe or using a multi-element probe.

Piezoelectric ultrasonic phased array probes are the most common type of multi-element probes. A couplant is required for an efficient transmission of the mechanical perturbation from the piezoelectric crystal to the inspected material. In the case of shear waves, this couplant must be viscous. Indeed, the gels commonly used do not allow the transmission of shear stresses. This property implies a rapid deterioration of the coupling between the probe and the plate when scanning the probe. A solution to overcome this problem would be to use a linear array of EMAT.
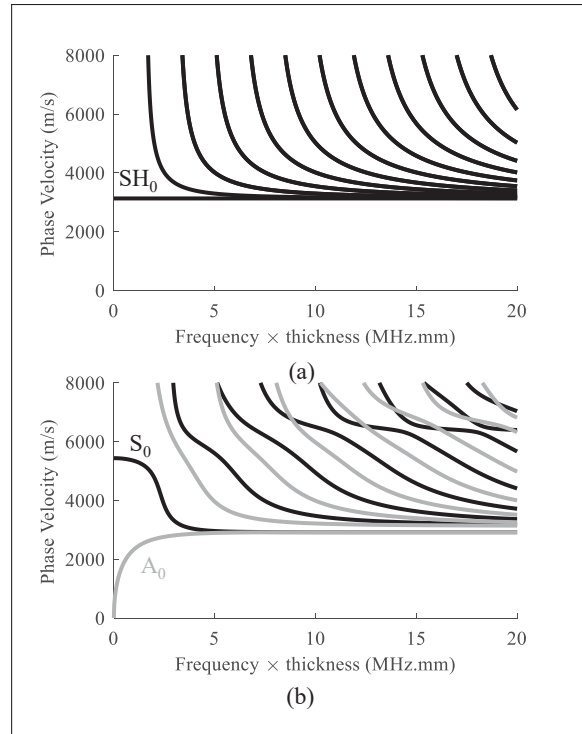
Figure 3.1   (a) SH waves phase velocity dispersion curves and (b) Lamb wave phase velocity dispersion curves in a steel plate (ρ = 8000 kg/m^3, E = 210 GPa, ν = 0.30)

3.2.2   Excitation methods

As previously stated, when using ultrasonic guided waves, the number of modes increases with the frequency. The number of modes, as well as their characteristics, such as their phase velocity and their excitation frequency, can be controlled in several ways as described hereinafter. The simplest method is to use a single-element transducer. The excitation is done without control of the phase velocity of the modes and the amplitude of each mode depends only on the frequency spectrum of the input signal and its excitability. This technique is limited in the sense that the only controllable parameter is the frequency content of the signal transmitted to the probe.

3.2.2.1   Comb excitation

A comb transducer is a multi-element probe whose elements are all activated at the same time with the same signal. This technology allows control of the excited modes as a function of the
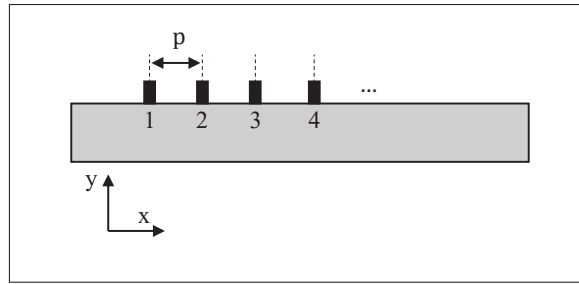
Figure 3.2   Schematic of a multi element probe on a plate. The numbers indicate the order of the elements

distance between each element or the pitch. The modes can only be excited at certain wavelengths corresponding to a multiple of the pitch. For such an excitation, the amplitude $A_n(\omega, x)$ of the mode n will be (Rose, 2014) :

$$A_n(\omega, x) = U \cdot F(\omega) \cdot C_n(x) \cdot H(\omega, x) \tag{3.3}$$

where U is the particle displacement, $F(\omega)$ is the frequency response of the elements, $C_n(x)$ is the coupling coefficient between the waveguide surface traction and the guided wave mode, and

$$H(\omega, x) = \sum_{i=1}^{N} e^{j[\omega t \pm k_x \cdot (x-x_i)]} = \frac{\sin(N\frac{k_x p}{2})}{\sin(\frac{k_x p}{2})} e^{j[\omega t \pm k_x \cdot (x-x_c)]} \tag{3.4}$$

where $\pm$ is negative for the direction of propagation +x and positive for the direction of propagation -x (see Fig. 3.2 for axis system), p is the pitch, N is the number of elements, ω is the angular frequency, $k_x = \frac{\omega}{V_p}$ is the wavenumber component along the direction of propagation x and x_c is the center of the transducer array. When p is equal to a multiple of the wavelength $\lambda = \frac{2\pi}{k_x}$, $|H(\omega, x)|$ reaches its maximum. The modes are then excited at wavelengths equal to a multiple of p. By changing the pitch of the probe p, it is then possible to generate modes at

other wavelengths. The multiplication of $|H(\omega)|$ by the frequency spectrum of the signal used allows to estimate the part of the dispersion curves on which the energy of the excitation will be distributed. Fig. 3.3 (a) shows the modes excited by a 20-element comb excitation around a wavelength of 6.4 mm when the excitation signal is a single-cycle Hann-windowed toneburst centered around 750 kHz. The figure assumes a flat frequency response of the probe.

3.2.2.2 Phase velocity excitation

Some researchers (Li & Rose, 2001; Zhu & Rose, 1999; Veit & Bélanger, 2020) improved the comb excitation method by adding a linear delay law between each element, contrary to the comb transducer described above, for which all the elements are activated at the same time. When considering a time delay increasing with a step t_0 between each element, Eq. 3.4 becomes :

$$H(\omega, x) = \sum_{i=1}^{N} e^{j[w(t-t_i))\pm k(x-x_i))]} = \frac{\sin(N\pi(\frac{p}{\lambda} \pm \frac{t_0}{T}))}{\sin(\pi(\frac{p}{\lambda} \pm \frac{t_0}{T}))} e^{j\left[w(t-\frac{N-1}{2}t_0)\pm k(x-x_c)\right]} \tag{3.5}$$

where T is the period. $|H(\omega, x)|$ is maximized when $\frac{p}{\lambda} \pm \frac{t_0}{T} = m$, with m being an integer. Therefore, the modes are excited at a wavelength depending on the pitch of the probe and the time step of the delay law t_0. It is then possible, by adjusting the delay law, to select the mode to be excited without changing the physical characteristics of the probe.

A specific case of the comb excitation with a linear delay law described above occurs when the pitch of the probe is small compared to the wavelength, i.e., $\frac{p}{\lambda} \ll 1$ (Veit & Bélanger, 2020). When considering the +x direction of propagation, the closest integer to m is 0. Eq. 3.5 is not defined for $m = 0$, but it shows that $|H(\omega, x)|$ is locally continuous in the neighborhood of $m = 0$. When $m = 0$, the excited phase velocity no longer depends on the frequency :

$$V_p = \frac{\lambda}{T} = \frac{p}{t_0} \tag{3.6}$$

This specific case allows an excitation at a constant phase velocity under the condition that $\frac{p}{\lambda} \ll 1$. Fig. 3.3 (b) shows the modes excited by a constant phase velocity excitation of 7300 m/s using a 64-element phased array probe with a pitch of 1.5 mm when the excitation signal is a single-cycle Hann-windowed toneburst centered around 750 kHz.
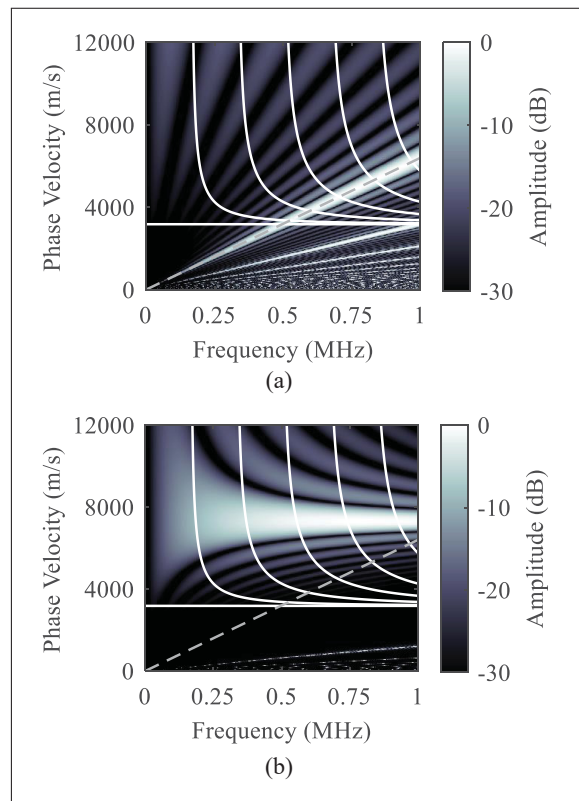
Figure 3.3   (a) Excitation map for a 20-element comb excitation around a wavelength of 6.4 mm when the excitation signal is a single-cycle Hann-windowed toneburst centered around 750 kHz, (b) Excitation map for a constant phase velocity excitation around 7300 m/s using a 64-element phased array probe with a pitch of 1.5 mm when the excitation signal is a single-cycle Hann-windowed toneburst centered around 750 kHz. The solid white line represents the phase velocity dispersion curves for SH waves in a 9.53 mm steel plate ($\rho = 8000$ kg/m^3, $E = 210$ GPa, $\nu = 0.30$). The grey dotted lines represent the minimal wavelength detectable by a linear array probe with a pitch of 3.2 mm

3.2.3   EMAT linear array

3.2.3.1   Electromagnetic acoustic transduction

EMAT refers to an ultrasound probe technology based on Lorentz and/or magnetostrictive forces. Since steel is a ferromagnetic and conductive material, both types of forces can be generated. The force F generated by an EMAT when used on steel can be calculated as follows :

$$F = F_L + F_M \tag{3.7}$$

where F_L are the Lorentz forces and F_M are the magnetostrictive forces.

A PPM EMAT (Fig. 3.4 (a)) (Vasile & Thompson, 1979; Ribichini, 2011) is composed of a racetrack coil and a magnet array whose direction of magnetization alternates with a spatial period λ. When considered for use on steel, this probe is likely to generate or detect an SH wave by a combination of Lorentz and magnetostrictive forces. Indeed, under the magnets, the direction of the magnetic field is normal to the plate, and thus perpendicular to the eddy current induced by the coil, and therefore, Lorentz forces are generated. However, when moving away from the center of the magnets, the magnetic field curves and ends up being parallel to the eddy current. In this situation, magnetostrictive forces are induced. These two phenomena occur simultaneously, at the same frequency and at the same wavelength. Sun et al. (Sun *et al.*, 2021a) showed that the coexistence of these two phenomena results in a loss of amplitude of about 30% when compared to a transduction relying purely on Lorentz forces. Since there is no change in the frequency and wavenumber excited by the probe, only the Lorentz forces will be considered for the analytical parts and the finite element simulation models. This assumption is also used multiple times in the literature s. The forces generated by the EMAT F can therefore be approximated by :

$$F \approx F_L = J_e \times B \tag{3.8}$$

where J_e is the eddy current induced by the coil in the inspected material and B is the magnetic field generated by the magnet array. From an ultrasonic transduction point of view, a PPM EMAT allows a comb excitation centered around a wavelength corresponding to the spatial period of the magnet array λ without having to use a multi-element probe. When applying Eq. 3.4 to a PPM EMAT, the pitch p corresponds to the distance between two magnets having the same magnetization direction, and the number of elements N is the number of magnets divided by two.

This basic configuration of PPM EMAT can be customized in several ways. Suresh et al. (Suresh & Balasubramaniam, 2020) (Fig. 3.4 (b)) proposed a variant where the distance between the magnets is no longer constant but varies along the transducer length thus allowing a wider spatial excitation of the SH modes. Using arc-shaped magnets, Hongyu Sun (Sun, Peng, Wang, Huang & Qu, 2021c) has shown that it is possible to focus the SH waves generated by a PPM EMAT at a given point and therefore almost doubling the amplitude of the reflected wave. A last interesting configuration is to use ring magnets with an encircling coil allowing the generation of an omnidirectional SH wave (Gauthier, Thon & Belanger, 2018; Liu, Huo, Li, He & Wu, 2021) which is particularly interesting for fast inspection of defects in plates.

The numerous configurations of PPM EMAT have allowed to multiply the applications using SH guided waves. By associating a PPM EMAT with a robotic system, it is possible to scan and reconstruct autonomously and accurately the geometrical features of a plate (Tabatabaeipour *et al.*, 2022). Complex shape such as rails (Hu *et al.*, 2021) or bent pipes (Wang, Xu & Chen, 2022) can also be inspected with these transducers. The properties of aluminum-epoxy-aluminum bonded joints can be estimated using high order SH modes (Koodalil *et al.*, 2021a; Koodalil, Rajagopal & Balasubramaniam, 2021b) by comparing the theoretical dispersion curves with the experimentally measured curves. A last application of the use of SH modes generated

by EMAT is remote thickness gauging of conductive wave guides such as plates or pipes (Suresh & Balasubramaniam, 2020; Thon *et al.*, 2022; Bélanger, 2014).
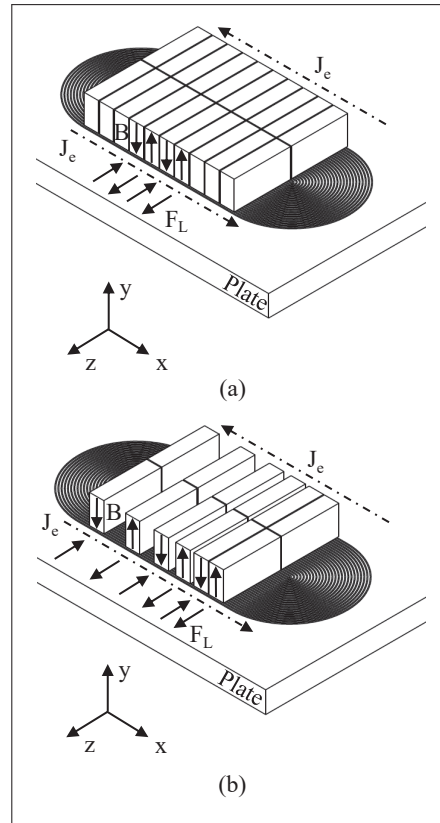
Figure 3.4   Schematic diagram of (a) a PPM EMAT and (b) a broadband PPM EMAT on a plate. B corresponds to the magnetic field generated by the magnets, J_e the eddy current induced by the coil in the plate, and F_L are Lorentz forces generated

3.2.3.2   Linear array structure

The main contribution of this paper is the development of a multi-element EMAT (Fig. 3.5 (a)). Each magnet and coil (also called elements), then generates a force field comparable to a PPM EMAT composed of a single magnet (Fig. 3.5 (b)). To facilitate the assembly of several elements, the direction of magnetization is reversed at each element so that the magnetic poles of the magnets alternate. This implies that for a given motion on a plate, two successive elements generate opposite currents. By reversing the wiring direction of the coil, it becomes possible to have a uniform Lorentz force field across all elements.

Such a probe allows a multi-element measurement compatible with an experimental measurement of SH wave dispersion curves by 2D-FFT. The minimum detectable wavelength, λ_{min}, or the maximum detectable wavenumber, is equal to twice the pitch, i.e., the distance between the center of two elements. Then, the aperture, equal to the pitch multiplied by the number of elements, determines the wavenumber step of the energy map obtained with the 2D-FFT.
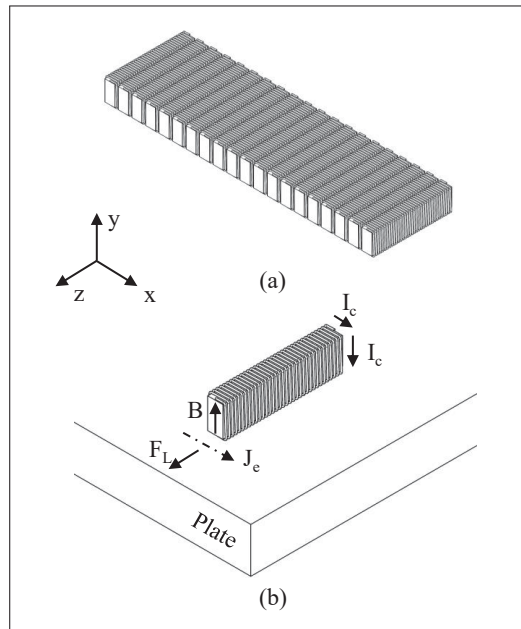
Figure 3.5   (a) EMAT linear array composed of 20 elements and (b) schematic of a single element of the EMAT linear array. B corresponds to the magnetic field generated by the magnets, I_c to the current supplied to the coil, and J_e the eddy current induced by the coil in the plate and F_L are Lorentz forces generated

3.2.4   Finite element simulation

3D finite element simulations were used to predict the capabilities of the developed EMAT linear array to detect and enable, with the help of 2D-FFT, the separation of high-order SH modes. To minimize the error inherent to FE simulations, the element size was set to allow 15 elements per wavelength using the shortest wavelength to be simulated. The time step was defined such that the fastest ultrasonic wave packet could not, in a time increment, skip an element (Drozdz, 2008). These constraints increase the required computing resources as well as the simulation

time. To remedy this problem, the propagation of the ultrasonic wave was carried out using Pogo FEA® (Huthwaite, 2014), an explicit time domain solver accelerated by graphics processing units (GPU), enabling the simulation of large models within a reasonable time frame and at a relatively low computing infrastructure cost.

Wave generation was performed by importing a force field in a Pogo mesh. For each probe, a uniform force field was imposed under the surface of each element with a time variation corresponding to the signal used. Therefore, the effect of the displacement field on the Lorentz force was not taken into account. On the receiving end, the displacements were measured on each of the nodes below the elements. The distance between the transmitting and receiving probes was set to 20 cm. Finally, absorbing boundaries, designed with the Absorbing Layer with Increasing Damping (ALID) method, were added on the edges of the plate to reduce the amplitude of the echoes and thus simulate an infinite plate (Drozdz, Moreau, Castaings, Lowe & Cawley, 2006; Cook *et al.*, 2007; Ribichini, 2011).

3.2.5   Experimental setup

3.2.5.1   Validation protocol

The linear array developed during this project has the advantage of allowing flexibility for the emission technique, which can be either a comb or a constant phase velocity excitation. On the reception side, the multi-element nature of the transducer allows to sample the propagating modes in space and time, making a 2D-FFT processing easy. To estimate the capacities of this probe, several scenarios were attempted, and in each case, the distance between the transmitter and the receiver was 20 cm :

1. The first test involved the use of a single element of the linear array structure in transmission and the 20 elements linear array probe described in Fig. 3.5 (a) and Fig. 3.7 (a) in reception. Narrow-band signals were used, with 15-cycle Hann-windowed tonebursts centered around 370 and 498 kHz. As explained at the beginning of section 3.2.2, this configuration corresponds to an excitation with a single element. The excited modes then depend mainly

on the frequency spectrum of the signals used. Fig. 3.6 shows the projection of the frequency contents of the two signals mentioned above on a phase velocity vs frequency map. Thus showing that these two configuration should allow an excitation of SH_0, SH_1, SH_2 and SH_3. This test was designed to verify the amplitude transmitted with a single element.
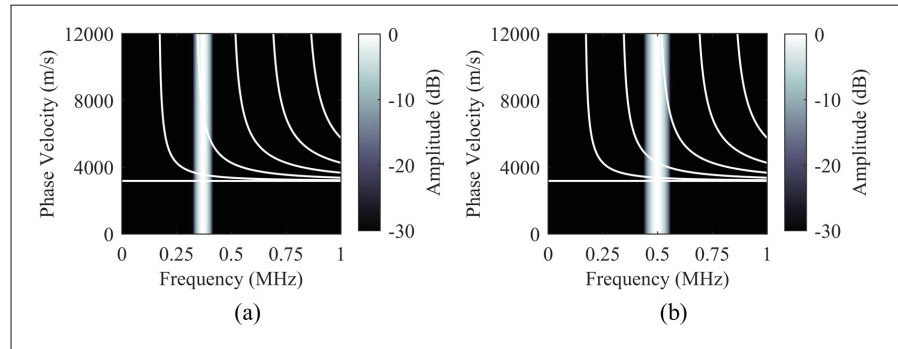
Figure 3.6   Excitation map for a single element excitation with a size of 4.3 mm when the excitation signal is a 15-cycle Hann-windowed toneburst centered around (a) 370 kHz and (b) 498 kHz

2. The second case investigated the use of a broadband PPM EMAT associated with a chirp sweeping from 300 to 800 kHz over 50 μs. By generating a multimodal wave, it was possible to evaluate whether the EMAT linear array developed allows, thanks to a 2D-FFT, to measure the amplitude of several high-order modes at the same time.

3. For the last case, the ability of the EMAT linear array to generate and detect an SH wave was compared to that of a piezoelectric shear ultrasonic phased array (PA) probe. Both probes were successively used in transmission and reception. When transmitting with the PA probe, a 1-cycle Hann-windowed toneburst centered around 750kHz was used and a delay law allowing a constant phase velocity excitation of around 7300 m/s was implemented Eq. 3.6. When the EMAT linear array was used in transmission, the acquisition was performed sequentially due to a lack of an EMAT array controller or of an interfacing system between the EMAT linear array and the Verasonics. A full matrix capture (FMC) was performed by combining all the transmitting elements of the EMAT linear array and the receiving elements of the PA probe. The signal used was a chirp sweeping from 300 to 800 kHz over 50 μs. An excitation around a constant phase velocity of 7300 m/s was generated in post-processing

by adding the corresponding delay to each transmission frame (Eq. 3.6Eq.(6)) to allow a comparison of the two technologies.

These three cases were evaluated using simulated and experimental measurements.

Finally, one of the main components of the EMAT linear array elements being a coil, it is important to evaluate the crosstalk between each element to verify that the measured signal is due to the propagation of the ultrasonic guided waves under the probe and not to interference with nearby elements. The importance of this phenomenon will be examined experimentally.

3.2.5.2   Probes

The probe developed is an EMAT linear array comprising 20 elements, each composed of a magnet and an encircling coil (Fig. 3.7 (a-b)). The coil is composed of 50 turns of 0.32 mm diameter copper wire (28 AWG). N55 grade neodymium magnets were used, and their dimensions and magnetization direction are described in Table 3.1. These magnets were used for all EMATs in this paper. Once the probe was assembled, the elementary pitch of the probe was measured equal to 4.3 mm. The minimum detectable wavelength was therefore 8.6 mm.

Tableau 3.1   Geometry and magnetization direction of the magnets (See Fig. 3.4 or Fig. 3.5 for axis system)

Width (x)	Length (z)	Height (y)	Magnetization
3.2 mm	25.4 mm	6.2 mm	Through height (y)

A broadband version of the PPM EMAT (Fig. 3.7 (c)) was realized with 2×9 magnets by progressively increasing the distance between two successive magnets according to the pattern described in Table 3.2. The coil located on the bottom side of the probe was manufactured on a flexible PCB (Fig. 3.7 (d)), thus allowing to obtain a dense and thin coil. The characteristics of the coil are summarized in Table 3.3.

A linear shear PA probe (Olympus 0.75L64-96X22-CA-P-2.5-OM-POL) composed of 64 elements centered around a frequency of 750 kHz with a pitch of 1.5 mm (Fig. 3.7 (e)), was used
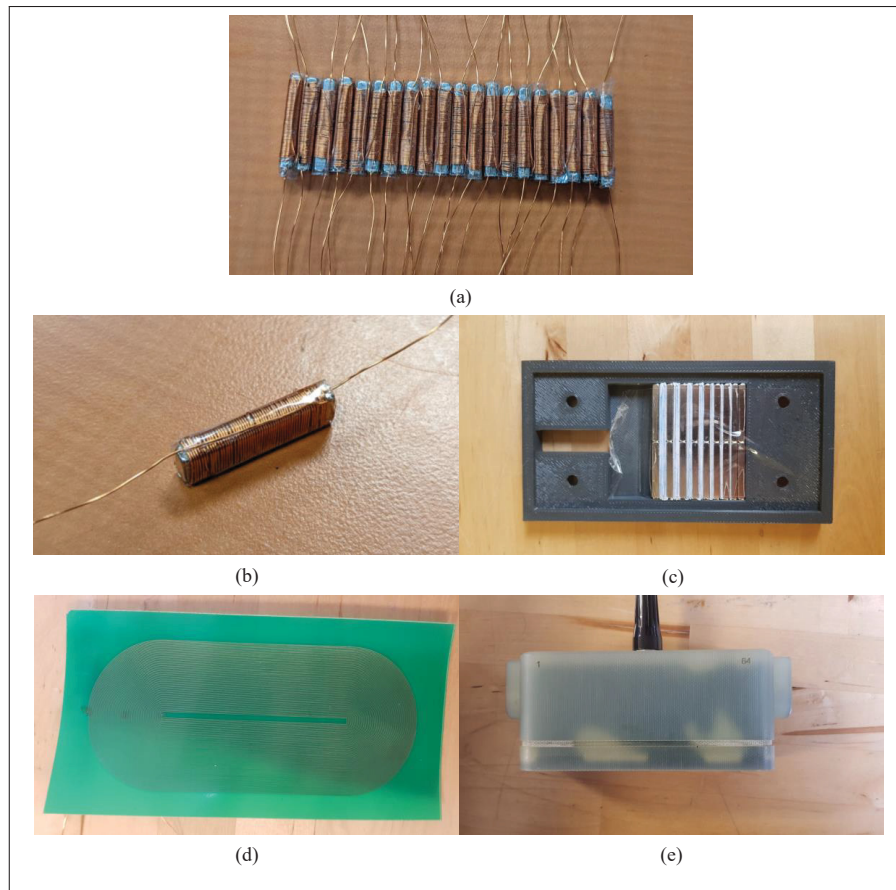
Figure 3.7   (a) 20-element EMAT linear array assembly, (b) a single element of the EMAT linear array, (c) magnet setup used for the broadband PPM EMAT in a 3D printed support, (d) 60-turn flexible coil used for the broadband PPM EMAT and (e) Olympus 0.75L64-96X22-CA-P-2.5-OM-POL shear piezoelectric phased array probe

Tableau 3.2   Distance between the center of two consecutive magnets for the broadband PPM EMAT

	$\lambda_{12}/2$	$\lambda_{23}/2$	$\lambda_{34}/2$	$\lambda_{45}/2$	$\lambda_{56}/2$	$\lambda_{67}/2$	$\lambda_{78}/2$	$\lambda_{89}/2$
Distance between two consecutive magnets (mm)	3.2	3.7	4.2	4.7	5.3	5.8	6.3	6.8

to emit and receive an SH wave at a constant phase velocity. When comparing this elementary pitch with the minimum detectable wavelength by the EMAT linear array of 8.6 mm, a ratio of $\frac{p}{\lambda_{min}} = 0.17$ is obtained. As detailed in section 3.2.2.2, the ratio is under 1 at the minimum

Tableau 3.3 Dimensions of the 60-turn flexible coil

Number of turns	Track width	Distance between tracks	Linear region dimension	Total dimension
60	0.2 mm (8 mils)	0.2 mm (8 mils)	65 mm x 52 mm	115.5 mm x 52 mm

wavelength.When using this probe, a viscous couplant was used to ensure transmission of the shear stresses.

Finally, a pair of laser Doppler vibrometers (Polytech OFV-2570) mounted on a motorized XY table allowing to take regularly spaced measurements according to the direction of propagation was used. This enabled non-contact measurement of the wavefield, and thus allowed an independent validation of the travelling wave packets.

3.2.5.3   Acquisition equipment

An electronic system allowing the complete control of the linear array structure is being designed but as it is not yet available, the elements of the EMAT linear array have been individually controlled both in transmission and reception. In transmission the signal was generated with a Keysight 33500B function generator, amplified by a RITEC RPR-4000 and then supplied to the desired EMAT or element for the EMAT linear array. On the reception side the receiving element or EMAT was connected to an 80 dB low-noise differential amplifier which made the signal detectable by a Keysight infiniiVision DSOX3014T oscilloscope.

The phased array probe was controlled with a Verasonics Vantage 64 LE Low Frequency in transmission and in reception. The Verasonics was synchronized with the oscilloscope when receiving with the EMAT linear array.

Finally, the crosstalk between the coils of the EMAT linear array was evaluated with a TiePie HS5 unit.

3.3 Results and discussion

3.3.1 Crosstalk between elements

Crosstalk is a phenomenon inherent to any measurement using alternating current. It refers to the coupling between two unconnected cables. In the case of the EMAT linear array developed, inductive crosstalk is the main source of concern : if this coupling is too strong, the current generated by one of the elements will be instantly transmitted to the other elements in the vicinity, which will pollute the measured waveforms.

To evaluate the crosstalk between the different elements, an EMAT linear array of 10 elements was assembled and positioned on the steel plate in order to simulate usage in real conditions. The first element of the structure was connected to the arbitrary function generator port of a TiePie HS5. The signal used was a 5-cycle Hann windowed toneburst centered around a frequency of 500 kHz with an amplitude of 4 V peak to peak. The results are presented in Fig. 3.8 and show the relative amplitude of the waveform due to crosstalk as compared to the signal supplied to the transmitter coil.

As can be noted, a 28 dB loss of amplitude can be seen between the first and second elements, corresponding to a division of the amplitude by 25 on a linear scale. From the fifth element, this loss is between 37 and 41 dB. The amplitude of a crosstalk signal induced between the elements will therefore be at least 28 dB below the amplitude of the waveform generated by the propagation of a wave below one of the elements. The crosstalk between the elements was therefore considered negligible for the designed EMAT.

3.3.2 Mode sensitivity

As stated in section 3.2.5, the developed EMAT linear array was tested in three scenarios. The first configuration uses an EMAT composed of an element of the linear array structure in transmission. The propagation distance was 20 cm. According to section 3.2.2, this excitation should allow a broad band excitation in the wavenumber domain. The signals used were 15-cycle
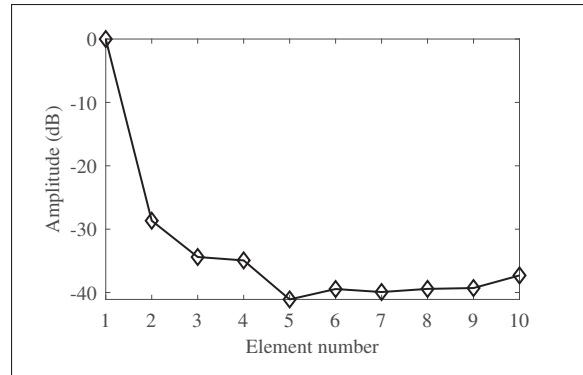
Figure 3.8   Measured crosstalk between the element of the developed EMAT linear array
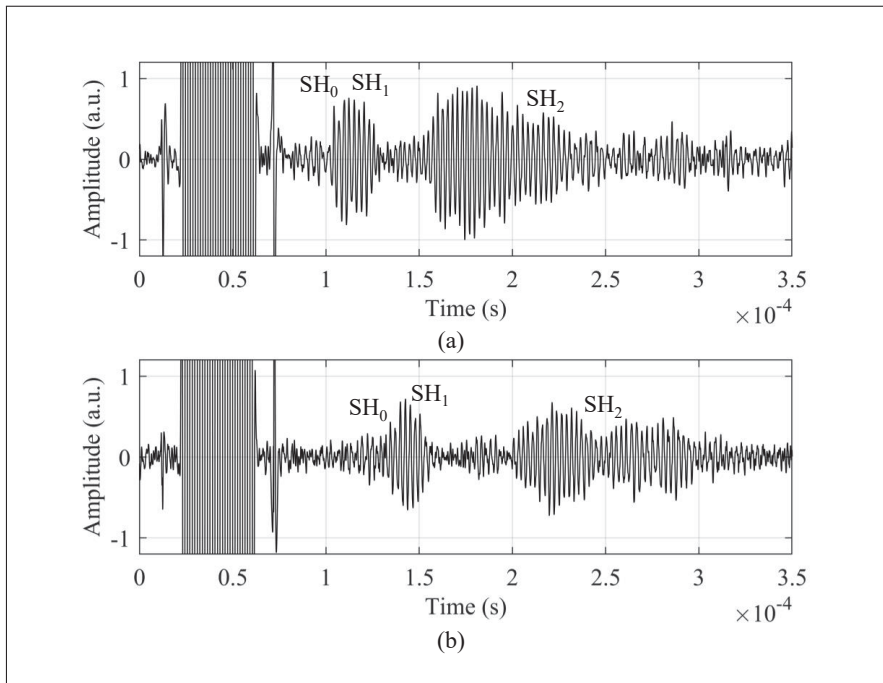
Figure 3.9   Ascans measured with the first (a) and last element (b) of the developed EMAT linear array (20 element, pitch = 4.3 mm) when transmitting a 15-cycle Hann-windowed toneburst centered around 370 kHz with a single element of the linear array structure, the propagation distance is 20 cm

Hann-windowed tonebursts centered around a frequency of 370 and 498 kHz. Fig. 3.9 shows the waveform measured by the first (Fig. 3.9 (a)) and last (Fig. 3.9 (b)) element of the EMAT linear array when a signal centered around 370 kHz is used. These waveforms can be used to make a
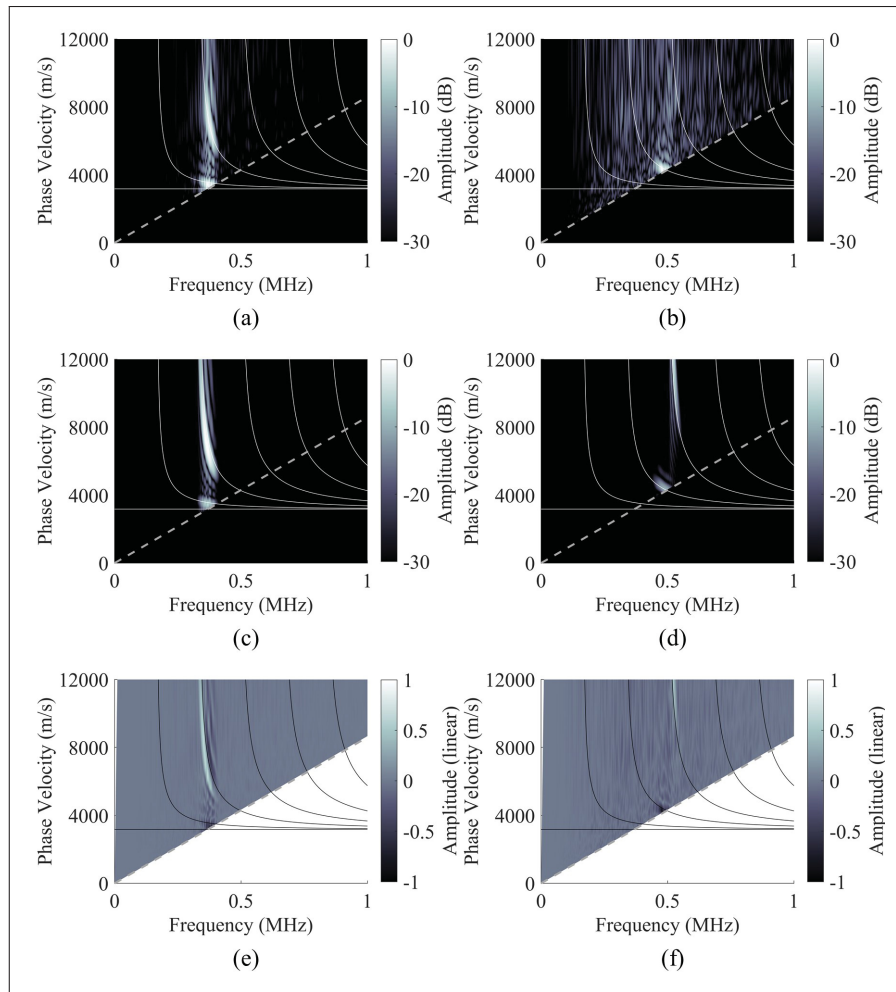
Figure 3.10   (a-c-e) 2D-FFT of the signals received with the developed EMAT linear array (20 element, pitch = 4.3 mm) when transmitting a 15-cycle Hann-windowed toneburst centered around 370 kHz with a single element of the linear array structure. (b-d-f) 2D-FFT of the signals received with the developed EMAT linear array when transmitting a 15-cycle Hann-windowed toneburst centered around 498 kHz with a single element of the linear array structure. In each case, the propagation distance was 20 cm. (a) and (b) were obtained experimentally, (c) and (d) by simulation, and (e) and (f) represent the difference on a linear scale between the simulation and experimental figure. The grey dotted lines represent the minimal wavelength detectable by a linear array probe with a pitch of 4.3 mm

preliminary analysis of the modes propagating in the steel plate. Considering Fig. 3.6 (a) it is possible to see that three modes are propagating : SH_0, SH_1 and SH_2. Among these modes SH_0 and SH_1 are excited at a similar velocity that do not allow their separation in the time domain when considering a propagation distance of 20 cm, and the length of the input signal of 15

cycles centered around 370 kHz. SH_2 is excited at a higher phase velocity and therefore has a lower group velocity than SH_0 and SH_1. Now close examination of Fig. 3.9 (a) shows that two waveforms seem to have been detected. In view of the observations made previously a fair hypothesis is that the first wave packet, around 0.12 µs, is composed of a combination of SH_0 and SH_1, the second, going from 0.15 to 0.25 µs, is SH_2. These observations are confirmed by the fact that, in view of the shape of the wave packets, the first waveform seems to be composed of weakly dispersive modes while the second is much more dispersive. To confirm these assumptions a 2D-FFT was applied to the Ascans measured by the different elements of the EMAT linear array. Fig. 3.10 shows the energy distribution of the different modes on a phase velocity vs. frequency map. Fig. 3.10 (e) and Fig. 3.10 (f) were obtained by subtracting the corresponding simulation figure from the experimental one on a linear scale. The two graphs allow to better compare the difference between the simulated and the experimental cases. When the amplitude on a pixel of the image is 1, it means that the simulations have detected a mode at this position (frequency, phase velocity) and that no mode was detected experimentally. For a value of -1, the opposite is true. When values close to 0 are obtained, simulations and experiments are in agreement and the amplitudes detected for this pixel are identical. As can be seen, during a transmission centered around 370 kHz three modes were excited. SH_0 and SH_1 were excited at a phase velocity of about 3600 m/s and SH_2 at a phase velocity higher than 4800 m/s. For the excitation around 498 kHz, only SH_2 was excited around a phase velocity of 4400 m/s. A closer look at Fig. 3.10 (e) reveals a shift of about 20 kHz on the excitation frequency of SH_2. This error can simply be explained by the fact that the properties of the steel plate for the simulations were approximated. An inaccuracy in the material properties can shift the dispersion curves on both the phase velocity and frequency axes. The preceding notwithstanding, the experimental results were very similar to the predictions obtained by simulations and prove (1) that one an element of the array is able to generate an SH wave measurable by the other elements and (2) the capabilities of the EMAT linear array when it comes to detecting and separating one or more high-order SH modes in the case of a narrow frequency band emission.
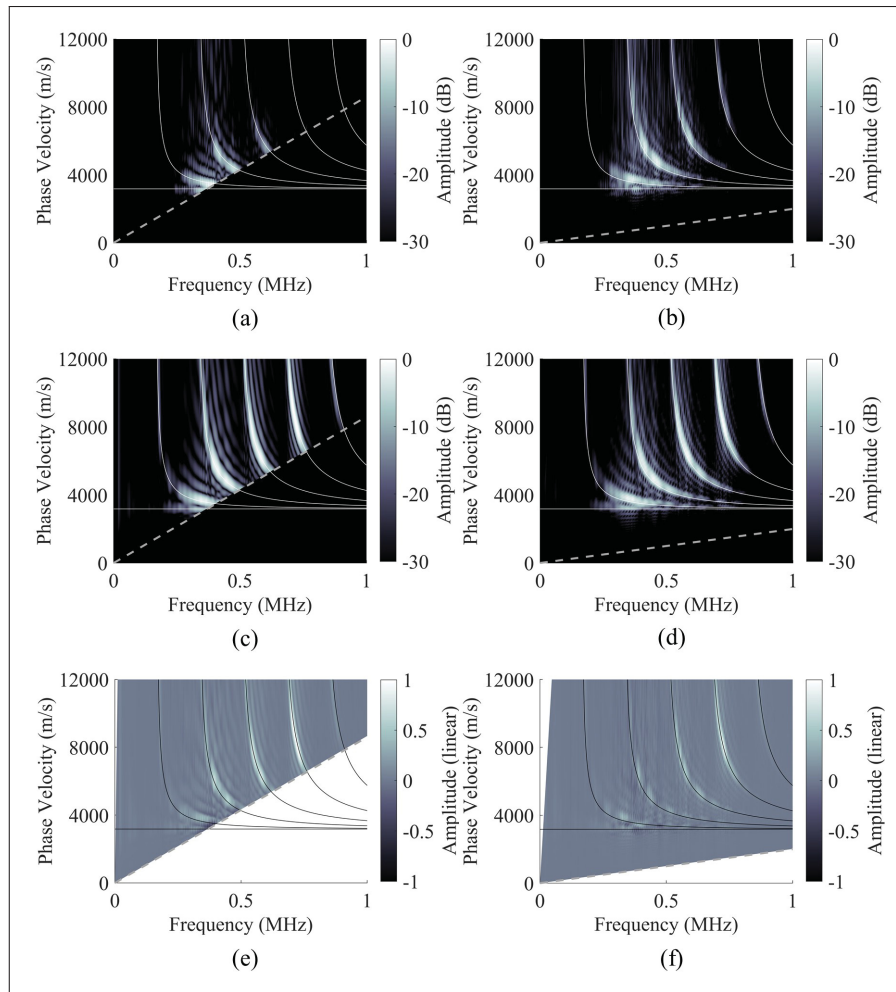
Figure 3.11 (a-c-e) 2D-FFT of the signals received with the developed EMAT linear array (20 element, pitch = 4.3 mm) when transmitting a chirp sweeping from 300 to 800 kHz over 50 μs with the broadband PPM EMAT. (b-d-f) 2D-FFT of the signals received with a laser vibrometer (90 points spaced 1 mm apart) when transmitting a chirp sweeping from 300 to 800 kHz over 50 μs with the broadband PPM EMAT. In each case, the propagation distance was 20 cm. (a) and (b) were obtained experimentally, (c) and (d) by simulation, and (e) and (f) represent the difference on a linear scale between the simulation and experimental figure. The grey dotted lines represent the minimal wavelength detectable by a linear array probe with a pitch of 4.3 mm (a-c-e) and 1 mm (b-d-f)

The second configuration tested uses a broadband PPM EMAT with a pitch varying from 3.2 to 6.8 mm over 9 magnets. The input signal transmitted to the probe was a chirp varying from 300 to 800 kHz over 50 μs. The reception was performed with the EMAT linear array and a laser vibrometer. The latter technology was used mainly to allow a comparison without the

influence of the bandwidth of the receiving probe. Fig. 3.11 (a-c-e) presents the 2D-FFT, on a phase velocity vs frequency diagram, of the signals obtained experimentally and by simulation using the EMAT linear array in reception, and Fig. 3.11 (b-d-f), using the laser vibrometer. Experimentally, SH_0 to SH_3 were detected by the EMAT linear array. However, the amplitude decreases with the mode order. The modes with the highest amplitudes were SH_0 and SH_1, while the amplitude of SH_2 was -5 dB and that of SH_3 was -12 dB. Measurements with the laser vibrometer also showed a loss of amplitude with the order of the mode but on a smaller scale. SH_0 to SH_2 were detected with a maximum amplitude of 0 dB, while that of SH_3 was -5 dB and for SH_4 it was -15 dB. The predictions by simulations were identical in both cases, and looking at Fig. 3.11 (c), it can be seen that the simulations predicted that SH_0 to SH_4 should be excited homogeneously and that SH_5 was outside the bandwidth of the signal used, and would be detected with a lower amplitude. The difference between the experimental and simulation results can be explained by the fact that no attenuation was considered in the finite element models. The amplitude of high-order modes at a higher frequency is therefore overestimated in the simulations. One explanation for the discrepancy between the results using the EMAT linear array and those using the laser vibrometer could be that the bandwidth of the EMAT and of its receiving electronics is narrower than that of the laser.

The last validation step was to compare the EMAT linear array with the Olympus 0.75L64-96X22-CA-P-2.5-OM-POL shear PA probe. Each of these two probes was used successively in transmission and reception. When using the phased array probe, the transmission was done with a single-cycle Hann-windowed toneburst centered around 750 kHz, corresponding to the central frequency of the PA probe. A delay law was implemented to enable a constant phase velocity excitation around 7300 m/s. On the reception side, the EMAT linear array was used. The separation distance was 20 cm. Sampling in time and space was performed to apply a 2D-FFT. Fig. 3.12 (a) shows the experimental results obtained in this configuration; Fig. 3.12 (c) shows those obtained by simulation and Fig. 3.12 (e) shows the difference between the figure obtained by simulation and the one obtained experimentally on a linear scale. First, it could be observed that the excitation of the modes occurs around 7300 m/s. However, only SH_3 and SH_4
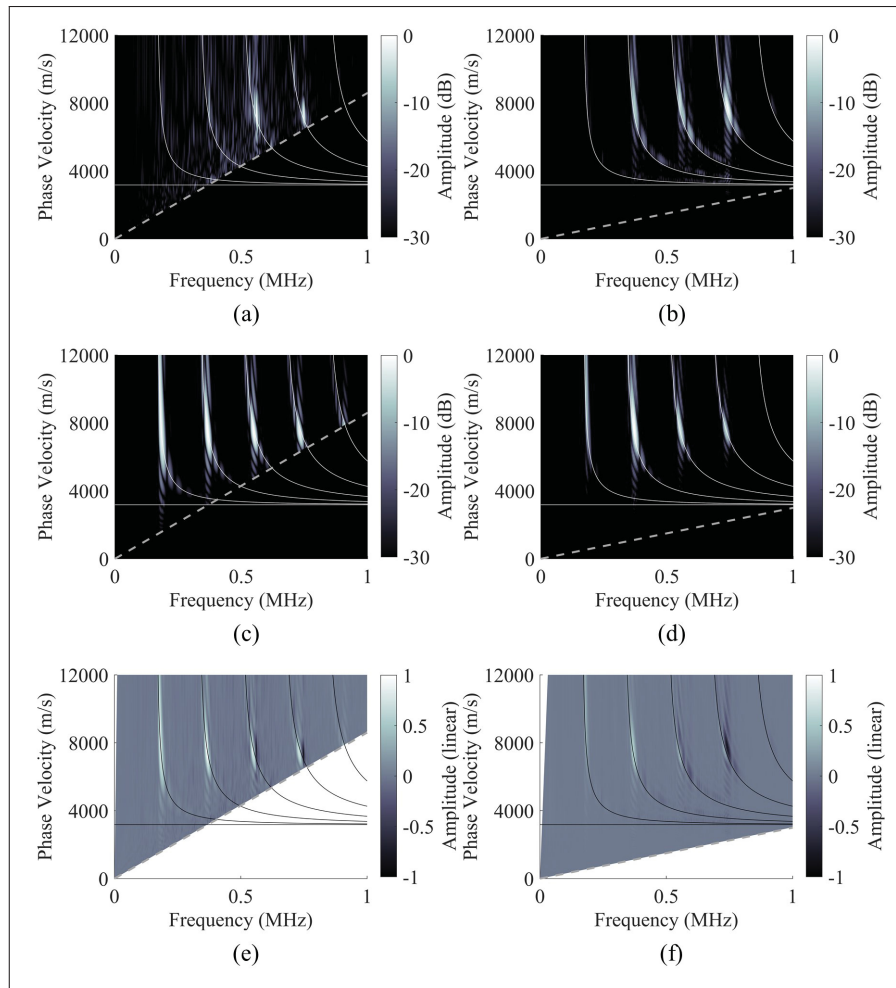
Figure 3.12   (a-c-e) 2D-FFT of the signals received with the developed EMAT linear array (20 element, pitch = 4.3 mm) when transmitting a single-cycle Hann-windowed toneburst centered around 750 kHz with the Olympus 0.75L64-96X22-CA-P-2.5-OM-POL (64-element, pitch = 1.5 mm) with a delay law enabling a constant phase velocity excitation around 7300 m/s. (b-d-f) 2D-FFT of the signals received with the Olympus 0.75L64-96X22-CA-P-2.5-OM-POL when transmitting a chirp sweeping from 300 to 800 kHz over 50 μs with the developed EMAT linear array. A constant phase velocity excitation around 7300 m/s was reconstructed in post-processing. In each case, the propagation distance was 20 cm. (a) and (b) were obtained experimentally, (c) and (d) by simulation, and (e) and (f) represent the difference on a linear scale between the simulation and experimental figure. The grey dotted lines represent the minimal wavelength detectable by a linear array probe with a pitch of 4.3 mm (a-c-e) and 1.5 mm (b-d-f)

are detected experimentally, whereas the simulations predicted an excitation from SH_1 to SH_4.

The most likely reason for this difference between the simulation and experiments relates to

the bandwidth of the phased array probe. According to the probe documentation, the amplitude of the transfer function at 500 kHz is 24 dB below its value at 750 kHz. SH_1 and SH_2 were likely generated at an amplitude too low to be detected. The second part of this validation step consisted in using the EMAT linear array in transmission and the shear PA probe in reception. The signal used was a chirp sweeping from 300 to 800 kHz over 50 μs. Due to equipment limitations, only one element of the EMAT could be activated at a time, making a constant phase velocity excitation impossible. The solution used was to proceed to an FMC by combining all the transmitting elements of the EMAT linear array and the receiving elements of the PA probe. The corresponding delay was then added, in post-processing, to each transmission frame to reconstruct a constant phase velocity excitation around 7300 m/s (Eq. 3.6). As can be seen experimentally (Fig. 3.12 (b)) or by simulation (Fig. 3.12 (d)) the modes were excited around a phase velocity of 7300 m/s. SH_1 could not be detected experimentally. SH_2 is visible, but has an amplitude 6 dB below the amplitude predicted by simulation. As before, this phenomenon is most likely due to the bandwidth of the phased array probe, since it is not present in the results of configurations involving only EMATs (Fig. 3.10 and Fig. 3.11). These results are nevertheless very encouraging because the capabilities of the EMAT linear array developed to generate and detect SH modes are similar to those of a piezoelectric phased array probe. The main difference between the EMAT linear array and the piezoelectric probe used is the frequency bandwidth since the EMAT showed transduction capabilities from 300 kHz to 800 kHz while the PA probe was limited to between 500 and 750 kHz. An increase in the frequency bandwidth of a probe has many advantages. For imaging a broadband probe will produce shorter pulses than a narrowband transducer, thus increasing the resolution of the image. And if we consider guided wave inspections numerous techniques benefit from a broadband probe such as such as material characterization (Comot, Bocher & Belanger, 2017) or remote thickness gauging (Bélanger, 2014; Thon & Bélanger, 2019; Thon *et al.*, 2022). The latter two techniques rely on the use of dispersion curves to extract parameters of a waveguide such as its nominal thickness, its mechanical moduli, or the minimum thickness along the propagation path. For this purpose, it is often necessary to excite high order SH modes in various regions of the dispersion curves. A limitation appears in the highly dispersive regions, where the phase and group velocities of the

modes are too different. This dispersion generally leads to a loss of amplitude and a stretching of the waveforms which can make the identification of a mode complex. In the three configurations tested, the EMAT linear array developed showed capabilities to generate and detect high order SH modes even in highly dispersive regions.

3.4   Conclusion

A novel multi-element electromagnetic acoustic transducer design has been reported in this paper. This probe provides great flexibility in the choice of the excitation mechanism used, such as a comb or a constant phased velocity excitation, for example. In reception, this transducer enables the propagating wave to be sampled in time and space, making it easy to apply 2D-FFT, which is particularly interesting to separate propagating modes.

The different elements are each composed of a rectangular neodymium magnet and a handmade encircling coil with copper wire. The complete structure is modeled and built to validate the performance of the probe. The crosstalk between the coils of the different elements was evaluated and a loss of 28 dB was noted between two successive elements, proving that this phenomenon is negligible. Different simulations and experimental measurements showed that the EMAT linear array is able to detect and extract the amplitude of the SH_0 to SH_4 modes, with performances similar to those of other technologies such as a laser vibrometer or a shear phased array probe on a 9.53 mm steel plate.

CHAPITRE 4

ON THE USE OF A LINEAR ARRAY EMAT FOR REMOTE THICKNESS GAUGING USING THE REFLECTED MODES ON A STEEL PIPE

Aurélien THON[1,2] , Guillaume Painchaud-April[3] , Alain Le Duff[3] , Pierre Bélanger[1,2]

[1] Piezoelectricity and Ultrasonics Technologies and Materials Laboratory at ÉTS (PULÉTS), 1100 Notre-Dame Ouest, Montréal, Québec, Canada H3C 1K3

[2] Département de Génie mécanique, École de Technologie Supérieure, 1100 Notre-Dame Ouest, Montréal, Québec, Canada H3C 1K3,

[3] Evident Industrial, 3415 Rue Pierre-Ardouin, Québec, Québec, Canada G1P 0B3

4.1 Abstract

Guided wave nondestructive testing refers to a set of fast and reliable techniques used to scan structures such as plates or pipes over medium to long range distances. The structural filtering method uses high-order modes and their cutoff frequency-thickness products to estimate the thickness along an inspection line. A corroded region, which can be approximated by a local loss of thickness, will act as a filter on the propagating modes. Because of their cutoff frequency-thickness product, some modes will not be able to propagate and will be either reflected or converted. Shear horizontal guided waves are the main candidate for structural filtering due to the simplicity of interpretation of their dispersion curves and their low sensitivity to non-viscous surface fluid loading. Electromagnetic acoustic transducers (EMAT) provide fast and efficient SH wave transduction but the most common designs, namely, periodic and permanent magnet EMAT is a mono element probe allowing modes to be excited only around a fixed wavelength. Recent work has shown that a linear array EMAT can be combined with a phase velocity excitation to allow almost complete control of the emitted waves in the frequency wavenumber space. In this paper, the linear array EMAT developed is used to estimate the minimum thickness of a defect machined on a 10.2 mm thick steel pipe with an external diameter of 323.8 mm. The measurements and finite element simulations carried out enabled us to estimate the thickness in

several positions, with a maximum error of 0.4 mm and locate the defect with an error of 10 mm over a propagation distance of 600 mm.

4.2   Introduction

Ultrasonic guided waves provide a set of nondestructive testing techniques to verify the integrity of critical parts in the oil and gas, energy, petrochemical and aeronautical industries, among others. Below the cutoff frequency of the first high-order mode, only fundamental modes can propagate, and they are now routinely used to rapidly scan large structures such as rails or pipes (Cawley *et al.*, 2003; Alleyne *et al.*, 2001, 1998). The low number of modes propagating under these conditions also allows for easy interpretation of the resulting A-scans, but the results are generally limited by their resolution due to the low frequency used. At higher frequencies or above the cutoff frequency of the first high-order mode, multiple modes can propagate. This phenomenon has allowed the development of many inspection techniques. Cracks can be detected and their growth monitored using high frequency guided waves (Chan, Masserey & Fromme, 2015; Travaglini, Bescond, Viens & Belanger, 2017). The properties of bonded joints can be estimated by inverting dispersion curves obtained with two-dimensional Fourier transforms (Pereira & Belanger, 2019) and the presence of defects can be revealed by imaging techniques such as the synthetic focusing algorithm (Yu, Fan, Puliyakote & Castaings, 2018). A final area of research is remote thickness gauging with two main methods : 1) tomography (Zimmermann *et al.*, 2021; Bélanger *et al.*, 2010; Huthwaite & Simonetti, 2013) and 2) structural filtering (Bélanger, 2014; Thon & Bélanger, 2019; Thon *et al.*, 2022; Suresh & Balasubramaniam, 2020). On the one hand, tomography uses a set of precisely positioned probes to map the velocity of guided waves propagating over the inspected area, which is then converted into a thickness map using dispersion relationships. On the other hand, structural filtering uses the cutoff phenomenon for high-order modes according to their frequency-thickness product. The latter technique typically uses shear horizontal (SH) waves as these have a lower sensitivity to surface fluid loading, and allow an easier identification of the propagating modes than with Lamb waves. The complexity here lies in the generation and detection of SH waves. Piezoelectric transducers

require the use of viscous couplants to allow efficient transmission of shear stresses from the probe to the part being inspected. This viscosity makes measurements more complicated than with conventional gel or water, especially when scanning is required. The most common solution in this context is to use electromagnetic acoustic transducers or EMATs. Several forms of EMAT can be assembled, but in most cases, a variant of a periodic and permanent magnet (PPM) EMAT is used. This structure has the advantage of allowing the emission and detection of an SH wave with a single element probe, while its main disadvantage is its lack of flexibility when it comes to the selective excitation of specific modes, as exciting or detecting a mode anywhere other than around the designed wavelength of the probe is a complex affair. Excitations around a given phase velocity can solve this problem, but these require the use of a multi-element probe. Although rare, multi-element EMATs, do exist. Isla and Cegla (Isla & Cegla, 2017) proposed a prototype 8-element EMAT phased array optimized to excite and detect bulk shear waves and Pucci et al. (Pucci *et al.*, 2019) designed a 12-element EMAT phased array operating at 2 MHz for the excitation and detection of bulk longitudinal waves. More recently, a linear array EMAT (Thon, Painchaud-April, Le Duff & Bélanger, 2023), which provides great flexibility in the excitation of SH modes, was developed, and had performances similar to that of a piezoelectric shear phased array probe.

The aim of this article is to adapt the linear array EMAT for remote thickness gauging on a steel pipe. The associated measurements herein will be carried out in reflection along the pipe axis. the multi-element nature of the probe will allow phase velocity excitations in emission and 2D-FFT in reception with an EMAT.

The paper begins with a materials and methods section, which addresses the required theoretical background on SH waves, EMATs and the excitation method. This section ends with a presentation of the experimental setup as well as the finite element model used. The results section compares and discusses finite element simulations with experiments to evaluate the capabilities of the method both in terms of thickness estimation and defect positioning. The results are discussed as they are presented. Finally conclusions are drawn.

4.3 Materials and methods

4.3.1 Guided wave propagation

Shear horizontal guided waves, or SH waves, are a type of guided wave with a polarization direction perpendicular to the propagation direction with no out-of-plane displacement. When the waveguide is a plate, the phase and group velocities of SH waves can be calculated using Eq. 4.1 and Eq. 4.2.

$$V_{p,n} = V_S \left(\frac{2fb}{\sqrt{4(fb)^2 - n^2 V_S^2}} \right) \tag{4.1}$$

$$V_{g,n} = V_S \sqrt{1 - \frac{(n/2)^2}{(fb/V_S)^2}} \tag{4.2}$$

where $V_{p,n}$ and $V_{g,n}$ are respectively the phase and group velocity of the nth-order mode, V_S is the bulk shear wave velocity, f is the frequency, and b is the thickness of the waveguide. As with all guided waves, SH modes can be separated into two categories : (1) the fundamental mode SH_0 capable of propagating regardless of the frequency-thickness product, and (2) high-order modes constrained to propagate only above a specific product called the cutoff product, which can can be calculated using Eq. 4.3 :

$$fb = \frac{nV_S}{2} \tag{4.3}$$

When this cut-off value is reached, the mode's phase velocity tends towards infinity and its group velocity towards 0. The mode can then no longer propagate. Nurmalia et al (Nurmalia *et al.*,

2012) demonstrated that two phenomena can occur. If the thickness variation is progressive, then the affected mode is reflected. On the contrary, for abrupt changes in thickness, a conversion to a mode capable of propagating will occur, and when the thickness of the waveguide allows it, the mode will return to its initial order.

Detecting a defect and estimating its minimum thickness during a structural filtering inspection is highly dependent on the size of the inspected defect. For defects that are too small in the direction of propagation, the rapid variation in thickness may result in mode conversions (Nurmalia *et al.*, 2012). Modes that were supposed to be cut off may therefore propagate through the defect, resulting in an overestimation of the minimum thickness. If the defect is too narrow, perpendicular to the direction of propagation, then it may not have a sufficient effect on the ultrasonic guided wave to be detected, whether by transmission or reflection measurement. For the latter, however, it is possible to reduce the width of the ultrasonic field at the defect by increasing the probe elevation. A wider probe will result in a less divergent beam and greater concentration of energy around the inspection line.

One crucial point in using this method involves extracting the amplitude of each mode. For this, the most versatile method is to use a two-dimensional Fast Fourier transform (2D-FFT) (Alleyne & Cawley, 1991). This technique requires sampling the propagating wave at regular intervals along the propagation direction. Experimentally, this can be done in different ways, such as scanning several points with a single-element probe or a laser vibrometer, or using a multi-element probe.

The structure inspected during this project was a steel pipe Fig. 4.1 (a), ($\rho = 8000 \, \text{kg}/\text{m}^3$, E $= 210$ GPa and $v = 0.30$) with an external diameter of 323.8 mm and a nominal thickness of 10.2 mm. A progressive corrosion zone was simulated on the outer surface of the pipe using milled spherical pockets Fig. 4.1 (b). This choice was made to allow the addition of a certain degree of variability to the thickness profile for waves propagating through it. The dimensions of the corrosion zone are detailed in Table 4.1. The equations used above assume that the waveguide is a plate, but they will be considered as valid for a pipe. This assumptions was shown to be valid

for large diameter pipes (Luo *et al.*, 2005; Velichko & Wilcox, 2009), and more specifically for the pipe used in this article (Thon *et al.*, 2022).

Tableau 4.1   Dimensions of each region of the simulated corrosion zone

Zone	Axial Dimensions (mm)	Circumferential Dimensions (mm)	Minimum Thickness (mm)
1	100	200	7.2
2	80	150	6
3	60	100	4
4	40	50	2.5
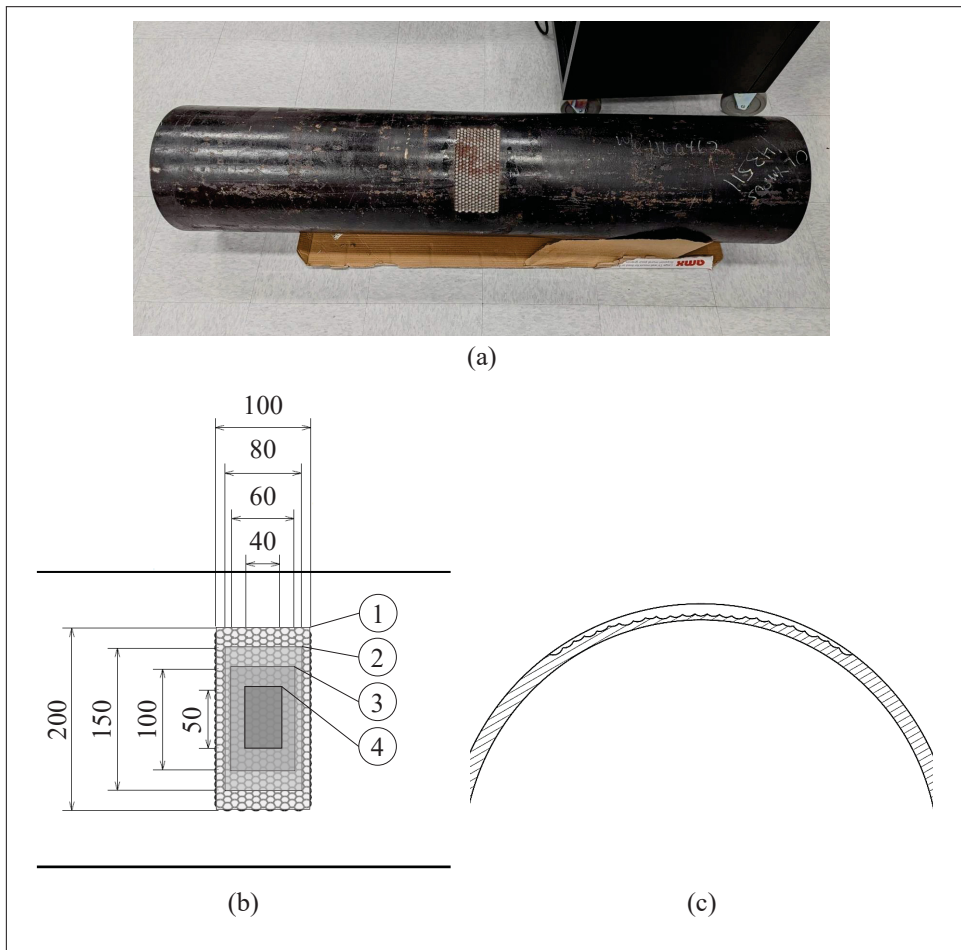
Figure 4.1   (a) Steel pipe used for the project, (b) dimensions of the progressive simulated corroded region, and (c) cross-section of the pipe at the center of the defect showing the minimum thickness profile of the pipe. All dimensions are in mm

4.3.2 Electromagnetic Acoustic Transducer

Electromagnetic acoustic transducers (EMATs) are probes that generate and detect mechanical waves in conductive and/or ferromagnetic structures. In most cases, the technology undergirding EMATs relies on two forces : (1) Lorentz forces, or the interaction between a magnetic field and currents induced in a conductive material, or (2) magnetostrictive forces arising from the ability of ferromagnetic materials to deform according to the orientation of a magnetic field. An EMAT consists of at least two elements, namely, a coil and a magnetic field generator, usually a permanent magnet.

Numerous configurations of EMAT have been developed in recent years. For bulk wave inspections, single-element EMATs can be used for thickness measurements and crack detection (Parra-Raad *et al.*, 2020). Periodic and permanent magnet EMATs (PPM EMAT) are composed of a racetrack coil and a magnet array with a polarity alternating with a spatial period equal to the wavelength excited by the transducer (Vasile & Thompson, 1979; Ribichini, 2011). PPM EMATs are commonly used for applications such as corroded waveguide thickness estimation (Suresh & Balasubramaniam, 2020; Bélanger, 2014; Thon *et al.*, 2022; Thon & Bélanger, 2019). Recently, Pialucha et al. (Pialucha, Pavlakovic, Alleyne & Cawley, 2020) used a combination of transmitted and reflected modes when measuring along the circumference of the pipe to enable a quantitative measurement of remnant thickness in corrosion under pipe support. The device used in their work is the QSR1® a scanner composed of two PPM EMAT with movable magnets allowing to select the excited wavelength. An extension of this technology was also developed, still using PPM EMAT, to enable axial inspection of pipes, the Axial QSR® . These probes are nonetheless limited in the sense that : (1) data processing techniques such as 2D-FFT cannot be used without having to move the probe, (2) to change the wavelength of the excitation the size or the space between the magnets must be changed. Several multi-element EMATs have been developed, including the 8-element prototype phased array EMAT by Isla and Cegla (Isla & Cegla, 2017), which is optimized to excite and detect bulk shear waves in steel at 1 MHz, or the 12-element phased array EMAT by Pucci et al. (Pucci *et al.*, 2019) which operates at 2 MHz for the excitation and detection of bulk longitudinal waves ; more recently, there was a

linear array EMAT developed for SH guided wave inspection (Thon *et al.*, 2023), compatible with advanced guided waves generation such as phase velocity excitation.
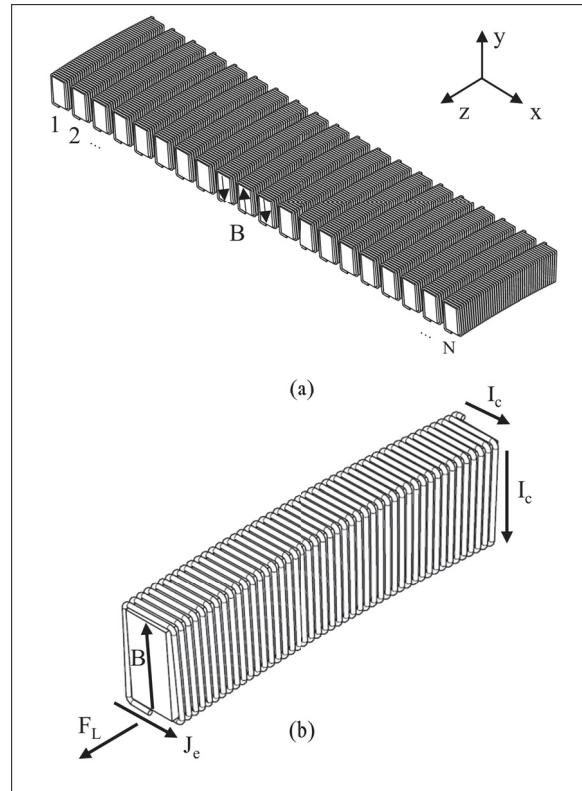
Figure 4.2   (a) Curved linear array EMAT composed of N elements, (b) a single element of the curved linear array structure. The numbers 1 to N represents the place of the element in the structure, B corresponds to the magnetic field generated by the magnets, I_c to the current supplied to the coil, and J_e the eddy current induced by the coil on the plate and F_L are Lorentz forces generated

This project used a variant of a linear array EMAT with curved magnets to better adapt to the pipe curvature (Fig. 4.2 (a)). This transducer is used on steel, and thus, Lorentz and magnetostrictive forces can be generated, but only the former will be considered for analysis part and for finite element simulations. This is a common assumption (Isla & Cegla, 2017, 2016; Ribichini *et al.*, 2012a,b) which has been shown to be valid since in the case of a PPM EMAT the superposition of Lorentz forces and magnetostrictive forces does not change the excited frequencies or wavelengths, but only the amplitude (Sun *et al.*, 2021a). The forces generated by the EMATs F will therefore be approximated by the Lorentz forces F_L :

$$F \approx F_L = J_e \times B \qquad (4.4)$$

where J_e is the eddy current induced by the coil and B is the magnetic field generated by the magnets. The different linear array EMATs built in this project were all identical and consisted of 20 curved magnets (Fig. 4.2 (b)), whose dimensions are described in Table 4.2, and a 50-turn copper coil with a wire diameter of 0.315 mm. Once the probe was assembled, its pitch was measured at 4.3 mm. The pitch limits the range of estimated remnant thickness. Indeed, when applying a 2D-FFT, the pitch, p, or distance between each measurement point, sets the minimum wavelength that will be detectable, $\lambda_{min} = 2 \cdot p = 8.6$ mm. By plotting this value on the dispersion curves, the maximum detectable frequencies, and therefore, the minimum detectable thicknesses for each mode, can be determined. As can be seen in Fig. 4.3 for SH_1 and SH_2 these maximum frequencies are respectively 400 and 483 kHz. Using Eq. 4.3, it can therefore be deduced that with the linear array EMAT built for this project, SH_1 will detect at least a thickness of 4 mm and SH_2 of 6.6 mm. SH_1 should theoretically allow the detection of zones 1 and 2 of the defect Fig. 4.1. Zone 3 has a minimum thickness equal to the detection limit. Given that SH_1 is close to SH_0 in this region on the dispersion curves, the estimation of the thickness here will be complex, if not impossible. SH_2 will only allow the detection of zone 1.

Tableau 4.2   Dimension of the curved magnet used

Width (mm)	Inner Radius (mm)	Arc (degree)	Height (mm)	Magnetization direction
3.2	162.9	9	6.4	Radial in both direction

4.3.3   Phase velocity excitation

Previous studies have shown that it is possible to use a multi-element probe and to activate elements according to a delay law to achieve an excitation around a constant phase velocity
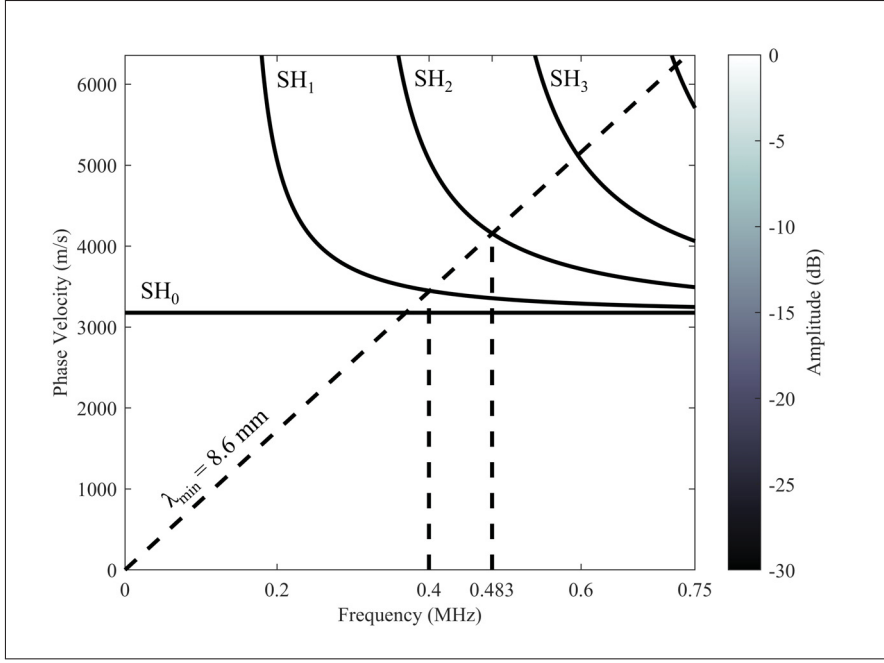
Figure 4.3   Phase velocity dispersion curves on a 10.2 mm thick steel (ρ = 8000 kg/m³, E = 210 GPa, v = 0.30) pipe with an internal diameter of 323.8 mm. The dashed inclined line represents the minimum detectable wavelength for a probe with a pitch of 4.3 mm. The two vertical dotted lines correspond to the maximum frequencies of SH1 and SH2 detectable by a probe with a pitch of 4.3 mm

(Li & Rose, 2001; Zhu & Rose, 1999; Veit & Bélanger, 2020). If t_0 is the time increment of the delay law, the amplitude of $A_n(\omega, x)$ of the mode n will be (Rose, 2014) :

$$A_n(\omega, x) = U \cdot F(\omega) \cdot C_n(x) \cdot H(\omega, x) \tag{4.5}$$

where U is the particle displacement, $F(\omega)$ is the frequency response of the elements, $C_n(x)$ is the coupling coefficient between the waveguide surface traction and the guided wave mode, and

$$H(\omega, x) = \sum_{i=1}^{N} e^{j[w(t-t_i)) \pm k_x(x-x_i))]} = \frac{\sin(N\pi(\frac{p}{\lambda} \pm \frac{t_0}{T}))}{\sin(\pi(\frac{p}{\lambda} \pm \frac{t_0}{T}))} e^{j\left[w(t-\frac{N-1}{2}t_0) \pm k_x(x-x_c)\right]} \tag{4.6}$$

where ± is negative for the direction of propagation +x and positive for the direction of propagation −x (see Fig. 4.2 for axis system), p is the pitch, N is the number of elements, ω is the angular frequency, T is the period, λ and k_x are respectively the wavelength and wavenumber component along the direction of propagation x, and x_c is the center of the transducer array. The amplitude of the excited modes can be estimated by calculating $|H(\omega, x)|$. $|H(\omega, x)|$ is maximized when $\frac{p}{\lambda} \pm \frac{t_0}{T} = m$, with m being an integer. If a propagation in the +x direction is considered where ± is negative, then a special case can be considered where $m = 0$. $|H(\omega, x)|$ is not defined for $m = 0$, but it is continuous in the neighborhood of $m = 0$. In this particular configuration, the excited phase velocity no longer depends on the frequency and will be equal to :

$$V_p = \frac{\lambda}{T} = \frac{p}{t_0} \tag{4.7}$$

It is then possible to change the excited region of the dispersion curves by changing only the delay law and no properties of the probe. By associating the right delay law and the right signal, the excitation can then be focused on a defined point of the dispersion curves to purely excite a given mode.

4.3.4   Experimental setup

The originality of this project lies in the use of linear array EMAT for structural filtering measurement. The inspection is carried out in reflection and along the axis of the pipe. The multi-element nature of the transducer is a significant advantage, enabling the use of phase velocity excitation in transmission and 2D-FFT processing in reception.

Fig. 4.4 provides an illustration of the experimental setup when the probes are placed in front of the defect. As with most applications requiring an EMAT, the receiving signal needs to be pre-amplified. This step was done with a custom home-made differential amplifier set to an
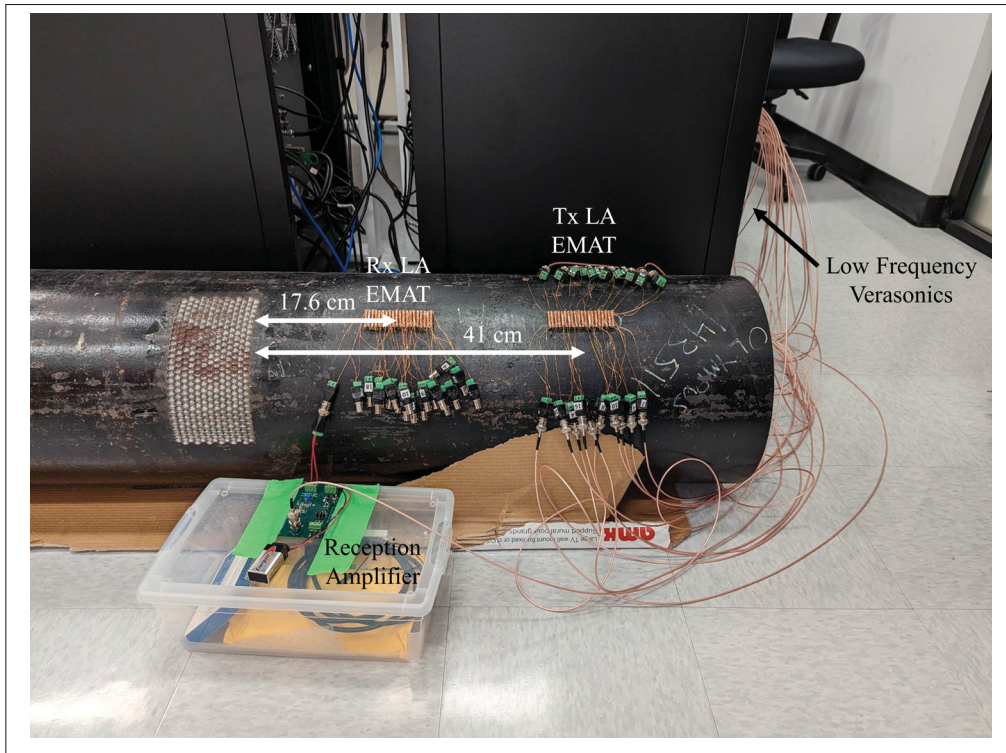
Figure 4.4   Experimental setup with the inspection line positioned in front of the region with a minimum thickness of 6 mm. The distances are from the center of the probes to the beginning of the defect and correspond to those used in all measurements involving the presence of the defect

amplification of 80 dB. This amplifier makes it impossible to carry out pulse-echo measurements with a single probe, which is why two linear array EMATs were assembled, one acting as a transmitter and the other as a receiver.

The linear array EMATs were controlled in transmission by a Vantage 64 LE Low Frequency system equipped with a UTA 160DH/32 LEMO front panel. The 20 elements of the emitter probe were each connected directly to a specific LEMO ports and activated according to a specific delay law (Table 4.3 and Table 4.4). Since only one reception amplifier was available the signals were acquired successively on each element of the receiving linear array EMAT.

Multiple signals, with an amplitude of 20 V, i.e. 40 Vpp, were used to scan a wide band of the SH_1 and SH_2 dispersion curves. Although the voltage may be higher when firing with only one

element (90 V or 180 Vpp) it was limited by the Verasonics system when firing with the 20 elements of the linear array EMAT. In each case, the signals were 10 cycles Hann-windowed toneburst. SH_1 was excited from 175 to 400 kHz to allow a detection range from 4 to 9 mm, and SH_2 was excited from 400 to 475 kHz for a detection range from 6.7 to 7.9 mm. Knowing the excitation frequency ranges of each mode, the phase velocities and excitation frequencies were calculated from Eq. 4.1. Delay laws were implemented to allow a pure excitation of the desired mode, as detailed in section 4.3.3. The parameters of each signal are detailed in Table 4.3 and Table 4.4.

On the reception side, the Ascans were filtered by a bandpass filter going from 50 kHz to 1 MHz. The limits of the filter were selected to prevent the removal of any feature from the signal inside the frequency range of interest (175 to 475 kHz). The signals were also averaged 5000 times, which with the Verasonics system used, was done at a rate of 15 s per measured A-scan. The number of averages used is not a minimum number, but led to low noise 2D-FFT figures. Each scanned position took about 1 and a quarter to 1 and a half hours of measurement for both SH_1 and SH_2. This time is attributable to the fact that the reception was done one at a time on all the elements because of the single receiving amplifier used. A system allowing the parallel (or simultaneous) amplification of all the elements of the receiving probe would reduce this acquisition time considerably.

Tableau 4.3　Parameters of the 10 cycles Hann-windowed toneburst used for the excitation of SH_1

Frequency (kHz)	175	200	225	250	275
Targeted phase velocity (m/s)	6968	5065	4403	4062	3855
Delay law time increment (μs)	0.62	0.85	0.98	1.06	1.12
Frequency (kHz)	300	325	350	375	400
Targeted phase velocity (m/s)	3718	3620	3548	3493	3450
Delay law time increment (μs)	1.16	1.19	1.21	1.23	1.25

Tableau 4.4   Parameters of the 10 cycles Hann-windowed toneburst used for the excitation of SH_2

Frequency (kHz)	400	425	450	475
Targeted phase velocity (m/s)	5065	4671	4403	4209
Delay law time increment (μs)	0.85	0.92	0.98	1.02

4.3.5   Finite element simulation

Before performing the experiments in the previous section, each configuration was simulated with a finite element model. For an ultrasonic wave propagation simulation, it is recommended to select a mesh size allowing at least 10 elements per wavelength and a time step such that in one time increment, the ultrasonic wave cannot skip a node (Drozdz *et al.*, 2006). For safety reasons, the element size was chosen to allow 20 elements of the smallest excited wavelength. This led to heavy models both in terms of computation time and resources required. To allow a resolution of the simulations within a suitable time frame, Pogo FEA (Huthwaite, 2014) an explicit time domain solver accelerated by graphics processing units (GPU), was used.

The geometries of the pipe and of the defect region were created using the plan used for the machining. Wave generation was performed under each element position by importing a uniform force field into Pogo with a time variation corresponding to the signal and delay law used. This makes the hypothesis of a weak coupling meaning that the effect of the displacement field on the Lorentz forces was not taken into account. The positions of the probes were identical to those from the experimental measurements. Finally, to reduce the size of the model, the pipe was cut, and absorbing boundaries, designed with the Absorbing Layer with Increasing Damping (ALID) method, were added on the edges to reduce the amplitude of the echoes (Rajagopal, Drozdz, Skelton, Lowe & Craster, 2012).

4.4   Results and discussion

4.4.1   Thickness estimation

The first step of the experimental measurements was to verify the modes generated by the probe and that were capable of propagating in the waveguide. To this end, the two linear array EMATs were placed 30 cm apart on a healthy region of the pipe. Then, the signals described in Table 4.3 and Table 4.4 were used. The 2D-FFT obtained from the experimental measurements and the simulations are shown in Fig. 4.5. In this figure (a-b), SH_1 was experimentally excited from 171 kHz to 400 kHz and from 163 kHz to 400 kHz during simulations. Using Eq. 4.3 it is therefore possible to predict that SH_1 should be able to detect thicknesses between 4 and 9.3 mm. The main difference in the experimental measurements is the presence of an important feature around 240 kHz. This feature was detected continuously along the phase velocity axis, which indicates that it is not due to a guided wave mode. Multiple tests were carried out, but did not allow to identify this phenomenon. This parasitic component will not be considered in the measurement of the cutoff frequencies. The amplitude around 240 kHz won't be used, which means that it will be difficult to measure thicknesses close to 6.6 mm Eq. 4.3. For Fig. 4.5 (c-d) SH_2 was detected from 410 to 475 kHz experimentally and from 380 to 475 kHz by simulation without any parasitic component implying a detection range for SH_2 ranging from 6.6 to 7.8 mm. For both modes, the upper limits were equal, thanks to the maximum frequency detectable by the probe, and thus, the minimum detectable wavelength, $\lambda_{min} = 2 \cdot p = 8.6$ mm. The differences for the lower limits of the detection ranges can be explained either by an inaccuracy in the simulations, particularly the modulus of the material used, or by the fact that the impedance of the emission chain composed of the probe and the Verasonics can alter the shape of the signals used. However, the errors between the experimental measurements and the predictions obtained by simulations remain very small.

The transmitting EMAT was then placed 41 cm in front of the defect, while the receiving EMAT was place 17.6 cm away. These distances were chosen to ensure that the first pass of the wave and the measured echo did not overlap in the time domain, and would therefore, produce no
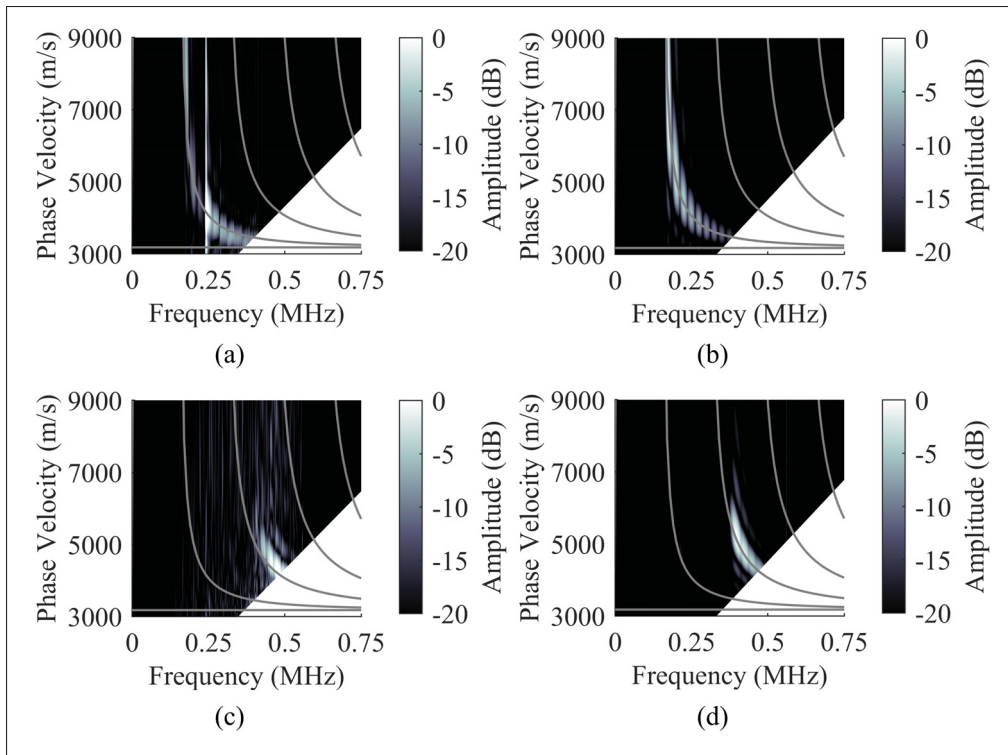
Figure 4.5   Experimental (a-c) and simulated (b-d) 2D-FFT obtained using a scan of SH_1 (a-b) and SH_2 (c-d) when the linear array EMATs are placed on a steel pipe (ρ = 8000 kg/m^3, E = 210 GPa and ν = 0.30) of nominal thickness of 10.2 mm with an inner diameter of 323.8 mm

interference in the Ascan. The inspection line was centered : (1) in an area with a minimum thickness of 6 mm, (2) in the transition zone ranging from 6 to 7.2 mm, and (3) in an area with a minimum thickness of 7.2 mm. In experimental measurements and simulations, a mode is considered cut off when its amplitude drop 20 dB below the maximum detected amplitude on 2D-FFT figures (Fig. 4.6 and Fig. 4.7), excluding the amplitude due to the parasitic feature in the case of the experimental measurement with SH_1.

In the first position, Fig. 4.6 (a-b) and Fig. 4.7 (a-b), the experimental cutoff of SH_1 was measured at 257 kHz, and from simulations, the predicted value was 259 kHz. Using Eq. 4.3 these cutoff frequencies can be converted to an estimation of the minimum thickness, respectively 6.2 and 6.1 mm, for a maximum error of 0.2 mm. SH_2 was received over its entire excitation range, meaning that the minimum thickness was smaller than that detectable by SH_2, i.e. 6.6mm.
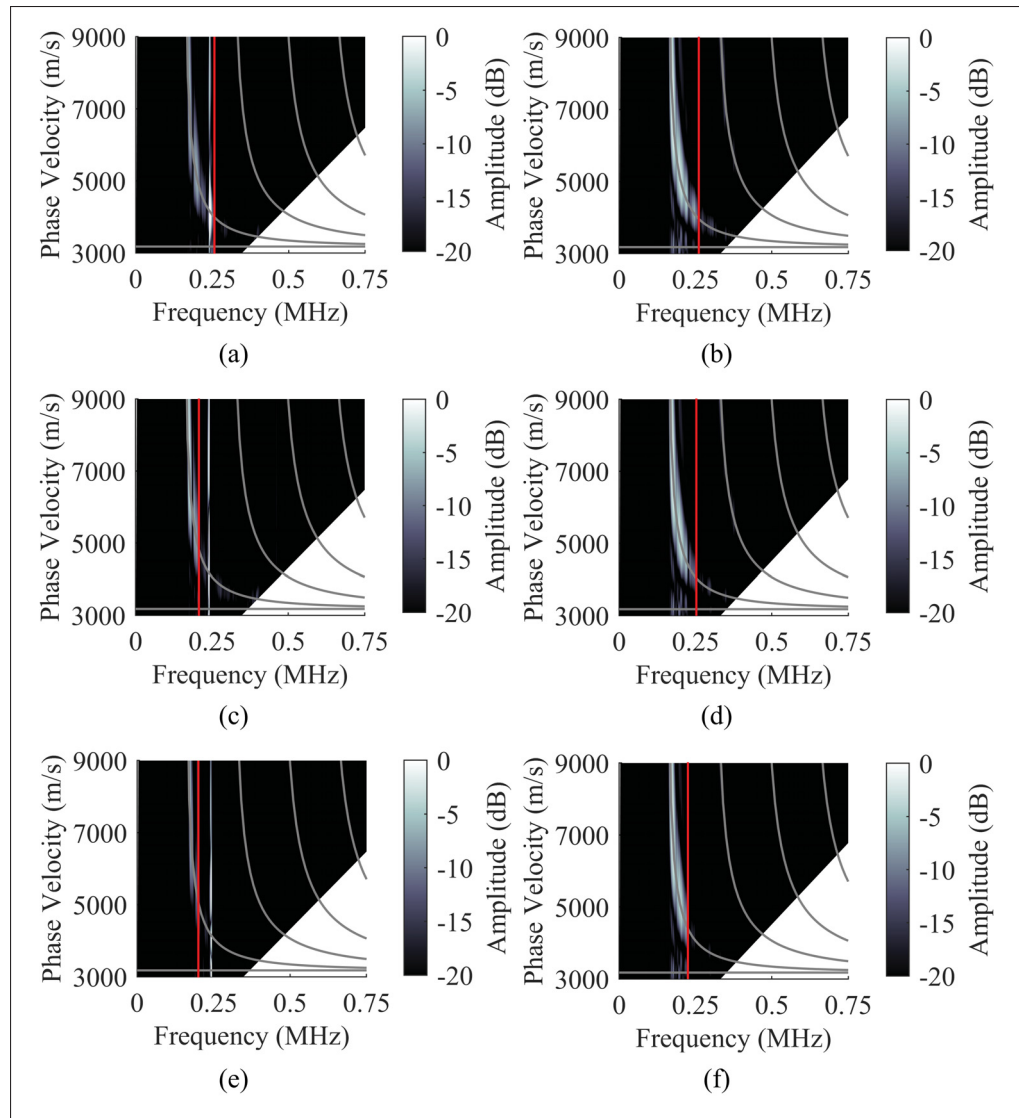
Figure 4.6   Experimental (a-c-e) and simulated (b-d-f) 2D-FFT obtained using a scan of SH$_1$ when the linear array EMATs are centered in the middle of the 6 mm (a-b), 7.2 (e-f) mm deep region and at the edge of these regions (c-d). The vertical lines represent the detected cutoff frequencies

When the probes were at the second position (Fig. 4.6 (c-d) and Fig. 4.7 (c-d)), SH$_1$ was cut at 232 kHz in accordance with the experimental data and at 250 kHz in accordance with the simulations. The corresponding thicknesses for SH$_1$ were 6.8 and 6.4 mm. The use of SH$_2$ still did not show clear cuts, but disturbances started to appear around 467 kHz in both the experimental measurements and the simulations, corresponding to a minimum thickness of 6.8

mm. In each case, the predicted thickness was consistent with the position of the probes since EMATs were positioned in front of a region with a minimum thickness transitioning from 6 to 7.2 mm. The difference between the experimental and finite element estimates using SH_1 is probably due to the proximity to the parasitic frequency mentioned above.

At the last position, with an actual minimum thickness of 7.2 mm (Fig. 4.6 (e-f) and Fig. 4.7 (e-f)), the cutoff of SH_1 was detected at 208 kHz during measurements and at 220 kHz by simulation, allowing to estimate the minimum thickness as equal to 7.6 and 7.2 mm. When SH_2 was excited, the cutoff frequency was measured equal to 452 kHz against 441 kHz according to the simulations, and the corresponding minimum thicknesses are 7 and 7.2 mm.

These series of measurements showed that associating a linear array EMAT and phase velocity excitations allow to excite purely SH modes, as well as to estimate the thickness of the pipe for thicknesses greater than 6.2 mm. The theoretical limit in the actual configuration for SH_1 is 4 mm (section 4.3.2). Using SH_2 is more limiting than using SH_1 since theoretically, the detection range is 6.6 to 7.8 mm against 4 to 9.3 mm, but in the case of the experimental setup used, this mode allows to detect minimum thicknesses that would imply cutoff frequencies close the parasitic frequency observed with SH_1.

4.4.2   Defect positioning

One advantage of reflection measurement is the ability to localize the defect. Fig. 4.8 show the Ascans obtained by exciting SH_1 when the probes were centered on the region with a minimum thickness of 6 mm. The signal used allows a phase velocity excitation around a frequency of 300 kHz and a phase velocity of 3718 m/s. Even if the signal quality is poor three feature can be identified : (1) the initial burst, (2) the waveform due to a direct transmission between the transmitter and the receiver, and (3) the echo due to the defect.

The reflected mode was detected 223 μs after the maximum amplitude of the initial burst leading to a propagation distance of 606 mm, for a group velocity of 2715 m/s (Eq. 4.2). By subtracting the distance between the emitter and the receiver the estimated defect location was
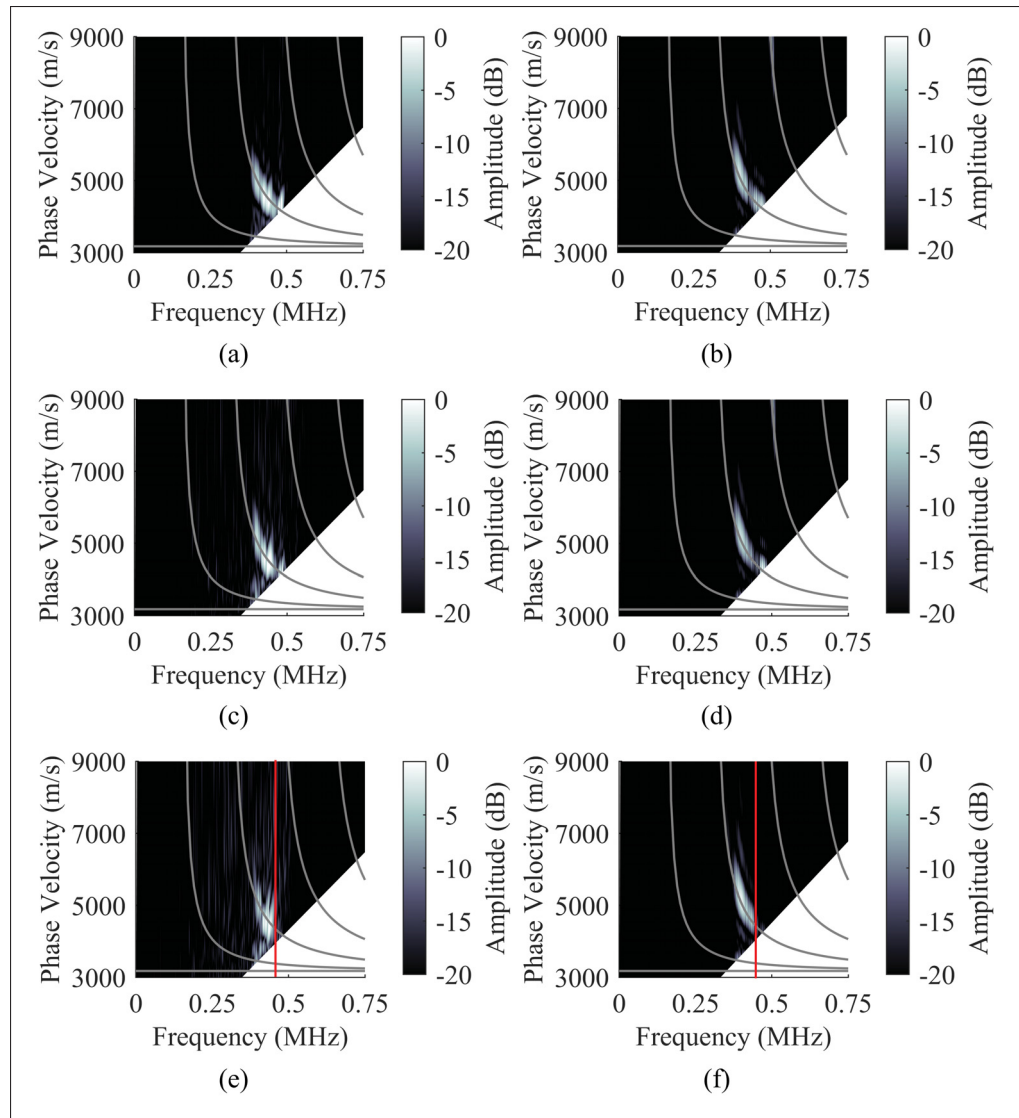
Figure 4.7   Experimental (a-c-e) and simulated (b-d-f) 2D-FFT obtained using a scan of SH$_2$ when the linear array EMATs are centered in the middle of the 6 mm (a-b), 7.2 (e-f) mm deep region and at the edge of these regions (c-d). The vertical lines represent the detected cutoff frequencies

166 mm ahead of the receiving element. The actual distance was measured equal to 176 mm. This position estimate remains approximate due to the low signal-to-noise ratio of the signal used, but shows that an inspection using the prototype linear array EMAT developed enables the defect position to be estimated using a reflection measurement, which is a major advantage over transmission-only inspection.
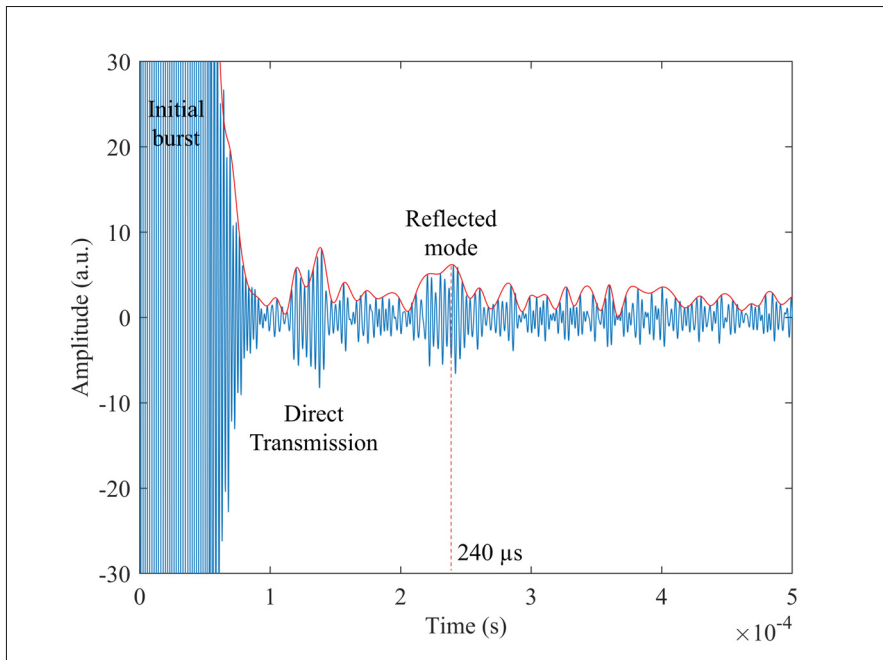
Figure 4.8   Experimental Ascan (blue) and its envelope (red) obtained with the 10th element of the receiving probe when the inspection is done at the center of region 2, with a minimum thickness of 6 mm, with an excitation of SH_1 using a 10-cycle Hann windowed toneburst centered around 300 kHz

4.5   Conclusion

In this study, two linear array EMATs were used to assess the minimum thickness of a machined defect on a steel pipe arising from a reflected wave and structural filtering. By using several phase velocity excitations, it was possible to excite SH_1 and SH_2 purely for frequency ranges of 171 to 400 kHz and 410 to 475 kHz, respectively, allowing theoretical detection ranges of 4 to 9.3 mm and 6.7 to 7.8 mm. To verify these values and to estimate the accuracy of the method, the probes were used at three positions, namely, in front of a zone of minimum thickness of 6 mm, at a transition zone ranging from 6 to 7.2 mm, and a region at 7.2 mm. The results showed that SH_1 estimated the thickness at the three positions with a maximum error of 0.4 mm. In the case of SH_2, it was used to compensate for the appearance of a parasitic frequency around 240 kHz during the experimental measurements using SH_1, estimating a thickness of 7 mm, for a real minimum thickness of 7.2 mm, and for an error of 0.2 mm. The measurement using the

wave reflected by the defect also allowed to position the defect 166 mm ahead of the receiving probe, the measured value being 176 mm. This represents an error of 10 mm.

CONCLUSION ET RECOMMANDATIONS

Les principales contributions des travaux réalisés sont : (1) l'optimisation de la structure PPM EMAT pour une utilisation sur des tuyaux en acier, et (2) la conception d'une sonde multi-éléments linéaire EMAT permettant la transduction d'une onde guidée SH dans divers guides d'onde comme des tuyaux ou des plaques. Ces points ont été validés par des simulations et des mesures expérimentales sur un tuyau en acier comportant un défaut usiné à partir de poches sphériques permettant ainsi l'obtention d'une surface de corrosion simulée.

Les contraintes lors d'inspection par contrôle non destructif sont multiples. Dans le cas d'une estimation d'épaisseur par filtrage structurel le principal objectif est de fournir rapidement et de manière fiable la valeur minimale de l'épaisseur sur un guide d'onde comme une plaque ou un tuyau. Le critère de rapidité implique que l'inspection doit se réaliser de préférence sans étape supplémentaire comme une interruption de service, un démontage d'un support de tuyau ou bien une excavation dans le cas d'une structure enterrée. Ce premier point est résolu en sélectionnant les ondes guidées SH capables de se propager sur de longues distances et faiblement sensibles au chargement de surface. Dans le cas de la fiabilité des résultats cela revient à réduire les sources d'erreurs. Les deux sources majeures sont l'amélioration du rapport signal sur bruit et une séparation plus efficace des modes.

Pour ce qui est de l'amélioration du rapport signal sur bruit le choix a été fait d'optimiser la structure PPM EMAT pour une utilisation sur un tuyau en acier. Cette étude a considéré quatre modèles : un premier composé d'aimants rectangulaires et d'une bobine plane, un second utilisant cette fois-ci une bobine incurvée, les deux derniers modèles d'EMAT permettent une prise en compte de la courbure du tuyau en utilisant des plus petits aimants et des aimants incurvés. Cette étude a été réalisée en considérant plusieurs phénomènes physiques tels que l'effet du surélèvement de la bobine sur les courants de Foucault induits ou bien encore la prise en compte du caractère ferromagnétique du tuyau sur la déviation des lignes de champs

magnétiques générées par les aimants. Les capacités de chaque sonde ont été testées lors d'une mesure d'épaisseur par filtrage structurel et ont permis la reconstruction du profil d'épaisseur du tuyau selon quatre paliers : moins de 5.4 mm, entre 5.4 et 7 mm, entre 7 et 8 mm et entre 8 mm et l'épaisseur nominale du tuyau soit 10.2 mm, permettant ainsi une détection de perte d'épaisseur pouvant atteindre jusqu'à 50% de l'épaisseur nominale. Les meilleurs résultats ont été obtenus avec la configuration comportant des aimants et une bobine incurvée mais celle composée de plus petits aimants permet des résultats similaires tout en permettant une meilleur adaptation à des diamètres différentes de tuyau.

La seconde partie de cette thèse a été séparée en deux parties : la conception d'un EMAT multi-éléments linéaire et une application sur le même tuyau que celui utilisé précédemment. Cette sonde est faite de plusieurs éléments chacun composé d'un aimant, plat ou incurvé selon le guide d'onde, et d'une bobine encerclante. Un tel transducteur a deux principaux intérêts. Tout d'abord le caractère multi-éléments de la sonde permet la transduction d'une onde guidée SH avec la méthode d'excitation par vitesse de phase, permettant suivant les lois de retard et les signaux utilisés une excitation pure de modes SH d'ordre élevés. Ensuite au niveau de la réception il est possible d'utiliser une transformée de Fourier à deux dimensions pour permettre de séparer les différents modes se propageant même s'ils se situent à la même fréquence. Des premiers tests ont montré que cette sonde a des performances similaires à celle d'une sonde piézoélectrique en cisaillement pour des fréquences allant de 300 à 800 kHz, sans nécessiter l'utilisation de couplant visqueux. Ce transducteur a ensuite été utilisé pour effectuer plusieurs mesures d'épaisseur sur un tuyau en acier en utilisant les modes réfléchis par le défaut permettant une estimation d'épaisseur avec une erreur maximale de 0.4 mm et un positionnement avec une erreur de 10 mm pour une distance de propagation totale de 600 mm.

Pour les prochaines étapes liées à ce projet je souhaite effectuer quelques recommandations :

1. Tout d'abord divers tests réalisés lors de cette thèse et de projets annexes ont permis de montrer que l'utilisation de fils fins permettant une bobine dense et donc une amélioration significative de la qualité des signaux obtenues et une diminution de la puissance requise. Dans le cas des PPM EMAT il a été décidé d'utiliser une bobine imprimée sur un PCB flexible avec un largeur de trace de 0.2 mm, permettant un bobinage plus dense et régulier que dans le cas de la bobine de l'EMAT multi-éléments, le diamètre du fil de cuivre utilisé est ici de 0.315 mm. Cette option est difficilement applicable pour l'EMAT multi-éléments composé de bobines encerclantes et donc non planes.

2. Initialement une circuit d'adaptation d'impédance n'a pas été considéré pour éviter de trop réduire la bande passante de la sonde mais au fur et à mesure des applications les fréquences utilisées ont été réduites pour permettre une détection continue de l'épaisseur entre 4 et 9.3 mm pour des fréquences allant de 175 à 400 kHz. Un tel circuit pourrait permettre une meilleure transmission d'énergie entre les EMAT et les chaînes d'acquisition d'émission et de réception.

3. Les signaux utilisés sont des signaux sinusoïdaux composés d'un nombre de cycles finis puis fenêtrés par une fonction de Hann. Des signaux codés de Golay pourraient grandement améliorer le rapport signal sur bruit sans allonger la durée totale d'acquisition. Deux signaux longs ayant subi un codage suivant les séquences de Golay sont utilisés successivement en émissions. Les corrélations entre les signaux utilisés et les signaux mesurés sont ensuite sommées. Cette technique permet d'obtenir avec une faible puissance et sans moyenner les signaux mesurés un fort rapport signal sur bruit. La difficulté réside ici dans la sélection d'un équipement pouvant permettre d'émettre des signaux longs dans des charges majoritairement inductives comme des bobines d'EMAT.

ELECTROMAGNETIC ACOUSTIC PROBE

Aurélien THON[1,2] , Pierre Bélanger[1,2]

[1] Piezoelectricity and Ultrasonics Technologies and Materials Laboratory at ÉTS (PULÉTS), 1100 Notre-Dame Ouest, Montréal, Québec, Canada H3C 1K3

[2] Département de Génie mécanique, École de Technologie Supérieure, 1100 Notre-Dame Ouest, Montréal, Québec, Canada H3C 1K3,

1.   Cross-reference to related application

The present application claims the benefit of United States Provisional Patent Application No. 63/203,550 filed on July 27, 2021, the contents of which are hereby incorporated by reference in their entirety.

2.   Technical Field

The application relates generally to measurement devices and, more particularly, to measurement devices that use ultrasonic guided waves for non-destructive testing.

3.   Background

The inspection of corroded structures is crucial across many industries. Affected areas are often difficult to access due to other impeding structures, such as pipe support or insulation. This makes standard thickness gauging methods such as point-by-point ultrasonic thickness gauging impossible.

The use of ultrasonic guided waves in nondestructive testing enables rapid inspections over long distances. In a pipe, several modes can propagate, such as flexural (axisymmetric and non-

axisymmetric) and torsional modes (axisymmetric and non-axisymmetric). Various techniques are known to propagate waves in pipes and detect defects. While these techniques are suitable for their purposes, improvements are desired.

4. Summary

In one aspect, there is provided a probe for non-destructive testing of a curved object, the probe comprising an arrangement of magnets and coils configured for generating shear horizontal guided waves for propagating longitudinally in the object, the probe having a top surface, a bottom surface, and two opposed ends extending between the top surface and the bottom surface, the bottom surface having a non-zero curvature between the two opposed ends and matable with an outer surface of the curved object.

In another aspect, there is provided a measurement system comprising at least one probe, a signal generating circuit for generating an emission signal, and a signal receiving circuit for receiving a detection signal. The probe comprises an arrangement of magnets and coils configured for generating shear horizontal guided waves for propagating longitudinally in the object, the probe having a top surface, a bottom surface, and two opposed ends extending between the top surface and the bottom surface, the bottom surface having a non-zero curvature between the two opposed ends and matable with an outer surface of the curved object.

5. Description of the drawings

Reference is now made to the accompanying figures in which :

Fig. I-1 to Fig. I-4 are cross-sectional views of a probe arranged on a curved object for inspection thereof ;

Fig. I-5 and Fig. I-6 are example configurations of a magnet array for a probe having a curved undersurface ;

Fig. I-7 is an example configuration of a coil for a probe having a curved undersurface ;

Fig. I-8 shows excitation energy obtained with a 20 magnets array when the excitation signal is a 20 cycle Hann windowed toneburst centered at 500 kHz;

Fig. I-9 shows the phase velocity curves in a 10.2 mm thick steel plate;

Fig. I-10 and Fig. I-11 are block diagrams of example measurement systems;

Fig. I-12 to Fig. I-15 illustrate a maximum amplitude of Lorentz Forces generated on a steel pipe with a diameter of 323.8 mm and a thickness of 10.2 mm by probes having different configurations;

Fig. I-16 to Fig. I-19 illustrate an ultrasonic field generated on a steel pipe with a diameter of 323.8 mm and a thickness of 10.2 mm by probes having different configurations; and

Fig. I-20 to Fig. I-23 show experimental A-scans obtained with an excitation from SH_1 to SH_4 with 20 cycle Hann windowed signals centered respectively at 524, 588, 682 and 795 kHz in a configuration using curved magnets and coils with an inspection line positioned at 130 mm (a) and 60 mm (b) from the center of the defect as well as their respective frequency contents (c) and (d).

6.   Detailed Description

The present disclosure is directed to methods and devices for inspection of curved ferromagnetic objects, such as but not limited to steel pipes, using ultrasonic waves. Guided waves are mechanical perturbations that propagate between two boundaries forming a waveguide such as a plate or a pipe. These can be separated into Lamb waves (symmetric and anti-symmetric), and shear horizontal (SH) guided waves. When impinging a defect or a feature parallel to the direction of polarization SH waves will not convert to Lamb modes. Unlike Lamb waves, SH waves are less sensitive to these forces when the fluid is not viscous. In addition, the cutoff frequencies-thickness product of high-order SH modes are evenly distributed along the frequency-thickness product axis, which allows the estimation of a thickness on regular intervals.

The equations A I-1 and A I-2 are used to compute the phase and group velocity of shear horizontal modes :

$$V_{p,n} = V_S \left(\frac{2fb}{\sqrt{4(fb)^2 - n^2 V_S^2}} \right) \tag{A I-1}$$

$$V_{g,n} = V_S \sqrt{1 - \frac{(n/2)^2}{(fb/V_S)^2}} \tag{A I-2}$$

$V_{(p,n)}$ and $V_{(g,n)}$ are respectively the phase and group velocity of the n-order mode, V_S is the bulk shear wave velocity, f is the frequency, and b is the thickness of the waveguide. The fundamental mode SH_0 can propagate at all frequency thickness products. High order modes are constrained to propagate only above a given cutoff frequency thickness product. When this value is reached, the mode's phase velocity tends towards infinity and the group velocity towards zero. This mode can no longer propagate and is then reflected or converted to a lower order mode. When a high order mode impinges an abrupt thickness reduction, it will be converted to a lower order mode, and when the thickness of the waveguide allows, it will be converted back to its original state. Conversely, if the defect is smooth most of its energy will be reflected.

In metallic materials, corrosion is a chemical weathering by an oxidizer. This implies wear of the affected surfaces, which can be likened to a local loss of thickness. For a high-order horizontal shear mode, this will shift the frequency-thickness product. If the severity of the defect is sufficient, then the mode can reach its cut-off threshold. The energy of this mode will then no longer be able to propagate. By identifying the last mode capable of propagating and the first mode filtered out, estimating the waveguide thickness is possible. Considering a plate of given thickness b, the cutoff frequency-thickness product of SH_n can be obtained using equation A I-3 :

$$fb = \frac{nV_S}{2} \tag{A I-3}$$

V$_S$ is the bulk shear wave velocity. The use of multiple of modes makes it possible to increase the number of detection thresholds. However, the excitation and detection of high order mode become more complex as the frequency increases. The attenuation may be modeled using equation A I-4 :

$$I = I_0 e^{-2\alpha x} \tag{A I-4}$$

I is the intensity of the wave at a distance x from its source, I$_0$ is the initial intensity, and α is the attenuation coefficient depending on the material properties and increasing with the frequency. Further than attenuation, the ultrasonic wave is also subject to scattering when it encounters a defect. High-order modes can be described as dispersive. The difference between their phase and group velocities implies an alteration in the waveform in the time domain along with its propagation. These phenomena affect higher order modes more strongly. Their experimental uses over a large propagation distance are therefore more complex than for the first SH modes.

The probe described herein uses shear horizontal (SH) ultrasound waves for non-destructive testing. In some embodiments, the ultrasonic probe is used to determine a thickness profile of the curved ferromagnetic object. Generally, the probe is designed with a geometry that maximizes proximity of the probe with the object over a large surface area. In particular, a curved undersurface of the probe is used to minimize the influence of distance on a force field generated by the probe in the object. In some embodiments, the probe is custom-made to match the shape and outer-diameter of the object under inspection, thus allowing for a constant and minimal spacing between the probe and the object. Alternatively, a probe design may be used with objects having a range of outer-diameters while still benefitting from an optimized generation of Lorentz forces for a ferromagnetic object, which can alter the direction of a magnetic field due to the attraction forces between the probe and the object. The Lorentz force created by the probe is dependent on the amplitude and the direction of the magnetic field as generated and the curved nature of the undersurface of the probe helps mitigate the effect of the ferromagnetic material on the magnetic field.

With reference to Fig. I-1, there is illustrated a cross-sectional view of an example ultrasonic probe 100 coupled to an object 102 having an inner surface 106B and an outer surface 106A. The probe 100 defines an outer surface 104A and an inner surface 104B adjacent to the outer surface 106A of the object 102. The probe 100 has an arrangement of magnets and coils that allow the generation and the detection of SH guided waves. In particular, eddy currents are created in the object 102 that lead to a Lorentz force, allowing the transduction of the SH waves longitudinally in the object 102. The inner surface 104B of the probe 100 has a non-zero curvature C1, which is used herein to denote an amount by which the inner surface 104B deviates from a straight line. The curved inner surface 104B optimizes the generation of the Lorentz force by creating a better coupling between the probe 100 and the object 102. In some embodiments, and as illustrated in Fig. I-1, the curvature C1 of the inner surface 104B of the probe 100 is substantially equal to a curvature C2 of the outer surface 106A of the object 102, such that the distance between the probe 100 and the object 102 is substantially uniform across a circumferential direction of the object 102 from a first end 108A of the probe 100 to a second and opposite end 108B of the probe 100, and C1 = C2. In this example, the entire inner surface 104B of the probe forms a region of contact with the outer surface 106A of the object 102.

In some embodiments, the curvature C1 of the inner surface 104B of the probe 100 and the curvature C2 of the outer surface 106A of the object 102 are different. A first example is shown in Fig. I-2, where the curvature C1 of the inner surface 104A of the probe 100 is greater than the curvature C2 of the outer surface 106A of the object 102, i.e. C1 > C2. This configuration results in a gap G1 between the inner surface 104B and the outer surface 106A, and regions of contact between the probe 100 and the object 102 proximate to and/or at the ends 108A, 108B of the probe 100. A radial dimension of the gap G1 relative to a central axis of the object 102 decreases in a circumferential direction of the object 102 towards the opposed ends 108A, 108B of the probe. A maximum radial dimension for gap G1 depends on many criteria, such as the properties of the material inspected, the power of the magnets, the thickness and the density of the coil, etc. The greater the gap, the less the Lorentz forces generated will be strong in emission and the harder it will be to detect the SH wave in reception.

Another example is shown in Fig. I-3, where the curvature C1 of the inner surface 104B of the probe 100 is less than the curvature C2 of the outer surface 106A of the object 102, i.e. C1 < C2. Gaps G2, G3 are formed between the object 102 and the probe 100 at respective ends 108A, 108B of the probe 100. A radial dimension of the gaps G2, G3 decreases in a circumferential direction of the object 102 towards a center of the probe 100 until contact is made between the inner surface 104B of the probe and the outer surface 106A of the object at a region of contact. The size of the region of contact will depend on the difference between the curvatures C1 and C2. Generally, an optimal configuration is when the region of contact extends from the first opposed end 108A to the second opposed end 108B of the probe, i.e. C1 = C2. When starting from a flat probe, the results improve as the region of contact increases, such that the curvatures of the inner surface 104B of the probe 100 and the outer surface 106A of the object 102 move towards a same value.

In some embodiments, the probe 100 is spaced apart from the object 102 by one or more support, such that contact between the probe 100 and the object 102 occurs via the one or more support. The supports are made of a material that does not impede the creation of eddy currents in the object, such as rubber, ceramic, plastic, and other non-conductive materials. An example is shown in Fig. I-4, where a first support 110A is proximate to the first end 108A and a second support 110B is proximate to the second end 108B. A gap G4 is formed between the inner surface 104B of the probe 100 and the outer surface 106A of the object 100 between the supports 110A, 110B. In some embodiments, a radial dimension of the gap G4 is substantially uniform in the circumferential direction. Alternatively, the radial dimension of the gap G4 varies circumferentially.

Although the probe 100 is illustrated in the examples of Fig. I-1 to Fig. I-4 as having an outer surface 104A that mirrors the shape of the inner surface 104B, the outer surface 104A may be configured with any shape, including straight, concave, convex, and other geometries. A handle may be provided on the outer surface 104A for ease of manipulation by an operator. The probe 100 may be provided in a casing or housing.

The ultrasonic probe 100 has an arrangement of magnets and coils that allow the generation and the detection of SH guided waves. With reference to Fig. I-5, an example configuration of magnets and coils is shown for the probe 100. An array 202 of magnets 204 is disposed on an elongated electrical coil 206. The probe 100 generates an ultrasonic pulse within the object 102 to which the probe 100 is coupled. The magnets 204 are disposed with periodically alternating north (N) and south (S) poles, which sets the primary wavelength of the ultrasound generated. Although the array 202 is shown with two rows 202A, 202B of magnets 204, a single row or more than two rows may be used. The electrical coil 206 runs in a direction of the alternation of the magnet poles, and when current (i) is pulsed through the coil 206, eddy currents are created in the object 102 that lead to a Lorentz force, allowing the transduction of the SH waves. More specifically, the interaction between induced eddy currents J in the conductive material of the object 102 and a magnetic field B generates Lorentz forces f_L :

$$\mathbf{f_L} = \mathbf{J} \times \mathbf{B} \tag{A I-5}$$

The proximity of the coil 206 to the conductive waveguide (i.e. the object 102) induces the eddy currents necessary for transduction. To optimize the generation of Lorentz forces, the magnet array 202 and coil 206 are curved. Since the object 102 is ferromagnetic, it has a lower reluctance than air and will tend to attract magnetic flux lines. The amplitude of the eddy currents generated by the coil 206 decreases as a function of its distance to the conductor, which has the effect of locally altering the direction of the magnetic flux lines, the amplitude of the eddy currents, and thus the shape of the Lorentz forces. The curved coil 206 minimizes the influence of the distance from the coil 206 on the generated force field. The curved array 202 ensures constant and minimal spacing of the magnets 204 and coil 206 from the object 102. In some embodiments, curved magnets 204 are used to form the curved array 202. In one specific and non-limiting embodiment, two rows of twenty curved permanent magnets are used, as shown in Fig. I-5. Alternatively, and as shown in Fig. I-6, small rectangular magnets 214 may be used and provided in multiple rows that are relatively positioned to provide the desired curvature. This

embodiment allows magnet liftoff relative to the object 102 to be reduced using only readily available magnets.

As shown in Fig. I-7, the coils 206 may be provided on a flexible substrate 300, such as a flexible printed circuit board (PCB), or a rigid substrate have a pre-defined shape that corresponds to the desired shape. In this example, the coils 206 are formed as a race track, whereby a first section 302A is associated with the first row 202A of the array 202 of magnets 204 and a second section 302B is associated with the second row 202B of the array 202 of magnets 204. The configuration of the coils 206 will vary as a function of the arrangement of the magnet array 202.

The wavenumber bandwidth of the probe 100 depends on the size and number of magnets 204, 214 in the direction of propagation. These two values make it possible to obtain a polarization pattern. By applying a Fourier transform, the amplitude of excitation as a function of the wavenumber can then be obtained. Combining this spatial spectrum with the frequency spectrum of the excitation signal allows the generation of a map of the transmitted energy and a prediction of the generated modes. A map as a function of phase velocity V_p and frequency (as shown in Fig. I-8) can be obtained using the equation A I-6 :

$$V_p = \frac{2\pi f}{k} \tag{A I-6}$$

where f is the frequency, and k is the wavenumber. By considering the excitation of a the probe 100 around a wavelength corresponding to twice the pitch of the magnets, it is then possible to predict that on the dispersion curves, the majority of the energy of the ultrasonic wave will be concentrated around a straight line inclined with a slope equal to λ (as shown in Fig. I-9). The intersection of this line with the phase velocity dispersion curves of the different SH modes makes it possible to obtain the excitation frequencies of these modes. It is then possible to compute the cutoff thicknesses of the high order SH modes using equation A I-3. It is then possible to target certain modes during the emission of an ultrasonic wave.

The angle of divergence of the ultrasound beam and the near field's size may be used to estimate the capacities of an inspection. If the defect is too close to the probe 100 or too small compared to the ultrasonic beam's width, it may not have sufficient influence on the propagation of the ultrasonic wave to be detected. These two dimensions can be calculated as follows :

$$N = \frac{D^2}{4\lambda} \tag{A I-7}$$

$$\sin(\theta) = 0.44\frac{\lambda}{D} \tag{A I-8}$$

where N is the near field's length, D the dimension of the transducer in the direction perpendicular to the propagation direction, λ is the wavelength, and θ is the divergence angle from the centreline to the -6 dB line. In some embodiments, a single probe 100 is used to generate and detect SH waves. An example embodiment is shown in Fig. I-10. A measurement system 508 comprises a signal generating circuit 502 that generates an emission signal and transmits the emission signal to an amplifier 504 for amplification thereof. The amplifier 504 is connected to each end of the coil 206, and the amplified signal is input into the coil 206. The amplifier 504 is also connected to a signal receiving circuit 506, such that a detected signal is received from the coil 206 into the amplifier 504 and transmitted to the signal receiving circuit 506 for processing thereof. In this configuration, transmission and detection is performed by the probe 100 sequentially. In some embodiments, two probes 100 are used, one for generation of SH waves and one for detection of SH waves. An example is shown in Fig. I-11, a measurement system 510 comprises two probes 100, a signal generating circuit 502, a signal receiving circuit 506, and two amplifiers 504. It will be understood that the circuitry used for generating and detecting the SH waves, including amplification, may be packaged separately from the probe 100, which may be identical whether used in the generation or detection of the SH waves. In this manner, a casing may house the probe 100 and provide input and output ports for connection to the various circuitry needed to operated the probe 100. Alternatively, the measurement system 508 is provided in a single

housing. Also alternatively, the measurement system 510 may be provided in a first housing for generation (signal generating circuit 502, amplifier 504, probe 100) and a second housing for detection (signal receiving circuit 506, amplifier 504, probe 100).

In order to demonstrate the improved performance of the probe 100 having a curved undersurface, a comparison was performed between various configurations. A reference was set using a flat probe on a flat object (i.e. a plate), with a pitch of 3.2 mm, an elevation of 50.8 mm, and an aperture of 64 mm (20 magnets in the direction of propagation) Values for near-field N and divergence angle θ of the ultrasonic beam were found to be 100.8 mm and 3.2°, respectively. The first point of comparison between the configurations is the shape of the ultrasonic field generated, which can be approximated analytically using Eq.(7) and Eq.(8). With reference to Fig. I-12 to Fig. I-15, there are illustrated examples of a maximum amplitude of Lorentz Forces generated on a steel pipe with a diameter of 323.8 mm and a thickness of 10.mm by four different probe configurations. The image of Fig. I-12 was obtained with a probe having rectangular magnets and a flat coil on the steel pipe. The effective elevation of the probe is 24.3 mm. This large deviation from the reference value is due to the increasing liftoff of the coil and magnets at the edge of the probe, due to the flatness of the undersurface. Fig. I-13 was obtained with a probe having rectangular magnets and a curved coil. The elevation increases to 41.7 mm due to a uniform spacing of the curved coil with the pipe. Fig. I-14 was obtained with curved magnets and a curved coil, as illustrated in the example of Fig. I-5, and Fig. I-15 was obtained with small rectangular magnets and a curved coil, as illustrated in the example of Fig. I-6. In both cases, an elevation close to the reference value is obtained, respectively at 50.7 and 50.6 mm. This variation in the effective elevation of the probe, according to equations A I-7 and A I-8, will induce an alteration in the shape of the generated ultrasonic field.

A reduction of the elevation reduces the size of the near field of the probe and increases the angle of divergence of the ultrasound beam. Diffraction patterns of the different probe configurations are shown in Fig. I-16 to Fig. I-19. Fig. I-16 corresponds to the diffraction pattern for the probe configuration having a flat coil and rectangular magnets on the steel pipe. This case represents the most divergent configuration since the angle obtained is 106% greater than the reference

value obtained for an elevation of 50.8 mm. By using a flexible coil that best follows the curvature of the pipe (Fig. I-17 : rectangular magnets and a curved coil) this effect is reduced since an increase of 19% is noted. Finally, the cases with a curved magnet array and coil (Fig. I-18 : curved magnets and a curved coil ; Fig. I-19 : small rectangular magnets and a curved coil), present results similar to the reference case.

As shown in Fig. I-12 to Fig. I-15 and 7A-7D, the least divergent cases are for probe configurations havinge a curved magnet array and coil. Fig. I-20 to Fig. I-19 show two scans performed at two different positions along the circumference of a pipe with probes made up of curved magnets. Fig. I-20 and Fig. I-22 correspond to a reference measurement without defect on the inspection line. More precisely, these measurements were taken 130 mm from the center of the defect on the circumferential axis. At this position, the thickness on the inspection line corresponds to the nominal thickness of the pipe. By analyzing the frequency content of the various A-Scans, it can be seen that all the modes from SH_1 to SH_4 can propagate. It should be noted that the amplitude of SH_4 is much lower than that of the other modes. It is therefore deduced that the thickness of the waveguide must be between the nominal thickness of the pipe (10.2 mm) and the cut-off thickness of SH_4 (8 mm). In Fig. I-21 and Fig. I-23, the inspection line passes through the defect, and the minimum thickness is 6 mm. Here we see a significant reduction in the amplitude of the reception signals, which is characteristic of the presence of a defect. It is nevertheless possible to note the presence of SH_1 and SH_2 in the frequency content of the signals. SH_3 and SH_4 were not detected. The thickness must therefore be between the cut-off thickness of SH_3 (7 mm) and that of SH_2 (5.4 mm).

The comparative study of the four probe configurations and their ability to reconstruct the thickness profile of a steel pipe has demonstrated that the lift-off distance between magnets and the coil from the pipe can have a significant effect on the generation of the ultrasonic wave. Experimentally, this has manifested itself as a significant loss of signal-to-noise ratio which can complicate the excitation or detection of high-order SH modes. The probe having a curved undersurface allowed the pipe thickness profile to be reconstructed using the cutoffs from SH_2 to

SH_4. This technique, therefore, makes it possible to detect at most a loss of 50% of the thickness of the waveguide.

As can be seen therefore, the examples described above and illustrated are intended to be exemplary only. The scope is indicated by the appended claims.

7.   Claims

1. A probe for non-destructive testing of a curved object, the probe comprising an arrangement of magnets and coils configured for generating shear horizontal guided waves for propagating longitudinally in the object, the probe having a top surface, a bottom surface, and two opposed ends extending between the top surface and the bottom surface, the bottom surface having a non-zero curvature between the two opposed ends and matable with an outer surface of the curved object.

2. The probe of claim 1, wherein the arrangement of magnets and coils comprises a curved array of magnets disposed on an elongated electrical coil residing on a curved substrate.

3. The probe of claim 2, wherein the curved array of magnets comprises at least one row of curved magnets disposed with periodically alternating north and south poles.

4. The probe of claim 3, wherein the at least one row of curved magnets comprises two rows of curved, permanent magnets.

5. The probe of claim 2, wherein the curved array of magnets comprises a plurality of rows of rectilinear magnets positioned along a curved path.

6. The probe of claim 1, wherein the non-zero curvature of the bottom surface of the probe matches a curvature of the outer surface of the curved object.

7. The probe of claim 1, wherein the non-zero curvature of the bottom surface of the probe is greater than a curvature of the outer surface of the curved object.

8. The probe of claim 1, wherein the non-zero curvature of the bottom surface of the probe is less than a curvature of the outer surface of the curved object.

9. The probe of claim 1, wherein the magnets are permanent magnets.

10. The probe of claim 1, wherein the coils are mounted to a flexible substrate.

11. The probe of claim 1, wherein the coils are mounted to a rigid substrate.

12. The probe of claim 1, wherein the bottom surface of the prove is matable with the outer surface of the curved object via at least one support.

13. A measurement system comprising : at least one probe according to any one of claims 1 to 12 ; a signal generating circuit for generating an emission signal ; and a signal receiving circuit for receiving a detection signal.

14. The measurement system of claim 13, further comprising at least one amplifier connected to ends of the coils of the at least one probe, to the signal generating circuit, and to the signal receiving circuit, the signal generating circuit configured for transmitting the emission signal to the at least one amplifier for amplification thereof.

15. The measurement system of claim 14, wherein the at least one amplifier is configured for receiving the emission signal from the signal generating circuit, for generating an amplified signal based on the emission signal, and for inputting the amplified signal into the coils.

16. The measurement system of claim 15, wherein the at least one amplifier is configured for receiving the detection signal from the coils, and for transmitting the detection signal to the signal receiving circuit.

17. The measurement system of claim 13, wherein the at least one probe comprises a single probe configured for sequentially generating and detecting the shear horizontal guided waves.

18. The measurement system of claim 13, wherein the at least one probe comprises a first probe configured for generating the shear horizontal guided waves and a second probe configured for detecting the shear horizontal guided waves.

8.   Abstract

There is described a probe for non-destructive testing of a curved object, the probe comprising an arrangement of magnets and coils configured for generating shear horizontal guided waves for propagating longitudinally in the object, the probe having a top surface, a bottom surface, and two opposed ends extending between the top surface and the bottom surface, the bottom

surface having a non-zero curvature between the two opposed ends and matable with an outer surface of the curved object.
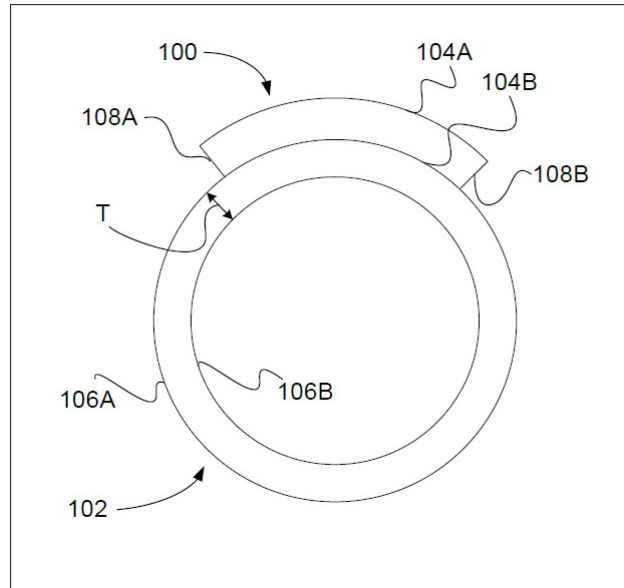
Figure-A I-1   Cross-sectional views of a probe arranged on a curved object. Tirée du brevet correspondant à l'annexe I
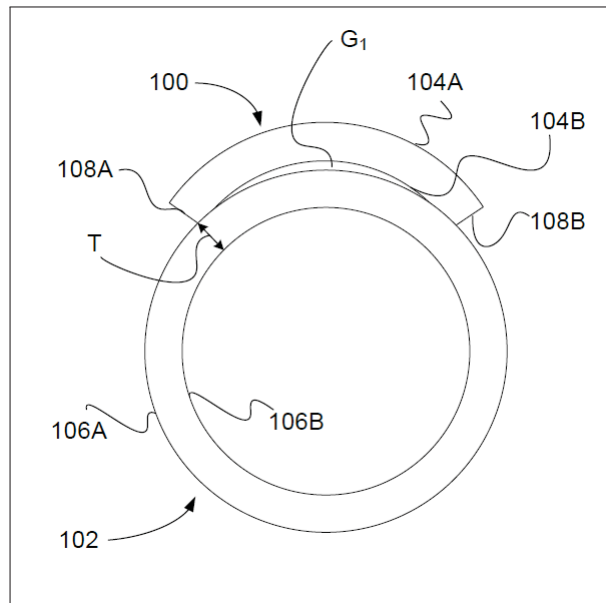
Figure-A I-2   Cross-sectional views of a probe arranged on a curved object. Tirée du brevet correspondant à l'annexe I
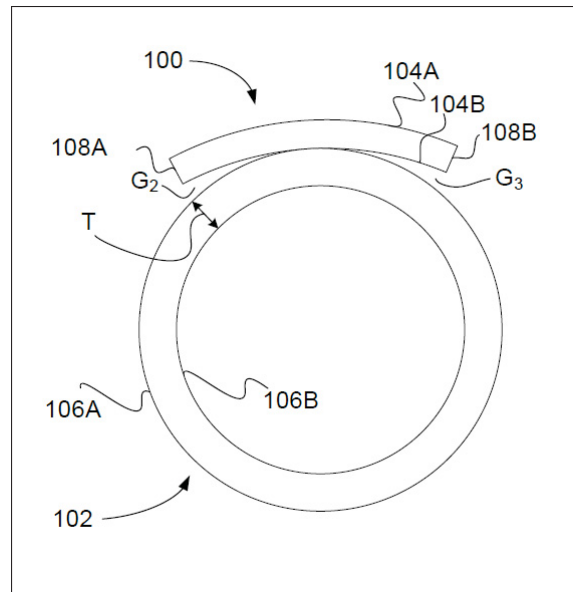
Figure-A I-3 Cross-sectional views of a probe arranged on a curved object. Tirée du brevet correspondant à l'annexe I
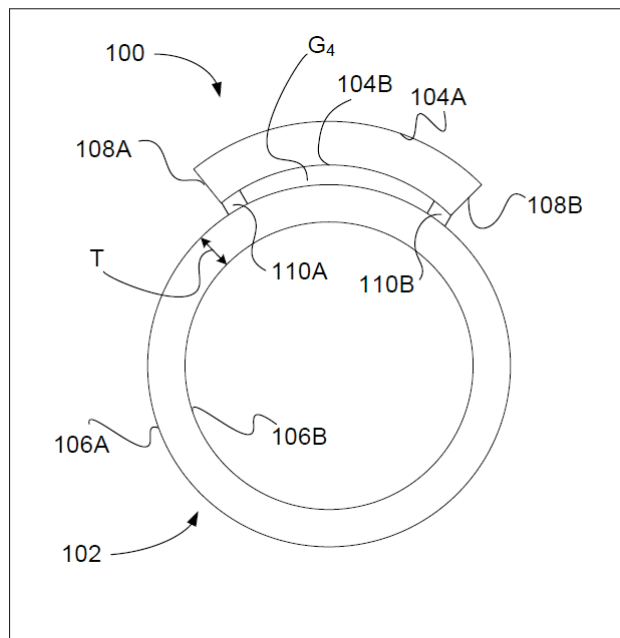
Figure-A I-4 Cross-sectional views of a probe arranged on a curved object. Tirée du brevet correspondant à l'annexe I
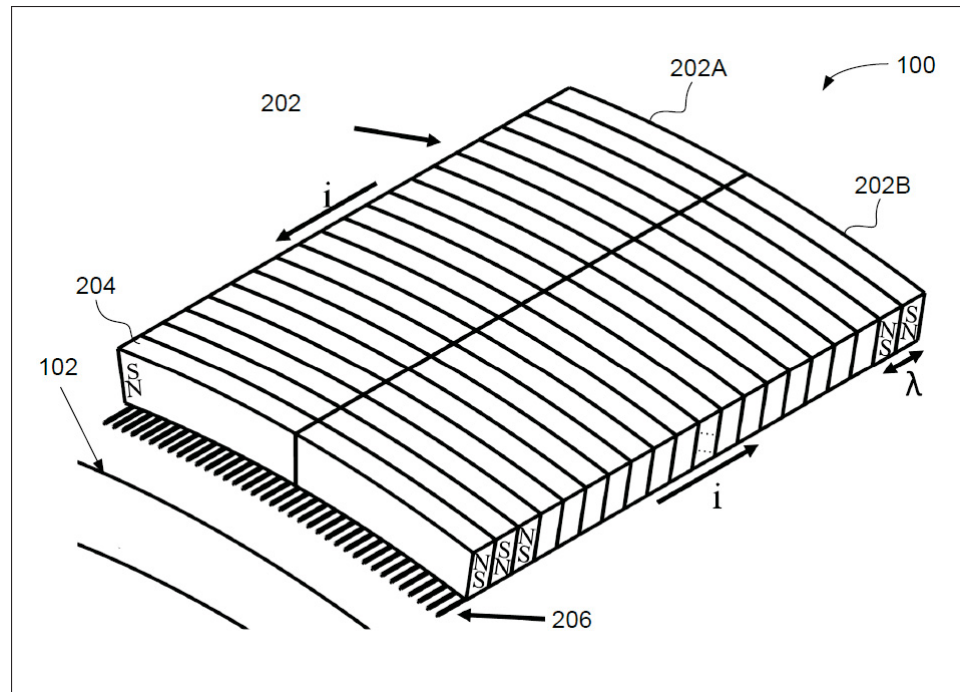
Figure-A I-5   Schematic diagram of a PPM EMAT with curved magnets and coil on a pipe.
Tirée du brevet correspondant à l'annexe I
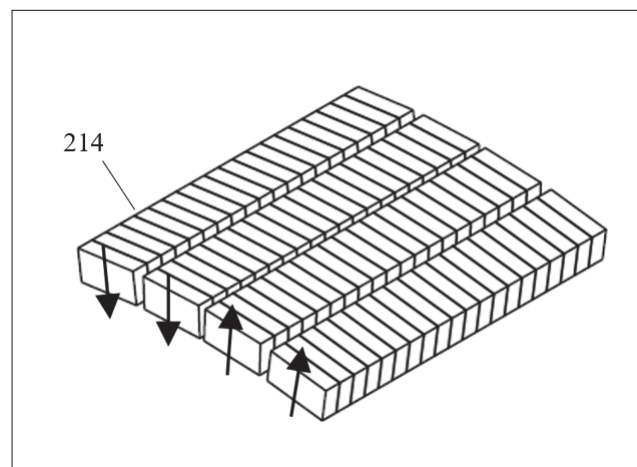
Figure-A I-6   Schematic diagram of a PPM EMAT with multiple rows of small magnets.
Tirée du brevet correspondant à l'annexe I
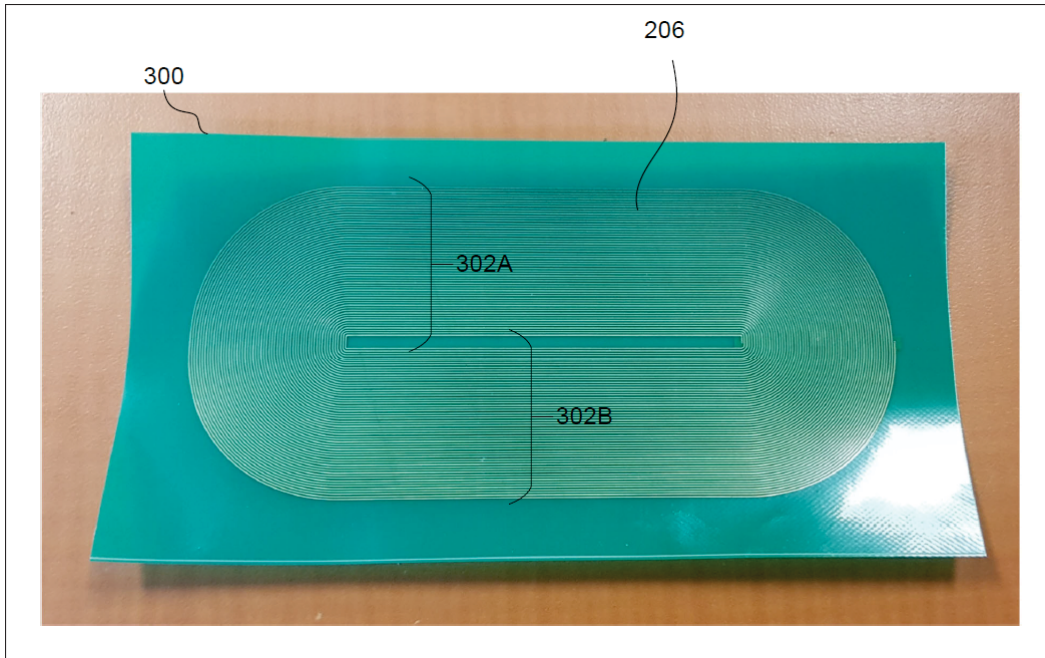
Figure-A I-7   Picture of a racetrack coil printed on a flexible PCB. Tirée du brevet
correspondant à l'annexe I
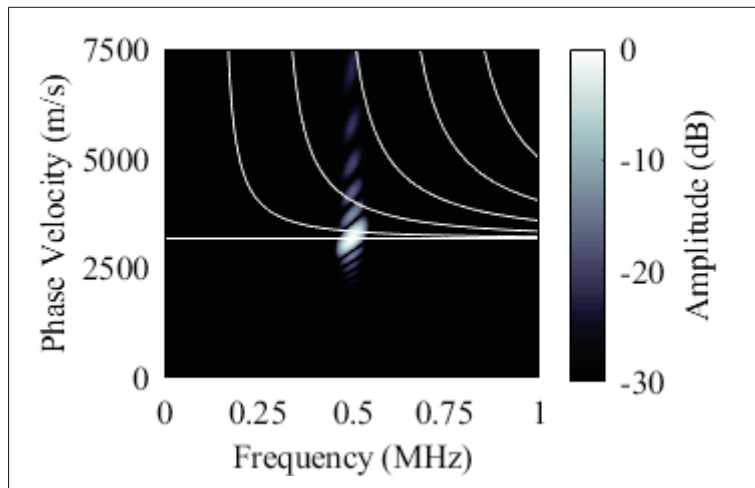
Figure-A I-8   Excitation energy obtained with a 2x20 magnets PPM EMAT when the
excitation signal is a 20 cycle Hann windowed toneburst centered at 500 kHz. Tirée du
brevet correspondant à l'annexe I
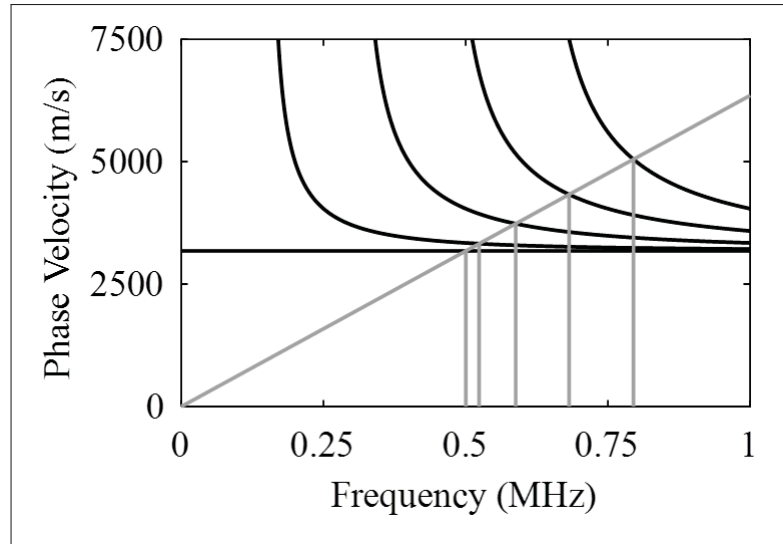
Figure-A I-9   Phase velocity curves for SH waves in a 10.2 mm thick steel plate. Tirée du
brevet correspondant à l'annexe I
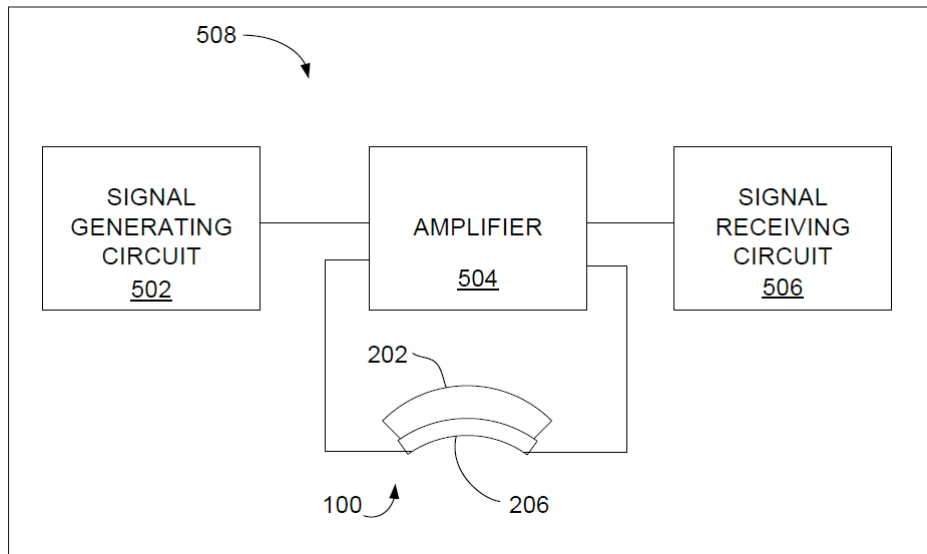
Figure-A I-10   Block diagram of example measurement systems. Tirée du brevet
correspondant à l'annexe I
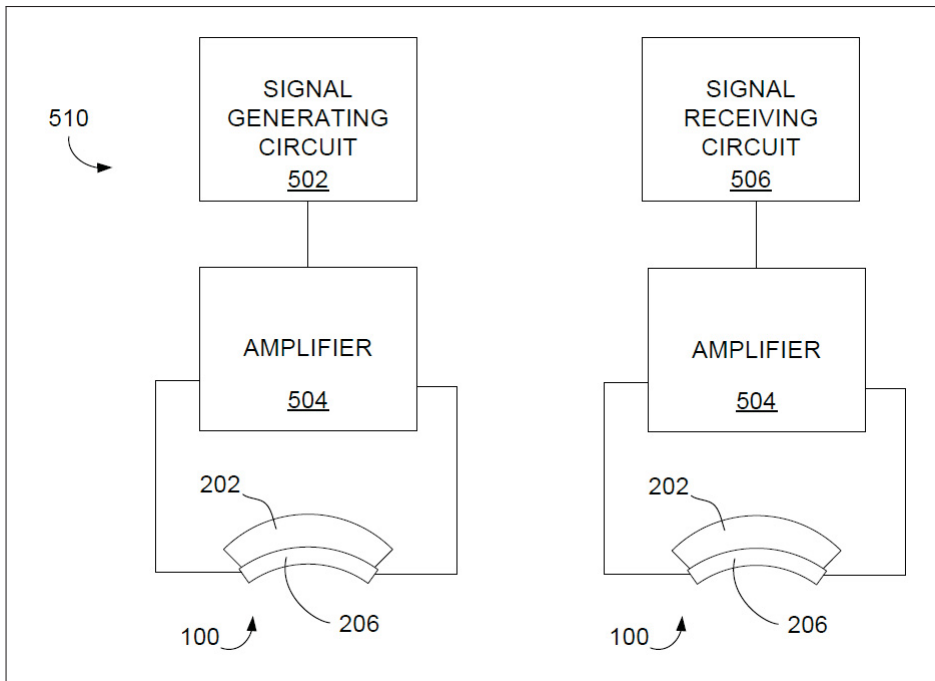
Figure-A I-11   Block diagrams of example measurement systems. Tirée du brevet correspondant à l'annexe I
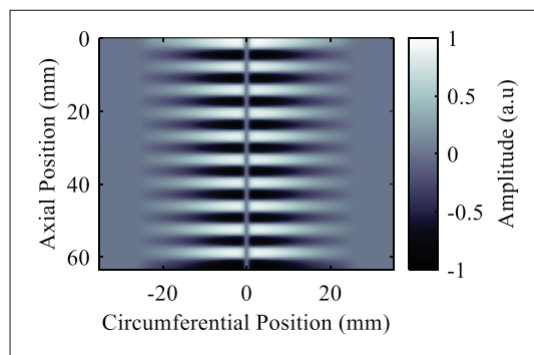
Figure-A I-12   Maximum amplitude of Lorentz Forces generated along the shear horizontal direction on a steel pipe with a diameter of 323.8 mm and a thickness of 10.2 mm by a PPM EMAT with rectangular magnets and flat coil. Tirée du brevet correspondant à l'annexe I
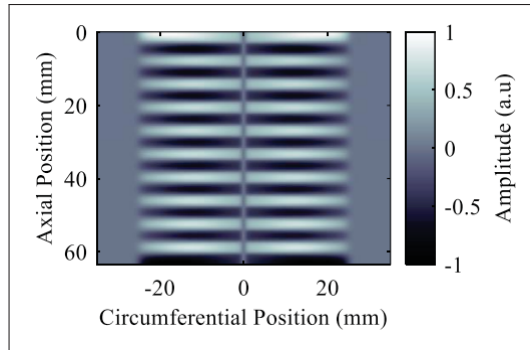
Figure-A I-13   Maximum amplitude of Lorentz Forces generated along the shear horizontal direction on a steel pipe with a diameter of 323.8 mm and a thickness of 10.2 mm by a PPM EMAT with rectangular magnets and curved coil. Tirée du brevet correspondant à l'annexe I
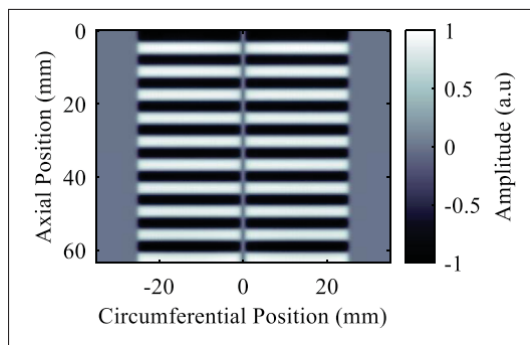
Figure-A I-14   Maximum amplitude of Lorentz Forces generated along the shear horizontal direction on a steel pipe with a diameter of 323.8 mm and a thickness of 10.2 mm by a PPM EMAT with curved magnets and coil. Tirée du brevet correspondant à l'annexe I
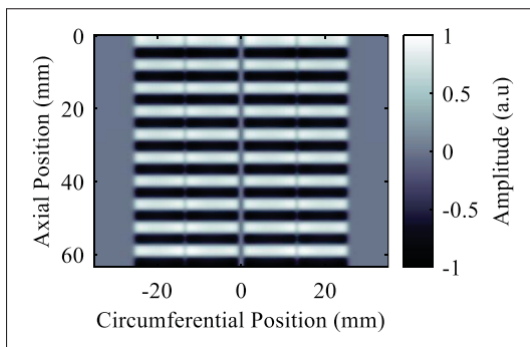
Figure-A I-15   Maximum amplitude of Lorentz Forces generated along the shear horizontal direction on a steel pipe with a diameter of 323.8 mm and a thickness of 10.2 mm by a PPM EMAT with small magnets and curved coil. Tirée du brevet correspondant à l'annexe I
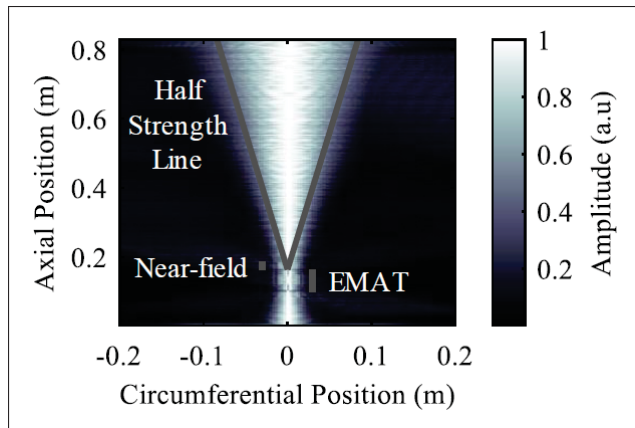
Figure-A I-16   Ultrasonic field generated on a steel pipe with a diameter of 323.8 mm and a thickness of 10.2 mm by a PPM EMAT with rectangular magnets and flat coil, (b) Rectangular magnets and curved coil, (c) Curved magnets and coils, and (d) Small magnets and curved coil. Tirée du brevet correspondant à l'annexe I
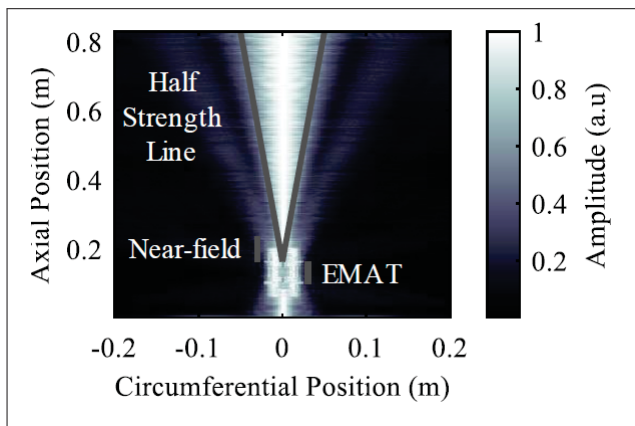
Figure-A I-17   Ultrasonic field generated on a steel pipe with a diameter of 323.8 mm and a thickness of 10.2 mm by a PPM EMAT with rectangular magnets and curved coil. Tirée du brevet correspondant à l'annexe I
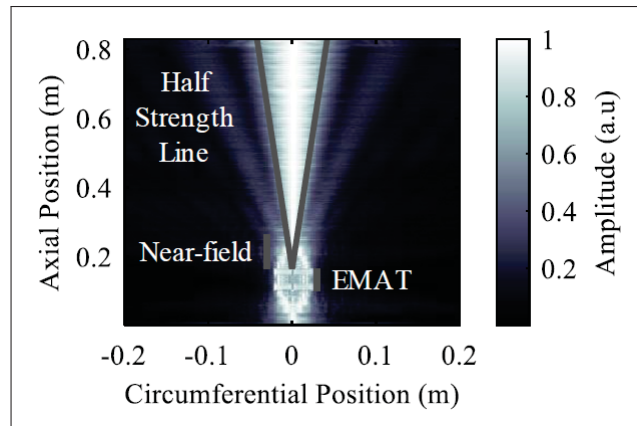
Figure-A I-18   Ultrasonic field generated on a steel pipe with a diameter of 323.8 mm and a thickness of 10.2 mm by a PPM EMAT with curved magnets and coil. Tirée du brevet correspondant à l'annexe I
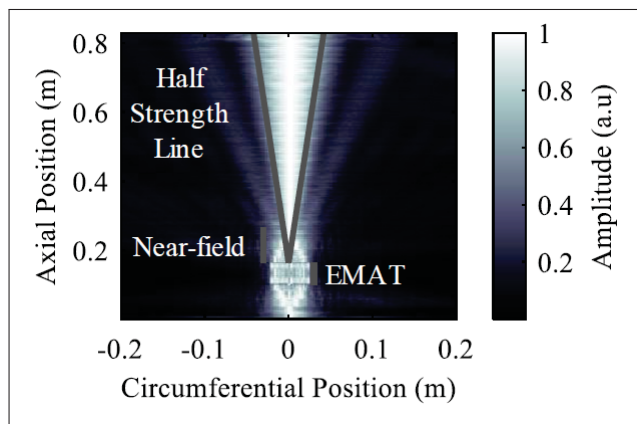
Figure-A I-19   Ultrasonic field generated on a steel pipe with a diameter of 323.8 mm and a thickness of 10.2 mm by a PPM EMAT with small magnets and curved coil. Tirée du brevet correspondant à l'annexe I
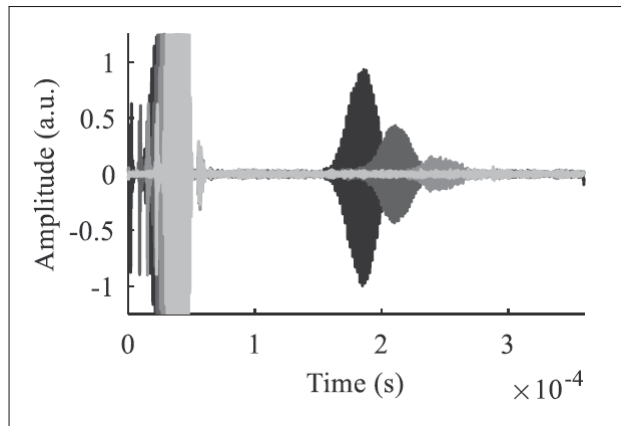
Figure-A I-20   Experimental A-scans obtained with an excitation from SH_1 to SH_4 with 20 cycle Hann windowed signals centered respectively at 524, 588, 682 and 795 kHz in a configuration using curved magnets and coils with an inspection line positioned at 130 mm. Tirée du brevet correspondant à l'annexe I
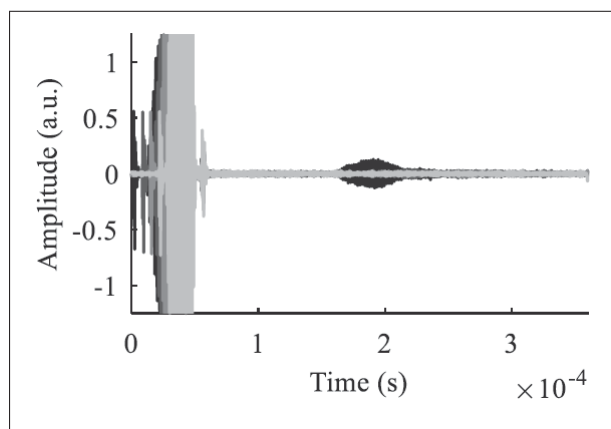
Figure-A I-21   Experimental A-scans obtained with an excitation from SH_1 to SH_4 with 20 cycle Hann windowed signals centered respectively at 524, 588, 682 and 795 kHz in a configuration using curved magnets and coils with an inspection line positioned at 60 mm. Tirée du brevet correspondant à l'annexe I
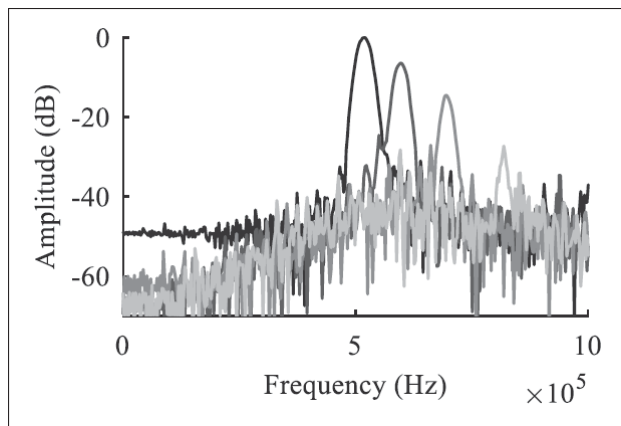
Figure-A I-22   Frequency spectrum of the A-scans presented on Fig. I-20. Tirée du brevet
correspondant à l'annexe I
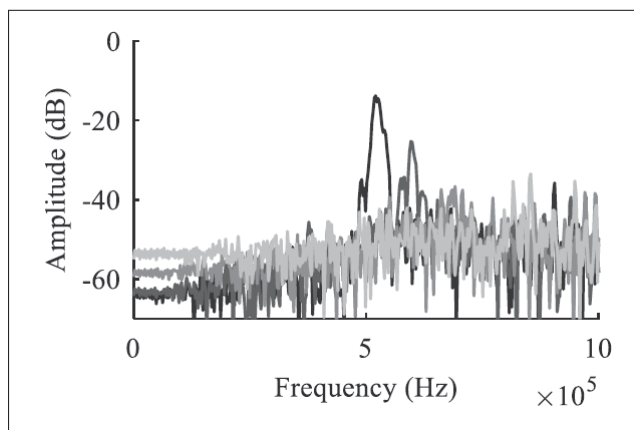
Figure-A I-23   Frequency spectrum of the A-scans presented on Fig. I-21. Tirée du brevet
correspondant à l'annexe I

MULTI-ELEMENT ELECTROMAGNETIC ACOUSTIC TRANSDUCER FOR GUIDED WAVE GENERATION AND DETECTION

Aurélien THON[1,2] , Pierre Bélanger[1,2]

[1] Piezoelectricity and Ultrasonics Technologies and Materials Laboratory at ÉTS (PULÉTS), 1100 Notre-Dame Ouest, Montréal, Québec, Canada H3C 1K3

[2] Département de Génie mécanique, École de Technologie Supérieure, 1100 Notre-Dame Ouest, Montréal, Québec, Canada H3C 1K3,

1.   Field

The present disclosure generally relates to guided wave inspection of materials, and more particularly to the use of a multi-element electromagnetic acoustic transducer for guided wave generation and detection.

2.   Introduction or background

Ultrasonic guided wave screenings have proven to be fast and reliable to detect various types of defects in plate-like structures. Low frequency ultrasonic guided waves are nowadays routinely used to screen long sections of pipelines. For a number of years, ultrasonic guided waves at a frequency beyond the cutoff of the first high order mode have attracted interest due to the plurality of modes that can propagate. When operating at a frequency beyond the cutoff of the first high order mode, the excitation mechanism becomes important to selectively excite a single high order mode or a group of high order modes. Ultrasonic comb transducers offer the possibility to selectively excite and detect high order ultrasonic guided waves at a desired wavelength. Linear array transducers are even more flexible and allow virtually full control in the frequency wavenumber space. High order shear horizontal (SH) modes have multiple potential applications including, for example, remote thickness gauging and crack monitoring. However,

these modes are notoriously difficult to excite and detect using conventional piezoelectric transducers. Electromagnetic acoustic transducers (EMAT) make the excitation and detection of SH modes relatively simple. Periodic permanent magnet (PPM) EMAT can be used to selectively excite and detect high order SH modes based on a desired wavelength. However, in some applications, it may be desirable to excite and detect high order SH modes with more control in the frequency wavenumber space.

Accordingly, there remains a need for improvement.

3.   Summary

Many further features and combinations thereof concerning embodiments described herein will appear to those skilled in the art following a reading of the instant disclosure.

4.   Description of the figures

In the figures,

Fig. II-1 is a schematic diagram of a multi-element electromagnetic acoustic transducer, in accordance with an illustrative embodiment;

Fig. II-2 is a perspective view of the multi-element electromagnetic acoustic transducer of Fig. II-1, in accordance with an illustrative embodiment;

Fig. II-3 is a perspective view of one element of the multi-element electromagnetic acoustic transducer of Fig. II-2, in accordance with an illustrative embodiment;

Fig. II-4 is a perspective view of a multi-element electromagnetic acoustic transducer, in accordance with another illustrative embodiment;

Fig. II-5 is a plot of Lamb wave phase velocity dispersion curves as a function of the frequency-thickness product, in accordance with an illustrative embodiment;

Fig. II-6 is a plot of SH wave phase velocity dispersion curves as a function of the frequency-thickness product, in accordance with an illustrative embodiment;

Fig. II-7 is a plot showing dispersion curves for the electromagnetic acoustic transducer of Fig. II-1, in accordance with an illustrative embodiment;

Fig. II-8 is a flowchart illustrating an example method for assembling an electromagnetic acoustic transducer, in accordance with an illustrative embodiment;

Fig. II-9, Fig. II-10, and Fig. II-11 illustrate two-dimensional Fourier transform (2D-FFT) signals received with the electromagnetic acoustic transducer of Fig. II-1, in accordance with an illustrative embodiment; and

Fig. II-12 is a plot of measured crosstalk between elements of the electromagnetic acoustic transducer of Fig. II-1, in accordance with an illustrative embodiment.

It will be noticed that throughout the appended drawings, like features are identified by like reference numerals.

5.   Detailed desciion

Referring now to Fig. II-1 and Fig. II-2, a multi-element electromagnetic acoustic transducer (EMAT) 100 for performing ultrasonic guided wave generation and/or detection will now be described, in accordance with one embodiment. The EMAT 100 comprises a plurality (N) of elements 102_1, 102_2, 102_3, . . ., 102_N provided on a surface 104 of a waveguide 106. While four (4) elements 102_1, 102_2, 102_3, 102_4 are illustrated in Fig. II-1 (i.e. N = 4), it should be understood that this is for illustrative purposes only and the EMAT 100 may comprise any suitable number (N) of elements 102_1, 102_2, 102_3, . . ., 102_N. In some embodiments, the plurality of elements 102_1, 102_2, 102_3, . . ., 102_N may be arranged in a linear (i.e. one-dimensional) array, although other possibilities may apply as further described herein below.

Any two adjacent elements of the plurality of elements 102_1, 102_2, 102_3, . . ., 102_N are spaced apart by a given distance (also referred to herein as a "pitch"). More specifically, the pitch is the distance between the center of two adjacent ones of the elements 102_1, 102_2, 102_3, . . ., 102_N. For example, as illustrated in Fig. II-1, the element 102_1 is spaced apart from the element 102_2 by a pitch P_{12}, the element 102_2 is spaced apart from the element 102_3 by a pitch P_{23}, and the element 102_3 is spaced apart from the element 102_4 by a pitch P_{34}. In some embodiments, the pitch between adjacent elements of the plurality of elements 102_1, 102_2, 102_3, . . ., 102_N may be equal, while in other embodiments, the pitch between adjacent elements of the plurality of elements 102_1, 102_2, 102_3, . . ., 102_N may be different. For example, in the embodiment illustrated in Fig. II-1, the pitches P_{12}, P_{23}, and P_{34} have an equal value, such that the EMAT 100 has a regular pitch. It should however be understood that the pitches P_{12}, P_{23}, and P_{34} may have different values, such that the EMAT 100 has an irregular pitch that varies along a length of the EMAT 100.

In some embodiments, the plurality of elements 102_1, 102_2, 102_3, . . ., 102_N may be provided on the surface 104 of the waveguide 106 without the use of a couplant (e.g., gel, or the like) that may be required in piezoelectric ultrasonic phased array probes (to ensure efficient transmission of the mechanical perturbation from the piezoelectric crystal to the inspected material). In other words, the plurality of elements 102_1, 102_2, 102_3, . . ., 102_N may be in direct contact with the surface 104 of the waveguide 106. Although the plurality of elements 102_1, 102_2, 102_3, . . ., 102_N are shown as being provided on the surface 104 of the waveguide 106, it should also be understood that the plurality of elements 102_1, 102_2, 102_3, . . ., 102_N may alternatively be provided on any other suitable surface of the waveguide 106. In the embodiment of Fig. II-1, the waveguide 106 has a first (or top) surface 104, a second (or bottom) surface 104' opposite the first surface 104, a first edge (or boundary) 108_a, and a second edge (or boundary) 108_b opposite the first edge 108a. Depending on the application, the plurality of elements 102_1, 102_2, 102_3, . . ., 102_N may, for example, be provided on the bottom surface 104' rather than on the top surface 104 of the waveguide 106.

The waveguide 106 may comprise any suitable conductive material and may have any suitable shape. The waveguide material may be homogeneous and isotropic. In some embodiments, the waveguide 106 comprises a ferromagnetic and conductive material, for instance steel. In some embodiments, the waveguide 106 may be substantially planar (for example, a sheet of metal). In some embodiments, the waveguide 106 may comprise a plate-like structure having a complex region to be inspected (not shown). In some embodiments, the plate-like structure may comprise a section of pipeline (not shown). In other embodiments, the waveguide 106 may be substantially curved (for example, a cylindrical section). Other embodiments may apply depending on the application.

A guided ultrasonic wave 110 propagates in the waveguide 106, for instance between the first edge 108a and the second edge 108b of the waveguide 106, along a direction of propagation A. It should be noted that although the direction of propagation A is shown in Fig. II-1 as being in the positive x-direction (+x), i.e. from the first (or left) edge 108a to the second (or right) edge 108b, the guided ultrasonic wave 110 may also propagate in another direction, for instance in the negative x-direction (-x), i.e. from the second (or right) edge 108b to the first (or left) edge 108a. In some embodiments, the guided ultrasonic wave 110 may be generated and/or detected by the EMAT 100 as further described herein below. The guided ultrasonic wave 110 may comprise a Lamb wave, including both symmetrical modes (S_0, S_1, S_2, . . .) and antisymmetrical modes (A_0, A_1, A_2, . . .). In some embodiments, the guided ultrasonic wave 110 may comprise a shear horizontal (SH) wave and/or modes thereof (of which SH_0 designates the fundamental mode and SH_1, SH_2, etc. designate higher order modes).

Referring to Fig. II-1, Fig. II-2, and Fig. II-3, each element of the plurality of elements 102_1, 102_2, 102_3, . . ., 102_N (with only element 102_1 being shown in Fig. II-3 for sake of clarity and illustration) comprises a magnet 202 and a coil 204 (see Fig. II-3). The size of the magnets 202 and the diameter of each coil 204 determines the pitch of the EMAT 100. The coil 204 may comprise at least one turn of electrically conductive wire wound around the magnet 202 in a clockwise or counterclockwise direction, thereby defining a direction of magnetization for each transducer element (with the magnetic field generated by each magnet 202 being indicated by

arrow B). In the illustrated embodiment, the magnets 202 are elongated and have a substantially rectangular cross-section, and each coil 204 is wrapped along a length of a corresponding magnet 202 (i.e. along the z direction). It should however be understood that, depending on the application, the magnets 202 may have any other suitable shape (including, but not limited to, a curved shape), and may be wound in any other suitable manner, as described further below. The magnets 202 may also have any suitable size and may be made of any suitable magnetic material.

In order to assemble the elements 102_1, 102_2, 102_3, ..., 102_N as an array (which may be one-dimensional or two-dimensional), the directions of magnetization of any two adjacent elements of the plurality of elements 102_1, 102_2, 102_3, ..., 102_N are oriented opposite to each other, such that the direction of magnetization of the transducer elements alternates with a given spatial period corresponding to twice the transducer's pitch. By reversing the direction of magnetization at each transducer element 102_1, 102_2, 102_3, ..., or 102_N, the magnetic poles of the magnets 202 alternate. This implies that, for a given motion of the waveguide 106, two successive elements 102_1, 102_2, 102_3, ..., 102_N generate opposite currents. By reversing the wiring direction of each coil 204, it becomes possible to have a uniform Lorentz force field across all elements 102_1, 102_2, 102_3, ..., 102_N.

For instance, in the embodiment of Fig. II-1, the element 102_1 has a first direction of magnetization (and the magnetic field generated by the magnet is indicated by arrow B1), the element 102_2 has a second direction of magnetization (and the magnetic field generated by the magnet is indicated by arrow B2) opposite to the first direction of magnetization, the element 102_3 has a third direction of magnetization (and the magnetic field generated by the magnet is indicated by arrow B3) opposite to the second indicated (and thus same as the first direction of magnetization), and the element 102_4 has a fourth direction of magnetization (and the magnetic field generated by the magnet is indicated by arrow B4) opposite to the third direction of magnetization (and thus same as the second direction of magnetization). In the illustrated embodiment, the direction of magnetization of each of the plurality of elements 102_1, 102_2, 102_3, ..., 102_N is orthogonal to the surface 104 of the waveguide 106 on which the plurality of elements 102_1, 102_2, 102_3, ..., 102_N are placed. The direction of magnetization may however vary, depending on the application,

the geometry of the waveguide 106, and/or the positioning of the plurality of elements 102_1, 102_2, 102_3, . . ., 102_N onto the waveguide 106. For instance, while the coils 204 are illustrated and described herein as being wound along the length of the magnets 202, the coils 204 may be wound differently, resulting in a change in a direction of Eddy currents and thus in the Lorentz forces generated by the EMAT 100. For example, each coil 204 may be wound along the width (i.e. along the x direction) of the corresponding magnet 202. This may allow for inspection of different defects of a material under inspection.

As shown in Fig. II-3, the coil 204 may be supplied with an excitation signal generated by an excitation system 206 electrically coupled (e.g., via electrical wire 208 or any other suitable electrical coupling means) to the coil 204. In some embodiments, the excitation signal may cause an excitation current Ic to circulate in the coil 204. In some embodiments, the excitation signal may be a single or multi-cycle Hann-windowed toneburst centered around a central frequency. When the coil 204 is supplied with the excitation signal, the coil 204 may be said to be "on" or "activated". When the coil 204 is not supplied with the excitation signal, the coil 204 may be said to be "off" or "deactivated". A transducer, for instance the EMAT 100, may be said to in an "on" or "activated" mode (also referred to herein as an "excited" mode) when at least some of its elements, for instance one or more of the plurality of elements 102_1, 102_2, 102_3, . . ., 102_N, are "on" or "activated".

[0029] In the embodiment shown in Fig. II-3, when the coil 204 is supplied with an excitation signal (and the transducer element is placed on a conductive material), an eddy current vector Je may be generated by the element 102_1 in the positive x-direction (+x), as shown in Fig. II-3. A Lorentz force F_L is caused by the interaction between the magnetic field vector B (due to the presence of the magnet 202) and the eddy current vector J_e as follows :

$$F_L = J_e \times B \hspace{3cm} \text{(A II-1)}$$

In embodiments where the direction of magnetization of each of the plurality of elements 102_1, 102_2, 102_3, ..., 102_N is orthogonal to the surface 106 of the waveguide 106, the magnetic field vector B and the eddy current vector J_e are substantially perpendicular, and the Lorentz force F_L may be generated by the element 204 in the positive z-direction (+z), as shown.

In the case of the EMAT 100, each of the elements 104a, 104b, 104c, 104d, ... of the plurality of elements 102_1, 102_2, 102_3, ..., 102_N may be separately supplied with respective excitation signals via an excitation system, for instance the excitation system 206, which may be electrically coupled to the plurality of elements 102_1, 102_2, 102_3, ..., 102_N. Although a single excitation system 206 is shown, it should be understood that multiple excitation systems 206 may apply.

In some embodiments, the excitation system 206 may activate (or excite) the plurality of elements 102_1, 102_2, 102_3, ..., 102_N of the EMAT 100 at substantially the same time and with the same signal. This technique may be referred to as "comb excitation", and allows control of the excited modes of the guided ultrasonic wave 110 as a function of the distance (or the pitch) between adjacent elements 102_1, 102_2, 102_3, ..., 102_N. Using comb excitation, the modes of the ultrasonic guided wave 110 can only be excited as certain wavelengths corresponding to a multiple of the pitch. For comb excitation, the amplitude $A_n(\omega, x)$ of the mode n is given by :

$$A_n(\omega, x) = U \cdot F(\omega) \cdot C_n(x) \cdot H(\omega, x) \qquad \text{(A II-2)}$$

where U is the particle displacement, $F(\omega)$ is the frequency response of the elements, $C_n(x)$ is the coupling coefficient between the waveguide surface traction and the guided wave mode, and

$$H(\omega, x) = \sum_{i=1}^{N} e^{j[\omega t \pm k_x \cdot (x - x_i)]} = \frac{\sin(N \frac{k_x p}{2})}{\sin(\frac{k_x p}{2})} e^{j[\omega t \pm k_x \cdot (x - x_c)]} \qquad \text{(A II-3)}$$

where ± is negative for the direction of propagation (for instance the direction of propagation A of the wave 110) and positive for the direction opposite to the direction of propagation, p is the pitch, N is the number of elements, ω is the angular frequency, $k_x = \frac{\omega}{V_p}$ is the wavenumber component along the direction of propagation and x_c is the center of the transducer array, for instance the geometrical center (not shown) of the EMAT 100. When p is equal to a multiple of the wavelength $\lambda = \frac{2\pi}{k_x}$, then $|H(\omega, x)|$ reaches its maximum. The modes will then be excited at wavelengths equal to a multiple of p. By changing the pitch of the transducer it is then possible to generate modes at other wavelengths. The multiplication of $|H(\omega, x)|$ by the frequency spectrum of the signal used allows to estimate in which part of the dispersion curves the energy of the excitation will be distributed, as discussed in further detail herein below.

In other embodiments, the excitation system 206 may activate each of the plurality of elements 102_1, 102_2, 102_3, ..., 102_N with a time delay, such that the activation of each the plurality of elements 102_1, 102_2, 102_3, ..., 102_N is staggered relative to one another. In some embodiments, the delay may be linear, although other possibilities may apply. This modified form of comb excitation with a linear delay law is also known as "phase velocity excitation".

When considering a time delay increasing with a step t_0 between each element, equation (2) becomes :

$$H(\omega, x) = \sum_{i=1}^{N} e^{j[w(t-t_i))\pm k(x-x_i))]} = \frac{\sin(N\pi(\frac{p}{\lambda} \pm \frac{t_0}{T}))}{\sin(\pi(\frac{p}{\lambda} \pm \frac{t_0}{T}))} e^{j\left[w(t-\frac{N-1}{2}t_0)\pm k(x-x_c)\right]} \qquad \text{(A II-4)}$$

where T is the period. $|H(\omega, x)|$ will be maximized when $\frac{p}{\lambda} \pm \frac{t_0}{T} = m$, where m is an integer. Therefore, the mode will now be excited at a wavelength depending on the pitch of the transducer and the time step of the delay law t_0. It is then possible, by adjusting the delay law, to select the mode to be excited without changing the physical characteristics of the transducer (e.g., the EMAT 100).

A specific case of the phase velocity excitation described above occurs when the pitch of the transducer is small compared to the wavelength, i.e. $\frac{p}{\lambda} \ll 1$. When considering the +x direction of propagation, then the closest integer to m is 0. Equation (3) is not defined for $m = 0$ but the equation shows that $|H(\omega, x)|$ is locally continuous in the neighborhood of $m = 0$. When $m = 0$ then the excited phase velocity no longer depends on the frequency :

$$V_p = \frac{\lambda}{T} = \frac{p}{t_0} \tag{A II-5}$$

This specific case allows an excitation at a constant phase velocity under the condition that $\frac{p}{\lambda} \ll 1$.

In general, the net force F generated by an EMAT transducer, for instance by the EMAT 100, is calculated as follows :

$$F = F_L + F_M \tag{A II-6}$$

where F_L is the Lorentz force and F_M is the magnetostrictive force induced by the plurality of elements 102_1, 102_2, 102_3, . . ., 102_N (or a single element as in 102_1) of the EMAT 100.

The net force F generated by an EMAT transducer may be approximated by the Lorentz force F_L, neglecting the magnetostrictive force F_M :

$$F \approx F_L = J_e \times B \tag{A II-7}$$

where J_e is the eddy current vector, B is the magnetic field vector, and F_L is the Lorentz force induced by the plurality of elements 102_1, 102_2, 102_3, . . ., 102_N (or by the single element 102_1) of the EMAT 100.

Fig. II-4 shows another embodiment of the EMAT 100 in which the plurality of transducer elements comprises a first set (i.e. a first plurality) of elements 3021, 3022, 3023, . . ., 302N and a second set (i.e. a first plurality) of elements 304_1, 304_2, 304_3, . . ., 304_N. The first plurality of elements 3021, 3022, 3023, . . ., 302N and the second plurality of elements 304_1, 304_2, 304_3, . . ., 304_N are arranged in a linear (one-dimensional) array (with individual transducer elements being arranged adjacent to one another along the x axis), such that the transducer elements together form a two-dimensional (or matrix) array. It should be understood that any suitable number of sets of transducer elements may apply. For instance, although two sets of elements are shown in Fig. II-4, it should be understood that the EMAT 100 may comprise three (3) or more sets of transducer elements. In one embodiments, all individual transducer elements in a given set comprise a magnet 202 and coil 204 combination wound in the manner described above with reference to Fig. II-3.

Fig. II-5 shows a first plot 400 of dispersion curves for a Lamb wave. Fig. II-6 shows a second plot 402 of dispersion curves for a SH wave. The Lamb wave and the SH wave propagate in a structure, for instance in the waveguide 106. The plots 400 and 402 represent phase and group velocities of the different modes that can propagate as a function of the frequency-thickness product. In general, as frequency increases, the number of modes propagating also increases.

In Fig. II-5, symmetrical modes S_0, S_1, S_2, S_3, . . . and asymmetrical modes A_0, A_1, A_2, A_3, . . . of the Lamb wave are plotted. Intersection points may be observed, on the dispersion curves of plot 400, between symmetrical and asymmetrical modes of the Lamb wave, for instance at points p1, p2, and p3 (other points not shown). These intersections may be undesirable in some conditions.

Depending on a thickness of the waveguide 106, two types of modes may propagate. On the one hand, the fundamental modes S_0 and A_0 (for Lamb waves) and SH_0 (for SH waves) can propagate regardless of the frequency-thickness product, as seen from plots 400 and 402. On the other hand, the higher-order modes (S_1 and above and A_1 and above for Lamb waves, and SH_1

and above for SH waves) are constrained to propagate only above a certain frequency-thickness product threshold, known as the cutoff frequency or cutoff frequency-thickness product.

In some embodiments, ultrasonic guided wave tomography may be used to map the phase velocity of a mode of the guided ultrasonic wave 110 in a given plate-like structure, for instance the waveguide 106, which can then, using the dispersion curves, for instance the ones in plots 400 and 402, be converted into a thickness map of the waveguide 106.

In some embodiments, thickness reductions in the waveguide 106 may act as low pass filters. By propagating the guided ultrasonic wave 110 in the waveguide 106 of a given thickness and detecting the modes cut off, it may be possible to infer the minimum remnant thickness of the waveguide 106 along the propagation path of the guided ultrasonic wave 110. Using this method, the thickness of the waveguide 106 over longer distances may be determined.

Fig. II-6 shows a plot 402 of dispersion curves for a SH wave propagating in a structure, for instance in the waveguide 106, representing phase and group velocities of the different modes that can propagate as a function of the frequency-thickness product. Modes SH_0, SH_1, SH_2, SH_3, SH_4, . . . are plotted. The absence of intersection points on the dispersion curves 402 between modes of the SH wave (compare with dispersion curves in plot 400) may allow a simpler interpretation of the data and a more regular thickness estimation of the waveguide 106 than with Lamb waves.

Fig. II-7 shows a plot 500 for a SH wave propagating in a structure, for instance in the waveguide 106. Dispersion curves for the propagating SH wave are shown, similar to the dispersion curves in plot 402 of Fig. II-6. Line 502 represents the minimal wavelength detectable by a transducer, for instance the EMAT 100, having a certain pitch. Frequencies 504, 506, 508, 510, and 512 for modes SH_0, SH_1, SH_2, SH_3, and SH_4, respectively, of the propagating SH wave are indicated. The frequencies 504, 506, 508, 510, and 512 each represent the maximum frequency at which a given mode can be generated or detected. In some embodiments, the excitation of higher order modes in the high frequency range (i.e. above a given cutoff frequency) using the systems and methods disclosed herein may be of particular interest.

While the EMAT 100 is described and illustrated herein with reference to the excitation and detection of SH modes, it should be understood that other guided wave modes may be excited and/or detected using the EMAT proposed herein. This may be achieved by modifying the configuration of the transducer elements (e.g., modifying the winding of the coils as in 204 or the polarization of the magnets as in 202).

Referring now to Fig. II-8, a method 600 for assembling an electromagnetic acoustic transducer, for instance the EMAT 100, will now be described in accordance with one embodiment. At step 602, a plurality of elements, for instance the plurality of elements 102_1, 102_2, 102_3, . . ., 102_N, described above with reference to Figs. 1, 2A, 2B, and 3, are provided. Each element comprises a magnet and a coil wound around the magnet. At step 604, the plurality of elements are arranged in an array on a surface of a waveguide (waveguide such as the waveguide 106 describe above with reference to Fig. II-1), with a direction of magnetization that alternates from one element to the next.

In order to validate the EMAT proposed herein, three-dimensional (3D) finite element simulations were performed. The element size was set to allow fifteen (15) elements per wavelength using the shortest wavelength to be simulated. The time step was defined such that the fastest ultrasonic wave packet could not, in a time increment, skip an element. The propagation of the ultrasonic wave was carried out using Pogo FEA®, an explicit time domain solver accelerated by graphics processing units (GPU), enabling the simulation of large models within a reasonable time frame and at a relatively low computing infrastructure cost. Wave generation was performed by importing a force field in a Pogo mesh. For each probe, a uniform force field was imposed under the surface of each element with a time variation corresponding to the signal used. Therefore, the effect of the displacement field on the Lorentz force was not taken into account. On the receiving end, the displacements were measured on each of the nodes below the elements. The distance between the transmitting and receiving probes was set to 20 cm. Finally, absorbing boundaries, designed with the Absorbing Layer with Increasing Damping (ALID) method, were added on the edges of the waveguide to reduce the amplitude of the echoes and thus simulate an infinite plate.

Several scenarios were then tested. First, a single element of the linear array structure proposed herein was used in transmission and a 20-element linear array probe (as described herein with reference to Fig. II-2) was used in reception. Each element was composed of a magnet and an encircling coil. The coil was composed of 50 turns of 0.32 mm diameter copper wire (28 AWG) and N55 grade neodymium magnets having a witdth (along the x direction) of 3.2 mm, a length (along the z direction) of 25.4 mm, a height (along the y direction) of 6.2 mm, and a through height (y) magnetization were used. The propagation distance was set to 20 cm. Narrow-band signals were used, with 15-cycle Hann-windowed tonebursts centered around 370 and 498 kHz. According to the dispersion curves (described herein with reference to Figs. 4A, 4B, and 5), this should allow the excitation of SH_0, SH_1 and SH_2. This test was designed to verify the amplitude transmitted with a single element. Fig. II-9 shows the energy distribution of the different modes on a phase velocity vs. frequency map. Fig. II-9 (e) and Fig. II-9 (f) were obtained by subtracting the corresponding simulation figure from the experimental one on a linear scale. The two graphs allow to better compare the difference between the simulated and the experimental cases. When the amplitude on a pixel of the image is 1, it means that the simulations have detected a mode at this position (frequency, phase velocity) and that no mode was detected experimentally. For a value of -1, the opposite is true. When values close to 0 are obtained, simulations and experiments are in agreement and the amplitudes detected for this pixel are identical.

As can be seen from Fig. II-9, during a transmission centered around 370 kHz, three modes were excited. SH_0 and SH_1 were excited at a phase velocity of about 3600 m/s and SH_2 at a phase velocity higher than 4800 m/s. For the excitation around 498 kHz, only SH_2 was excited around a phase velocity of 4400 m/s. A closer look at Fig. II-9 (e) reveals a shift of about 20 kHz on the excitation frequency of SH_2. This error can simply be explained by the fact that the properties of the steel plate for the simulations were approximated. An inaccuracy in the material properties can shift the dispersion curves on both the phase velocity and frequency axes. The preceding notwithstanding, the experimental results were very similar to the predictions obtained by simulations and prove the capabilities of the proposed EMAT linear array when it

comes to detecting and separating one or more high-order SH modes in the case of a narrow frequency band emission.

A second case investigated the use of a broadband PPM EMAT associated with a chirp sweeping from 300 to 800 kHz over 50 μs. The PPM EMAT was realized with 2x9 magnets by progressively increasing the distance between two successive magnets. The pitch was varied from 3.2 to 6.8 mm. By generating a multimodal wave, it was possible to evaluate whether the EMAT linear array proposed herein allows to measure (using two-dimensional Fourier transform (2D-FFT)) the amplitude of several high-order modes at the same time. For this purpose, the input signal transmitted to the probe was a chirp varying from 300 to 800 kHz over 50 μs. The reception was performed with the EMAT linear array and a laser vibrometer used mainly to allow a comparison without the influence of the bandwidth of the receiving probe.

Fig. II-10 (a-c-e) presents the 2D-FFT, on a phase velocity vs frequency diagram, of the signals obtained experimentally and by simulation using the EMAT linear array in reception, and Fig. II-10 (b-d-f), using the laser vibrometer. Experimentally, SH_0 to SH_3 were detected by the EMAT linear array. However, the amplitude decreases with the mode order. The modes with the highest amplitudes were SH_0 and SH_1, while the amplitude of SH_2 was -5 dB and that of SH_3 was -12 dB. Measurements with the laser vibrometer also showed a loss of amplitude with the order of the mode but on a smaller scale. SH_0 to SH_2 were detected with a maximum amplitude of 0 dB, while that of SH_3 was -5 dB and for SH_4 it was -15 dB. The predictions by simulations were identical in both cases, and looking at Fig. II-10 (c), it can be seen that the simulations predicted that SH_0 to SH_4 should be excited homogeneously and that SH_5 was outside the bandwidth of the signal used, and would be detected with a lower amplitude. The difference between the experimental and simulation results can be explained by the fact that no attenuation was considered in the finite element models. The amplitude of high-order modes at a higher frequency is therefore overestimated in the simulations. One explanation for the discrepancy between the results using the EMAT linear array and those using the laser vibrometer could be that the bandwidth of the EMAT and of its receiving electronics is narrower than that of the laser.

For the last validation case, the ability of the EMAT linear array to generate and detect an SH wave was compared to that of a piezoelectric shear ultrasonic phased array (PA) probe (e.g., the Olympus 0.75L64-96X22-CA-P-2.5-OM-POL shear PA probe). Both probes were successively used in transmission and reception. When transmitting with the PA probe, a single-cycle Hann-windowed toneburst centered around 750kHz was used and a delay law allowing a constant phase velocity excitation of around 7300 m/s was implemented. When the EMAT linear array was used in transmission, the acquisition was performed sequentially due to a lack of an EMAT array controller. A full matrix capture (FMC) was performed by combining all the transmitting elements of the EMAT linear array and the receiving elements of the PA probe. The signal used was a chirp sweeping from 300 to 800 kHz over 50 μs. An excitation around a constant phase velocity of 7300 m/s was generated in post-processing by adding the corresponding delay to each transmission frame (see Eq.(5)) to allow a comparison of the two technologies. The separation distance was 20 cm. Sampling in time and space was performed to apply a 2D-FFT. Fig. II-11 (a) shows the experimental results obtained in this configuration, Fig. II-11 (c) shows those obtained by simulation, and Fig. II-11 (e) shows the difference between the figure obtained by simulation and the one obtained experimentally on a linear scale. First, it can be observed that the excitation of the modes occurs around 7300 m/s. However, only SH_3 and SH_4 are detected experimentally, whereas the simulations predicted an excitation from SH_1 to SH_4. The most likely reason for this difference between the simulation and experiments relates to the bandwidth of the phased array probe. According to the probe documentation, the amplitude of the transfer function at 500 kHz is 24 dB below its value at 750 kHz. SH_1 and SH_2 were likely generated at an amplitude too low to be detected.

The second part of this validation step consisted in using the EMAT linear array in transmission and the shear PA probe in reception. The signal used was a chirp sweeping from 300 to 800 kHz over 50 μs. Due to equipment limitations, only one element of the EMAT could be activated at a time, making a constant phase velocity excitation impossible. The solution used was to proceed to an FMC by combining all the transmitting elements of the EMAT linear array and the receiving elements of the PA probe. The corresponding delay was then added, in post-processing,

to each transmission frame to reconstruct a constant phase velocity excitation around 7300 m/s. As can be seen experimentally (Fig. II-11 (b)) or by simulation (Fig. II-11 (d)), the modes were excited around a phase velocity of 7300 m/s. SH_1 could not be detected experimentally. SH_2 is visible, but has an amplitude 6 dB below the amplitude predicted by simulation. As before, this phenomenon is most likely due to the bandwidth of the phased array probe, since it is not present in the results of configurations involving only EMATs (Fig. II-9 and Fig. II-10). These results are nevertheless encouraging because the capabilities of the EMAT array developed to generate and detect SH modes are similar to those of a piezoelectric phased array probe.

Crosstalk between elements of the EMAT array was also investigated. Crosstalk refers to the coupling between two unconnected cables and is a phenomenon inherent to any measurement using alternating current. If the coupling is too strong, the current generated by one of the transducer elements will be instantly transmitted to the other elements in the vicinity, which will pollute the measured waveforms. To evaluate the crosstalk between the different elements, an EMAT linear array of ten (10) elements was assembled and positioned on a steel plate in order to simulate usage in real conditions. The first element of the structure was connected to the arbitrary function generator port of a TiePie HS5. The signal used was a 5-cycle Hann windowed toneburst centered around a frequency of 500 kHz with an amplitude of 4 V peak to peak. The results are presented in Fig. II-12 and show the relative amplitude of the waveform due to crosstalk as compared to the signal supplied to the transmitter coil. As can be noted, a 28 dB loss of amplitude can be seen between the first and second elements, corresponding to a division of the amplitude by 25 on a linear scale. From the fifth element, this loss is between 37 and 41 dB. The amplitude of a crosstalk signal induced between the elements will therefore be at least 28 dB below the amplitude of the waveform generated by the propagation of a wave below one of the elements. The crosstalk between the elements may therefore be considered negligible for the EMAT proposed herein.

From the above, it can be seen that, in one embodiment, the EMAT proposed herein may advantageously allow for flexibility with regards to the choice of the excitation mechanism (i.e. the emission technique) used, which can be a comb or a constant phase velocity excitation, for

example. On the reception side, the multi-element nature of the EMAT may allow to sample propagating modes in space and time, allowing for the use of 2D-FFT processing to separate and extract the amplitude of the different modes. In particular, in one embodiment, the minimum detectable wavelength, or the maximum detectable wavenumber, is equal to twice the pitch. The aperture, equal to the pitch multiplied by the number of transducer elements (as in 102_1, 102_2, 102_3, . . ., 102_N, in Fig. II-2), may then determine the wavenumber step of the energy map obtained with the 2D-FFT.

Although the embodiments have been described in detail, it should be understood that various changes, substitutions and alterations can be made herein without departing from the scope as defined by the appended claims.

Moreover, the scope of the present application is not intended to be limited to the particular embodiments of the process, machine, manufacture, composition of matter, means, methods and steps described in the specification. As one of ordinary skill in the art will readily appreciate from the disclosure of the present invention, processes, machines, manufacture, compositions of matter, means, methods, or steps, presently existing or later to be developed, that perform substantially the same function or achieve substantially the same result as the corresponding embodiments described herein may be utilized. Accordingly, the appended claims are intended to include within their scope such processes, machines, manufacture, compositions of matter, means, methods, or steps

As can be understood, the examples described above and illustrated are intended to be exemplary only. The scope is indicated by the appended claims.

6.   What is claimed is :

1. An electromagnetic acoustic transducer comprising : a plurality of spaced elements arranged in an array on a surface of a waveguide with a direction of magnetization of the plurality of elements alternating from one of the plurality of elements to a next one of the plurality of

elements, each element of the plurality of elements comprising a magnet and a coil wound around the magnet.

2. The transducer of claim 1, wherein the waveguide is made of a ferromagnetic and conductive material.

3. The transducer of claim 2, wherein the plurality of elements is provided directly on the surface of the waveguide.

4. The transducer of claim 1, wherein the waveguide is a plate-like structure.

5. The transducer of claim 1, wherein the waveguide is a section of pipeline.

6. The transducer of claim 1, wherein the direction of magnetization of each element of the plurality of elements is orthogonal to the surface of the waveguide.

7. The transducer of claim 1, wherein the plurality of elements are arranged in a linear array.

8. The transducer of claim 1, wherein the plurality of elements are arranged in a two-dimensional array.

9. The transducer of claim 1, wherein each coil is configured to be supplied with an excitation signal via comb excitation.

10. The transducer of claim 1, wherein each coil is configured to be supplied with an excitation signal via phase velocity excitation.

11. The transducer of claim 1, wherein the plurality of elements are spaced from one another by a regular distance.

12. The transducer of claim 1, wherein the plurality of elements are spaced from one another by an irregular distance.

13. A method for assembling an electromagnetic acoustic transducer, the method comprising : providing a plurality of elements, each element of the plurality of elements comprising a magnet and a coil wound around the magnet ; and arranging the plurality of elements in an array on a surface of a waveguide, with a direction of magnetization alternating from one of the plurality of elements to a next one of the plurality of elements.
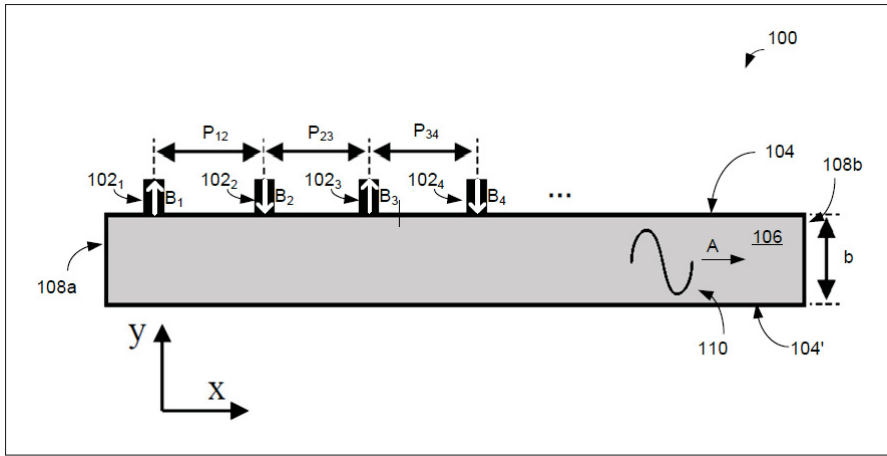
Figure-A II-1   Schematic diagram of a multi-element electromagnetic acoustic transducer.
Tirée du brevet correspondant à l'annexe II
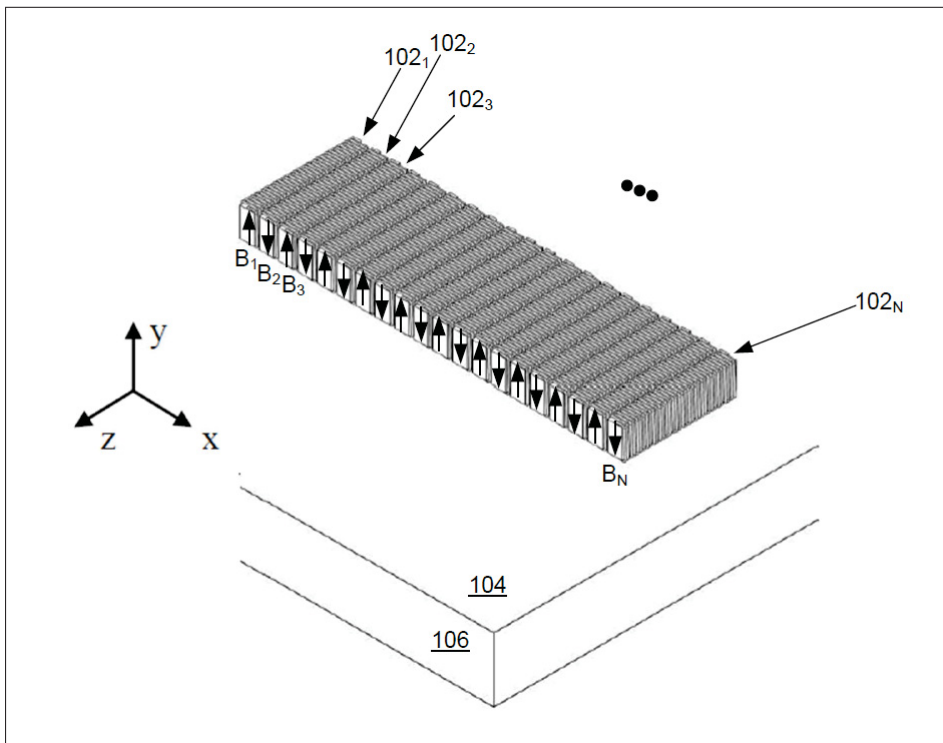
Figure-A II-2   Perspective view of the multi-element electromagnetic acoustic transducer
of Fig. II-1. Tirée du brevet correspondant à l'annexe II
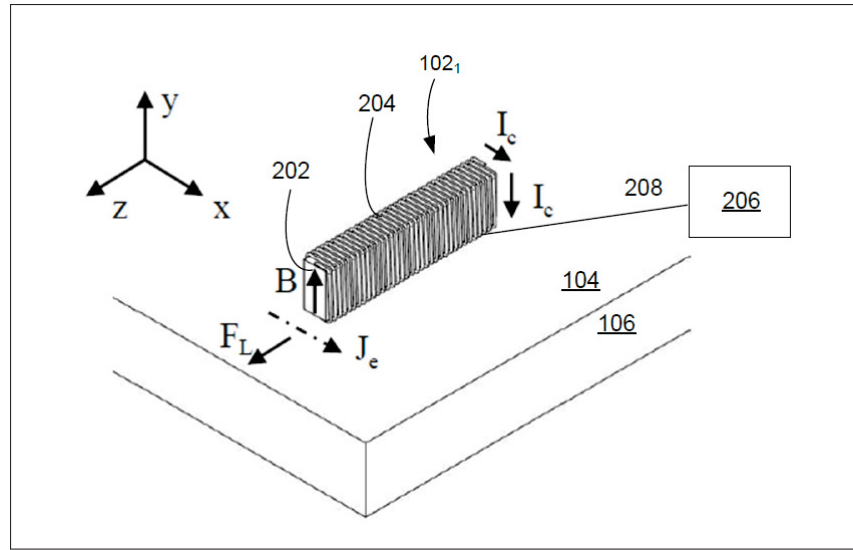
Figure-A II-3   Perspective view of one element of the multi-element electromagnetic acoustic transducer of Fig. II-2. Tirée du brevet correspondant à l'annexe II
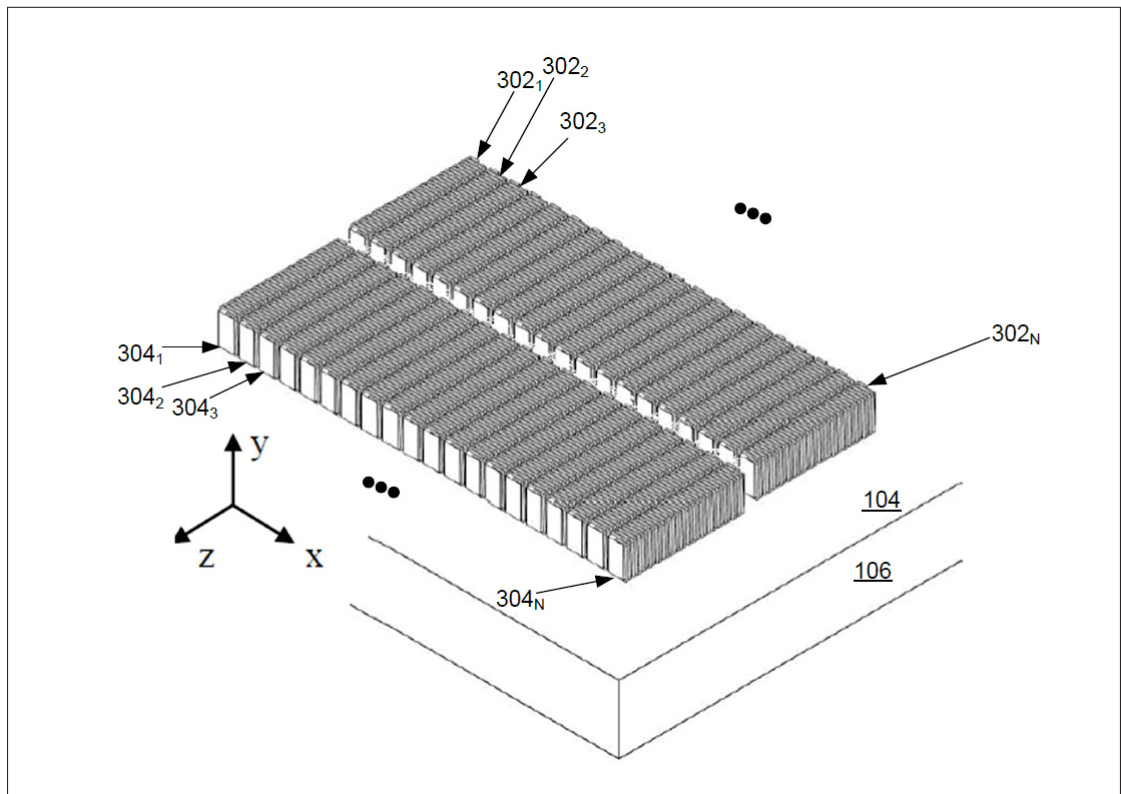
Figure-A II-4   Perspective view of multiple multi-element electromagnetic acoustic transducers side by side. Tirée du brevet correspondant à l'annexe II
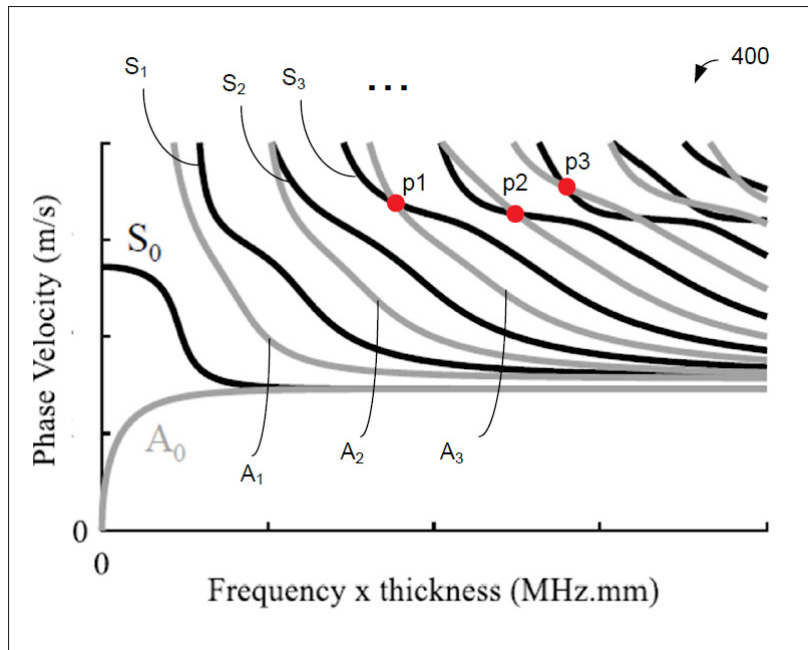
Figure-A II-5　Lamb wave phase velocity dispersion curves as a function of the frequency-thickness product in a steel plate. Tirée du brevet correspondant à l'annexe II
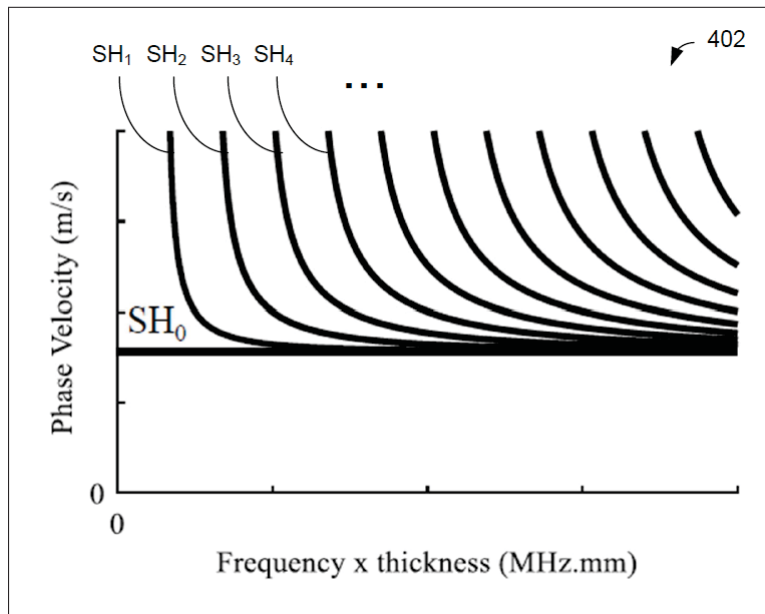
Figure-A II-6　SH wave phase velocity dispersion curves as a function of the frequency-thickness product in a steel plate. Tirée du brevet correspondant à l'annexe II
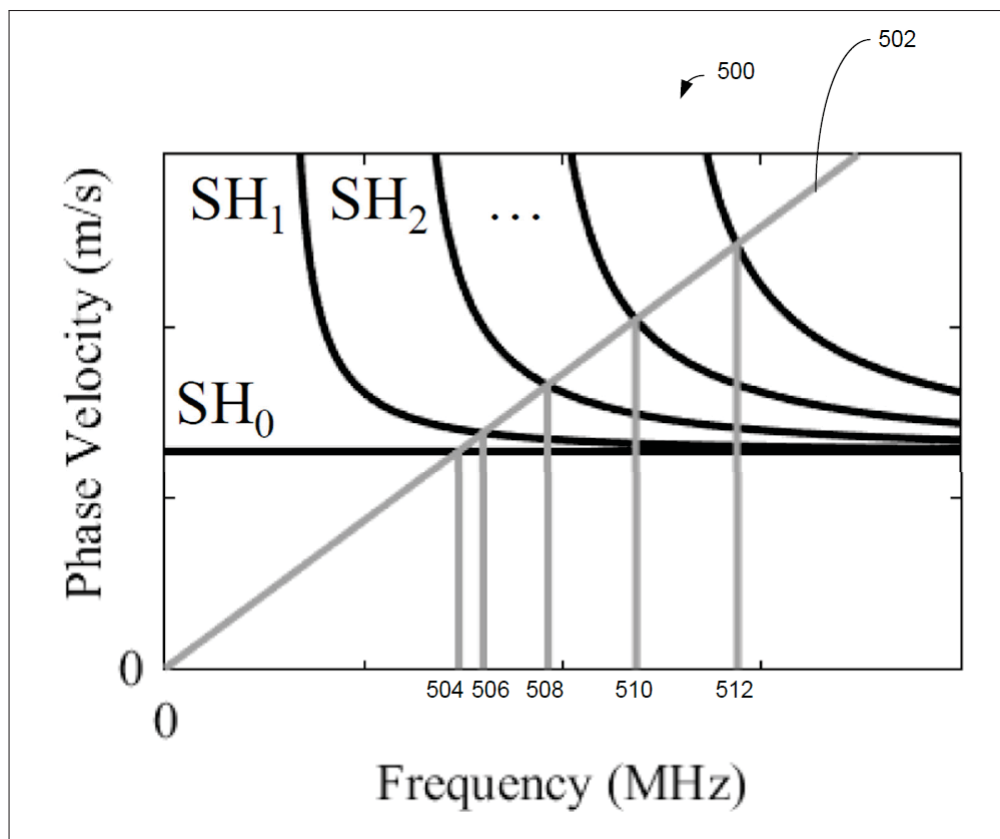
Figure-A II-7 Maximum detectable frequencies for each SH_0 to SH_4 when the excitation is made with a multi-element electromagnetic acoustic transducer with a pitch of 4.3 mm.
Tirée du brevet correspondant à l'annexe II
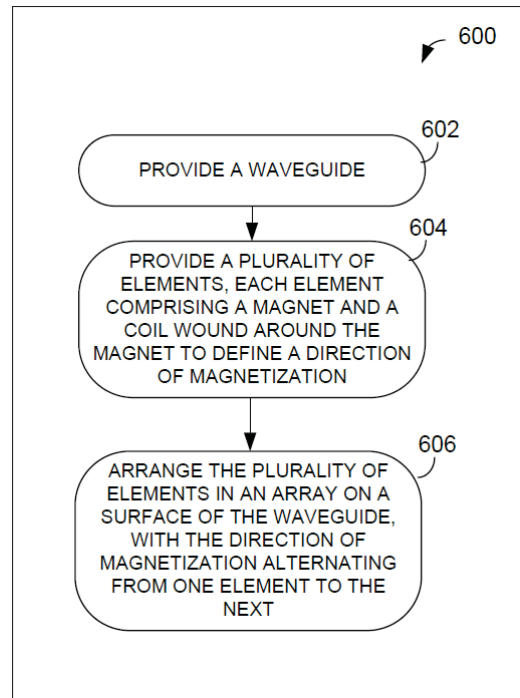
Figure-A II-8   Flowchart illustrating an example method for assembling an electromagnetic acoustic transducer. Tirée du brevet correspondant à l'annexe II
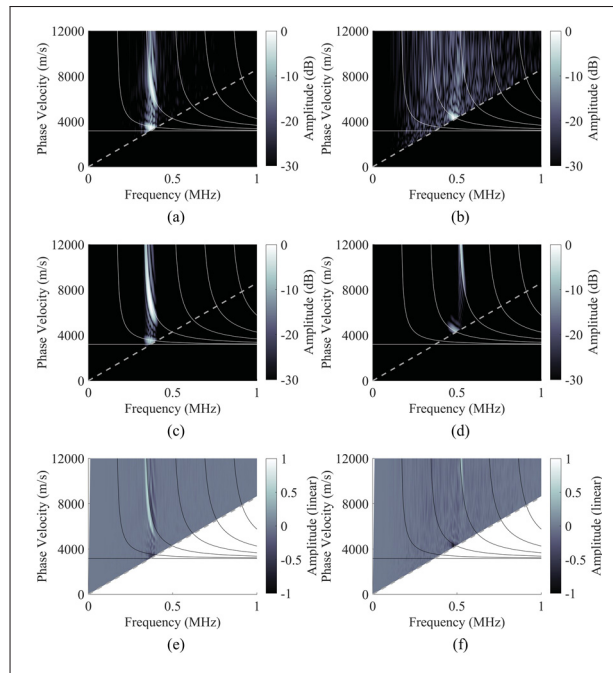
Figure-A II-9   (a-c-e) 2D-FFT of the signals received with the developed EMAT linear array (20 element, pitch = 4.3 mm) when transmitting a 15-cycle Hann-windowed toneburst centered around 370 kHz with a single element of the linear array structure. (b-d-f) 2D-FFT of the signals received with the developed EMAT linear array when transmitting a 15-cycle Hann-windowed toneburst centered around 498 kHz with a single element of the linear array structure. In each case, the propagation distance was 20 cm. (a) and (b) were obtained experimentally, (c) and (d) by simulation, and (e) and (f) represent the difference on a linear scale between the simulation and experimental figure. The grey dotted lines represent the minimal wavelength detectable by a linear array probe with a pitch of 4.3 mm. Tirée du brevet correspondant à l'annexe II

Figure-A II-10   (a-c-e) 2D-FFT of the signals received with the developed EMAT linear array (20 element, pitch = 4.3 mm) when transmitting a chirp sweeping from 300 to 800 kHz over 50 μs with the broadband PPM EMAT. (b-d-f) 2D-FFT of the signals received with a laser vibrometer (90 points spaced 1 mm apart) when transmitting a chirp sweeping from 300 to 800 kHz over 50 μs with the broadband PPM EMAT. In each case, the propagation distance was 20 cm. (a) and (b) were obtained experimentally, (c) and (d) by simulation, and (e) and (f) represent the difference on a linear scale between the simulation and experimental figure. The grey dotted lines represent the minimal wavelength detectable by a linear array probe with a pitch of 4.3 mm (a-c-e) and 1 mm (b-d-f). Tirée du brevet correspondant à l'annexe II
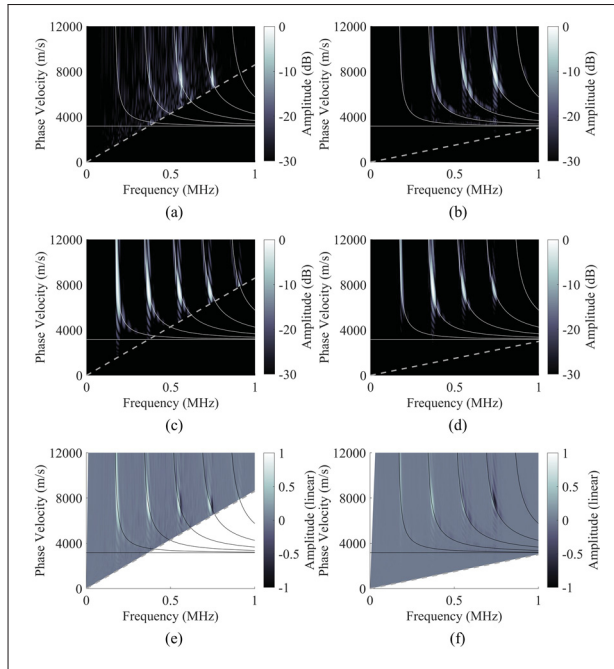
Figure-A II-11   (a-c-e) 2D-FFT of the signals received with the developed EMAT linear array (20 element, pitch = 4.3 mm) when transmitting a single-cycle Hann-windowed toneburst centered around 750 kHz with the Olympus 0.75L64-96X22-CA-P-2.5-OM-POL (64-element, pitch = 1.5 mm) with a delay law enabling a constant phase velocity excitation around 7300 m/s. (b-d-f) 2D-FFT of the signals received with the Olympus 0.75L64-96X22-CA-P-2.5-OM-POL when transmitting a chirp sweeping from 300 to 800 kHz over 50 μs with the developed EMAT linear array. A constant phase velocity excitation around 7300 m/s was reconstructed in post-processing. In each case, the propagation distance was 20 cm. (a) and (b) were obtained experimentally, (c) and (d) by simulation, and (e) and (f) represent the difference on a linear scale between the simulation and experimental figure. The grey dotted lines represent the minimal wavelength detectable by a linear array probe with a pitch of 4.3 mm (a-c-e) and 1.5 mm (b-d-f). Tirée du brevet correspondant à l'annexe II
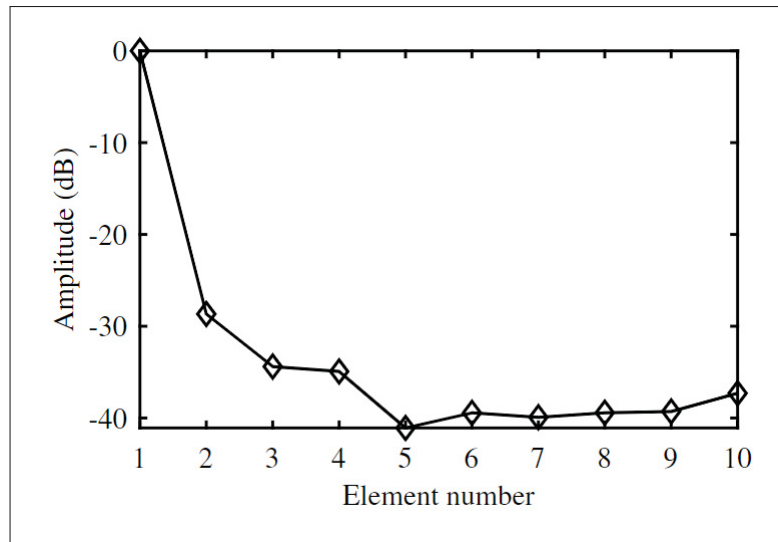
Figure-A II-12   Measured crosstalk between the element of the developed EMAT linear array. Tirée du brevet correspondant à l'annexe II

NONDESTRUCTIVE TESTING SYSTEM AND METHOD USING REFLECTED SHEAR HORIZONTAL GUIDED WAVES

André Dionne[1,2] , Aurélien Thon[1,2] , Pierre Bélanger[1,2]

[1] Piezoelectricity and Ultrasonics Technologies and Materials Laboratory at ÉTS (PULÉTS), 1100 Notre-Dame Ouest, Montréal, Québec, Canada H3C 1K3

[2] Département de Génie mécanique, École de Technologie Supérieure, 1100 Notre-Dame Ouest, Montréal, Québec, Canada H3C 1K3,

1.   Field

The improvements generally relate to the field of nondestructive testing, and, more particularly, to the use of ultrasonic guided waves for nondestructive testing.

2.   Introduction or background

The inspection of corroded structures is crucial across many industries. Affected areas are often difficult to access due to other impeding structures, such as pipe support or insulation. This makes standard thickness gauging methods such as point-by-point ultrasonic thickness gauging impossible.

The use of ultrasonic guided waves in nondestructive testing enables rapid inspections over long distances. In a pipe, several modes can propagate, such as flexural (axisymmetric and non-axisymmetric) and torsional modes (axisymmetric and non-axisymmetric). Various techniques are known to propagate waves in pipes and detect defects. While these techniques are suitable for their purposes, improvements are desired.

3.   Summary

In accordance with one aspect, there is provided a method for nondestructive testing of a structure. The method comprises driving at least one ultrasonic probe to cause at least one shear horizontal (SH) guided wave to propagate in the structure, receiving at least one reflected guided wave signal from the structure in response to driving the at least one ultrasonic probe, performing a comparison between an amplitude of the at least one reflected guided wave signal and an amplitude threshold, and determining a thickness of the structure based on the comparison and detecting, based on the thickness as determined, a presence or an absence of at least one defect in the structure.

In accordance with another aspect, there is provided a system for nondestructive testing of a structure. The system comprises an ultrasonic probe configured to be coupled to the structure and to cause, when driven, at least one shear horizontal (SH) guided wave to propagate in the structure, a processing unit, and a non-transitory computer-readable medium having stored thereon instructions executable by the processing unit for driving at least one ultrasonic probe, receiving at least one reflected guided wave signal from the structure in response to driving the at least one ultrasonic probe, performing a comparison between an amplitude of the at least one reflected guided wave signal and an amplitude threshold, and determining a thickness of the structure based on the comparison and detecting, based on the thickness as determined, a presence or an absence of at least one defect in the structure.

Many further features and combinations thereof concerning embodiments described herein will appear to those skilled in the art following a reading of the instant disclosure.

4. Description of the figures

Reference is now made to the accompanying figures in which :

Fig. III-1 is a schematic diagram of an example nondestructive testing system, in accordance with an illustrative embodiment;

Fig. III-2 is a block diagram of the determination unit of Fig. III-1, in accordance with an illustrative embodiment;

Fig. III-3 is a schematic diagram of an ultrasonic phased array probe, in accordance with an illustrative embodiment;

Fig. III-4, Fig. III-5, and Fig. III-6 are flowcharts of an example nondestructive testing method, in accordance with an illustrative embodiment;

Fig. III-7 illustrates simulation results for a structure having a defect and Fig. III-8 illustrates simulation results for a structure having no defect, in accordance with an illustrative embodiment;

Fig. III-9, Fig. III-10, Fig. III-11, and Fig. III-12 illustrate simulation results obtained for a SH1 propagation on a 3/8 inches steel plate, in accordance with an illustrative embodiment; and

Fig. III-13 is a block diagram of an example computing device, in accordance with an illustrative embodiment.

It will be noticed that throughout the appended drawings, like features are identified by like reference numerals.

5.   Detailled description

The present disclosure is directed to systems and methods for nondestructive testing (or inspection) of objects including, but not limited to, steel pipes, using ultrasonic guided waves. Ultrasonic guided waves are mechanical perturbations that propagate between two boundaries forming a waveguide such as a plate or a pipe. In a plate, ultrasonic guided waves can be separated into Lamb waves (symmetrical and anti-symmetrical), and shear horizontal (SH) waves. Within each category, there are fundamental modes and high order modes. When impinging a defect or a feature parallel to the direction of polarization, SH waves will not convert to Lamb modes. In addition, the cutoff frequencies-thickness product of high-order SH modes are evenly distributed

along the frequency-thickness product axis (indicative of the product of waveguide thickness and frequency), which allows the estimation of a thickness on regular intervals.

$$V_{p,n} = V_S \left(\frac{2fb}{\sqrt{4(fb)^2 - n^2 V_S^2}} \right) \tag{A III-1}$$

$$V_{g,n} = V_S \sqrt{1 - \frac{(n/2)^2}{(fb/V_S)^2}} \tag{A III-2}$$

where $V_{(p,n)}$ and $V_{(g,n)}$ are respectively the phase and group velocity of the n-order mode, V_S is the bulk shear wave velocity, f is the frequency, and b is the thickness of the waveguide. The fundamental mode SH_0 can propagate at all frequency-thickness products whereas high order modes are constrained to propagate only above a given cutoff frequency-thickness product. Below the cutoff frequency-thickness product, high order modes are considered as vanishing and their energy is reflected or converted into lower order modes. When the frequency-thickness product approaches the cutoff frequency-thickness product of high order modes, the mode's phase velocity tends towards infinity and the group velocity tends towards zero. This mode can no longer propagate and is then reflected or converted to a lower order mode. When a high order mode impinges an abrupt (i.e. sudden or discontinuous) thickness reduction, it will be converted to a lower order mode, and when the thickness of the waveguide allows, it may be converted back to its original state. Conversely, if the defect is smooth most of its energy will be reflected.

In metallic materials, corrosion is a chemical weathering by an oxidizer. This implies wear of the affected surfaces, which can be likened to a local loss of thickness. For a high-order SH mode, this will shift the frequency-thickness product below its cutoff frequency-thickness product. If the severity of the defect is sufficient, then the mode can reach its cutoff threshold. The energy of this mode will then no longer be able to propagate. Considering a plate of given thickness b, the cutoff frequency-thickness product of SHn can be obtained using equation (3) :

$$fb = \frac{nV_S}{2} \hspace{4cm} \text{(A III-3)}$$

where V_S is the bulk shear wave velocity. The use of multiple of modes makes it possible to increase the number of detection thresholds. However, the excitation and detection of high order mode become more complex as the frequency increases. The attenuation of a wave may be modeled using equation (4) :

$$I = I_0 e^{-2\alpha x} \hspace{4cm} \text{(A III-4)}$$

where I is the intensity of the wave at a distance x from its source, I_0 is the initial intensity, and α is the attenuation coefficient depending on the material properties and increasing with the frequency. Further than attenuation, the ultrasonic wave is also subject to scattering when it encounters a defect. High-order modes can be described as dispersive. The difference between their phase and group velocities implies an alteration in the waveform in the time domain along with its propagation. These phenomena affect higher order modes more strongly. Their experimental uses over a large propagation distance are therefore more complex than for the first SH modes.

The systems and methods described herein use SH ultrasonic guided waves for nondestructive testing. In particular, it is proposed herein to analyze guided wave signal(s) reflected from a structure in order to determine a thickness of the structure and detect the presence or absence of one or more defects in the structure. When a defect is present in the structure, the structure's thickness at the location of the defect can be referred to as a "remaining", "residual" or "remnant" thickness.

Referring to Fig. III-1, an example nondestructive testing system 100 will now be described. The system 100 is used to inspect a structure 102 (also referred to herein as a "structure under test" or a "structure under inspection"). The structure 102 is illustratively elongated (i.e. with

a length greater than its transverse dimension or diameter) and comprises a wall 103 having a substantially uniform thickness T. In one embodiment, the structure 102 may be a curved object and the wall 103 may have a smooth curvature in the transverse direction (i.e. with no abrupt changes in thickness or orientation). The structure 102 may also be a wall- or plate-like structure. The structure 102 may include, but is not limited to, a pipe, rod, rail, rectangular conduit, cylindrical vessel, plate, wall, or hollow bar. The structure 102 may be made of any suitable solid material, including, but not limited to, a metal, ferromagnetic material, metal alloy, plastic, or the like. The structure 102 may be used in any suitable application or industry (e.g., oil and gas, pipelines, power stations, industrial plants, and the like), for instance to carry oil, gas, petrochemicals, water, coolants, or the like.

The structure 102 may comprise a defect 104, which, in the illustrated embodiment, is a reduced wall thickness arising from corrosion of the wall 103. In other words, the defect 104 corresponds to a region of the structure 102 (also referred to herein as a "corroded area") that is thinner than the thickness T of a surrounding region of the structure 102. The defect 104 may be due to a cavity (not shown) in the structure 102, the cavity being caused by corrosion. The cavity illustratively extends from a surface (e.g., an inner or outer surface) of the structure 102. In the illustrated embodiment, the defect 104 has a depth Td, which represents a portion of the original wall thickness T (i.e. a thickness reduction of the structure 102), such that the structure 102 has a remnant thickness Tr at the location of the defect 104, where T = Tr + Td. It should however be understood that defects other than corrosion-type defects may apply. It should also be understood that the defect 104 may be provided at any suitable location of the structure 102, such as in upper or lower parts of the structure 102. The structure 102 also comprises an impeding member 106, such as a pipe support or insulation. The defect 104 (e.g., the corroded area) and the impeding member 106 together form an area 108 (also referred to herein as a "partially accessible" or "inaccessible" area or zone) which is difficult to access.

An ultrasonic probe 110 is coupled to an outer surface 112 of the structure 102 for determining a thickness profile of the structure 102. As will be discussed further below, the probe 110 may be any suitable probe configured to allow the generation and the detection of SH guided waves.

In some embodiments, a single probe 110 is used to sequentially generate and detect SH waves. In other embodiments, two probes 110 are used, a first probe for generation of SH waves and a second probe for detection of SH waves. Thus, although illustrated herein as one probe, it should be understood that the probe 110 may comprise one or more probes.

The system 100 further comprises a determination unit 114 coupled to the probe 110 and configured to determine a thickness of the structure 102 based on reflection of the SH waves generated by the probe 110. As illustrated in Fig. III-2, in one embodiment, the determination unit 114 comprises a signal generating circuit 202 and a signal receiving circuit 204 comprising a thickness determination unit 206. In the illustrated embodiment, the electronic circuitry used for generating and detecting the SH waves (i.e. the signal generating circuit 202 and the signal receiving circuit 204) may be provided (e.g., packaged) separately from the probe 110. The probe 110 may then be connected (using any suitable connection means) to the signal generating circuit 202 and the signal receiving circuit 204. For example, a casing (not shown) may house the probe 110 and provide input and output ports for connection to the various circuitry needed to operate the probe 110. In other embodiments, the electronic circuitry used for generating and detecting the SH waves may be incorporated into the probe 110.

The signal generating circuit 202 is configured to generate a signal (referred to herein as an "emission signal") and transmit the emission signal to the probe 110. In one embodiment, the emission signal is a radio frequency (RF) signal having a suitable frequency (e.g., in the order of tens or hundreds of kilohertz (kHz)) and a suitable shape. The probe 110 is then configured to convert the emission signal into a guided wave and to excite a given SH mode of the guided wave at a time.

In one embodiment illustrated in Fig. III-3, the probe 110 is a multi-element probe, such as an ultrasonic phased array probe 300 comprising a plurality (N) of probe elements 302. The ultrasonic phased array probe 300 may be used to target a specific wavelength λ. The elementary pitch p (i.e. the pitch between two consecutive probe elements 302) may be selected to be smaller than the targeted wavelength λ, with $\frac{p}{\lambda} \ll 1$. In this embodiment, the ultrasonic phased

array probe 300 is able to excite high order guided wave modes at a constant phase velocity, independently of frequency. The phase velocity can be obtained as :

$$V_{ph} = \frac{p}{t_0} \qquad \text{(A III-5)}$$

where V_{ph} is the phase velocity, p is the fixed elementary pitch, and t_0 is the delay in emission between two consecutive probe elements 302, the delay being selected in order to excite the desired phase velocity V_{ph}. In order to excite a specific phase velocity, the ultrasonic phased array probe 300 may be aligned with the desired direction of propagation (indicated as z+ in Fig. III-3). A delay may then be added between each probe element 302, creating an angled plane wavefront 304. The delay required for each probe element 302 in order to excite a specific phase velocity may be written as :

$$t_i = \frac{p \times (i - 1)}{V_{ph}} \qquad \text{(A III-6)}$$

where t_i is the delay of element i, V_{ph} is the targeted phase velocity, and p is the elementary pitch of the probe 300. The angle α of the transmitted wavefront 304 may be directly related to the shear velocity (V_S) of the waveguide 306 and the targeted phase velocity (V_{ph}), as follows :

$$\alpha = \operatorname{asin} \frac{V_S}{V_{ph}} \qquad \text{(A III-7)}$$

The wave transmitted into the waveguide 306 travels dominantly in the direction from the first emitting probe element to the last. When using an ultrasonic phased array transducer as in 300, the wavefront 304 is discretized with small elements in accordance with Huygens' principle, and the wavefront angle α can be changed. More specifically, the wavefront angle α and the bandwidth of the input signal may be controlled (e.g., using electronic circuits) by adjusting the

number of signal cycles. The constant phase velocity excitation technique described herein may therefore be used to excite a large number of waveguide modes, using a single beam.

It should however be understood that other probes and excitation techniques may apply. For example, the probe 110 may comprise one or more comb transducers and comb excitation may be used to target a specific wavelength. In this case, mode selection may be based on the pitch between each probe element, with the pitch being a multiple or equal to the wavelength of the mode(s) of interest. The probe 110 may also comprise one or more electromagnetic acoustic transducers (EMAT). EMAT is a transducer technology consisting of an array of magnets and a coil and which uses either Lorentz forces, magnetostrictive forces or magnetization forces. In one embodiment, the probe 110 is as described in co-pending U.S. Patent Application No. 63/203,55017/874,474 filed on July 27, 20212022, the entire contents of which are incorporated herein by reference. Other embodiments may apply. The probe 10 described and illustrated herein may therefore include, but is not limited to, a phased array probe, an EMAT, or an EMAT array.

Referring back to Fig. III-1 and Fig. III-2, the guided wave generated by the probe 110 (i.e. the excited SH mode) travels within the structure 102. The guided wave can be reflected (as indicated by arrow A in Fig. III-1) at a discontinuity caused by the defect 104. The guided wave may also travel (as indicated by arrow B in Fig. III-1) across the area where the defect 104 is present, such that the guided wave is transmitted across the structure 102. It should be understood that the guided wave may be partially or fully reflected, or partially or fully transmitted. The probe 110 (which is positioned on one side of the defect 104) may be configured to receive the reflected guided wave signal, as will be described further below. A second probe (not shown) may be positioned on an opposite side of the defect 104 in order to receive the transmitted (or converted) guided wave signal. Mode conversion may also occur as a result of propagation of the guided wave within the structure 102.

In some embodiments, due to the presence of the defect 104, the guided wave is fully reflected and no transmission occurs. Conversely, in other embodiments, due to the absence of any defect

104, the guided wave is fully transmitted across the defect 104, such that no reflection occurs. Following travel of the guided wave within the structure 102, the probe 110 may receive a reflected guided wave and converts the reflected guided wave into an electrical signal, referred to herein as a "reflected guided wave signal". The amplitude of the reflected guided wave signal may vary depending on whether the guided wave propagating within the structure 102 is partially reflected, fully reflected, partially transmitted, or fully transmitted. For example, the amplitude of the reflected guided wave signal is below a predetermined amplitude threshold when the guided wave is fully transmitted across the structure 102 due to the absence of the defect 104. The amplitude of the reflected guided wave signal is above the amplitude threshold when the guided wave is fully reflected within the structure 102 due to the presence of the defect 104 (referred to herein as a "gradual defect") causing a gradual (i.e. progressive or continuous) thickness change (or reduction). Such a gradual defect is in contrast to a defect referred to herein as an "abrupt defect" (i.e. a defect exhibiting a discontinuous change in thickness) which causes an abrupt thickness change.

The reflected guided wave received at the probe 110 is then fed to the signal receiving circuit 204, which is configured to process the received signal in order to determine the thickness of the structure 102. For this purpose, the thickness determination unit 206 is configured to compare the amplitude of the reflected guided wave signal to the amplitude threshold. The value of the amplitude threshold may be determined through testing (e.g., before the nondestructive testing system 100 is deployed to inspect the structure 102) and stored in memory or other suitable storage. The value of the amplitude threshold may then be retrieved (e.g., by the thickness determination unit 206) from the memory or storage in order to perform the comparison.

When the amplitude of the reflected guided wave signal exceeds the amplitude threshold (indicating that the majority - i.e. more than half - of the guided wave signal is reflected due to the presence of the defect 104), the thickness determination unit 206 determines that the frequency-thickness product of the excited SH mode is below the cutoff frequency-thickness product. It can therefore be determined that the thickness of the structure 102 (i.e. the remnant thickness at the location of the defect 104) is below a minimal thickness for the structure 102,

which in turn indicates the presence of a defect. The value of the minimal thickness may be determined through testing (e.g., before the nondestructive testing system 100 is deployed to inspect the structure 102) and stored in memory or other suitable storage for subsequent retrieval (e.g., by the thickness determination unit 206).

In some embodiments, when the entirety of the excited SH mode(s) is detected by the probe 110, the thickness determination unit 206 detects that a gradual defect as in 104 having a thickness corresponding to the cutoff frequency-thickness is present. When one (or more) lower order SH mode(s) is detected by the probe 110, the thickness determination unit 206 detects that an abrupt defect as in 104 having a thickness corresponding to the cutoff frequency-thickness is present. Moreover, in some embodiments, when the thickness determination unit 206 detects the presence of the defect 104 (based on the amplitude of the reflected guided wave signal and on the thickness as determined), the thickness determination unit 206 may further be configured to determine, based on the at least one reflected guided wave signal, a distance between the probe 110 and the location of the defect. In particular, the distance between the probe 110 and the location of the defect may be determined based on the group velocity of the reflected guide wave and on the amount of time that has elapsed between the moment the guided wave is generated by the probe 110 and the moment the reflected guided wave is received at the probe 110. The value of the distance may be obtained by multiplying the group velocity by the elapsed amount of time.

When the amplitude of the reflected guided wave signal is below the amplitude threshold (indicating that the majority of the guided wave signal is transmitted, with little to no guided wave signal being reflected), the thickness determination unit 206 determines that the frequency-thickness product of the excited SH mode is above the cutoff frequency-thickness product. It can therefore be determined that the thickness of the structure is above the minimal thickness, which indicates the absence of the defect 104. In other words, when no SH mode is detected by the probe 110, the thickness determination unit 206 determines that no defect as in 104 is present.

Referring now to Fig. III-4, an example nondestructive testing method 400 that uses the reflection of SH guided waves to determine a thickness profile of a structure, such as the structure 102 of

Fig. III-1, will now be described. At step 402, at least one ultrasonic probe is driven to cause at least one SH guided wave to propagate in a structure, in the manner described above with reference to Figs. 1 to 3. At step 404, at least one reflected guided wave signal is received and a thickness of the structure is determined at step 406 based on an amplitude of the at least one reflected guided wave signal, as described herein above with reference to Figs. 1 to 3. In particular and as illustrated in Fig. III-5, step 406 comprises, at step 408, comparing the amplitude of the at least one reflected guided wave signal to an amplitude threshold. At step 410, an assessment is made as to whether the amplitude of the at least one reflected guided wave signal exceeds the amplitude threshold. In other words, step 410 allows to determine whether the majority of the guided wave signal is transmitted or reflected, which is in turn indicative of whether the frequency-thickness product of the excited SH mode is above or below the cutoff frequency-thickness product and whether the thickness of the structure is above or below the minimal thickness. If it is determined at step 410 that the amplitude of the at least one reflected guided wave signal exceeds the amplitude threshold, the next step 412 comprises determining that the thickness of the structure is below the minimal thickness for the structure and that a defect is present. If it is determined at step 410 that the amplitude of the at least one reflected guided wave signal does not exceed (i.e. is above) the amplitude threshold, the next step 414 comprises determining that the thickness of the structure is above the minimal thickness and that no defect is present. In some embodiment, after the presence of a defect has been detected at step 412, the method 400 comprises a step 416 of determining the defect type based on the at least one reflected guided wave signal. The method 400 may further comprises a step 418 of determining a distance between the probe and the location of the defect based on the at least one reflected guided wave signal.

Referring now to Fig. III-6, in one embodiment, step 416 of determining the defect type comprises assessing at step 420 whether the entirety of the excited SH mode(s) has been detected. If this is the case, the next step 422 comprises detecting the presence of a gradual defect (i.e. exhibiting a continuous change in thickness). If it is determined at step 420 that the entirety of the excited SH mode(s) has failed to be detected, the next step 424 comprises assessing whether low order

SH mode(s) have been detected. If this is the case, the next step 426 comprises detecting the presence of an abrupt detect. Otherwise, step 416 exits.

In order to validate the systems and methods described herein, Finite Element (FE) simulations may be used. An excitation with a 64-element phased array probe may be applied to nodes corresponding to a transducer having a 1 mm pitch between probe elements. A steel plate having a thickness of 3/8 inches may be used to model the structure under test. For this example, the minimal thickness for the structure may be set to 4 mm and the cutoff frequency-thickness product may be set to 5.7 mm. During the simulation, an SH guided wave is generated by a first probe (positioned on one side of the defect) and propagates in the modelled structure where the SH guided wave interacts with a defect. A reflected guided wave signal is detected by the first probe. A transmitted (or converted) guided wave signal may also be detected by a second probe positioned on an opposite side of the defect.

Simulation results are illustrated in Figs. 5A and 5B, where SH4 is the main mode that propagates through the simulated structure. Plot 502 of Fig. III-7 illustrates that, when a defect is present in the structure, the probe (e.g., the first probe) detects a reflected guided wave signal in the opposite (or negative) direction as that of the propagating signal, the reflected guided wave signal having a significant amplitude (i.e. having an amplitude above the predetermined amplitude threshold). Fig. III-7 further illustrates that the reflected guided wave signal has the same phase velocity in absolute value as the propagating signal. In contrast, plot 504 of Fig. III-8 illustrates that, when no defect is present in the structure, the probe (e.g., the second probe) detects a transmitted guided wave signal in the same (or positive) direction as the propagating signal. Moreover a signal with negligible amplitude (i.e. having an amplitude below the amplitude threshold) may be detected in the opposite (or negative) direction.

Further FE simulations may be performed with a 3/8 inch steel plate and a 64-element phased array transducer with a pitch of 1.5 mm. For this example, a defect resulting in a minimal thickness going from 3.5 mm to 7.5 mm with a step of 0.5 mm was added in the middle of the steel plate. Similarly to the FE simulations described above with reference to Figs. 5A and

5B, an SH guided wave is generated by a first probe (positioned on one side of the defect) and propagates in the modelled structure where the SH guided wave interacts with a defect. A reflected guided wave signal is detected by the first probe and a transmitted (or converted) guided wave signal may also be detected by a second probe positioned on an opposite side of the defect.

Simulation results are illustrated in Fig. III-9, 5D, 5E, and 5F. SH_1 was excited and scanned between 200 kHz and 500 kHz using multiple narrowband phased velocity excitation and its amplitude as a function of the frequency and the phase velocity when propagation is performed on a defect-less plate can be seen on plot 506 of Fig. III-9. Plots 508 of Fig. III-10 and plot 510 of Fig. III-11 show the amplitude of SH1 reflected by the defect, with the minimum thickness being 3.5 mm and 5.5 mm, respectively. The detected cutoff frequencies are indicated by lines 514_1 (at 420 kHz) and 514_2 (at 270 kHz) in Figs. 5D and 5E. Using equation (3) above, one can estimate the minimum thickness, which is 3.78 mm in the embodiment of Fig. III-10 and 5.87 mm in the embodiment of Fig. III-11. Additional cases were simulated for minimum thicknesses ranging from 3.5 mm to 7.5 mm with a step of 0.5 mm and the results are shown in plot 512 of Fig. III-12. As can be seen from plot 512, among all the simulated cases, the maximum error is 0.44 mm, or less than 5% of the nominal thickness of the steel plate.

With reference to Fig. III-13, an example of a computing device 600 is illustrated. For simplicity only one computing device 600 is shown but more computing devices 600 operable to exchange data may be provided. The computing devices 600 may be the same or different types of devices. The electronic circuitry used for generating and detecting the SH waves (e.g., the signal generating circuit 202 and/or the signal receiving circuit 204 of Fig. III-2) and/or the method (reference 400 of Fig. 4) may be implemented with one or more computing devices 600.). The computing device 600 may also be used to control operation of the probe 110 described herein with reference to Figs. 1 to 3. Other embodiments may also apply.

The computing device 600 comprises a processing unit 602 and a memory 604 which has stored therein computer-executable instructions 606. The processing unit 602 may comprise any suitable devices configured to implement the method 400 such that instructions 606, when executed by

the computing device 600 or other programmable apparatus, may cause the functions/acts/steps performed as part of the method 400 as described herein to be executed. The processing unit 602 may comprise, for example, any type of general-purpose microprocessor or microcontroller, a digital signal processing (DSP) processor, a central processing unit (CPU), an integrated circuit, a field programmable gate array (FPGA), a reconfigurable processor, other suitably programmed or programmable logic circuits, or any combination thereof.

The memory 604 may comprise any suitable known or other machine-readable storage medium. The memory 604 may comprise non-transitory computer readable storage medium, for example, but not limited to, an electronic, magnetic, optical, electromagnetic, infrared, or semiconductor system, apparatus, or device, or any suitable combination of the foregoing. The memory 604 may include a suitable combination of any type of computer memory that is located either internally or externally to device, for example random-access memory (RAM), read-only memory (ROM), compact disc read-only memory (CDROM), electro-optical memory, magneto-optical memory, erasable programmable read-only memory (EPROM), and electrically-erasable programmable read-only memory (EEPROM), Ferroelectric RAM (FRAM) or the like. Memory 604 may comprise any storage means (e.g., devices) suitable for retrievably storing machine-readable instructions 606 executable by processing unit 602.

The methods and systems described herein may be implemented in a high level procedural or object oriented programming or scripting language, or a combination thereof, to communicate with or assist in the operation of a computer system, for example the computing device 600. Alternatively, the methods and systems described herein may be implemented in assembly or machine language. The language may be a compiled or interpreted language. Program code for implementing the methods and systems described herein may be stored on a storage media or a device, for example a ROM, a magnetic disk, an optical disc, a flash drive, or any other suitable storage media or device. The program code may be readable by a general or special-purpose programmable computer for configuring and operating the computer when the storage media or device is read by the computer to perform the procedures described herein. Embodiments of the methods and systems described herein may also be considered to be implemented by way of a

non-transitory computer-readable storage medium having a computer program stored thereon. The computer program may comprise computer-readable instructions which cause a computer, or more specifically the processing unit 602 of the computing device 600, to operate in a specific and predefined manner to perform the functions described herein, for example those described in the method 400.

Computer-executable instructions may be in many forms, including program modules, executed by one or more computers or other devices. Generally, program modules include routines, programs, objects, components, data structures, etc., that perform particular tasks or implement particular abstract data types. Typically the functionality of the program modules may be combined or distributed as desired in various embodiments.

As can be understood, the examples described above and illustrated are intended to be exemplary only. Although the embodiments have been described in detail, it should be understood that various changes, substitutions and alterations can be made herein without departing from the scope as defined by the appended claims.

Moreover, the scope of the present application is not intended to be limited to the particular embodiments of the process, machine, manufacture, composition of matter, means, methods and steps described in the specification. As one of ordinary skill in the art will readily appreciate from the disclosure of the present invention, processes, machines, manufacture, compositions of matter, means, methods, or steps, presently existing or later to be developed, that perform substantially the same function or achieve substantially the same result as the corresponding embodiments described herein may be utilized. Accordingly, the appended claims are intended to include within their scope such processes, machines, manufacture, compositions of matter, means, methods, or steps.

6.   What is claimed is :

1. A method for nondestructive testing of a structure, the method comprising : driving at least one ultrasonic probe to cause at least one shear horizontal (SH) guided wave to propagate

in the structure; receiving at least one reflected guided wave signal from the structure in response to driving the at least one ultrasonic probe; performing a comparison between an amplitude of the at least one reflected guided wave signal and an amplitude threshold; and determining a thickness of the structure based on the comparison and detecting, based on the thickness as determined, a presence or an absence of at least one defect in the structure.

2. The method of claim 1, wherein driving the at least one ultrasonic probe comprises causing the at least one ultrasonic probe to excite high order SH guided wave modes at a constant phase velocity.

3. The method of claim 1, wherein driving the at least one ultrasonic probe comprises causing at least one comb transducer to excite SH guided wave modes using comb excitation.

4. The method of claim 1, wherein driving the at least one ultrasonic probe comprises driving at least one electromagnetic acoustic transducer (EMAT).

5. The method of claim 4, wherein driving the at least one ultrasonic probe comprises driving an EMAT array.

6. The method of claim 1, wherein driving the at least one ultrasonic probe comprises driving a phased array probe.

7. The method of claim 1, wherein determining the thickness of the structure comprises, upon determining, based on the comparison between the amplitude of the at least one reflected guided wave signal and the amplitude threshold, that the amplitude of the at least one reflected guided wave signal exceeds the amplitude threshold, determining that the thickness of the structure at a location of the at least one defect is below a minimal thickness for the structure and detecting the presence of the at least one defect in the structure.

8. The method of claim 1, wherein determining the thickness of the structure comprises, upon determining, based on the comparison between the amplitude of the at least one reflected guided wave signal and the amplitude threshold, that the amplitude of the at least one reflected guided wave signal is below the amplitude threshold, determining that the thickness of the structure exceeds a minimal thickness for the structure and detecting the absence of the at least one defect in the structure.

9. The method of claim 7, further comprising determining that the at least one reflected guided wave signal comprises an entirety of excited modes of the at least one SH guided wave, and that the at least one defect exhibits a continuous change in thickness.

10. The method of claim 7, further comprising determining that the at least one reflected guided wave signal comprises at least one low order mode of the at least one SH guided wave, and that the at least one defect exhibits a discontinuous change in thickness.

11. The method of claim 7, further comprising determining a group velocity of the at least one reflected guided wave signal, determining an amount of time elapsed between generation of the at least one SH guided wave signal and receipt of the at least one reflected guided wave signal, and computing a product of the group velocity and the amount of time to determine a distance between the at least one ultrasonic probe and a location of the at least one defect.

12. A system for nondestructive testing of a structure, the system comprising : an ultrasonic probe configured to be coupled to the structure and to cause, when driven, at least one shear horizontal (SH) guided wave to propagate in the structure ; a processing unit ; and a non-transitory computer-readable medium having stored thereon instructions executable by the processing unit for : driving the at least one ultrasonic probe ; receiving at least one reflected guided wave signal from the structure in response to driving the at least one ultrasonic probe ; performing a comparison between an amplitude of the at least one reflected guided wave signal and an amplitude threshold ; and determining a thickness of the structure based on the comparison and detecting, based on the thickness as determined, a presence or an absence of at least one defect in the structure.

13. The system of claim 12, wherein the at least one ultrasonic probe, when driven, is caused to excite high order SH guided wave modes at a constant phase velocity.

14. The system of claim 12, wherein the at least one ultrasonic probe comprises at least one comb transducer configured to, when driven, excite SH guided wave modes using comb excitation.

15. The system of claim 12, wherein the at least one ultrasonic probe comprises at least one electromagnetic acoustic transducer (EMAT).

16. The system of claim 15, wherein the at least one ultrasonic probe comprises an EMAT array.

17. The system of claim 12, wherein the at least one ultrasonic probe comprises a phased array probe.

18. The system of claim 12, wherein the instructions are executable by the processing unit for determining the thickness of the structure comprising, upon determining, based on the comparison between the amplitude of the at least one reflected guided wave signal and the amplitude threshold, that the amplitude of the at least one reflected guided wave signal exceeds the amplitude threshold, determining that the thickness of the structure at a location of the at least one defect is below a minimal thickness for the structure and detecting the presence of the at least one defect in the structure.

19. The system of claim 12, wherein the instructions are executable by the processing unit for determining the thickness of the structure comprising, upon determining, based on the comparison between the amplitude of the at least one reflected guided wave signal and the amplitude threshold, that the amplitude of the at least one reflected guided wave signal is below the amplitude threshold, determining that the thickness of the structure exceeds a minimal thickness for the structure and detecting the absence of the at least one defect in the structure.

20. The system of claim 18, wherein the instructions are executable by the processing unit for determining a group velocity of the at least one reflected guided wave signal, determining an amount of time elapsed between generation of the at least one SH guided wave signal and receipt of the at least one reflected guided wave signal, and computing a product of the group velocity and the amount of time to determine a distance between the at least one ultrasonic probe and a location of the at least one defect.

7. Abstract

A method and a system for nondestructive testing of a structure are provided. At least one ultrasonic probe is driven to cause at least one shear horizontal (SH) guided wave to propagate in the structure. At least one reflected guided wave signal is received from the structure to the at least one ultrasonic probe being driven. A comparison between an amplitude of the at least one reflected guided wave signal and an amplitude threshold is performed. A thickness of the

structure is determined based on the comparison and a presence or an absence of at least one defect in the structure is detected based on the thickness as determined.
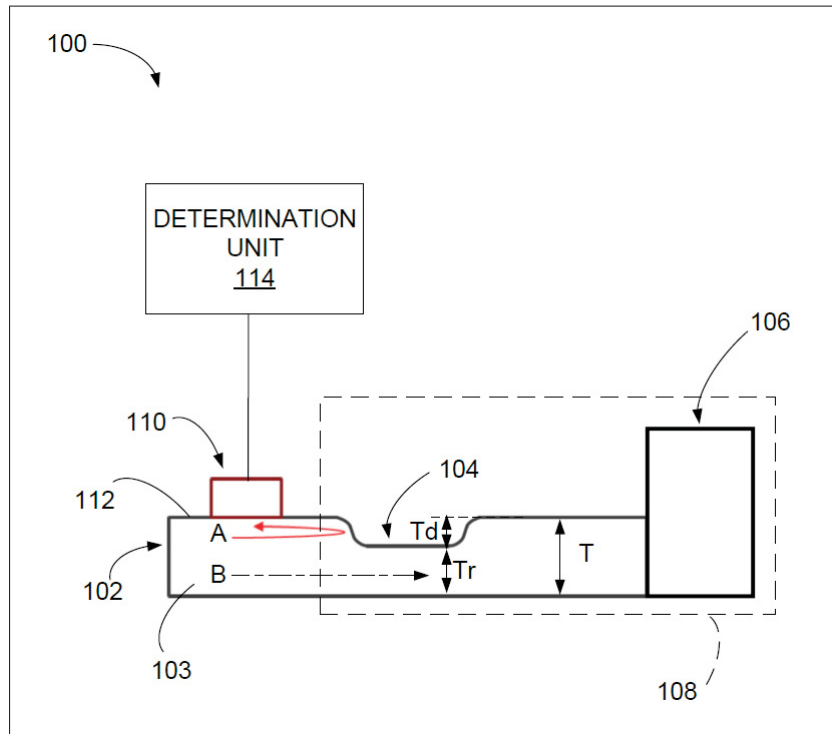

Figure-A III-1   Schematic diagram of an example nondestructive testing system. Tirée du brevet correspondant à l'annexe III
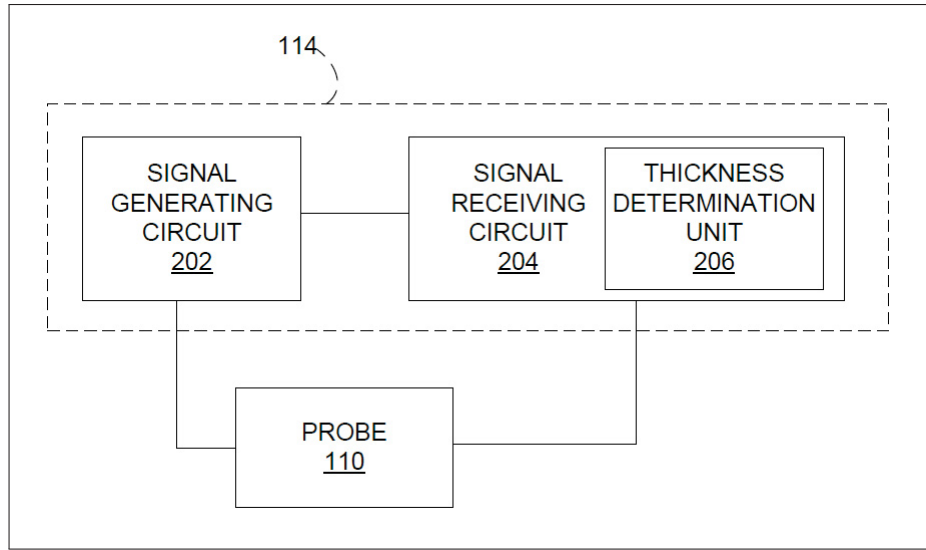
Figure-A III-2   Block diagram of the determination unit of Fig. III-1. Tirée du brevet
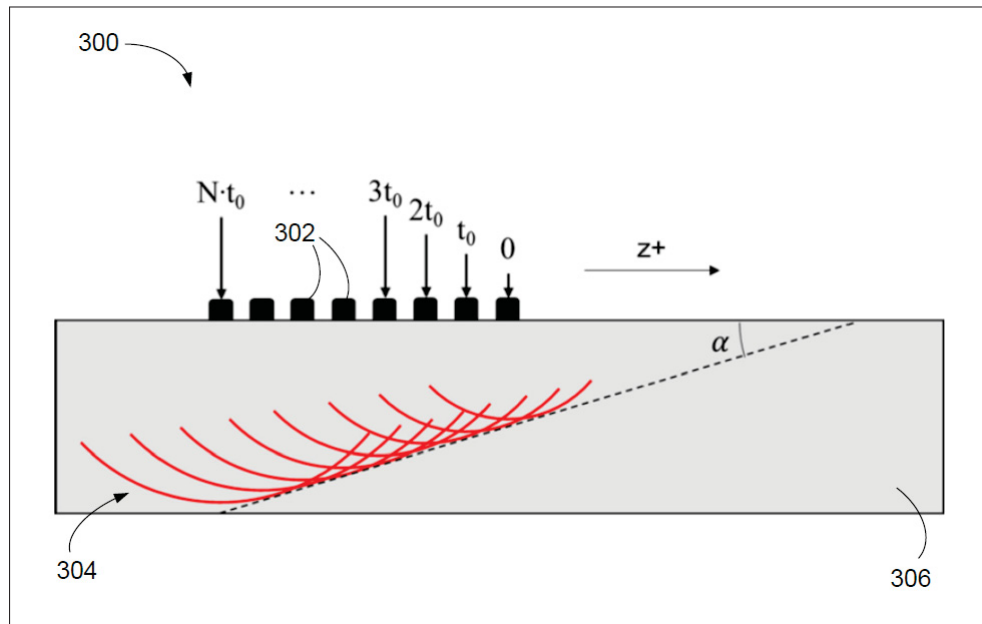correspondant à l'annexe III

Figure-A III-3   Schematic diagram of an ultrasonic phased array probe. Tirée du brevet
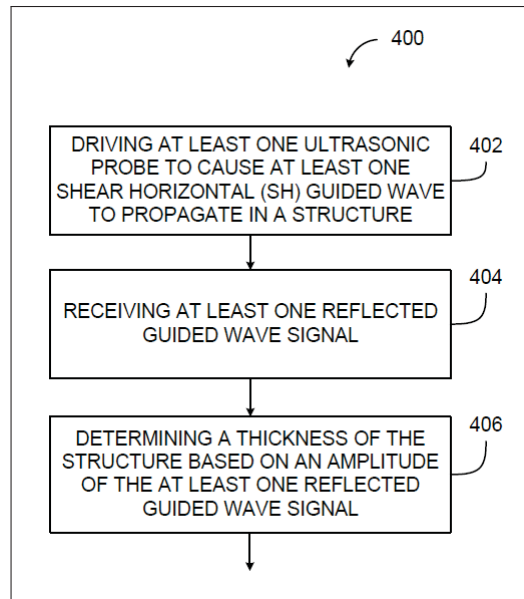correspondant à l'annexe III

Figure-A III-4   Flowchart of an example nondestructive testing method. Tirée du brevet correspondant à l'annexe III
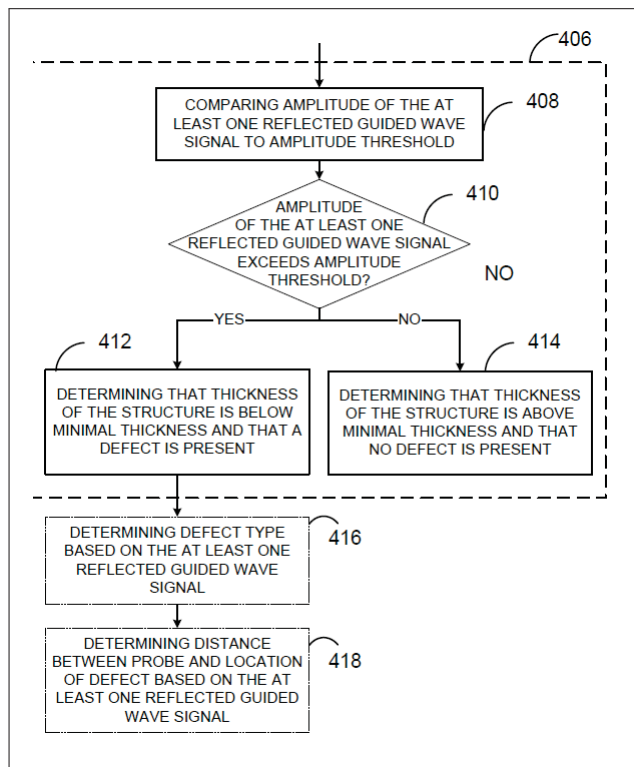

Figure-A III-5   Flowchart of an example nondestructive testing method. Tirée du brevet correspondant à l'annexe III
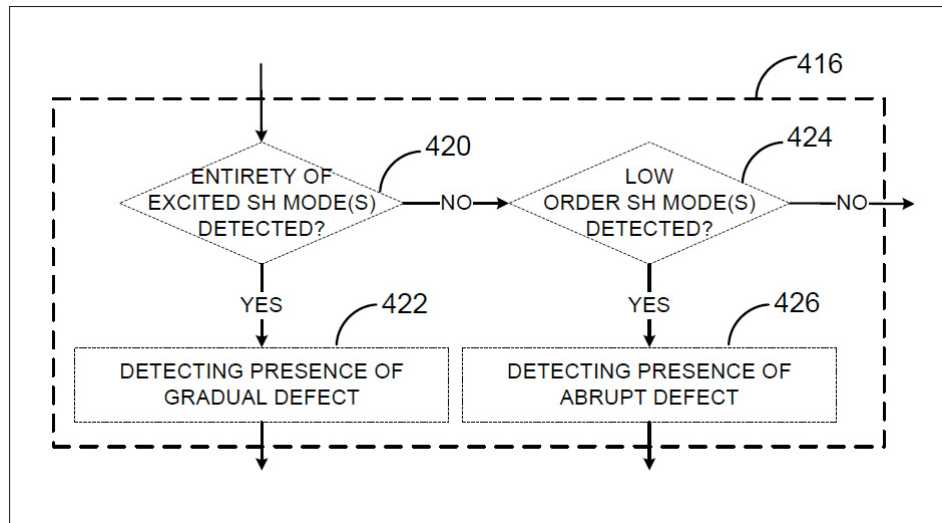
Figure-A III-6   Flowchart of an example nondestructive testing method. Tirée du brevet
correspondant à l'annexe III
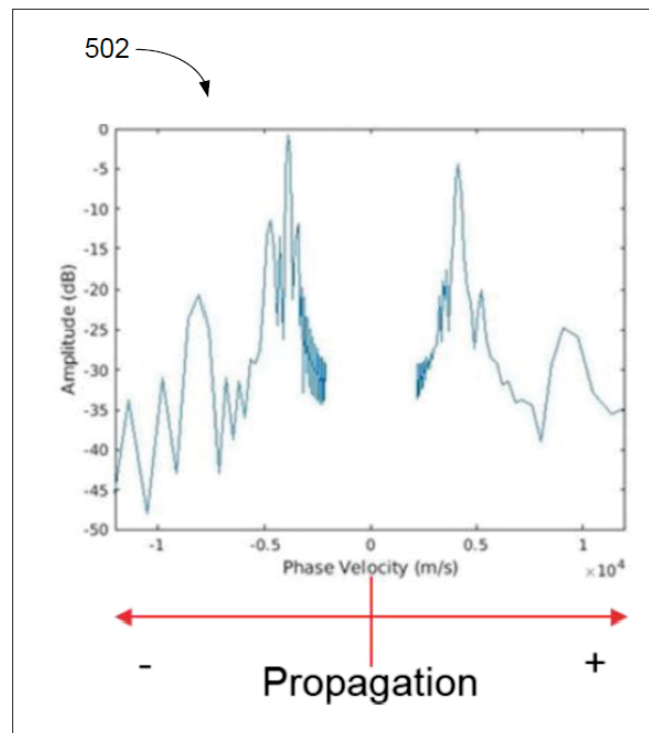
Figure-A III-7   Example of simulation results for a structure having a defect. Tirée du
brevet correspondant à l'annexe III
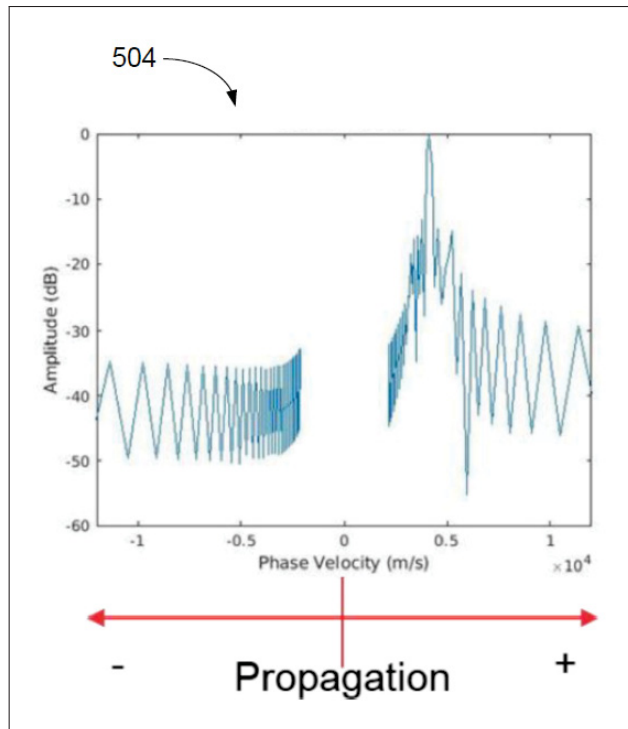
Figure-A III-8   Example of simulation results for a structure having no defect. Tirée du brevet correspondant à l'annexe III
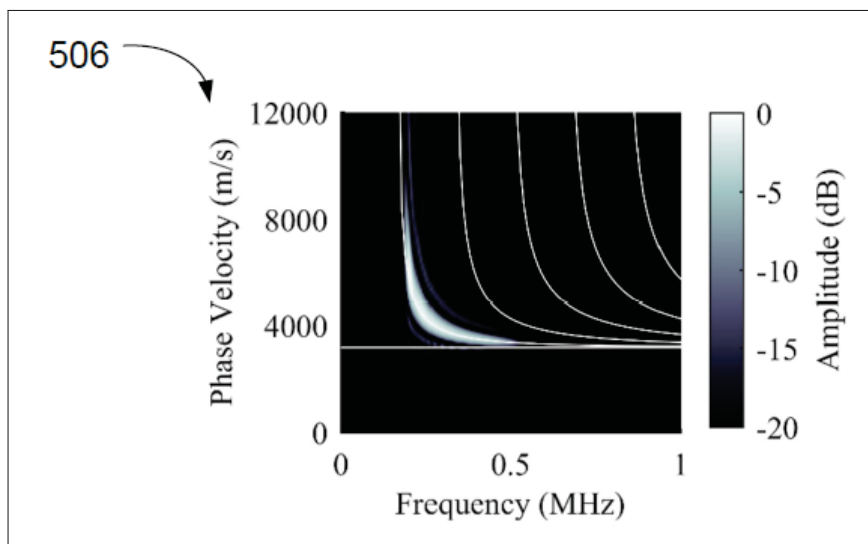
Figure-A III-9   Simulated 2D-FFT obtained on a defect-free region when SH_1 is scanned on a 9.53 mm steel plate between 200 kHz and 500 kHz using multiple narrowband phased velocity excitation and a 64 element phased array probe with a pitch of 0.5 mm. Tirée du brevet correspondant à l'annexe III
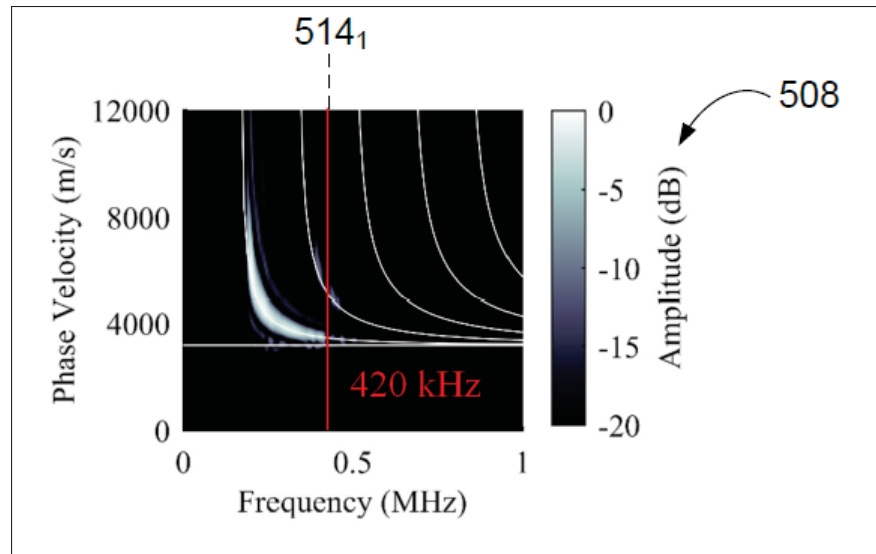
Figure-A III-10   Simulated 2D-FFT obtained in front of a defect with a minimum thickness of 3.5 mm when SH_1 is scanned on a 9.53 mm steel plate between 200 kHz and 500 kHz using multiple narrowband phased velocity excitation and a 64 element phased array probe with a pitch of 0.5 mm. Tirée du brevet correspondant à l'annexe III

Figure-A III-11   Simulated 2D-FFT obtained in front of a defect with a minimum thickness of 5.5 mm when SH_1 is scanned on a 9.53 mm steel plate between 200 kHz and 500 kHz using multiple narrowband phased velocity excitation and a 64 element phased array probe with a pitch of 0.5 mm. Tirée du brevet correspondant à l'annexe III

Figure-A III-12   Reconstructed thickness and error as a function of the minimum real thickness. Tirée du brevet correspondant à l'annexe III

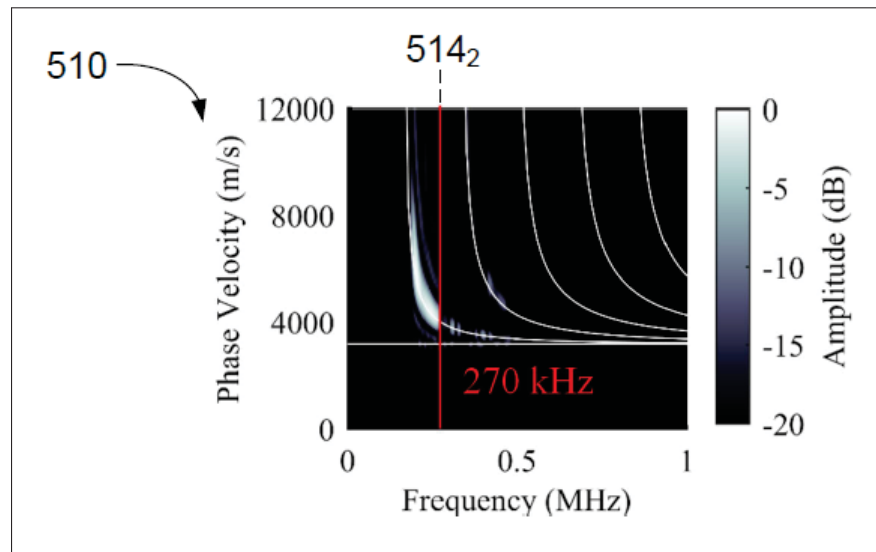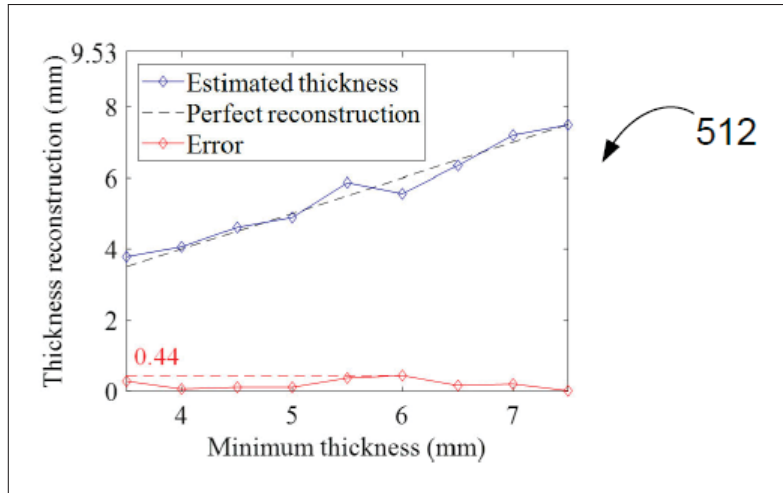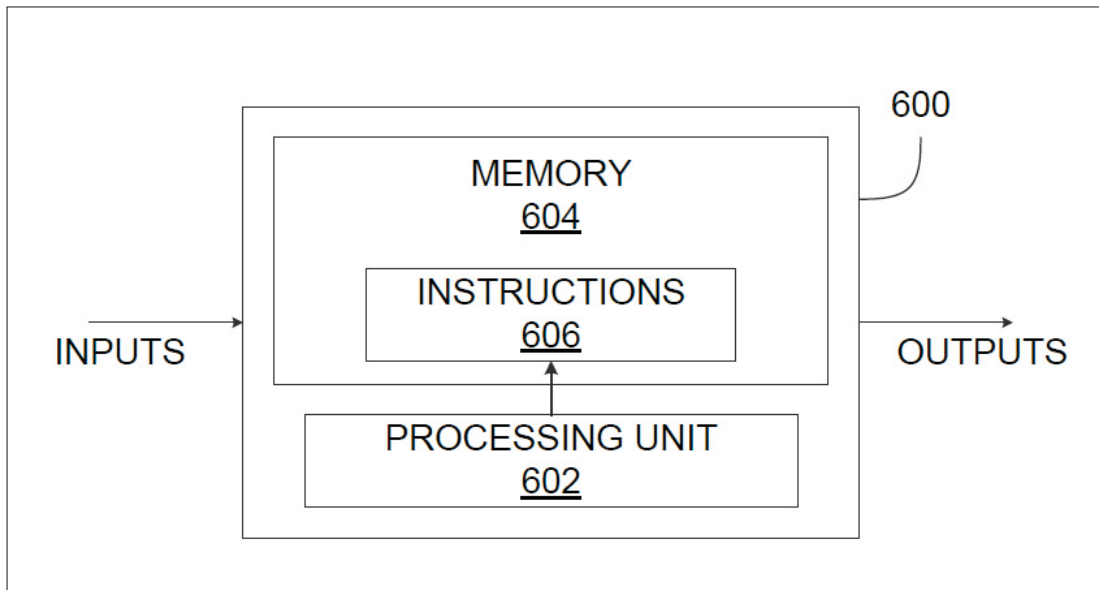Figure-A III-13   A block diagram of an example computing device. Tirée du brevet correspondant à l'annexe III

BIBLIOGRAPHIE

Alleyne, D. & Cawley, P. (1991). A two-dimensional Fourier transform method for the measurement of propagating multimode signals. *The Journal of the Acoustical Society of America*, 89(3), 1159–1168. doi : 10.1121/1.400530.

Alleyne, D. N., Lowe, M. J. S. & Cawley, P. (1998). The Reflection of Guided Waves From Circumferential Notches in Pipes. *Journal of Applied Mechanics*, 65(3), 635–641. doi : 10.1115/1.2789105.

Alleyne, D. N., Pavlakovic, B., Lowe, M. J. S. & Cawley, P. (2001). Rapid, long range inspection of chemical plant pipework using guided waves. *AIP Conference Proceedings*, 557(1), 180–187. doi : 10.1063/1.1373757.

Belanger, P. & Cawley, P. (2009). Feasibility of low frequency straight-ray guided wave tomography. *NDT & E International*, 42(2), 113–119. doi : 10.1016/j.ndteint.2008.10.006.

Britton, J. (2002). *Corrosion at pipe supports : Causes and solutions*.

Bélanger, P., Cawley, P. & Simonetti, F. (2010). Guided wave diffraction tomography within the born approximation. *IEEE Transactions on Ultrasonics, Ferroelectrics, and Frequency Control*, 57(6), 1405–1418. doi : 10.1109/TUFFC.2010.1559.

Bélanger, P. (2014). High order shear horizontal modes for minimum remnant thickness. *Ultrasonics*, 54(4), 1078–1087. doi : 10.1016/j.ultras.2013.12.013.

Cawley, P. (2002). Practical Long Range Guided Wave Inspection - Applications To Pipes And Rail. *National Seminar of ISNT*, 16.

Cawley, P., Lowe, M. J. S., Alleyne, D. N., Pavlakovic, B. & Wilcox, P. (2003). Practical long range guided wave inspection-applications to pipes and rail. *Mater. Eval*, 61(1), 66–74.

Chan, H., Masserey, B. & Fromme, P. (2015). High frequency guided ultrasonic waves for hidden fatigue crack growth monitoring in multi-layer model aerospace structures. *Smart Materials and Structures*, 24(2), 025037. doi : 10.1088/0964-1726/24/2/025037. Publisher : IOP Publishing.

Cheeke, J. D. N. (2012). *Fundamentals and Applications of Ultrasonic Waves*. CRC Press. doi : 10.1201/b12260.

Comot, P., Bocher, P. & Belanger, P. (2017). Ultrasonic guided wave inspection of Inconel 625 brazed lap joints : Simulation and experimentation. *NDT & E International*, 91, 71–78. doi : 10.1016/j.ndteint.2017.06.007.

Cook, R. D., Malkus, D. S., Plesha, M. E. & Witt, R. J. (2007). *Concepts and Applications of Finite Element Analysis*. USA : John Wiley & Sons, Inc.

Cooley, J. W. & Tukey, J. W. (1965). An Algorithm for the Machine Calculation of Complex Fourier Series.

Drozdz, M., Moreau, L., Castaings, M., Lowe, M. J. S. & Cawley, P. (2006). Efficient Numerical Modelling of Absorbing Regions for Boundaries Of Guided Waves Problems. *AIP Conference Proceedings*, 820(1), 126–133. doi : 10.1063/1.2184520.

Drozdz, M. B. (2008). *Efficient finite element modelling of ultrasound waves in elastic media*. (Ph.D., Imperial College London). Repéré à http://hdl.handle.net/10044/1/7974.

García-Martín, J., Gómez-Gil, J. & Vázquez-Sánchez, E. (2011). Non-Destructive Techniques Based on Eddy Current Testing. *Sensors*, 11(3), 2525–2565. doi : 10.3390/s110302525. Number : 3 Publisher : Molecular Diversity Preservation International.

Garverick, L. (1994). *Corrosion in the Petrochemical Industry*. ASM International.

Gauthier, B., Thon, A. & Belanger, P. (2018). Comparison of a piezoceramic transducer and an EMAT for the omnidirectional transduction of SH0. *AIP Conference Proceedings*, 1949(1), 230005. doi : 10.1063/1.5031652. Publisher : American Institute of Physics.

Gazanhes, C. & Jessel, M. (1976, jun). Ultrasons [Text]. Repéré le 2018-11-06 à https://www.techniques-ingenieur.fr/base-documentaire/archives-th12/archives-electronique-tiaea/archive-2/ultrasons-e2690/.

Graff, K. F. (1991). *Wave Motion in Elastic Solids*. Dover Publications.

Hinders, M. K. & McKeon, J. C. P. (1999, jan). Lamb Wave Tomography for Corrosion Mapping. Repéré à https://ntrs.nasa.gov/citations/19990028753.

Ho, K. S., Billson, D. R. & Hutchins, D. A. (2007). Ultrasonic Lamb wave tomography using scanned EMATs and wavelet processing. *Nondestructive Testing and Evaluation*, 22(1), 19–34. doi : 10.1080/10589750701327890.

Hu, S., Shi, W., Lu, C., Chen, Y., Chen, G. & Shen, G. (2021). Rapid detection of cracks in the rail foot by ultrasonic B-scan imaging using a shear horizontal guided wave electromagnetic acoustic transducer. *NDT & E International*, 120, 102437. doi : 10.1016/j.ndteint.2021.102437.

Huthwaite, P. & Simonetti, F. (2011). High-resolution imaging without iteration : a fast and robust method for breast ultrasound tomography. *The Journal of the Acoustical Society of America*, 130(3), 1721–1734. doi : 10.1121/1.3613936.

Huthwaite, P. (2014). Accelerated finite element elastodynamic simulations using the GPU. *Journal of Computational Physics*, 257, 687–707. doi : 10.1016/j.jcp.2013.10.017.

Huthwaite, P. & Simonetti, F. (2013). High-resolution guided wave tomography. *Wave Motion*, 50(5), 979–993. doi : 10.1016/j.wavemoti.2013.04.004.

Isla, J. & Cegla, F. (2016). Optimization of the Bias Magnetic Field of Shear Wave EMATs. *IEEE Transactions on Ultrasonics, Ferroelectrics, and Frequency Control*, 63(8), 1148–1160. doi : 10.1109/TUFFC.2016.2558467.

Isla, J. & Cegla, F. (2017). EMAT phased array : A feasibility study of surface crack detection. *Ultrasonics*, 78, 1–9. doi : 10.1016/j.ultras.2017.02.009.

Koodalil, D., Rajagopal, P. & Balasubramaniam, K. (2021a). Bond stiffness estimation with shear horizontal guided waves generated using PPM-EMATs. *International Journal of Adhesion and Adhesives*, 104, 102761. doi : 10.1016/j.ijadhadh.2020.102761.

Koodalil, D., Rajagopal, P. & Balasubramaniam, K. (2021b). Quantifying adhesive thickness and adhesion parameters using higher-order SH guided waves. *Ultrasonics*, 114, 106429. doi : 10.1016/j.ultras.2021.106429.

Krautkrämer, J. & Krautkrämer, H. (1990). *Ultrasonic Testing of Materials*. Berlin, Heidelberg : Springer Berlin Heidelberg. Repéré à http://public.eblib.com/choice/publicfullrecord. aspx?p=3099756.

Lamb, H. (1917). On waves in an elastic plate. *Proc. R. Soc. Lond. A*, 93(648), 114–128. doi : 10.1098/rspa.1917.0008.

Leonard, K. R. & Hinders, M. K. (2005). Multi-mode Lamb wave tomography with arrival time sorting. *The Journal of the Acoustical Society of America*, 117(4), 2028–2038. doi : 10.1121/1.1867792.

Li, J. & Rose, J. (2001). Implementing guided wave mode control by use of a phased transducer array. *IEEE Transactions on Ultrasonics, Ferroelectrics, and Frequency Control*, 48(3), 761–768. doi : 10.1109/58.920708. Conference Name : IEEE Transactions on Ultrasonics, Ferroelectrics, and Frequency Control.

Liu, Z., Huo, Z., Li, A., He, C. & Wu, B. (2021). Development of an Omnidirectional SH0 Mode Electromagnetic Acoustic Transducer Employing a Circumferential Periodic Permanent Magnet Array. *IEEE Sensors Journal*, 21(6), 7691–7701. doi : 10.1109/J-SEN.2021.3051289. Conference Name : IEEE Sensors Journal.

Lopez, A., Bacelar, R., Pires, I., Santos, T. G., Sousa, J. P. & Quintino, L. (2018). Non-destructive testing application of radiography and ultrasound for wire and arc additive manufacturing. *Additive Manufacturing*, 21, 298–306. doi : 10.1016/j.addma.2018.03.020.

Luo, W., Zhao, X. & Rose, J. L. (2005). A Guided Wave Plate Experiment for a Pipe. *Journal of Pressure Vessel Technology*, 127(3), 345–350. doi : 10.1115/1.1989351.

Mudeg, P. J. (2001). Field application of the Teletest ; Long-range ultrasonic testing technique. *Insight*, 43(2), 74–77. Repéré à https://ci.nii.ac.jp/naid/80012178578/.

Nakamura, N., Ogi, H. & Hirao, M. (2013). Mode Conversion and Total Reflection of Torsional Waves for Pipe Inspection. *Japanese Journal of Applied Physics*, 52(7S), 07HC14. doi : 10.7567/JJAP.52.07HC14.

Nurmalia, Nakamura, N., Ogi, H., Hirao, M. & Nakahata, K. (2012). Mode conversion behavior of SH guided wave in a tapered plate. *NDT & E International*, 45(1), 156–161. doi : 10.1016/j.ndteint.2011.10.004.

Olympus. (2004). *Introduction to Phased Array Ultrasonic Technology Applications*. Olympus.

Parra-Raad, J., Khalili, P. & Cegla, F. (2020). Shear waves with orthogonal polarisations for thickness measurement and crack detection using EMATs. *NDT & E International*, 111, 102212. doi : 10.1016/j.ndteint.2019.102212.

Pavlakovic, B., Lowe, M., Alleyne, D. & Cawley, P. (1997). Disperse : A General Purpose Program for Creating Dispersion Curves. Dans *Review of Progress in Quantitative Nondestructive Evaluation* (pp. 185–192). Springer, Boston, MA. doi : 10.1007/978-1-4615-5947-4_24.

Pereira, D. & Belanger, P. (2019). Inverse characterization of adhesive shear modulus in bonded stiffeners using ultrasonic guided waves. *AIP Conference Proceedings*, 2102(1), 050006. doi : 10.1063/1.5099772. Publisher : American Institute of Physics.

Petcher, P. A., Burrows, S. E. & Dixon, S. (2014). Shear horizontal (SH) ultrasound wave propagation around smooth corners. *Ultrasonics*, 54(4), 997–1004. doi : 10.1016/j.ultras.2013.11.011.

Pialucha, T., Pavlakovic, B., Alleyne, D. & Cawley, P. (2020). Quantitative measurement of remnant thickness in corrosion under pipe supports. *Insight - Non-Destructive Testing and Condition Monitoring*, 62(11), 642–648. doi : 10.1784/insi.2020.62.11.642.

Pucci, L., Raillon, R., Taupin, L. & Baqué, F. (2019). Design of a Phased Array EMAT for Inspection Applications in Liquid Sodium. *Sensors*, 19(20), 4460. doi : 10.3390/s19204460. Number : 20 Publisher : Multidisciplinary Digital Publishing Institute.

Rajagopal, P., Drozdz, M., Skelton, E. A., Lowe, M. J. S. & Craster, R. V. (2012). On the use of absorbing layers to simulate the propagation of elastic waves in unbounded isotropic media using commercially available Finite Element packages. *NDT & E International*, 51, 30–40. doi : 10.1016/j.ndteint.2012.04.001.

Ribichini, R., Cegla, F., Nagy, P. B. & Cawley, P. (2012a). Experimental and numerical evaluation of electromagnetic acoustic transducer performance on steel materials. *NDT & E International*, 45(1), 32–38. doi : 10.1016/j.ndteint.2011.08.007.

Ribichini, R., Nagy, P. B. & Ogi, H. (2012b). The impact of magnetostriction on the transduction of normal bias field EMATs. *NDT & E International*, 51, 8–15. doi : 10.1016/j.ndteint.2012.06.004.

Ribichini, R. (2011). *Modelling of Electromagnetic Acoustic Transducers*. (Thèse de doctorat, Imperial College London).

Rose, J. L. (2014). *Ultrasonic Guided Waves in Solid Media*. Cambridge : Cambridge University Press. doi : 10.1017/CBO9781107273610.

Rose, J. L., Cho, Y. & Avioli, M. J. (2009). Next generation guided wave health monitoring for long range inspection of pipes. *Journal of Loss Prevention in the Process Industries*, 22(6), 1010–1015. doi : 10.1016/j.jlp.2009.08.011.

Shull, P. J. (2016). *Nondestructive Evaluation : Theory, Techniques, and Applications*. CRC Press.

Sun, C. Z., Sinclair, A. & Filleter, T. (2021a). Influence of Magnetostriction Induced by the Periodic Permanent Magnet Electromagnetic Acoustic Transducer (PPM EMAT) on Steel. *Sensors (Basel, Switzerland)*, 21(22), 7700. doi : 10.3390/s21227700.

Sun, H., Peng, L., Lin, J., Wang, S., Zhao, W. & Huang, S. (2021b). Microcrack defect quantification using a focusing high-order SH guided wave EMAT : the physics-informed deep neural network GuwNet. *IEEE Transactions on Industrial Informatics*, 1–1. doi : 10.1109/TII.2021.3105537. Conference Name : IEEE Transactions on Industrial Informatics.

Sun, H., Peng, L., Wang, S., Huang, S. & Qu, K. (2021c). Development of Frequency-Mixed Point-Focusing Shear Horizontal Guided-Wave EMAT for Defect Inspection Using Deep Neural Network. *IEEE Transactions on Instrumentation and Measurement*, 70, 1–14. doi : 10.1109/TIM.2020.3033941. Conference Name : IEEE Transactions on Instrumentation and Measurement.

Suresh, N. & Balasubramaniam, K. (2020). Quantifying the lowest remnant thickness using a novel broadband wavelength and frequency EMAT utilizing the cut-off property of guided waves. *NDT & E International*, 116, 102313. doi : 10.1016/j.ndteint.2020.102313.

Tabatabaeipour, M., Trushkevych, O., Dobie, G., Edwards, R. S., McMillan, R., Macleod, C., O'Leary, R., Dixon, S., Gachagan, A. & Pierce, S. G. (2022). Application of ultrasonic guided waves to robotic occupancy grid mapping. *Mechanical Systems and Signal Processing*, 163, 108151. doi : 10.1016/j.ymssp.2021.108151.

Thon, A. & Bélanger, P. (2019). EMAT design for minimum remnant thickness gauging using high order shear horizontal modes. *Ultrasonics*, 95, 70–78. doi : 10.1016/j.ultras.2019.03.006.

Thon, A., Painchaud-April, G., Le Duff, A. & Bélanger, P. (2022). Optimization of a Lorentz forces EMAT for the reconstruction of the circumferential thickness profile of a steel pipe using high order shear horizontal modes. *NDT & E International*, 128, 102631. doi : 10.1016/j.ndteint.2022.102631.

Thon, A., Painchaud-April, G., Le Duff, A. & Bélanger, P. (2023). Development of a linear array electromagnetic acoustic transducer for shear horizontal guided wave inspection. *NDT & E International*, 136, 102807. doi : 10.1016/j.ndteint.2023.102807.

Travaglini, C., Bescond, C., Viens, M. & Belanger, P. (2017). Feasibility of high frequency guided wave crack monitoring. *Structural Health Monitoring*, 16(4), 418–427. doi : 10.1177/1475921716673567. Publisher : SAGE Publications.

Vasile, C. F. & Thompson, R. B. (1979). Excitation of horizontally polarized shear elastic waves by electromagnetic transducers with periodic permanent magnets. *Journal of Applied Physics*, 50(4), 2583–2588. doi : 10.1063/1.326265. Publisher : American Institute of Physics.

Veit, G. & Bélanger, P. (2020). An ultrasonic guided wave excitation method at constant phase velocity using ultrasonic phased array probes. *Ultrasonics*, 102, 106039. doi : 10.1016/j.ultras.2019.106039.

Velichko, A. & Wilcox, P. D. (2009). Excitation and scattering of guided waves : Relationships between solutions for plates and pipes. *The Journal of the Acoustical Society of America*, 10.

Vogelaere, F. D. (2009). Corrosion under insulation. *Process Safety Progress*, 28(1), 30–35. doi : 10.1002/prs.10276. _eprint : https ://aiche.onlinelibrary.wiley.com/doi/pdf/10.1002/prs.10276.

Volker, A., Mast, A. & Bloom, J. (2010). EXPERIMENTAL RESULTS OF GUIDED WAVE TRAVEL TIME TOMOGRAPHY. *AIP Conference Proceedings*, 1211(1), 2052–2059. doi : 10.1063/1.3362375.

Wang, L., Xu, J. & Chen, D. (2022). PPM EMAT for Defect Detection in 90-Degree Pipe Bend. *Materials*, 15(13), 4630. doi : 10.3390/ma15134630. Number : 13 Publisher : Multidisciplinary Digital Publishing Institute.

Willey, C. L., Simonetti, F., Nagy, P. B. & Instanes, G. (2014). Guided wave tomography of pipes with high-order helical modes. *NDT & E International*, 65, 8–21. doi : 10.1016/j.ndteint.2014.03.010.

Yu, X., Fan, Z., Puliyakote, S. & Castaings, M. (2018). Remote monitoring of bond line defects between a composite panel and a stiffener using distributed piezoelectric sensors. *Smart Materials and Structures*, 27(3), 035014. doi : 10.1088/1361-665X/aaa69b. Publisher : IOP Publishing.

Zhu, W. & Rose, J. (1999). Lamb wave generation and reception with time-delay periodic linear arrays : a BEM simulation and experimental study. *IEEE Transactions on Ultrasonics, Ferroelectrics, and Frequency Control*, 46(3), 654–664. doi : 10.1109/58.764852. Conference Name : IEEE Transactions on Ultrasonics, Ferroelectrics, and Frequency Control.

Zimmermann, A. A. E., Huthwaite, P. & Pavlakovic, B. (2021). High-resolution thickness maps of corrosion using SH1 guided wave tomography. *Proceedings of the Royal Society A : Mathematical, Physical and Engineering Sciences*, 477(2245), 20200380. doi : 10.1098/rspa.2020.0380. Publisher : Royal Society.